THE INFRA-RED ASTRONOMY OF SUPERNOVAE

by

GILLIAN PEARCE B.Sc.

A thesis submitted to the University of Keele
for the Degree of Doctor of Philosophy

Department of Physics,
University of Keele,
Keele,
Staffordshire.

November 1983

The 2 journal articles at the end of this thesis have been excluded at the request of the university

TO MY PARENTS

ACKNOWLEDGEMENTS

I would like to express profound thanks to:

My parents for the encouragement, help, and support they have given me throughout my life, for the sacrifices they have made, and for helping me achieve my ambition of becoming an astronomer.

My supervisor, Dr. A. Evans, for his enthusiasm, advice, help, and for his supervision of research.

Dr T.R. Geballe, Dr P.M. Williams, Dr A.J. Longmore, and Dr W.P.S. Meikle, for their enthusiastic help and instruction on using the United Kingdom Infra-red Telescope.

Mr A.J. Mayes B.A., and Dr M.F. Bode, for useful discussions.

Mrs B. Haywood, Mrs D. Walker and Miss L. Stanley for so patiently typing this thesis.

Mr A. Bennett for drawing some of the figures in my thesis.

Dr Paul Collis and the staff of the Computer Centre at Keele for their advice on computing.

The S.E.R.C. for travel funds.

The University of Keele for travel funds, and for financial support for the research.

The University of Manchester Regional Computer Centre for computing time on the CDC 7600.

My friends and teachers for their encouragement especially Mr B.F.H. Coleman M.Sc., Dr R.J. Mooney, Dr R.J. Hilleard, Dr D. Crow, Dr J.J. Cox, Dr R.C. Maddison, Mr R.J. Whitmore B.Sc., Mr D. Wright B.Sc., and Mr B. Jones B.Sc.

ABSTRACT

The heating of circumstellar and interstellar dust grains of various types by extragalactic supernovae is investigated. Models to compute the infra-red flux from such dust grains are devised. The optical constants of different grain materials are deduced, and the method to compute the temperature of a grain heated by a supernova is detailed. The evaporation and condensation of grains are considered and the effect of forces on the grains are investigated. Spectra and light curves are computed for radiation from interstellar graphite and silicate grains in a typical nearby galaxy heated by a type II supernova. Spectra of circumstellar silicate dust shells around the supernovae SN1979c and SN1980k are computed and compared with observational data. This comparison leads to a determination of the masses and sizes of the circumstellar dust shells which condense around these supernovae. Finally the formation of a composite double dust shell consisting of an inner shell of homogeneous grains and an outer shell of core-mantle grains is considered. The condensation of such a dust shell around a type II supernova is found to be possible. Spectra are computed for this type of circumstellar dust shell and compared with the spectra computed for a circumstellar dust shell of homogeneous silicate grains.

CONTENTS

CHAPTER ONE

A SUMMARY OF THE THESIS

This thesis investigates the heating of interstellar and circumstellar dust grains by extragalactic supernovae. Models are devised to compute the infra-red flux from various distributions of dust of different types. Where possible the computed fluxes are compared with observations.

In chapter 2, a review of recent literature on supernovae is described. Aspects of visual, infra-red, ultra-violet, X-ray and radio observations are detailed. Theoretical models are also described for type I and type II supernovae, including the evolution of likely respective progenitors. Two supernovae, those which occured in NGC6946 and NGC4321 are reviewed in considerable detail as these are modelled in the thesis.

In chapter 3, the method of computation of the flux from circumstellar and interstellar dust grains heated by supernovae is detailed. The luminosity and effective temperature of type I and type II supernovae are determined as a function of time. The optical constants are derived for graphite, silicate, silicon carbide and corundum at frequencies ranging from the far ultra-violet to millimetre wavelengths. The contribution to grain heating of ambient starlight is also considered.

The light travel time across the supernova is taken to be negligible, but the consequences of a significant light travel time across the supernova dust shell are detailed. The flux from a grain of given size and composition at a particular temperature is considered. When the grain's radiation is observed at time t, the grain is in thermodynamic equilibrium with supernova radiation observed at time τ. This time τ is derived in terms of t. Consideration is given as to how to allow for condensation of dust after outburst and the expansion of the cavity of dust around the supernova in the computations of radiation flux from circumstellar and

interstellar dust. The equation of transfer involved in the heating of circumstellar and interstellar dust grains by supernova radiation is considered and its solution detailed. The method used to determine grain temperature in terms of the Planck mean and the absorption efficiency is described in detail. The method involves computing the absorption efficiencies and the corresponding Planck means. Futhermore, in view of the complexity of the light curves and efficiencies a method of interpolating the Planck mean values is described.

In chapter 4, the evaporation temperatures of grains of the four types as a function of time after supernova outburst are considered. The cavity formed by the supernova due to the evaporation of pre-existing grains is also described. Grains of a number of radii and of various types forming circumstellar shells around type I and type II supernovae are considered. The time development of the cavity radius due to evaporation and to the gravitational, radiation pressure, and viscous forces acting on the grains is investigated. For type II supernovae the cavity evaporates to the final radius very quickly. However for type I supernovae the expansion of the cavity due to evaporation is more gradual and must be taken into consideration in flux computations. For the silicate and corundum and for homogeneous silicon carbide grains there is essentially no expansion of the cavity due to the forces on the grains. However for the other cases involving homogeneous graphite and graphite-mantle silicon carbide-core grains there is significant expansion of the cavity and this must be taken into consideration in flux computations. The condensation times of circumstellar dust grains from supernova ejecta are found to be too small to have any significant effect on the dust flux.

In chapter 5, the flux from interstellar grains heated by a type II supernova is considered. The interstellar grains are assumed to form an infinite plane parallel slab with a uniform distribution of both graphite and silicate grains. It is assumed that the total interstellar dust mass

density is 1.8×10^{-23} kg m^{-3} (Whittet 1981) of which 70% is silicate by mass and 30% is graphite by mass. By comparing the interstellar extinction curve with those produced by graphite and silicate grains of different radii, it is concluded that silicate and graphite grains of radii 0.15μm and 0.035μm respectively provide a reasonable approximation to the interstellar extinction curve. The assumptions of the interstellar dust grain model and the co-ordinate system used in flux computations are detailed; the method of flux computation is then described.

In chapter 6, the flux from circumstellar grains heated by type II supernovae is considered. The circumstellar grains are assumed to form a spherical shell with a power law distribution of silicate grains, the grain number density varying as $r^{-\beta}$ where $\beta = 0$, 1 or 2, and r is the distance of a grain from the supernova. The model assumptions are detailed and the method of flux computation is described. The coordinate system used is different to that for the interstellar grains and is also described. The circumstellar dust shell model is applied to observations of the supernovae in NGC4321 and NGC6946. In both cases, infra-red fluxes in the first 100 days or so after outburst can be explained entirely in terms of supernova photospheric radiation and it is concluded that the infra-red excess at later times is reasonably consistent with the condensation of a circumstellar dust shell of silicate grains at around 200 days after outburst. The parameters of the circumstellar dust shell are determined in each case. Spectra of the circumstellar dust shells and the supernovae are compared with the observations.

In chapter 7, the model and the flux computation method used in chapter 6 are modified to describe the method of computation of the flux from a double dust shell. This consists of an inner spherical shell of homogeneous grains which merges into an outer spherical shell of core-mantle grains. The inner radius of the outer shell is equal to the outer radius of the inner shell. The cores are identical to homogeneous

grains in the inner shell. A double dust shell of silicon carbide (SiC) cores and graphite mantles around a type I supernova is found to be improbable as the silicon carbide grain material condenses further from the supernova than does the graphite. A condensed (but not a pre-existing) double dust shell of corundum cores and silicate mantles around a type II supernova is however found to be possible therefore such a double dust shell is investigated. Spectra are computed for a double dust shell which condenses at 160 days after the supernova outburst. Particular attention is paid to the three maxima in the dust flux at 10μm, at 14μm, and at 21μm, all three being due to the core-mantle grains and to the 12.7μm corundum peak. The 14μm feature does not occur in homogeneous silicate or corundum grains and can be taken as a positive indication of corundum-core silicate-mantle grains. The 12.7μm peak can be taken as a positive indication of corundum grains. Two cases are considered, one of continuous ejection, and one of short-lived ejection. The first case leads to the formation of a geometrically thick dust shell and the second to the formation of a geometrically thin shell.

This concludes the investigation of the radiation from different distributions of dust of various grain types heated by extragalactic supernovae. In chapter 8, some ideas for further research are given.

In the appendices are given

(i) zero magnitude fluxes,

(ii) details of integrations used in chapter 7,

(iii) the reduction of data obtained at U.K.I.R.T.,

(iv) a list of symbols used in the thesis, and

(v) copies of the author's published papers.

CHAPTER 2

REVIEW OF THE LITERATURE ON SUPERNOVAE AND RELATED TOPICS

2.0 Introduction

This thesis is concerned with the study of infra-red radiation from dust grains heated by extra-galactic supernovae. The heating of four grain types (graphite, silicate, silicon carbide, and corundum) and the heating effects of type I and type II supernovae are considered. Flux computations are carried out for graphite, silicate, corundum, and corundum-core silicate-mantle grains heated by type II supernovae. The type II supernova dust grains are either those in a circumstellar shell around the supernova, pre-existing or condensing out of the supernova ejecta or the interstellar grains in the dust plane of the galaxy. This chapter reviews the research so far undertaken in this field.

2.1 Supernova Light Curves

Supernovae were originally distinguished on the basis of their light curves by Baade and Zwicky (1938). The distinction was made largely on the shape of the light curve. Certain type II supernovae showed the presence of a plateau region whereas other supernovae did not. A more rigorous classification of supernovae was undertaken later on in which supernovae were distinguished as type I or type II supernovae on the basis of their spectra, depending on whether or not hydrogen was present in their ejecta (Trimble 1982).

Composite light curves of type I supernovae are presented in Barbon, et al. (1973) in which it is concluded that there is a common

light curve for this type of supernova. The variation with time of the luminosity and effective temperature of type I supernovae is described in Chapter 3. The peak luminosity is 8.17×10^{35} Watts, corresponding to a bolometric magnitude of -18.55. The light curves of type II supernovae are considered in Barbon, et al. (1979). There are two classes of type II supernovae, the P and L classes. The P class is characterised by a rapid decline for 30 to 35 days following maximum light, in which the supernova falls about 1.2 magnitudes in B. A plateau of constant luminosity occurs between 30 to 35 days and about 80 days after maximum light, then a second rapid decline up to 120 to 130 days after maximum light in which the star drops 2.5 magnitudes in B. Then, a final phase occurs in which the flux at B drops by 0.006 magnitudes per day. Most type II supernovae are classified as belonging to the P class. The time variation of the luminosity and effective temperature of the L class, described in Weaver et al. (1980), is detailed in chapter 3. The peak luminosity is taken to be 2.7×10^{36}Watts, corresponding to a bolometric magnitude of -19.90. The L class does not have a constant luminosity plateau but is characterized by linear declines in magnitude. The two supernovae studied in chapter 6 of this thesis, SN1979c in NGC4321 and SN1980k in NGC6946, are both L class type II supernovae. The light curves at B and V of SN1979c are reproduced from Barbon, et al. (1982a) in figure 1 and the light curves at U, B and V of SN1980k are reproduced from Barbon, et al (1982b) in figure 2. The U, B, V, and R observations of SN1979c are presented in Balinskaya et al. (1980) and U, B, and V observations of SN1980k are presented in Buta (1982). These observations and a detailed analysis of the light curves of these two supernovae are presented in chapter 6. Like the L class of type II supernovae, the light curves of these two supernovae undergo changes in the rate of decline at certain times after maximum light.

FIGURE 1. The B (upper curve) and V (lower curve) magnitudes for SN1979C in NGC4321. The inset shows the (B-V) variation with time for SN1979c.

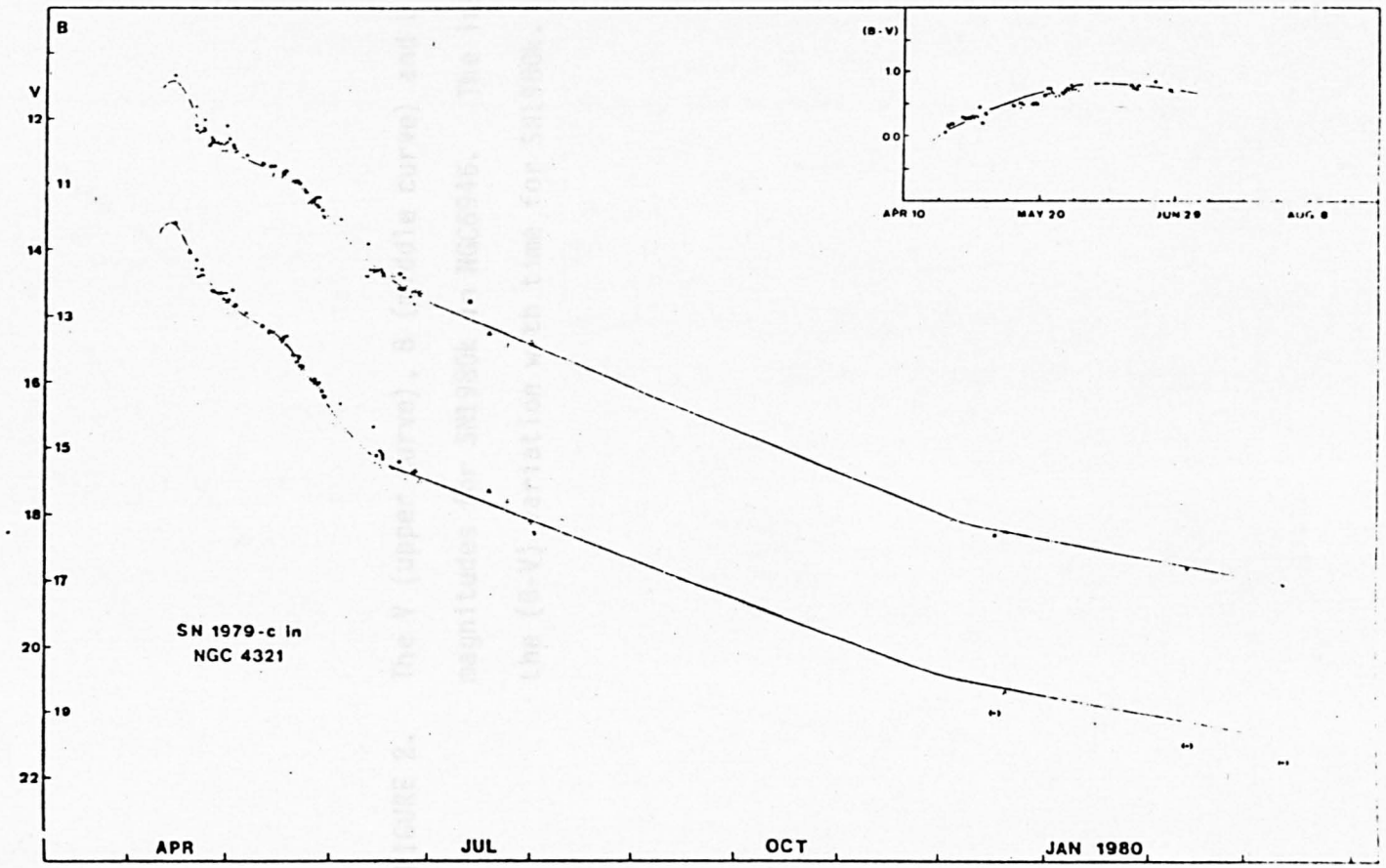
B
V
12
11
14
13
16
15
18
17
20
19
22
SN 1979-c in
NGC 4321
APR
JUL
OCT
JAN 1980
(B-V)
1.0
0.0
APR 10
MAY 20
JUN 29
AUG. 8

FIGURE 2. The V (upper curve), B (middle curve) and U (lower curve magnitudes for SN1980k in NGC6946. The inset shows the (B-V) variation with time for SN1980k.

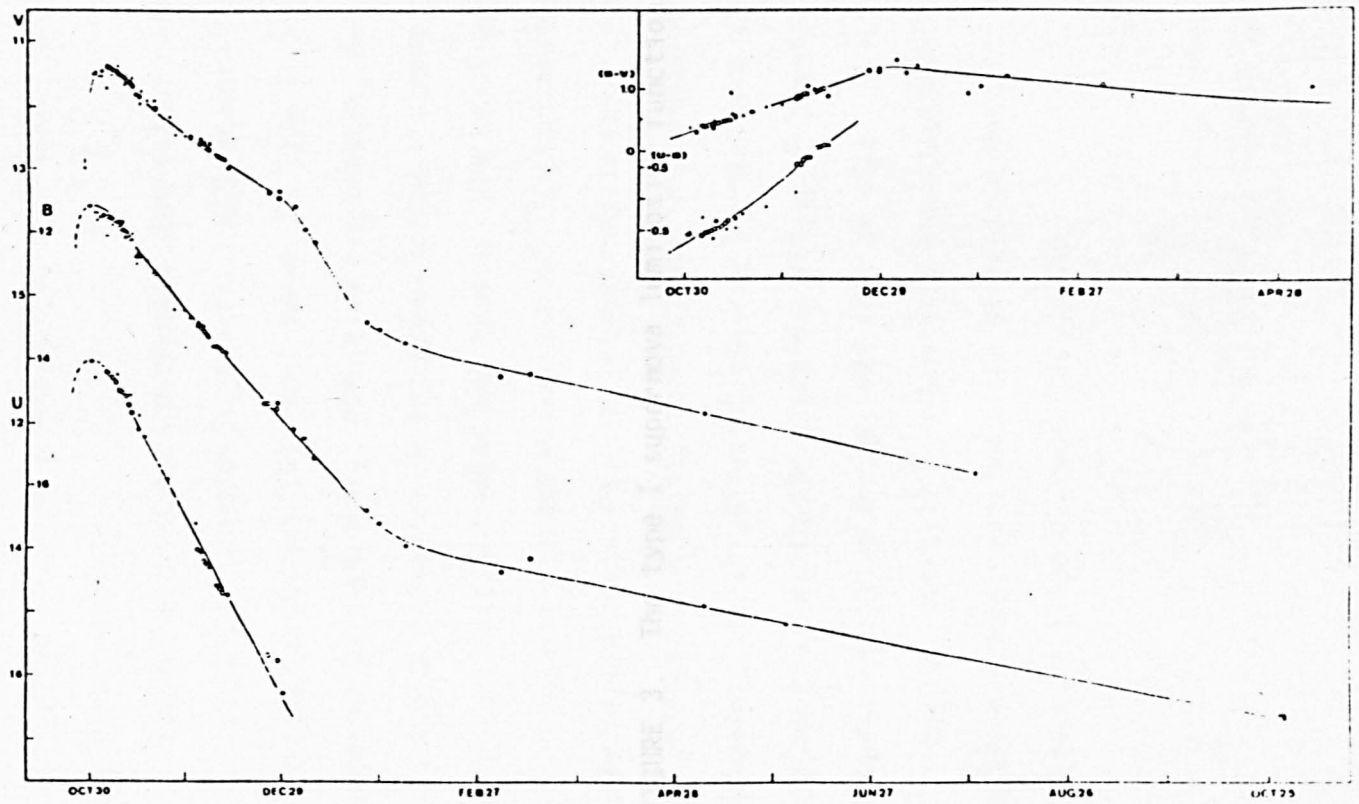
V
B
U
11
13
15
14
16
12
OCT30
DEC29
FEB27
APR28
JUN27
AUG26
OCT25
(B-V)
(U-B)
1.0
0
-0.5
-0.5

FIGURE 3. The type I supernova luminosity function

In the case of SN1979c, the U and B light curves undergo changes in the rate of decline at about 50 and about 100 days after outburst while U, B, V and R light curves all undergo changes of slope at about 100 days after outburst. In the case of SN1980k the U, B and V light curves all undergo changes in the rate of decline for about 50 days after outburst.

Various authors have attempted theoretical modelling of the light curves of supernovae. Arnett (1980) produced a series of analytical solutions for light curves of type II supernovae. The behaviour of luminosity, effective temperature, B-V colour and fluid velocity is presented, with dependence on the mass, energy of explosion, initial radius and opacity. The solutions allow estimates of the mass of ejected matter and of ^{56}Co synthesized to be made from observational data. From such solutions it may be possible to infer the absolute luminosity from distance independent characteristics of the event. Analytical solutions are an important aid as a means of scaling the results for different values of physical parameters such as mass, explosion energy, and initial size.

Arnett, essentially represents the supernova light curves as decaying exponential functions of various detailed forms. One such function is given by equation (2.1.1)

$$-\ln L_{*}(t) = \left(\frac{t}{1.59 \times 10^{8}s}\right) + \left(\frac{t}{1.134 \times 10^{2}s}\right)^{2} \qquad (2.1.1)$$

where $L_{*}(t)$ is the supernova luminosity as a function of the time t after outburst. The function described in equation (2.1.1) was fitted into the models for SN1979c and SN1980k in this thesis. However, this function did not yield a very good fit to the observational data, since the second term in equation (2.1.1) caused a decline which was

too rapid when compared to observational light curves. Arnett assumes that the variation with time of the supernova photosphere temperature $T_e(t)$ is given by

$$T_e(t) = T_e\,(0)\; L_*(t)^{1/4} \;/\; (1 + V_{sc}t \;/\; R_*(0))^{1/2} \qquad (2.1.2)$$

where $R_*(0)$ is the radius of the supernova at outburst and V_{sc} is the rate of increase of the supernova black-body radius.

Equation (2.1.2) gives rise to very high supernova temperatures at early times ($T_e \sim 25000$K at $t \sim 1$ day) whereas others have suggested that the temperature of the supernova at such early times may be as low as 10^4K.

A unified model for supernova light curves was attempted by Trivedi (1982). He showed that light curves of both type I and type II supernovae follow the equation

$$M = M_0 - 5 \log \left(\frac{t'_0}{t + t'_0} \right) - 2.5 \log (1 + K'_1 (t - t'_1)) + 2.5 \log (1 + K'_2 (t - t'_2)^2) \qquad (2.1.3)$$

where M_0 is the magnitude corresponding to the peak luminosity; M is the magnitude at anytime t after outburst of the supernova; t'_0 is the time at which the value M_0 occurs, t'_1 is the time when the inner shell starts contributing to the brightness; t'_2 is the time when surface radiation loss affects the brightness; K'_1 and K'_2 are constants. Trivedi argues that the brightness Σ at a time t is given by

$$\frac{\Sigma}{\Sigma_0} = (R_*(t'_0)/R_*(t)) = \left(\frac{t'_0}{t + t'_0} \right)^2 \qquad (2.1.4)$$

where Σ_0 is the brightness at time t_0 and $R_*(t)$ is the radius of the supernova at a time t after outburst.

Trivedi also examines the idea of the decay of $^{56}Ni \rightarrow {}^{56}Co \rightarrow {}^{56}Fe$. Such a mechanism has been used by Colgate and McKee (1969), Van Hise (1974), and Chevalier (1981), to explain light curves. Trivedi concludes that it would require 50% to 70% of the ejected material to be Ni^{56} and this would require 70% to 90% of the ejected material to be in the form of iron group elements. This, he concludes, appears to be contrary to observations. Also such models based on the decay of ^{56}Ni are used to explain the light curves of type I supernovae only and not type II supernovae.

2.2 Infra-red Observations of Supernovae

Lee et al. (1972) report on U, B, V, R, I, J, K photometry of the bright supernova 1972e in galaxy NGC5253. Observations obtained over a period of 43 days showed that the U, B, V measurements were similar in form to those obtained for other type I supernovae. Infra-red observations made at 1.25 μm and at 2.2 μm during two nights separated by a period of 38 days showed nearly identical magnitude. Measurements showed a decline in all the other wavebands, but this decline had definite irregularities.

Spectrophotometric observations of this supernova were obtained by Kirshner et al.(1973) within the wavelength range 0.33 μm to 2.2 μm. The overall shape of the energy distribution from 0.4 μm to 2.2 μm could be represented by a black body which decreased in temperature from about 10,000K on May 23rd 1972 to 7500K on June 5th 1972. It then remained at about 7000K until at least July 8th 1972. The results disagree with those obtained by Lee et al. (1972) for the period from May 22nd to June 29th. Lee reported no decrease in infra-red flux

between these dates. From June 4th to June 25th 1972 small changes in the shape of the energy distribution occurred, while the flux decreased. This behaviour is typical of an object whose photosphere shrinks while remaining at constant temperature. Assuming NGC5253 has a distance of 4Mpc the temperatures and magnitudes indicate photospheric radii of 1.1×10^{13}m on May 24th, 1.6×10^{13}m on June 4th, 1.1×10^{13}m on June 15th and 1.0×10^{13}m on June 26th. The rapid increase in the radius of the photosphere followed by a decrease could be the result of the increasing transparency of the expanding supernova envelope. The temperature of the photosphere remains constant suggesting that the prevailing source of opacity becomes important at that temperature, material at lower temperatures being transparent and material at higher temperatures opaque.

Further infra-red observations have been undertaken by Elias et al. (1981) and Dwek et al. (1983). Elias et al. (1981) observed the type I supernovae in NGC1316, NGC4532 and NGC5253, at J, H and K. The data available provide the best type I supernova light curves at these wavelenths. These light curves are characterized by a double maximum. The effect is apparently strongest at J and is probably due to the development of a transient absorption feature during the intervening minimum. There is a theory that the infra-red emission at later times (~ 6 months after outburst of the supernova) may be due to the presence of a circumstellar dust shell around such objects. However observations by the author, of type I supernovae (for example, the supernova in NGC4185 and NGC1316) have failed to detect any associated infra-red excesses which would indicate the presence of circumstellar dust shells. The theory is confined more to the case of type II supernovae.

Elias et al. (1981) suggest that the infra-red luminosities of type I supernovae may be useful as distance indicators within a few

tens of Mpc, as there is little variation in infra-red absolute magnitudes at maximum between different type I supernovae, at any given time after outburst.

Infra-red observations of the supernova SN1980k (in NGC6946) are presented in Dwek et al. (1983). They conclude that during the period between November 1st and December 19th, 1980, the infra-red emission probably originated from the photosphere of the expanding supernova layers. The J, H, K and L colours correspond to those of a black body with an average temperature of ~ 5000k. Further observations around 31st May 1981 showed that this supernova developed an infra-red excess after December 1980. This infra-red excess remained through October 1981 and is consistent with thermal emission from dust at ~700k to 900k, in addition to the hotter photosphere. The interpretation of the data is consistent with both the suggestion that dust may condense out of the supernova ejecta; or the hypothesis that the emission arises from pre-existing grains in a circumstellar dust shell.

Dwek (1983) examines models for the infra-red emission observed in NGC4321 and NGC6946. The results show that the evolution of the infra-red spectrum from both supernovae is consistent with a circumstellar dust shell model, in which the thermal infra-red radiation arises from pre-existing dust grains heated up by the UV-visual output of the supernova. The models suggest that both supernovae have circumstellar dust shells extending out to a distance of ~6.8 x 10^{15}m from the star, with optical depths of ~0.3 and 0.03 for SN1979c and SN1980k respectively.

2.3 Observations of Supernovae at other Wavelengths.

Radio observations undertaken by Weiler et al. (1981) using the Very Large Array suggest that pulsars may be associated with some type II supernovae. Observations were undertaken by Weiler et al. of the supernova in NGC4321. The flux was 5mJy at 5GHz in April 1980, approximately one year after outburst. According to these authors the emission was non-thermal, and they argued that the emission, which had an intrinsic luminosity at this frequency exceeding 180 times that of Cas-A was due to a pulsar embedded in this object.

Observational data at X-ray, optical, radio, and ultra-violet wavelenths have been collectively condensed in the paper by Panagia et al. (1980), and these authors examine coordinated observations of the supernova 1979c in NGC4321. It is concluded that most of the ultraviolet emission lines originate in a shell of compressed gas ejected by the supernova progenitor rather than the supernova itself. This is in contrast to the optical emission lines which originate in the outer layers of the main supernova envelope which is moderately ionized and expands at $\sim 10^4 kms^{-1}$.

Radio and X-ray observations yield an upper limit to the supernova emission which agrees with the ultra-violet results. Dwek et al. (1983) suggest that X-rays may heat the dust associated with the circumstellar shell thought to exist around the supernova in NGC6946. They speculate that the dust may be heated by X-rays, resulting from the interaction of the expanding shock wave with circumstellar material. However, observation of the supernova in NGC6946 by Canizares et al. (1981) showed that this was unlikely to be the case.

2.4 The Spectra of Supernovae

Type I and type II supernovae are distinguished from each other by the presence or absence of hydrogen lines in their spectra near light maximum. It is universally accepted that type I supernovae have no hydrogen lines in their spectra. It is also broadly accepted that type II supernovae tend to occur among population I stars and that type I supernovae occur among population II stars.

Zwicky (1965) also desribed spectra which he classified as belonging to other groups of supernovae called types III, IV and V. However Oke and Searle (1974) in their review of the observational spectra of supernovae could find no real evidence for distinguishing types III, IV and V from types I and II. In the case of a type V supernova only one example was known and the authors were again uncertain as to the need to classify this as a separate group.

The spectra of type II supernovae are divided essentially into three stages according to Oke and Searle (1974). Phase A occurs at 0 to 20 days. A few days after maximum the continuum spectral energy distribution is smooth. Except for H_α none of the spectral features are very prominent. H_β and H_γ have P-cygni-like profiles. This is followed by phase B, which occurs at 20 to 70 days. The overall continuum energy distribution is still smooth but redder than in phase A, and absorption lines appear to strengthen. The H_α feature remains prominent and consists of a strong emission and a weak violet-shifted absorption. Late phases show that a continuum is still present, and that H_α occurs in emission, and also forbidden lines of [OI] appear. The supernova IC4182 studied by Minkowski (1939) is a typical type I supernova, and its light curve is used to define what is meant by a type I supernova light curve. Type I supernova spectra form a far more homogeneous class, than do type II's. Kirschner *et*

al. (1973) have considered the spectra of type I and type II supernovae. Their analysis of type I spectra shows that the continuum cools as the supernova ages and that the line spectrum is much more complicated than those of type II supernovae.

Oke and Searle (1974) have shown that the spectra of type I supernovae can be divided into four phases. Phase A occurs 0 to 20 days after light maximum. The spectrum is a smooth continuum essentially, on which are superimposed strong P-Cygni type line profiles. The strongest lines remain much the same over the first 20 days but the weaker features become stronger with time. Balmer lines are not present either in emission or absorption. Phase B occurs 20 to 60 days after light maximum. The continuum is still relatively smooth but is redder in colour than in phase A. The overall spectrum remains largely the same over the whole period except that a very broad feature appears from λ5180Å to λ5600Å. Also a strong and new emission feature at λ6550Å appears.

Phase C occurs at 60 to 100 days. The feature at λ5600Å weakens and eventually disappears. The spectrum undergoes slight changes. Phase D occurs at 200 to 400 days. The spectrum has undergone radical changes in intensities of the lines. The emission at 6500Å remains, and a broad emission peak arises at 7200Å.

Barbon et al. (1982a) study the time development of the spectrum of SN1979c in NGC4321. The spectra obtained at 6 to 7 days past maximum were characterized by a nearly featureless continuum. About three weeks after maximum, the spectra displayed broad emission bands, including a wide P-Cygni feature centred at 4730Å which indicated a mean expansion velocity of around 8100kms^{-1}. Thirty to fourty days from maximum, the spectrum was dominated by broad emission features. It was noted by Branch et al. (1981) that there was a general weakness of absorption features in comparison with

other type II supernovae.

Barbon et al. (1982b) study the time development of the spectrum of SN1980k in NGC6946. At 7 to 9 days after maximum, the spectrum showed an almost pure continuum without perceptible traces of emission or absorption features. Fourteen days after maximum, an emission band with at least five secondary maxima centred at 6555Å appeared, indicating that the emitting layers were expanding at $\sim 6200 kms^{-1}$. At 19 to 31 days after maximum H_α became very prominent. At 35 to 54 days after maximum there was a pseudo-continuum of several emission lines from 5200Å to 5700Å. Observations taken between 67 and 94 days after maximum showed little change in the spectra from earlier spectra taken in December 1980. Measurements showed that the expansion velocities were smaller than those taken earlier.

Type II supernovae light curves and spectra tend to vary individually. There is no type II equivalent of IC4182 which can be used to define what is meant by a typical type II supernova.

2.5 The Progenitors of Type I and Type II Supernovae.

Type II supernovae tend to occur among population I stars, in the spiral arms of galaxies where there is generally an abundance of dust. Late type giant stars occur in the same regions where type II supernovae occur and it is believed that there is a likely association between the two objects in that these late type giant stars are the progenitors of type II supernovae. The supernova discovered in NGC1255 by Seitter and Duerbeck (1981) may support this hypothesis. It was concluded that there was a supergiant star of mass around 20 solar masses in the same position on the plate before the supernova occurred. The mass estimation for the progenitor was

arrived at using the mass-luminosity relationship, for supergiants, the luminosity and distance of the object having been determined from the redshift of the parent galaxy. It is thought that this object may have been the progenitor of the supernova. On the other hand the object may simply have been along the same line of sight.

Thompson (1982) has attempted to set an upper mass limit for the stellar progenitor to the supernova in NGC6946. He concludes that the progenitor was probably <18M. The estimate of mass is probably somewhat uncertain due to the lack of a faint stellar sequence for comparison. Circumstellar shells are associated with some late type giant stars. Such shells of dust are believed to be present around type II supernovae. The detonation of such a supernova would be brought about by the collapse of the core of the late type giant star. The evolution of the progenitor proceeds via the mechanism

$^{1}H \rightarrow {}^{4}He$ (proton chain or C-N-O cycle)

$^{4}He \rightarrow {}^{12}C, {}^{16}O$

$^{12}C \rightarrow {}^{20}Ne$ (and smaller amounts of magnesium etc.)

$^{20}Ne \rightarrow {}^{24}Mg, {}^{28}Si$

$^{16}O \rightarrow {}^{28}Si$ (and smaller amounts of ^{32}S and ^{40}Ar, and ^{40}Ca).

$^{28}Si \rightarrow {}^{56}Fe$ (or ^{56}Ni)

(Trimble, 1982).

Nuclear binding is at a maximum near ^{56}Fe, thus these cores are not capable of further exoergic reactions and some form of collapse is unavoidable. Eventually the electrons and protons in the core combine to form neutrons and neutrinos are released, via the reaction

$$e^- + p^+ \rightarrow n^0 + \nu_e$$

The neutrinos carry away so much of the stars thermal energy that eventually the core of the star plunges into total collapse. This causes a rapid rise in temperature in the layers around the core and the former expands rapidly outwards from the core (this expansion is further increased by the transfer of momentum from the collapsing core by way of the neutrinos and radiation pressure).

It is believed that type I supernova may arise from double star systems in which one of the components achieves a mass exceeding that given by the Chandrasekhar limit, by receiving additional mass transfered to it from the other component. Once the core mass exceeds the Chandrasekhar mass limit of $1.44M_\odot$ the core collapses leading to the rapid expansion of the outer layers as a type I supernova.

Models of type I supernovae arising from binary systems have been investigated by Truran et al. (1971), Hartwick (1972), Mazurek (1973) and Starrfield et al. (1981). All agree that explosions will occur for white dwarfs having a sufficiently high mass. If indeed type I supernovae do arise in such a manner this can account for the homogeneity of the spectra and the light curves of type I supernovae.

An alternative school of thought believes that type I supernovae may arise from single stars. Here it is believed that the cores of such stars evolve until they contain a mass of degenerate carbon and oxygen of slightly less than the Chandrasekhar mass. This is then detonated, possibly by the onset of carbon fusion. The hydrogen in the outer layers of such stars has either been lost in the stellar winds or almost entirely fused into helium by mixing during hydrogen shell burning. Weaver, et al. (1980) have investigated such models and have shown that if the cores are half incinerated to ^{56}Ni inside a helium envelope of mass $\sim 0.5M_\odot$, and sizes $\sim 10^9$m to 10^{11}m a type I

supernova could be produced.

2.6 Condensation Theory and Supernova Ejecta Composition

Many late type giant stars, some of which are thought to be supernovae progenitors, have circumstellar dust shells which probably condensed from material ejected in a variable phase of the stars' evolution. Consequently, one theory of the origin of circumstellar dust around supernovae is that it is the remainder of circumstellar dust around the progenitor after the evaporation of dust by supernova radiation at outburst.

An alternative theory to the pre-existing grain theory suggests that circumstellar dust shells around type II supernovae may arise due to grains condensing out of the ejecta of the supernova explosion. This idea of the condensation of dust grains from material ejected in violent stellar eruptions was first put forward by Hoyle and Wickramasinghe (1970). The condensation of circumstellar dust shells around novae was postulated by Clayton and Wickramasinghe (1976) to explain the time development of the infra-red excess. The theory was further developed for supernovae by Clayton (1982).

The composition of grains in novae ejecta (assuming solar abundance) has been investigated by Yamamoto and Nishida (1977). They conclude that the main compounds present in the ejecta of novae are Al_2O_3, $MgSiO_4$, $MgSiO_3$, SiO_2, and Fe. The corresponding condensation temperatures are 1404K, 1075K, 1068K, 1014K, and 988K respectively. These authors speculate that supernovae are responsible for synthesizing heavy elements and replenishing the interstellar medium and they are a totally different phenomenon to novae. They believe that aluminium abundance would be greatly enhanced in the ejecta of supernovae as compared to novae due to the higher temperatures in

supernovae.

Hoyle and Wickramasinghe (1970) put forward the idea that the adiabatic expansion and cooling of grain nuclei should be accompanied by condensation of silicate dust. It is believed that type II supernovae arise from oxygen-rich progenitors and silicate grains compose the circumstellar dust shells. Clayton (1982) coined the term SUNOCON (SUperNOva CONdensate) and he argues that alumium, which is synthesized in stars by the burning of carbon, would combine with oxygen to produce a grain core of Al_2O_3. He also argues that magnesium is produced under such conditions as those which prevail in a supernova explosion, and combines with the oxygen and silicon to produce such compounds as $MgSiO_3$. The magnesium produced in the extreme conditions that exist in a supernova explosion could also combine with aluminium and oxygen to form $MgAl_2O_4$. He argues that successive layers of these compounds can build up as the materials condense out in turn, as determined by their condensation temperatures. Clayton believed that supernovae replenish the aluminium in the interstellar medium on a time-scale of the order of 4×10^9 years. He states that if the aluminium atoms were to emerge in a gaseous state, the steady-state fraction in the gas would be

$$x_{Al}\ (\text{gas}) \ / \ x_{Al}\ (\text{solid}) \sim 40^{-1} \qquad (2.6.1)$$

Clayton and Wickramasinghe (1976) consider graphite grains condensing in an expanding shell of gas of constant thickness ejected in a nova outburst. They examine the effect of the growth of grain radius on the development of infra-red luminosity. If a_g denotes the grain radius, the rate at which a grain grows is given by

$$\frac{da_g}{dt} = \frac{\alpha\, n_v}{s_g} \left(\frac{mKT}{2\pi}\right)^{\frac{1}{2}} \qquad (2.6.2)$$

where α is the sticking probability; s_g the grain material density, (α/s_g is assumed to be approximately equal to $10^{-4}m^3Kg^{-1}$); n_v is the number density of carbon atoms in the ambient gas; T is the gas temperature and m the mass of a carbon atom. The authors assume that the depletion of carbon from the ambient gas is unimportant so only a small fraction of the carbon in the ambient gas actually condenses into grains. Consequently, n_v is simply proportional to $(t_c/t)^2$, where t_c is the time after outburst at which grains condense and t is the time after outburst being considered. The gas temperature is taken to be equal to the temperature of a black-body in thermodynamic equilibrium with nova radiation and so is proportional to $(t_c/t)^{1/2}$. Consequently, from (2.6.2) da_g/dt is proportional to $(t_c/t)^{5/4}$ and the final form of the integrated equation is

$$a_g = a_1 + (a_\infty - a_1) \quad (1 - (t_c/t)^{9/4}) \qquad (2.6.3)$$

where a_∞ is the final grain radius and a_1 is the radius of the nucleation centre. The authors argue that because the formation of nucleation centres is a result of the collision of gas atoms, their rate of formation is proportional to n_v^2 and so t^{-4} declines much more rapidly than does grain condensation. Consequently, the formation of nucleation centres is assumed to be instantaneous. It should be noted that according to the theory of Clayton and Wickramasinghe (1976), the grains are always growing and the time taken to reach a certain fraction of the final radius (assuming $a_1 \ll a_\infty$) is a function only of the time after outburst at which condensation occurs. For instance 90% of the final radius is reached at $t = 6.3t_c$ so the growth time is $5.3t_c$, which would be 530 days for t_c = 100 days or 1060 days for t_c = 200 days. If, however, it is assumed (as in chapter 4 of this thesis) that depletion of grain

monomers from the ambient gas is important and that almost all the grain material condenses, a very different result is arrived at. The grain condensation times are very much shorter than those predicted by Clayton and Wickramasinghe (1976) and they are dependent on other parameters as well as the condensation time, parameters such as the initial grain monomer number density in the ambient gas.

Grain growth was also considered by Lefevre (1979). Lefevre considers grain growth given by equation (2.6.3) for an exploding nova shell and near a late-type star and concludes that irrespective of the nucleation mechanism, grain growth is governed by the grain temperature, so there is a critical distance at which growth begins (e.g. $\sim 8 \times 10^{12}$m for the example quoted above).

Clayton and Wickramasinghe (1976) have studied grain heating by novae. They state that the infra-red luminosity L_{IR} is given by

$$\begin{aligned} L_{IR} &= c' a^3 (t)\, t^{-2} \qquad a \leq a_1 \\ L_{IR} &= c' a_1\, a^2 (t) t^{-2} \qquad a \geq a_1 \end{aligned} \tag{2.6.4}$$

for a thin nebula where $a_1 = 0.0178\mu$m is the grain radius for which the Planck mean grain absorption efficiency $\overline{Q_{abs}}\ (a, T_e) = 1$; T_e being the nova photosphere temperature, and c' is a constant. (The absorption efficiency is the ratio of the cross-section for absorption of radiation to the geometrical cross-section of the grain. The Planck mean efficiency is the efficiency average over the Planck function $B(\nu,T)$. This model is generally consistent with the observational data for Nova Serpentis.

2.7 Grain Destruction

Draine and Salpeter (1979) consider grain destruction by such mechanisms as sputtering and evaporation. The grain temperature T_{gsb} at which N_L layers of monomers sublime from a grain in a time t is given by

$$T_{gsb} = U_o \left(K \ln(\nu_L t / N_L)\right)^{-1} \qquad (2.7.1)$$

where U_o is the binding energy per molecule of material, ν_L is the molecular vibration frequency of the lattice atoms; for evaporation $N_L \sim 10^2$. Sputtering of grains will occur when the ejecta reach the grains. The sublimation rate of a grain is given in Wright (1981) by

$$\frac{da}{dt} = V_s e^{-T_o/T_{gi}} \qquad (2.7.2)$$

where V_s is the speed of sound in the solid, KT_o is the activation energy for sublimation, and a_i is the grain radius. It is assumed that dust heated to a temperature T_v vapourises instantly, while dust cooled to less than T_v never vapourizes. As the life-time of a supernova flash is of the order of 10^6s, a_i is of order 0.1μm and V_s is of order $10^3 ms^{-1}$, e^{-T_o/T_v} is of order 10^{16}. Therefore, T_v is of order $T_o/37$. The parameter T_v is fairly well defined as a grain of temperature ten per cent greater than T_v survives for less than three per cent of the life-time of the supernova flash. T_{gi} is the grain temperature.

Falk and Scalo (1975) have considered the behaviour of grains in early supernova environments. They examine the efficiency of grain destruction by collisional and radiative heating and sputtering at early times. The approximate time scale for diffusion of radiation through an isothermal circumstellar shell is given by

$$t \approx 75 \left(\frac{T}{10^3}\right)^{-3} (\Delta\tau)^2/\kappa \qquad (2.7.3)$$

where, T is the temperature of the incident radiation field; $\Delta\tau$ is the optical thickness of the shell of opacity κ.

Grains will be destroyed if the temperature they attain in this radiation field exceeds the grain evaporation temperature. In Falk and Scalo the equilibrium temperature of grains heated collisionally by the gas ejected in the supernova explosion is

$$T_{gi} \sim 1950\mu^{1/4}(n)^{-1/8}\overline{Q_{abs}}^{-1/4}(\overline{Q_{pr}}W)^{3/8}(T)^{3/4} \qquad (2.7.5)$$

where $\overline{Q_{pr}}$ is the Planck mean radiation pressure efficiency at temperature T, n is the number density of gas particles, $\overline{Q_{abs}}$ is the Planck mean grain absorption efficiency; μ is a constant and W is the dilution factor and is equal to $(R_*/r)^2$, where r is any distance from the supernova across the shell. The condition of radiative equilibrium implies that the equilibrium grain temperature is given by

$$T_{gi} = T_e\,(W\,\overline{Q_{abs}}\,(T_e)/4\,\overline{Q_{abs}}\,(T_{gi}))^{1/4} \qquad (2.7.6)$$

for an optically thin shell; here $\overline{Q_{abs}}\,(T)$ is the Planck mean grain absorption efficiency at temperature T. The authors conclude that graphite, silicon carbide, iron or ices, or quartz grains could survive evaporation but sputtering and fragmentation would destroy the larger grains. They believe that grains have no observable effect on early supernova development but that the smaller particles may at late times act as condensation nuclei.

2.8 Infra-red Emission from Supernovae, and its Interpretation

The infra-red emission arising from type II supernovae at early times is associated with the photosphere. However the infra-red emission at t > 6 months after the supernova outburst is believed to be due to radiation from a circumstellar dust shell. It is not known if such shells are due to pre-existing grains or condensed grains or perhaps both.

Bode and Evans (1980) theoretically examine the supernova which occurred in NGC4321. The heating function of the grains, that is the rate at which grains heated by all emitted supernova radiation would absorb radiant energy in the circumstellar shell is given by

$$H = L_{\star} \overline{Q_{abs}} \qquad (2.8.1)$$

where the Planck mean of the grain absorption efficiency is taken to be independent of time. The bolometric luminosity of the central object is denoted by $L_{\star}$. The peak luminosity L_0 is taken to be equal to 2.7×10^{36}Watts (after Panagia, 1980), and they assume that it decays as

$$L_{\star}(t) = L_0 e^{-\omega t} \qquad (2.8.2)$$

where $L_{\star}(t)$ is the luminosity at time t after outburst and ω is the e-folding time which is taken to be 50 days. They conclude that for a 0.2μm graphite grain to exist for a significant time the grains must lie at a distance of $\sim 8 \times 10^{14}$m. Accordingly they suppose that at the time of the Merrill (1979) observation, the dust envelope possessed a cavity of this size. Their results are consistent with observations of Merrill of a thermal infra-red excess in this object after ~260

days. They also consider that the infra-red emission may have arisen from interstellar grains in the galactic plane of M100 (NGC4321). However the infra-red fluxes they derive for this are too low by $\sim 10^3$ for such interstellar emission.

The infra-red emission from interstellar grains heated by supernovae has been examined also by Pearce and Evans (1983). A copy of the paper is printed in Appendix (v) of this thesis.

Chevalier (1981) considers the interaction of the radiation from a type II supernova with a circumstellar shell. He argues that the radiation from a supernova is expected to have two basic components: the photospheric emission which will approximate to a black-body spectrum; and bremsstrahlung emission from a hot shell of shocked gas ejected in the supernova explosion. He points out that bremsstrahlung emission has not yet been directly observed from a supernova, but Branch et al. (1981) has suggested that some of the ultra-violet emission from the supernova 1979c was due to the bremsstrahlung component.

The hydrodynamic interaction of the expanding supernova envelope with the circumstellar shell leads to the formation of a hot region which can influence the supernova emission spectrum. Chevalier computes that the total rate of energy generation by the shock moving into the circumstellar medium is $\sim 6.3 \times 10^{40} M_{-6} U_4^{+3} V_1^{-1}$ ergs s^{-1} where U_4 is the velocity of the shock wave in units of $10^4 Kms^{-1}$. The quantity M_{-6} is the mass loss rate in units of 10^{-6} M_o yr^{-1}; V_1 is the wind velocity in units of $10Kms^{-1}$ caused by the moving shock wave. This rate of energy generation by the shock gives rise to a post shock temperature of $\sim 1.3 \times 10^9 U_4^2$ Kelvin. Such a temperature could significantly heat a circumstellar shell.

Wright (1980) also considers the heating of grains by a supernova. The work of Wright (1980) investigates a model in which a supernova explodes in a molecular cloud. This is a light-echo model

and attempts to predict values for the infra-red flux produced by the heating of dust grains. His model assumes that the visible and ultra-violet output of the supernova is absorbed by dust with a linear absorption coefficient. It is further assumed that the cloud surrounding the supernova is optically thin in the infra-red but optically thick in the ultra-violet and visible.

The distance of the dust from the supernova is given simply as

$$r = (x^2 + \rho^2)^{1/2} \qquad (2.8.3)$$

where x is given by:-

$$x = \frac{\rho^2}{2ct} - \frac{1}{2} ct \qquad (2.8.4)$$

and ρ is in the plane of the sky.

The infra-red flux, arising from the heating of grains is given by

$$F_\nu = \frac{ct_f}{D^2} \int_{r_m}^{R_m} \kappa_\nu B(\nu_i, T_{gi}(r)) \, 2\pi r \, d r \qquad (2.8.5)$$

where R_m and r_m are quantities defined in Wright's paper (1980); r is the distance of the dust from the supernova; κ_ν is the linear absorption coefficient; D is the distance of the supernova from the observer. Wright assumes a square shape pulse for the supernova and takes supernova maximum luminosity $L_o = 10^9 \times L_\odot$; the life-time of a supernova flash $t_f = 3 \times 10^6$secs; and $T_v = 1000$K which yields a binding energy of ~4eV for the grains. The infra-red luminosity is given by

$$L_{IR} \sim \frac{ct_f}{2r_v} L_o \sim 7 \times 10^7 L_o \qquad (2.8.6)$$

where r_v is the distance from the supernova at which a grain vapourizes. Typical parameters for a supernova exploding in a cloud with n $\sim 10^3 cm^{-3}$ at a distance of 10Kpc produces a flux of $\sim 2 \times 10^4$ Jy at 3.5μm for some 500 days. However, at 10Mpc the predicted fluxes are not very large, and he points out that at very large distances the supernova would be fainter than the galaxy that contains it and so high spatial resolution would be required to separate the supernova and the galaxy.

The paper by Dwek et al. (1983) is concerned with the data for the supernova in NGC6946. They consider the various dust heating mechanisms such as collisional heating and radiative heating. The dust is heated up by collisions with the ambient gas out of which it condensed. They state that the mass of the gas in which these grains condensed can range from $10^{-3} M_\odot$ to $10 M_\odot$. The gas temperature is taken to be 2000K, the condensation temperature of the dust, so that the total thermal energy content of the gas ranges from $\sim 10^{33}$Joules to $\sim 10^{37}$Joules. They conclude that collision with the ambient gas is an inadequate energy source for the dust. Also, they conclude that heating by radioactivities in the ejecta can be rejected on the grounds of cosmic abundance and time scale constraints.

They alternatively consider the radiative heating aspects. Here the dust may be heated up by the absorption of black-body radiation emitted from the photosphere. A temperature of ~6000K will suggest that the photosphere is associated with the hydrogen recombination front and that the dust condenses out of the expanding hydrogen rich atmosphere above it. A temperature of ~4000K is associated with the uncovering of the mantle of the star, and that the dust is formed out of these metal-rich ejecta. Finally they consider that dust may be heated by X-rays, resulting from the interaction of the expanding shock wave with circumstellar material. However observation of the

supernova in NGC6946 by Canizares et al. (1981) showed that this was unlikely to be the case.

They conclude that the infra-red fluxes observed are consistent with both the infra-red echo model in which the emission is from pre-existing grains of circumstellar material heated up by the UV-visual output of the supernova, but also resemble that observed in several novae, and is suggestive of the formation of dust in the expanding supernova ejecta. In this latter case dust must be radiatively heated up by the underlying photosphere. As they point out only further observational evidence will discern which model is correct for SN1980k in NGC6946. Indeed it could be the case that circumstellar material for some supernovae is due to pre-existing grains whereas for others it arises from the condensation of material from the supernova ejecta.

The near infra-red emission from the supernova SN1982g in NGC1332 has been modelled by Graham et al. 1983. A copy of the paper may be found in Appendix (v) of this thesis. The data for SN1982g were obtained using the United Kingdom Infra-Red Telescope and the Anglo-Australian telescope.

2.9 Supernova Remnants.

The infra-red radiation from supernova remants is considered to be emitted by dust grains heated by collisions with hot gas and ambient starlight. This dust is either swept up dust in the interstellar medium or dust that condenses out of the ejecta of a supernova. Falk and Scalo (1975) consider the heating of grains in a supernova remnant and have considered the infra-red emission from supernova condensates. The envelope of the supernova which is expelled at high velocities into the surrounding medium eventually

begins to decelerate. This deceleration of the envelope transfers most of the kinetic energy of the ejecta to the interstellar medium, which results in the propagation of an adiabatic blast wave. This blast wave creates a cavity of hot interstellar gas in which the mantle ejecta are immersed. They consider the effect of sputtering of grains and compute that a grain's lifetime against destruction by sputtering in the cavity is approximately given by (for $t \sim 10^6 K$)

$$\tau_{sput} \sim 10^6 a_i(\mu m)/n(cm^{-3}) \text{ years} \qquad (2.9.1)$$

where a_i is the grain radius and n is the ambient gas density in cm^{-3}. The ambient gas density for supernova remnants is typically $0.08 cm^{-3}$ to $0.6 cm^{-3}$ (Spitzer 1982) and its temperature is $\sim 4 \times 10^6 K$ to $7 \times 10^6 K$. The sputtering time for such remnants would therefore be $\sim 2.5 \times 10^5$ to $\sim 2 \times 10^6$ years for a typical initial grain size of $0.2 \mu m$.

These authors also consider collisional heating of the condensates by the shocked gas. The hot supernova cavity gas in the remnant Cas A gives rise to temperatures of ~110K for $0.1 \mu m$ grains. The corresponding infra-red flux is 9×10^7 mJy at $35 \mu m$. The post-shock gas on the other hand will heat up grains and give rise to very much less infra-red emission. These authors predict that grains of radius $0.1 \mu m$ and temperature 100K will give rise to an infra-red flux of 0.6mJy at $35 \mu m$. It is therefore the hot supernova cavity gas which will heat up the grains predominantly.

Dinerstein et al. (1982) measured 8 knots in Cas A at $3.8 \mu m$ and/or $10.6 \mu m$. Two of these knots KB61 and KB42 were detected at $10 \mu m$ with fluxes of about 40mJy and 30mJy respectively. The corresponding dust temperatures would be ~430K and 370K respectively.

2.10 Background Sources

For a supernova in close proximity to the nucleus of a galaxy, there may be considerable problems with contamination. However, provided that the nucleus of the galaxy concerned, is not sited in the beam of the detector being used, the only major source of contamination is likely to be due to H II - molecular cloud complexes.

The type of variability found at far infra-red wavelengths of interstellar grains heated by supernovae is probably insufficient to exclude HII-molecular cloud complexes. It would by contrast, however, be expected that the infra-red emission of a HII-molecular cloud complex would be constant. However, it would be useful to have an alternative means of distinguishing between the two objects. This alternative method may be sought in their respective radio spectra. The radio emission of a HII-molecular cloud complex is expected to be that characteristic of free-free radiation (e.g. Panagia 1978) and that of the supernova, in particular after outburst, is expected to be non-thermal and extremely transient (e.g. Weiler et al. 1981). Therefore, suitable radio observations in the post-eruptive phase would determine whether the far infra-red source is associated with a supernova or whether it is infra-red emission from a HII-molecular cloud complex.

2.11 Conclusion

Type I supernovae will have similar light curves while type II supernovae can be classified into the P and L classes according to their light curves. The P class have a constant luminosity plateau phase but the L class decline exponentially in luminosity, no plateau

phase being present. The luminosity and effective temperature as a function of time after outburst are given for type I supernovae, and for the L class of type II supernovae in chapter 3. The supernovae 1979c and 1980k, both L class type II supernovae are further investigated in chapter 6. Their luminosities and effective temperatures as a function of time after outburst are derived by a black-body fit to the observational data and their infra-red excesses at more than 200 days after outburst are modelled by a circumstellar dust shell of silicate grains. The general luminosity and effective temperature variations of the L class of type II supernovae are used in chapter 5 in the computation of the infra-red radiation from interstellar dust heated by a type II supernova.

The idea of multiple layered grains is further investigated in chapter 7. As the ejecta of type I supernovae have an excess of carbon over oxygen and the ejecta of type II have an excess of oxygen over carbon, the formation of silicon carbide-core graphite-mantle grains is considered in the ejecta of the former and the formation of corundum-core silicate-mantle grains is considered in the ejecta of the latter. The formation of core-mantle grains around type I supernovae is found to be improbable, but the formation of core-mantle grains around type II supernovae is found to be possible. Therefore, computations are carried out to determine the radiative flux from such grains heated by a L class type II supernova with the general luminosity and effective temperature variation given in chapter 3.

In chapter 4, the derivation of the grain evaporation temperature described by Draine and Salpeter (1979) is used to determine the grain evaporation temperature. Also in chapter 4 the grain growth theory in Clayton and Wickramasinghe (1976) is further developed by considering the effect of depletion, which is considered

to be important for supernovae if not for novae.

CHAPTER 3

CALCULATION OF THE TEMPERATURE OF DUST HEATED BY A SUPERNOVA.

3.0 Introduction

When a supernova erupts in a galaxy, the infra-red emission from dust heated by the supernova seen by a distant observer lies within a parabloid of revolution (Bode and Evans 1979) with focus at the supernova and axis along the line of sight through the supernova. This infra-red emission arises through the absorption of ultra-violet radiation by grains of for example graphite and silicate, and the subsequent emission of radiation in the infra-red. These grains may be interstellar or circumstellar in origin. The case for heating of interstellar grains by the supernova is considered in chapter 5, and the case of circumstellar grains heated by a supernova is examined in chapter 6.

3.1 The Variation With Time Of The Luminosities And Temperature of Supernovae.

It is assumed that the supernova radiates as a black-body. The flux per unit frequency interval at frequency, ν, from unit normal area of a black-body of temperature T is given by:-

$$B(\nu,T) = \frac{2\pi h\nu^3}{c^2} \frac{1}{(e^{h\nu/kT} - 1)} \qquad (3.1.1)$$

For the study of infra-red fluxes from interstellar grains heated by a supernova, the following type II supernova temperature, T_e, and luminosity L_*, variations with time were used (from Weaver et al. 1980)

$$L_*(t) = 0 \qquad t < 0$$

$$L_*(t) = L_0 e^{-t/t_0} \qquad t > 0 \qquad (3.1.2)$$

$$T_e(t) = 25{,}000e^{-t/t_1} \qquad 0 < t < t_2$$

$$= 6{,}000 \qquad t \geq t_2 \qquad (3.1.3)$$

From Panagia(1979), the peak luminosity of the supernova at outburst, $L_0 = 2.7 \times 10^{36}$ Watts, the e-folding time of the supernova light curve t_0 = 50 days, $t_2 = 2.5 \times 10^6$ secs and $t_1 = t_2 / \ln (25/6)$. The peak luminosity of 2.7×10^{36} Watts is equivalent to an absolute bolometric magnitude of -19.90.

The luminosity, $L_*(t)$ and temperature $T_e(t)$ of the individual type II supernovae with infra-red excesses due to circumstellar grains are derived from a black-body fit to the observed supernova photospheric fluxes, f_ν, at N frequencies, ν, at which there is no contribution from the circumstellar dust. If there is no infra-red excess (relative to the photospheric radiation) this is true of all frequencies in the infra-red. If there is an infra-red excess it is true only of frequencies greater than the highest frequency at which an excess occurs. The optical depth A_ν, due to interstellar grains is determined observa tionally, and τ_ν^{cs}, the circumstellar contribution to the total extinction, is derived from the circumstellar dust model. For a set of temperatures T_e^i, ranging over several thousand degrees Kelvin with interval of 10K between consecutive temperatures the corresponding supernova luminosity L^i is derived as follows. The flux per unit frequency interval at frequency ν, from a black-body of temperature T_e^i, luminosity L, and distance D, is given by

$$L_\nu = P\nu^3 (e^{\beta^i \nu} - 1)^{-1} \; e^{-A_\nu - \tau_\nu^{cs}} \qquad (3.1.4)$$

$$P = h L / 2\sigma c^2 D^2 (T_e^i)^4 \qquad (3.1.5)$$

and

$$B^i = h/KT_e^i \qquad (3.1.6)$$

The luminosity L^i corresponding to the best fit to the observed fluxes of a black-body of temperature T_e^i is given by minimizing the deviations of the black-body fluxes from the observed fluxes at the same frequencies as follows:-

$$\frac{\partial}{\partial \ln P} \sum_{\nu} (\ln(f_\nu/L_\nu))^2 = 0 \qquad (3.1.7)$$

Substitiuting equation (3.1.4) into equation (3.1.7) for L_ν and putting $P=P^i$ when $L=L^i$ in equation (3.1.5)

$$\ln P^i = N^{-1} \sum_{\nu} (\ln f_\nu - 3\ln\nu + \ln(e^{B^i_\nu}-1) + \tau_\nu^{cs} + A_\nu) \qquad (3.1.8)$$

The value of T_e^i corresponding to the lowest of all the values of $(\ln(f_\nu/L_\nu^i))^2$ (i.e. the best of all the black-body fits) is taken to be the supernova temperature $T_e(t)$ and the corresponding luminosity L^i is taken to be the supernova luminosity $L_*(t)$.

The U, B, V data used to obtain the effective temperature and luminosity of the supernova in NGC4321 were obtained from Balinskaya *et al.* (1980) and the U, B, V, R data used to obtain the effective temperature and luminosity of the supernova in NGC6946 were obtained from Buta (1982).

The time variation of the luminosity of a type I supernova is illustrated in figure 3 and given in equation (3.1.9) and derived from Barbon *et al.* (1973). The time variation of the effective temperature of a type I supernova is derived from Meyerott (1980) and given in equation (3.1.12).

$$\begin{aligned} L_*(t) &= 0 && t < 0 \\ &= L_1 e^{t/t_1} && 0 < t < 15.4 \\ &= 8.17 \times 10^{35} && 15.4 < t < 24.6 \\ &= L_2 e^{-t/t_2} && 24.6 < t < t_4 \\ &= L_3 e^{-t/t_3} && t > t_4 \end{aligned} \qquad (3.1.9)$$

$$\begin{aligned} T_e(t) &= 9450 e^{-t/300} && 0 < t < t_5 \\ &= 6000 && t \geq t_5 \end{aligned} \qquad (3.1.10)$$

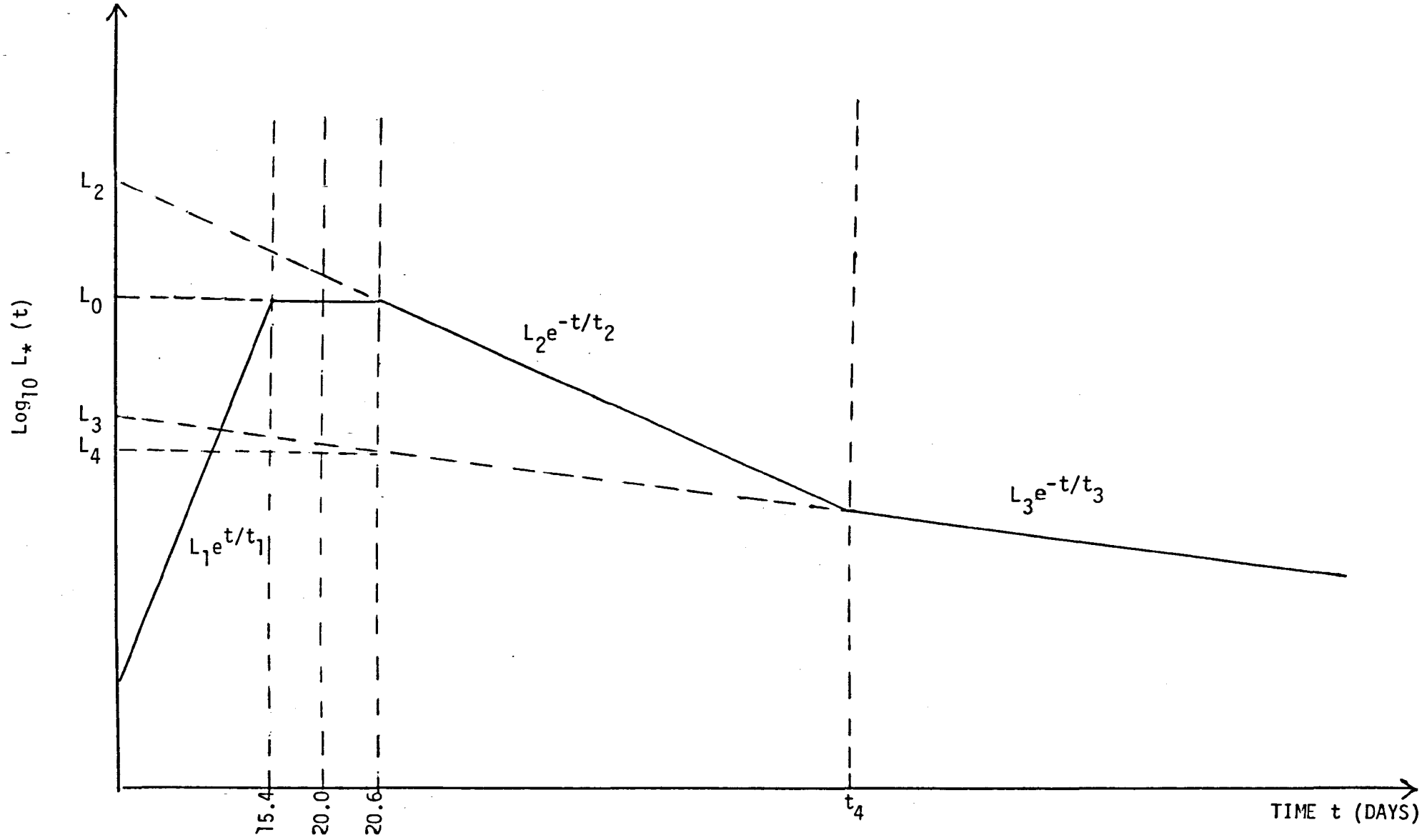
L_2
L_0
L_3
L_4
$\log_{10} L_*(t)$
$L_2 e^{-t/t_2}$
$L_3 e^{-t/t_3}$
$L_1 e^{t/t_1}$
15.4
20.0
20.6
t_4
TIME t (DAYS)

where L_* is in Watts, T_e is in Kelvin, t is in seconds and

$$L_1 = 8.17 \times 10^{35} \exp(-15.4 \ln 2/4.2)$$

$$L_2 = 8.17 \times 10^{35} \exp(24.6 \ln 2/6.6)$$

$$L_3 = 1.072 \times 10^{35} \exp(20 \ln 2/46)$$

$$t_1 = 4.2/\ln 2$$

$$t_2 = 6.6/\ln 2$$

$$t_3 = 46/\ln 2$$

$$t_4 = t_2\ t_3\ \ln(L_2/L_3)/(t_3 - t_2)$$

$$t_5 = 300\ \ln(9450/6000)$$

3.2 The Optical Constants Of Grain Materials.

The refractive index $m_1 - im_2$ is derived for the grain materials graphite, silicate, silicon carbide, and corundum.

The optical constants of silicate are illustrated in figures 4 and 5 and are listed in table 1. The optical constants of graphite are listed in table 2 for wavelengths less than or equal to 1μm and are given by equations (3.2.1) and (3.2.2), for wavelengths greater than 1μm:

$$m_1 = (2 + 2(1 + 4(\lambda/\mu m)^2)^{\frac{1}{2}})^{\frac{1}{2}} \qquad (3.2.1)$$

$$m_2 = (m_1^2 - 4)^{\frac{1}{2}} \qquad (3.2.2)$$

The data in table 2 were taken from Isobe (1971). The optical constants of silicate illustrated in figures 4 and 5 and given in table 1 are taken from Mayes (1983) and are derived originally from data in Day (1979) and Day (1981). The optical constants of silicon carbide were derived as follows. From Gilman et al. (1974) m_1 for $\lambda > 0.5112$ μm and m_2 for $\lambda > 6\mu m$ are given by the equations

$$m_1 = \Gamma \cos\delta \qquad (3.2.3)$$

$$m_2 = \Gamma \sin\delta \qquad (3.2.4)$$

where

$$\Gamma = (\varepsilon_1^2 + \varepsilon_2^2)^{0.25} \qquad (3.2.5)$$

and

$$\delta = \tan^{-1}\frac{\varepsilon_2}{\varepsilon_1} \quad \text{for } \varepsilon_1 > 0 \qquad (3.2.6)$$

$$\delta = \left(\tan^{-1}\frac{\varepsilon_2}{\varepsilon_1} + \pi\right) \quad \text{for } \varepsilon_1 < 0 \qquad (3.2.7)$$

TABLE 1

OPTICAL CONSTANTS FOR SILICATE.

WAVELENGTH/μm	m_1	WAVELENGTH/μm	m_2
$\lambda=\infty$	1.80	$\lambda=\infty$	0
$\lambda>250/3$	$1.80+(100/3\lambda)$	$\lambda>100$	$20/\lambda$
$\lambda=250/3$	2.20	$\lambda=100$	0.20
$(500/13)<\lambda<(250/3)$	$(71/35)+(100/7\lambda)$	$60<\lambda<100$	$0.14+6/\lambda$
$\lambda=500/13$	2.40	$\lambda=60$	0.24
$(100/3)<\lambda<(500/13)$	$2.79-(15/\lambda)$	$25<\lambda<60$	
$(-18/175)+(14.4/7\lambda)$			
$\lambda=100/3$	2.34	$150/7<\lambda<25$	0.72
$25<\lambda<100/3$	$3.00-(22/\lambda)$	$50/3<\lambda<150/7$	$2.05-(57/2\lambda)$
$\lambda=25$	2.12	$\lambda=50/3$	0.34
$20<\lambda<25$	$3.64-(38/\lambda)$	$150/11<\lambda<50/3$	$1.33-(33/2\lambda)$
$\lambda=20$	1.74	$500/39<\lambda<150/11$	0.12
$500/29<\lambda<20$	$2.615-(35/2\lambda)$	$75/7<\lambda<500/39$	
$(-1851/1150)+(510/23\lambda)$			
$\lambda=500/29$	1.60	$10<\lambda<75/7$	0.46
$500/33<\lambda<500/29$	1.60	$150/17<\lambda<10$	$3.01-(51/2\lambda)$
$\lambda=500/33$	0.60	$\lambda=150/17$	0.12
$150<\lambda<500/33$	$(149/155)+(300/31\lambda)$	$150/19<\lambda<150/17$	$1.055-(33/4\lambda)$
$\lambda=150/13$	0.80	$0.3<\lambda<150/19$	0.01
$75/7<\lambda<150/13$	1.80	$0.2<\lambda<0.3$	$0.16-\lambda/2$
$\lambda=75/7$	1.80	$\lambda=0.2$	0.06
$(100/11)<\lambda<(75/7)$	$3.704-(102/5\lambda)$	$0.17<\lambda<0.2$	$109/150-10\lambda/3$

TABLE 1 (cont.)

$\lambda=100/11$	1.46	$\lambda=0.17$	0.16
$50/7<\lambda<100/11$	$(109/150)+(20/3\lambda)$	$0.15<\lambda<0.17$	$3.05-17\lambda$
$\lambda=50/7$	1.66	$\lambda=0.15$	0.50
$0.36<\lambda<50/7$	1.66	$0.144<\lambda<0.15$	$6.50-40\lambda$
$\lambda=0.36$	1.66	$\lambda=0.144$	0.74
$0.22<\lambda<0.36$	$2.02-\lambda$	$0.14<\lambda<0.144$	$-4.30+35\lambda$
$\lambda=0.22$	1.80	$\lambda=0.14$	0.60
$0.17<\lambda<0.22$	$2.64-\lambda$	$0.112<\lambda<0.14$	$1.50-45\lambda/7$
$\lambda=0.17$	2.00	$\lambda=0.112$	0.78
$0.15<\lambda<0.17$	$4.125-12.5\lambda$	$0.1<\lambda<0.112$	$2.46-15\lambda$
$\lambda=0.15$	2.25	$\lambda=0.1$	0.96
$0.142<\lambda<0.15$	$-5.0625+48.75\lambda$	$0.09<\lambda<0.1$	$0.36+6\lambda$
$\lambda=0.142$	1.86	$0.078\leq\lambda\leq0.09$	0.90
$0.125<\lambda<0.142$	1.86	$0.05<\lambda<0.078$	$(-45/28)+(225\lambda/7)$
$\lambda=0.125$	1.86	$\lambda\leq0.05$	0.00
$0.105<\lambda<0.125$	$0.86+8\lambda$		
$\lambda=0.105$	1.70		
$0.09<\lambda<0.105$	$-1.10+80\lambda/3$		
$\lambda=0.09$	1.30		
$0.05<\lambda<0.09$	$0.625+7.5\lambda$		
$\lambda=0.05$	1.00		
$\lambda=0.05$	1.00		

TABLE 2

OPTICAL CONSTANTS FOR GRAPHITE.

WAVELENGTH/μm	m_1	m_2	WAVELENGTH/μm	m_1	m_2
0.0050	1.00	0.0000	0.1150	2.04	0.29
0.0075	0.99	0.0002	0.1200	1.90	0.19
0.1100	0.98	0.0002	0.1250	1.77	0.15
0.0125	0.97	0.0004	0.1300	1.64	0.13
0.0150	0.96	0.0008	0.1350	1.54	0.11
0.0175	0.95	0.0015	0.1400	1.43	0.11
0.0200	0.94	0.0030	0.1450	1.32	0.11
0.0225	0.92	0.0040	0.1500	1.21	0.16
0.0250	0.90	0.0050	0.1550	1.10	0.21
0.0275	0.87	0.0060	0.1600	0.99	0.27
0.0300	0.84	0.0080	0.1700	0.84	0.45
0.0325	0.76	0.0120	0.1700	0.84	0.45
0.0350	0.68	0.0200	0.1750	0.79	0.54
0.0375	0.63	0.0300	0.1800	0.74	0.66
0.0420	0.56	0.0800	0.1850	0.70	0.75
0.0450	0.46	0.1360	0.1900	0.69	0.85
0.0475	0.42	0.2100	0.1950	0.69	0.97
0.0500	0.40	0.3300	0.2000	0.69	1.10
0.0525	0.39	0.4200	0.2025	0.69	1.25
0.0550	0.39	0.5300	0.2050	0.70	1.41
0.0575	0.39	0.6500	0.2075	0.71	1.60
0.0600	0.39	0.7900	0.2100	0.73	1.82
0.0625	0.40	0.9200	0.2125	0.745	1.92
0.0650	0.42	1.0700	0.2150	0.76	2.02

TABLE 2 (cont.)

0.0675	0.45	1.2500	0.2175	0.78	1.13
0.0700	0.50	1.4500	0.2200	0.80	2.25
0.0725	0.57	1.5700	0.2225	0.825	2.30
0.0750	0.64	1.6900	0.2250	0.85	2.35
0.0775	0.71	1.7900	0.2275	0.875	2.39
0.0800	0.78	1.8300	0.2300	0.90	2.42
0.0825	1.08	1.7900	0.2325	0.925	2.42
0.0850	1.39	1.6900	0.2350	0.95	2.42
0.0875	1.70	1.5700	0.2375	0.975	2.42
0.0900	2.00	1.4500	0.2400	1.00	2.42
0.0925	2.10	1.3200	0.2425	1.06	2.41
0.0950	2.19	1.2000	0.2450	1.14	2.40
0.0975	2.30	1.1000	0.2475	1.22	2.39
0.1000	2.38	1.0000	0.2500	1.30	2.38
0.1025	2.34	0.8100	0.2525	1.375	2.35
0.1050	2.28	0.6600	0.2550	1.47	2.33
0.1075	2.23	0.5300	0.2575	1.555	2.31
0.1100	2.18	0.4200	0.2600	1.64	2.29
			0.2650	1.82	2.24
			0.2700	2.00	2.19
			0.2800	2.36	2.05
			0.2900	2.54	1.90
			0.3000	2.54	1.88
			0.5000	2.54	1.39
			0.6000	2.54	1.42
			0.7000	2.54	1.54
			0.8000	2.54	1.57
			1.0000	2.54	1.57

FIGURE 4. Optical constants for Olivine (represented by x)

Optical constants for silicate (represented by -)

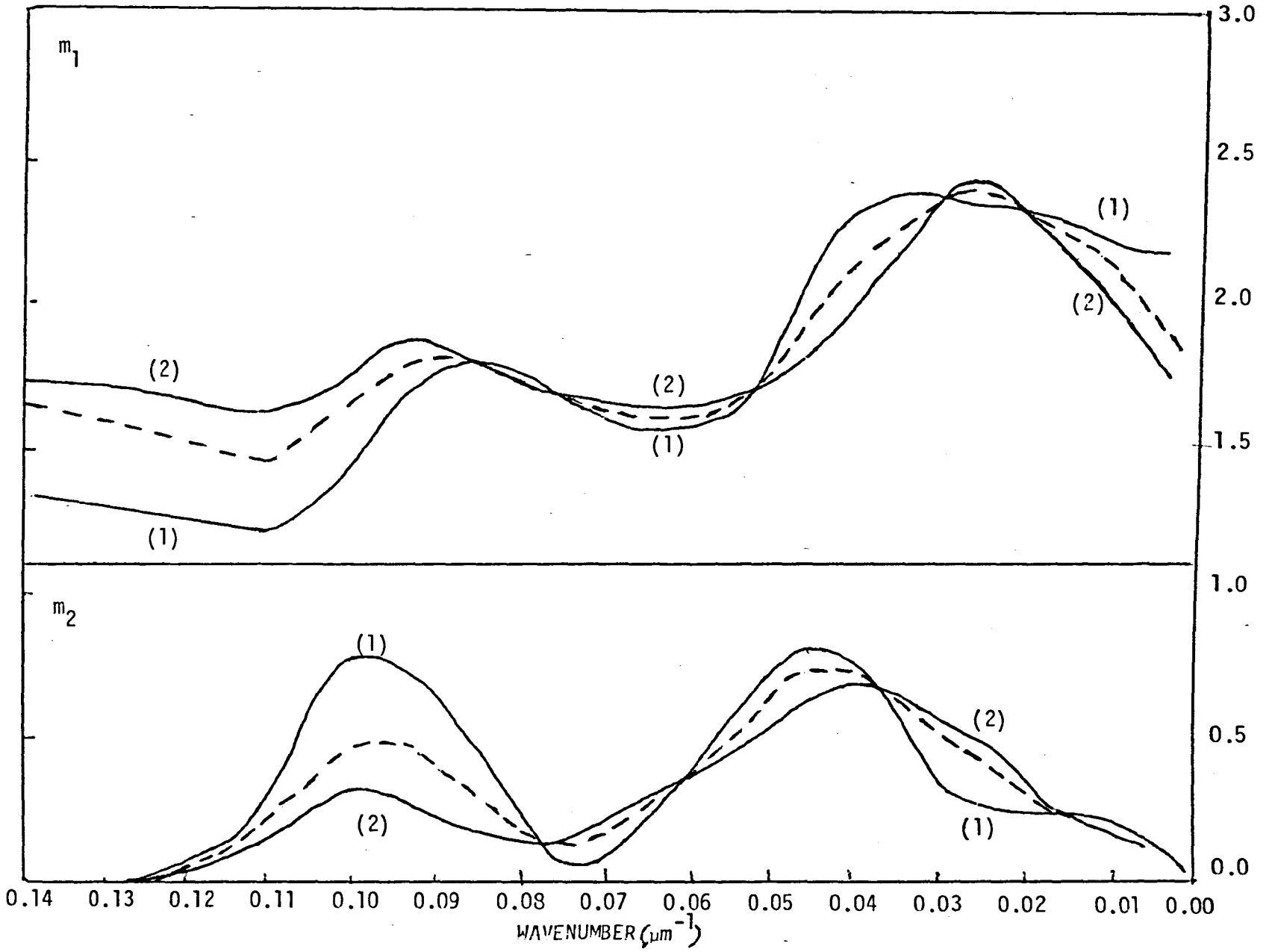
m1
m2
(1)
(2)
3.0
2.5
2.0
1.5
1.0
0.5
0.0
0.14 0.13 0.12 0.11 0.10 0.09 0.08 0.07 0.06 0.05 0.04 0.03 0.02 0.01 0.00
WAVENUMBER (μm⁻¹)

FIGURE 5. Optical constants for (1) $Mg_2 Si O_4$ (2) $Fe_2 Si O_4$
---- for the amorphous silicate

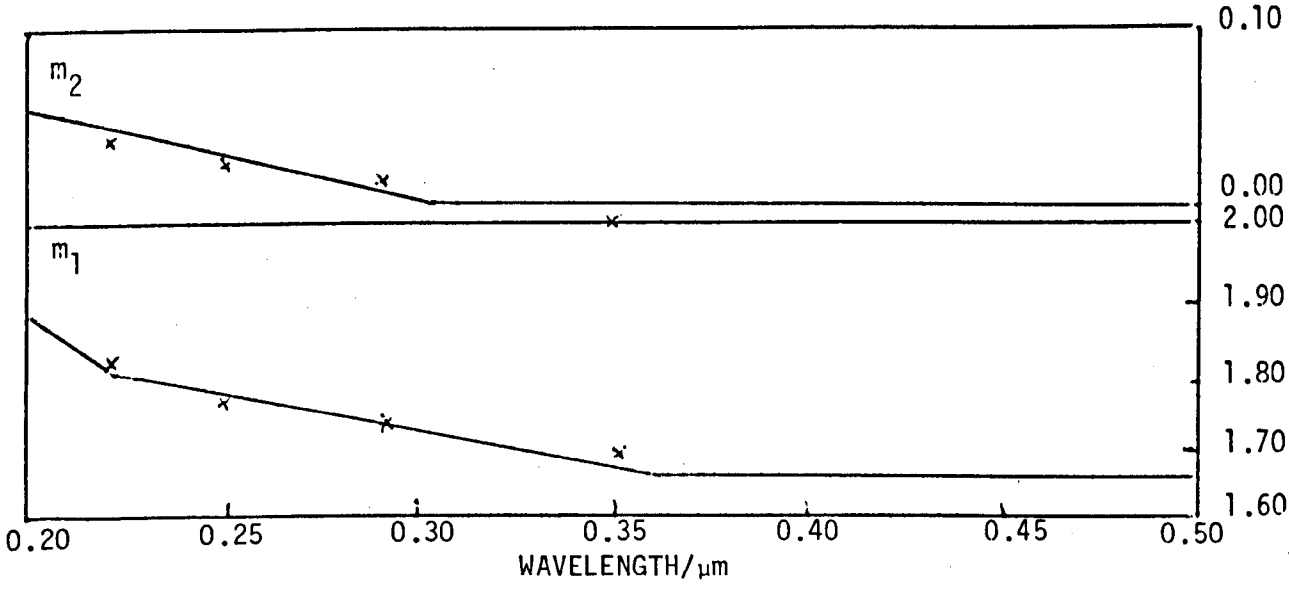
m_2
m_1
0.10
0.00
2.00
1.90
1.80
1.70
1.60
0.20
0.25
0.30
0.35
0.40
0.45
0.50
WAVELENGTH/μm

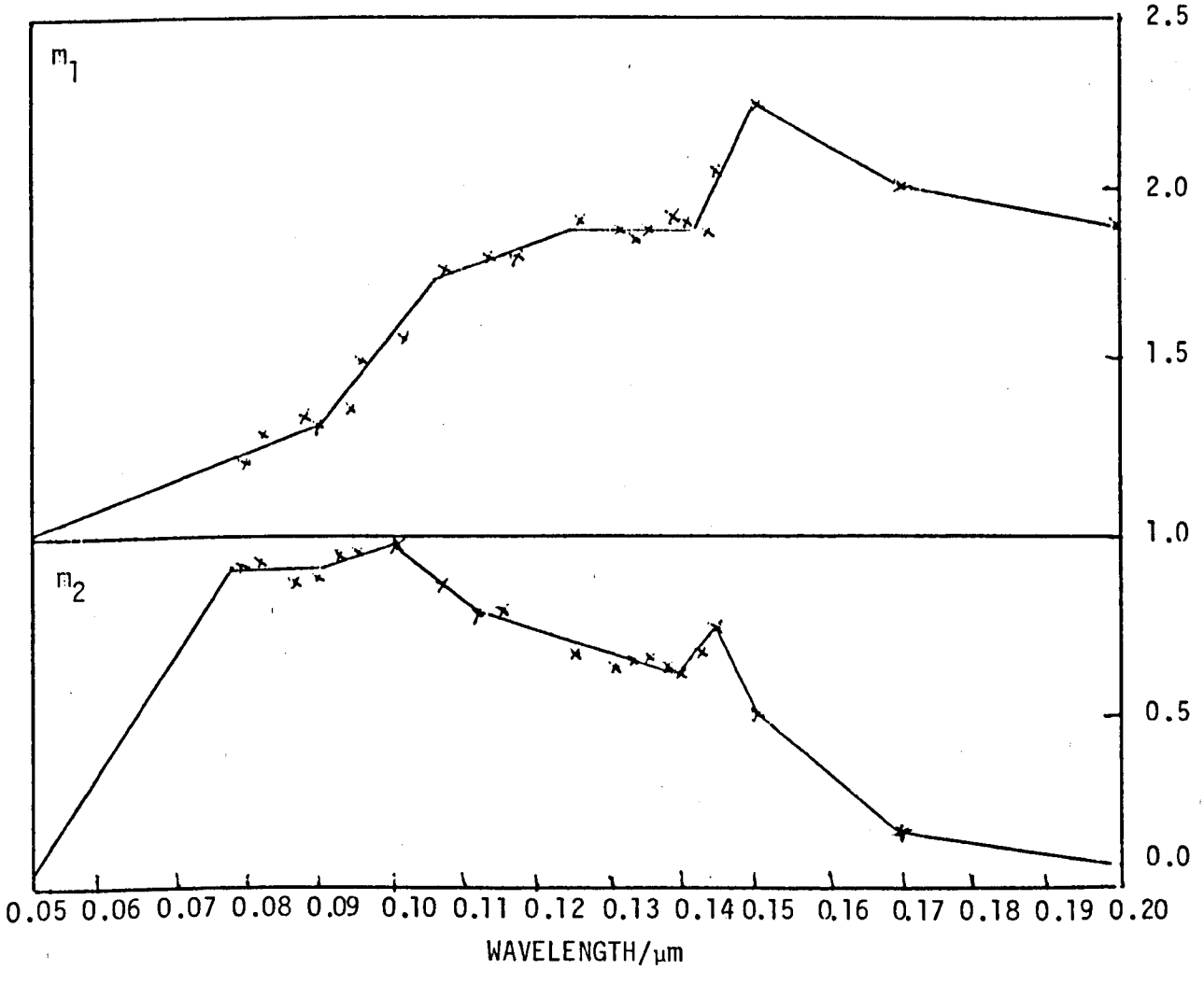
m_1
m_2
2.5
2.0
1.5
1.0
0.5
0.0
0.05 0.06 0.07 0.08 0.09 0.10 0.11 0.12 0.13 0.14 0.15 0.16 0.17 0.18 0.19 0.20
WAVELENGTH/μm

In the above

$$\varepsilon_1 = m_1^2 - m_2^2 = \varepsilon_o + \frac{4\pi\varepsilon_4(1-(\nu/\nu_o)^2)}{(1-(\nu/\nu_o)^2)^2+\varepsilon_3^2(\nu/\nu_o)^2}$$

and

$$\varepsilon_2 = 2m_1 m_2 = \frac{4\pi\varepsilon_4\varepsilon_3(\nu/\nu_0)}{(1-(\nu/\nu_0)^2)^2 + \varepsilon_3^2(\nu/\nu_0)^2} \qquad (3.2.8)$$

where

$\varepsilon_0=6.7$, $\varepsilon_4=0.263$, $\nu_0=2.380\times10^{13}$ Hz,

$\varepsilon_3=0.0107$, $\nu/\nu_0=\lambda_0/\lambda$ and $\lambda_0=12.60\mu m$

for

$0.5112\mu m < \lambda < 6\mu m$

m_2 is given by the equation

$$m_2 = \frac{10^{-3}}{\pi}\ (\lambda/\mu m) \qquad (3.2.9)$$

For $0.2480\mu m < \lambda < 0.5112\mu m$, m_2 is given by the equation

$$m_2 = \left(\frac{\varepsilon_5}{\lambda}\right)(1-\lambda/\lambda_0)^2 \qquad (3.2.10)$$

where $0.2480 < \lambda < 0.2794$, $\varepsilon_5 = 0.1598\mu m$, and $\lambda_0 = 0.3402\mu m$. When $0.2794 < \lambda < 0.3426$, $\varepsilon_5 = 0.03020\mu m$ and $\lambda_0 = 0.4796$. When $0.3426 < \lambda < 0.5112$, $\varepsilon_5 = 0.016385\mu m$ and $\lambda_0 = 0.5504$. For $\lambda < 0.125\mu m$ the optical constants of silicon carbide are given by the equations

$$m_1 = 1.0 + 1.86(\lambda/\mu m) \qquad (3.2.11)$$

$$m_2 = 14.5(\lambda/\mu m) \qquad (3.2.12)$$

where m_1 for $0.125\mu m < \lambda < 0.5112\mu m$ and m_2 for $0.125\mu m < \lambda < 0.2480\mu m$ are given by linear interpolations of the values of m_1 and m_2 for adjacent value of λ. (see table 3).

The optical constants of corundum were derived as follows. For all wavelengths > 2066.5Å (corresponding to 6eV) values of m_1 and m_2 were derived using a four frequency classical oscillator model. (Barker 1963) The relative permittivity is given by

TABLE 3

OPTICAL CONSTANTS FOR SILICON CARBIDE.

WAVELENGTH/μm	m_1	m_2
0.1250	1.2325	1.8125
0.1305	1.3400	1.8900
0.1380	1.4600	2.0000
0.1440	1.5500	2.2100
0.1510	1.6300	2.5000
0.1550	1.8300	2.7500
0.1675	2.9200	3.1100
0.1910	4.5700	1.5600
0.2070	4.2200	0.5300
0.2250	3.5900	0.1600
0.2480	3.2900	0.0470
0.3100	2.9400	
0.4130	2.7500	
0.5112	2.6150	

$$\varepsilon' - i\varepsilon'' = \varepsilon_0 + \sum_{i=1}^{4} \frac{\Delta_i((1-(\lambda_i/\lambda)^2)-i(\Gamma_i\lambda_i/\lambda))}{(1-(\lambda_i/\lambda)^2)^2+(\Gamma_i\lambda_i/\lambda)^2} \qquad (3.2.13)$$

where $\varepsilon_0 = 3.2$

λ_1=26.0μ	λ_2=22.6μm	λ_3=17.6μm	λ_4=15.7m
Δ_1=0.30	Δ_2=2.7	Δ_3=3.0	Δ_4=0.30
Γ_1=0.015	Γ_2=0.010	Δ_3=0.020	Δ_4=0.020

The relative permittivity and the optical constants are related by

$$\varepsilon' - i\varepsilon'' = (m_1 - im_2)^2 \qquad (3.2.14)$$

$$m_1 = \left(\tfrac{1}{2}\varepsilon' + \tfrac{1}{2}(\varepsilon'^2 + \varepsilon''^2)^{\frac{1}{2}}\right)^{\frac{1}{2}} \qquad (3.2.15)$$

$$m_2 = \left(-\tfrac{1}{2}\varepsilon' + \tfrac{1}{2}(\varepsilon'^2 + \varepsilon''^2)^{\frac{1}{2}}\right)^{\frac{1}{2}} \qquad (3.2.16)$$

From equations (3.2.13) and (3.2.14)

$$\varepsilon' = \varepsilon_0 + \sum_{i=1}^{4} \frac{\Delta_i(1-(\lambda_i/\lambda)^2)}{(1-(\lambda_i/\lambda)^2)^2+(\Gamma_i\lambda_i/\lambda)^2} \qquad (3.2.17)$$

$$\varepsilon'' = \sum_{i=1}^{4} \frac{\Delta_i\Gamma_i\lambda_i/\lambda}{(1-(\lambda_i/\lambda)^2)^2+(\Gamma_i\lambda_i/\lambda)^2} \qquad (3.2.18)$$

The values of m_1 and m_2 are given by equations (3.2.15), (3.2.16), (3.2.17) and (3.2.18). For all wavelengths < 2066.5Å, the optical constants of corundum are given by

$$m_1 = c_1 m_1(\lambda_1) + c_2 m_1(\lambda_2) \qquad (3.2.19)$$

$$m_2 = c_1 m_2(\lambda_1) + c_2 m_2(\lambda_2) \qquad (3.2.20)$$

where

$$c_1 = (\lambda-\lambda_2)/(\lambda_1-\lambda_2) \qquad (3.2.21)$$

and

$$c_2 = (\lambda_1-\lambda)/(\lambda_1-\lambda_2) \qquad (3.2.22)$$

where $\lambda_2 < \lambda < \lambda_1$. The wavelengths λ_1 and λ_2 used and the corresponding optical constants $m_1(\lambda_1)$ and $m_2(\lambda_2)$ were taken from Hagemann et al (1974). For wavelengths between 2066.5Å and 2μm values of m_1 and m_2 are derived from

$$m_1 = m_1(\lambda_1) \tag{3.2.23}$$

$$m_2 = m_2(\lambda_1)(\lambda/\lambda_1)^{c_3} \tag{3.2.24}$$

where

$$c_3 = \frac{\ln(m_2(\lambda_2)/m_2(\lambda_1))}{\ln(\lambda_2/\lambda_1)} \tag{3.2.25}$$

where λ_1 and λ_2 are the longest and second longest wavelengths taken from Hagemann et al. (1974).

For all wavelengths greater than or equal to 2μm, the optical constants of corundum are given by those derived in equations (3.2.15), (3.2.16), (3.2.17) and (3.2.18). For wavelengths between 2066.5Å and 2μm, however, two values of each m_1 and m_2 are derived; those derived in equations (3.2.15), (3.2.16), (3.2.17) and (3.2.18) and those derived in equations (3.2.23), (3.2.24) and (3.2.25). The values of m_1 and m_2 derived from equations (3.2.15), (3.2.16), (3.2.17) and (3.2.18) increase and decrease respectively as the wavelength is decreased. The value of m_1 derived from equation (3.2.23) however, is unchanging with wavelength and the value of m_2 derived from equations (3.2.24) and (3.2.25) increases as the wavelength decreases. Consequently, in the case of m_1, the minimum of the two values is taken to be correct but in the case of m_2, the maximum of the two values is taken. This choice is made for consistency with experimental data.

The ratios of the cross-sections for absorption, scattering and extinction of radiation at a particular wavelength by a grain to the geometrical cross-section of the grain are denoted by Q_{abs}, Q_{sca}, and Q_{ext} respectively. They are also known as the absorption, scattering and extinction efficiencies of a grain. For spherical, homogeneous or core-mantle grains composed of materials of known optical constants, the efficiencies can be computed using the procedures outlined in Wickramasinghe (1972).

The Planck means $\overline{Q}$ of the efficiencies Q are defined in equation (3.2.26).

$$\overline{Q} = \frac{\int_0^\infty B(\nu,T)Q(\nu)d\nu}{\int_0^\infty B(\nu,T)d\nu} \qquad (3.2.26)$$

where the Planck Function $B(\nu,T)$ is defined in equation (3.1.1). The Planck mean efficiencies give the ratios of the cross-sections averaged over the Planck function for absorption, scattering, and extinction, of black-body radiation by a grain, to the geometrical cross-section of the grain.

Grains condensing from carbon rich material are likely to be either homogeneous graphite or graphite-mantle silicon carbide-core grains while grains condensing from oxygen rich material are likely to be either homogeneous silicate or silicate-mantle corundum-core grains.

The mass fractions of silicon and carbon in silicon carbide are 0.7 and 0.3 respectively, while the ratio χ of the mass abundance of carbon to silicon in carbon rich material is assumed to be about 10, about twice the solar carbon to silicon abundance ratio. It is known that the ejecta of type I supernovae are hydrogen deficient and the abundances of the other elements are non-solar (Trimble 1982). Two possible progenitors are hydrogen deficient carbon stars (for instance, the RCB stars) and nova producing binary systems. As novae ejecta are carbon rich (Clayton and Wickramasinghe (1976)) and the carbon abundance in hydrogen deficient carbon stars is

greatly enhanced relative to the abundances of the other elements (Schönberner 1975), it is concluded that the ejecta of type I supernovae have a greater abundance of carbon than oxygen. Also the carbon abundance is likely to be enhanced relative to all the other elements by comparison with solar abundance. As silicon carbide has density $s_1 = 3217 kg\ m^{-3}$ and graphite density $s_2 = 2250 kg\ m^{-3}$, the core radius a_1 and grains radius a_2 of silicon carbide-core graphite-mantle grains will be given by

$$\chi = \frac{(a_2^3 - a_1^3)s_2 + 0.3a_1^3 s_1}{0.7a_1^3 s_1}$$

from which $$a_2/a_1 = (1+0.7s_1\chi/s_2 - 0.3s_1/s_2)^{\frac{1}{3}} \qquad (3.2.27)$$

which is 2.20 if χ is 10. This assumes that all carbon and silicon condenses into grain material. It will be shown in chapter 4 that this is likely to be the case.

The mass fractions of silicon in silicate and aluminium in corundum are 0.1609 and 0.4576 respectively, while the ratio χ of the mass abundance of silicon to aluminium in oxygen rich material is likely to be around the solar abundance ratio of 15.5, as the abundance in the ejecta of type II supernovae are probably solar (Trimble 1982). As corundum has density $s_1 = 3950 kgm^{-3}$ and silicate density $s_2 = 3320 kgm^{-3}$, the core radius a_1 and grain radius a_2 of corundum-core silicate-mantle grains will be given by

$$\chi = \frac{(a_2^3 - a_1^3)(28/174)s_2}{a_1^3 s_1\ (54/118)}$$

for which

$$a_2/a_1 = (1+\chi(54/118)s_1/(28/174)s_2)^{\frac{1}{3}} \qquad (3.2.28)$$

which is 3.77 for χ=15.5 assuming that all silicon and aluminium condenses into grain material (which chapter 4 shows to be likely).

3.3 The Assumptions Made In The Models About The Supernova

The supernova is taken to be situated at a distance D from the observer. The supernova is seen by the observer at time t to have luminosity $L_\star(t)$, radius $R_\star(t)$ and an effective black-body surface temperature $T_e(t)$. The effect of light travel time across the supernova on radiation flux from dust grains is taken to be negligible. The radius of the supernova $R_\star(t) \ll R_1$ or R_c, for all t, that is an effective point source supernova, where R_1 is the cavity radius for the interstellar case and R_c is the radius of the cavity formed around the erupting supernova for the circumstellar case. If this is not so, a grain is heated by supernova radiation emitted not at a single time but at a range of times. This range of emission times, is given by the range of light travel times to the grain, from the parts of the supernova photosphere emitting radiation which contributes to the heating of the grains. This is a source of error in the supernova luminosity and effective temperature used to compute the flux from a grain heated by the supernova. The order of size of the errors in the supernova luminosity and effective temperature are given by the change in the supernova luminosity and effective temperature over this range of times, which is negligible.

The flux per unit frequency interval at frequency ν from the supernova seen by the observer at time t, $L_\nu(t)$ is given by:-

$$L_\nu(t)=\frac{R_\star^2(t)}{D^2} B(\nu,T_e(t))e^{-\tau_\nu^{cs}-\tau_\nu^{is}-A_\nu} \qquad (3.3.1)$$

As the black body radius $R_\star(t)$ of the supernova is given by $(L_\star(t)/4\pi\sigma T_e^4(t))^{\frac{1}{2}}$, substituting equation (3.1.1) into equation (3.3.1) yields

$$L_\nu(t)=\frac{h\nu^3 L_*(t)e^{-\tau_\nu^{cs}-\tau_\nu^{is}-A_\nu}}{2D^2c^2\sigma T_e^4(t)(e^{h\nu/KT_e(t)}-1)} \qquad (3.3.2)$$

where τ_ν^{cs} and τ_ν^{is} are the optical depths from the supernova to the observer along the line of sight of the circumstellar dust shell (cs) and the interstellar (is) dust plane slab respectively at frequency ν, and A_ν is the extinction due to interstellar grains in the Milky Way galaxy.

3.4 The Grain Heating Due To Ambient Starlight.

Before discussing grain heating by the supernova, which is dealt with in the next section, the heating by background starlight is discussed briefly. This is used later on in the thesis (mainly in chapter 5).

The mean flux, F_ν, of the ambient starlight can be represented by a sum of three dilute black-body spectra, where the dilution factors W_j and temperatures are given by Werner and Salpeter (1969).

$$F_\nu=\sum_{j=1}^{3} W_j B(\nu,T_j) \qquad (3.4.1)$$

where $T_1=14500K$, $T_2=7500K$, $T_3=4000K$

and $W_1=4\times10^{-16}$, $W_2=1.5\times10^{-14}$, $W_3=1.5\times10^{-13}$

The rate at which spherical grains of composition i, and radius a_i, absorb ambient starlight radiation is given by

$$H_*=4\pi a_i^2\sigma\sum_j W_j Q_{abs}(j,a_i,T_j)T_j^4 \qquad (3.4.2)$$

From equation (3.4.2) the heating of interstellar grains by backgrounded starlight is evaluated, and subsequently used in chapter 5.

3.5 The Grain Heating By The Supernova

The flux per unit frequency interval at frequency ν emitted from unit area of a grain of temperature T_{gi}, type i, and radius a_i, is given by

$$Q_{abs}(i,a_i,\nu)B(\nu,T_{gi})=2\pi h\nu^3 c^{-2} Q_{abs}(i,a_i,\nu)(\exp(h\nu/kT_{gi})-1)^{-1} \qquad (3.5.1)$$

Let the temperature of a grain, distance r, from the centre of the supernova in thermodynamic equilibrium with radiation observed to be emitted by the supernova at time t after outburst be defined as $T_{gi}(r,t)$. For pre-existing dust, $B_\nu(r,t)$ is the flux per unit frequency interval at frequency ν observed to be emitted from unit area of a black-body temperature T, grain distance r from the centre of the supernova, in thermodynamic equilibrium with radiation seen to be emitted by the supernova at time t after outburst. For condensed dust, $B_\nu(r,t)$ is the same parameter as for pre-existing dust if the dust still has condensed, but is equal to zero if the dust has not condensed.

If $T_{gi}(r,t)$ denotes the temperature of a spherical dust grain radius a_i, type i, at distance r from the supernova in thermodynamic equilibrium with radiation from the supernova seen by the observer at time t, $B_\nu(r,t)$ is given by

$$B_\nu(r,t)=2\pi h\nu^3 c^{-2} H_\nu(r,t) \qquad (3.5.2)$$

and is used in chapters 5, 6 and 7.

Consider a grain, perpendicular distance ρ from the line of sight through the supernova and whose component of the supernova grain distance along the line of sight is x. Infra-red radiation from the grain as a result of heating by the supernova reaches the observer at time t. The corresponding direct radiation from the supernova reaches the observer at time τ where τ and t are related by:-

$$\tau = t-(r-x)/c$$
$$= t-((\rho^2+x^2)^{\frac{1}{2}}-x)/c \qquad \text{as} \quad r=(\rho^2+x^2)^{\frac{1}{2}} \tag{3.5.3}$$

Consequently if the dust grain existed before outburst,

$$H_\nu(r,\tau(\rho,x,t)) = (\exp(h\nu/KT_{gi}(r,\tau(\rho,x,t)))-1)^{-1} \tag{3.5.4}$$

When a circumstellar dust shell condenses around a supernova, the dust flux at any wavelength rises from zero to its maximum value as the dust shell condenses and then decreases monotonically as the supernova luminosity declines. The rise in the dust flux from zero to its maximum value depends on the way in which the circumstellar dust shell condenses. Even though grain condensation is effectively instantaneous, the grains do not necessarily condense in all parts of the circumstellar dust shell at the same time. Grains will obviously not condense at times earlier than the condensation time t_c. Consequently, it is assumed that a grain in any part of the circumstellar dust shell condenses when it is in thermodynamic equilibrium with supernova radiation emitted at time t_c. This is in fact at time $t_c + r/c$ for a grain condensing at distance r from the supernova. The observer first sees radiation from a grain at position r at time t_c so the condensation of the circumstellar dust shell appears to the observer to be described by the paraboloid of revolution $\tau=t_c$. This crosses the inner radius R_c of the circumstellar dust shell behind the supernova as seen from the observer at time $t_c + 2R_c/c$ and the outer edge at time t_c+2R_1/c. The dust flux is certain to decline monotonically after time $t_c + 2R_1/c$ and its maximum value will probably occur between the times $t_c + 2R_c/c$ and $t_c + 2R_1/c$.

For a condensed dust shell the function $H_\nu(r,\tau(\rho,x,t))$ is amended as follows,

$$H_\nu(r,\tau(\rho,x,t))=(\exp(h\nu/KT_{gi}(r,\tau(\rho,x,t)))-1)^{-1} \qquad \text{for } \tau > t_c$$

$$H_\nu(r,\tau(\rho,x,t))=0 \qquad \text{for } \tau < t_c$$

(3.5.5)

In a dusty region, at distance r from the supernova, the optical depth to supernova radiation due to interstellar and/or circumstellar dust at frequency ν, $\tau'_\nu(r)$ is given by

$$\tau'_\nu(r)=N_{os}\pi a_s^2 Q_{abs}(a_s,\nu)(r-R_1)$$

interstellar silicate only

$$=N_{og}\pi a_g^2 Q_{abs}(a_g,\nu)(r-R_1)$$

interstellar graphite only

$$=\pi(r-R_1)(N_{os}a_s^2 Q_{abs}(a_s,\nu)+N_{og}a_g^2 Q_{abs}(a_g,\nu))$$

interstellar case only

$$=N_{oc}\pi a_c^2 Q_{abs}(a_c,\nu)f_\beta(R_c,r)$$

circumstellar case only or circumstellar and interstellar cases. $R_c < r < R_1$

$$=\pi(r-R_1)(N_{os}a_s^2 Q_{abs}(a_s,\nu)+N_{og}a_g^2 Q_{abs}(a_g,\nu))$$
$$+ N_{oc}\pi a_c^2 Q_{abs}(a_c,\nu)f_\beta(R_c,R_1)$$

circumstellar and interstellar cases $r > R_1$

(3.5.6)

where $f_\beta(u,v)=\int_u^v r^{-\beta}dr$ $=v-u$ $\beta=0$

$=\ln(v/u)$ $\beta=1$

$=u^{-1}-v^{-1}$ $\beta=2$ (3.5.7)

The quantities N_{os} and N_{og} are the number densities of interstellar silicate and graphite grains respectively; N_{oc} is the coefficient of the circumstellar grain number density distribution which is described in chapter 6; f_β arises from the circumstellar grain number density distribution

$$N_c = N_{oc}\, r^{-\beta}.$$

The temperature $T_{gi}(r,t)$ of a spherical dust grain radius a_i, type i, at distance r from a supernova, in thermodynamic equilibrium with radiation from the supernova seen by the observer at time t, is given by

$$\begin{aligned} &4\pi a_i^2 \overline{Q_{abs}}(a_i, T_{gi}(r,t))\sigma T_{gi}^4(r,t) \\ &= \pi a_i^2 (R_*^2(t)/r^2) \int_o^\infty Q_{abs}(a_i,\nu) e^{-\tau'_\nu(r)} B(\nu, T_e,(t))d\nu \\ &+ H_* \end{aligned} \tag{3.5.8}$$

where the contribution H_* to grain heating radiation by ambient starlight is given by equation (3.4.2). The quantity $Q_{gi}(r,t)$ is defined by the following equation

$$Q_{gi}(r,t) = \overline{Q_{abs}}(a_i, T_{gi}(r,t)) T_{gi}^4(r,t) \tag{3.5.9}$$

so substituting equations (3.4.2) and (3.5.9) into equation (3.5.8)

$$\begin{aligned} Q_{gi}(r,t) &= (R_*^2(t)/4\sigma r^2) \int_o^\infty Q_{abs}(a_i,\nu) e^{-\tau'_\nu(r)} \\ &B(\nu, T_e(t))d\nu + \sum_{j=1,2,3} W_j Q_{abs}(j, a_i, T_j) T_j^4 \end{aligned} \tag{3.5.10}$$

As the supernova radius for a black-body is given by

$$R_*(t) = \left(L_*(t)/4\pi\sigma T_e^4(t)\right)^{\frac{1}{2}} \tag{3.5.11}$$

substit uting equations (3.1.1), (3.3.2) and (3.5.11) into equation (3.5.10) gives

$$\begin{aligned} Q_{gi}(r,t) = &\frac{h\, L_*(t)}{8\sigma^2 c^2 r^2 T_e^4(t)} \int_o^\infty \frac{\nu^3 Q_{abs}(a_i,\nu) e^{-\tau'_\nu(r)}\, d\nu}{e^{h\nu/KT_e(t)} - 1} \\ &+ \sum_{j=1,2,3} W_j \overline{Q_{abs}}(a_i, T_j) T_j^4 \end{aligned} \tag{3.5.12}$$

$Q_{gi}(r,t)$ is computed for a two-dimens ional array of values (r_p,t_q) where p and q are positive integers, using equation (3.5.12). The integral in equation (3.5.12) is computed using a points integration routine. The quantity $Q_{gi}(r,t)$ is obtained for any distance from the supernova and time t after outburst from the two-dimensional array of values $Q_{gi}(r_p,t_q)$ by interpolation. A power law interpolation is used for r because the grain temperature is likely to vary with r by some kind of power law. If $r_p < r < r_{p+1}$ and $t_q < t < t_{q+1}$ it is assumed that

$$\frac{Q_{gi}(r,t_q)}{Q_{gi}(r,t_q)} = \left(\frac{r}{r_p}\right)^{\chi'} \qquad (3.5.13)$$

and

$$\frac{Q_{gi}(r_{p+1},t_q)}{Q_{gi}(r_p,t_q} = \left(\frac{r_{p+1}}{r_p}\right)^{\chi'} \qquad (3.5.14)$$

From equations (3.5.13) and (3.5.14)

$$\chi' = \frac{\ln(Q_{gi}(r_{p+1},t_q)/Q_{gi}(r_p,t_q))}{\ln(r_{p+1}/r_p)} \qquad (3.5.15)$$

An exponential interpolation is used for t because the supernova luminosity declines exponentially with t, so the grain temperature will do likewise.

Computing

$$Q_{gi}(r,t_q)=Q_{gi}(r_p,t_q)\left(\frac{r}{r_p}\right)^{\frac{[\ln(Q_{gi}(r_{p+1},t_q))-\ln(Q_{gi}(r_p,t_q)]}{\ln(r_{p+1})-\ln(r_p)}} \qquad (3.5.16)$$

for t_q and t_{q+1}, $Q_{gi}(r,t)$ is then given by

$$Q_{gi}(r,t)=Q_{gi}(r,t_q)\exp\frac{(\ln Q_{gi}(r,t_{q+1}))-\ln(Q_{gi}(r,t_q)))(t-t_q)}{t_{q+1}-t_q} \qquad (3.5.17)$$

A power law fit is assumed to derive the grain temperature T_{gi} from Q_{gi} using the following set of grain temperatures $T_{ggi}(j)$ (in Kelvin).

$$\begin{aligned} T_{ggi}(j) &= 10(j+1) && 1 < j < 9 \\ &= 20(j-4) && 10 < j < 29 \\ &= 100(j-24) && 30 < j < 34 \\ &= 300(j-92/3) && 35 < j < 39 \end{aligned} \qquad (3.5.18)$$

Q_{ggi} is related to T_{ggi} by the following equations:-

$$Q_{ggi}(i)=\sigma^{-1}\int_0^\infty Q_{abs}(a_i,\nu)B(\nu,T_{ggi}(i))d\nu. \qquad (3.5.19)$$

If

$$Q_{ggi}(j-1) < Q_{gi}(r,t) < Q_{ggi}(j)$$

so

$$T_{ggi}(j-1) < T_{gi}(r,t) < T_{ggi}(j)$$

it is assumed that

$$\ln Q_{ggi}(j)=\ln Q_{goi}(j)+[\alpha'(j)]^{-1}\ln T_{ggi}(j) \qquad (3.5.20)$$

and

$$\ln Q_{ggi}(j-1)=\ln Q_{goi}(j)+[\alpha'(j)]^{-1}\ln T_{ggi}(j-1) \qquad (3.5.21)$$

From equations (3.5.20) and (3.5.21) the following expressions for the constants Q_{goi} and α' are derived:-

$$Q_{goi}(i)=\exp\left(\frac{\ln T_{ggi}(i)\ln Q_{ggi}(i-1)-\ln T_{ggi}(i-1)\ln Q_{ggi}(i)}{\ln(T_{ggi}(i)/T_{ggi}(i-1))}\right)$$

for $2 < i < 40$ (3.5.22)

$$\alpha'(i)=\frac{\ln(T_{ggi}(i)/T_{ggi}(i-1))}{\ln(Q_{ggi}(i)/Q_{ggi}(i-1))} \qquad (3.5.23)$$

for $2 < i < 40$

$Q_{goi}(1)$ and $\alpha'(1)$ are put equal to $Q_{goi}(2)$ and $\alpha'(2)$ respectively. Using the power law fit, for $Q_{ggi}(j-1) < Q_{gi}(r,t) < Q_{ggi}(j)$, the grain temperature $T_{gi}(r,t)$ corresponding to $Q_{gi}(r,t)$ is given by

$$T_{gi}(r,t)=(Q_{gi}(r,t)/Q_{goi}(j)) \qquad (3.5.24)$$

If $Q_{gi}(r,t) > Q_{ggi}(40)$, $T_{gi}(r,t) > 2800K$ (i.e. $T_{ggi}(40)$), and such grains are unphysical as they will have vapourized at such temperatures, so the model parameters must be altered. The integrals in equation (3.5.19) are computed using a points integration routine with a set of values of frequency ν. The set of values of ν used for graphite or silicate grains comprise a chosen set of 77 values corresponding to wavelengths greater than 1μm and the 97 values listed in table 2 corresponding to wavelengths less than or equal to 1μm. For graphite m_1 and m_2 are given for these 97 values alongside those values in table 2 and for the other 77 values by equations (3.2.1) and (3.2.2). For silicate, m_1 and m_2 are given for all the 174 frequencies by the formula in table 1. The 174 frequencies are chosen to accurately describe the variations with frequency of Q_{abs} for both silicate and graphite grains from the far ultra-violet to the far infra-red. For homogeneous silicon carbide and graphite silicon carbide core-mantle grains the 77 wavelengths > 1μm were replaced by a different set of 86 wavelengths selected to give adequate coverage of the desired range. For homogeneous corundum, and silicate corundum core-mantle grains, the 77 wavelengths > 1μm were replaced by a different set of 121 wavelengths, chosen to give the desired range of wavelengths. For each of the three sets of wavelengths, the desirabilty of a large number of wavelengths for accurate computation was constrained by the need to minimise computing times, and the intervals between consecutive wavelengths were made smallest around wavelengths where Q_{abs} for either of the grain types used varies most rapidly with wavelength.

In summary, to compute the temperature $T_{gi}(r,t)$ of a grain of type i

at distance r from the supernova in thermodynamic equilibrium with supernova radiation emitted at time t, firstly $Q_{gi}(r,t)$ is computed by interpolating the set of values $Q_{gi}(r_p,t_q)$ using equations (3.5.13) to (3.5.17) inclusive, then $T_{gi}(r,t)$ is derived from $Q_{gi}(r,t)$ using the interpolation described by equation (3.5.24). The set of values $Q_{gi}(r_p,t_q)$ is computed using equation (3.5.12). This method is used to compute the grain temperatures and so determine the radiation flux emitted by dust grains in chapters 5, 6 and 7.

CHAPTER 4

THE EVAPORATION AND CONDENSATION OF GRAINS

4.0 Introduction

A supernova at outburst evaporates any circumstellar or interstellar dust grains forming a cavity free of dust. A supernova also immediately evaporates any grains condensing so close to it that their temperatures are greater than their evaporation temperatures. In order to determine the sizes of the cavity around the supernova for a circumstellar dust shell or for interstellar grains, it is necessary to determine the evaporation temperatures of the grains. It is also necessary to determine the effect that the forces (due to the supernova radiation pressure, the gravitational pull of the supernova, and the viscous drag of the ejecta) acting on the grains have on the cavity radius. If the radiation pressure is sufficiently large the cavity will expand with time. Finally, it is necessary to determine the time taken for grains to condense. If the condensation times are greater than one day the grain radius must be taken to be a function of time in the model to compute the radiation flux from dust heated by a supernova.

4.1 Evaporation Of Grains

From Draine and Salpeter (1979), the grain temperature T_{gsb} required to sublime N_L layers of monomers from a grain in a time t is given by

$$T_{gsb} = U_o \, (K \, \ln(\nu t / N_L))^{-1} \qquad (4.1.1)$$

where ν is a molecular vibration frequency and is $\sim 10^{12}$ s^{-1}; U_o is the binding energy per molecule of material and $N_L \sim 10^2$ for the grain to evaporate. Consequently, the evaporation temperature T_{evap} for a grain at constant temperature for a time t (that is, the time required to sublime 100 monolayers) is given by

$$T_{evap}(t) = \frac{5040\ U_o\ (ev)}{10 + \log_{10} t(s)} \qquad (4.1.2)$$

Evaporation temperatures and U_o values for graphite, silicate, silicon carbide, and corundum are listed in table 4. The U_o values for silicate and graphite are values typically in the range of those given by Barlow (1978) and Draine and Salpeter (1979). The U_o value for silicon carbide is taken from Barlow (1979), and the U_o value for corundum is taken from Goldsmith et al (1961).

Interstellar and circumstellar grains existing before the supernova outburst will be evaporated after outburst out to a certain distance from the supernova. As supernovae are characterized by a peak luminosity at outburst, followed by a decline with an e-folding time of tens of days, most of the grain evaporation is likely to occur in the first day after outburst.

Consequently, as the evaporation temperature after 10 days is not much lower than that after one day (see table 4) and the temperature of the grain at a given distance from the supernova falls with time because the supernova becomes less luminous, it is unlikely that the cavity will continue to expand (as grains at increasing distance from the supernova evaporate), for more than a few days after outburst. The final cavity size and the time at which it is reached are computed for a particular grain size and composition by studying the variation with time t after outburst of the smallest distance from the supernova, $R_c'(t)$, at which such a grain can exist

TABLE 4

GRAIN EVAPORATION TEMPERATURES (K) AFTER TIME, t (secs)

$\log_{10} t$	Graphite	Silicate	Silicon Carbide	Corundum
5	2470	1915	2621	2218
6	2315	1796	2457	2079
7	2179	1690	2312	1957
8	2058	1596	2184	1848
9	1950	1512	2069	1751
10	1852	1436	1966	1663
11	1764	1368	1872	1584
12	1684	1306	1787	1512
13	1611	1249	1709	1446
U_0(ev)	7.35	5.7	7.8	6.6

$$R_c'(t) = \left(\frac{L_*(t)\overline{Q_{abs}}(i,a_i,T_e(t))}{16\pi\sigma\overline{Q_{abs}}(i,a_i,T_{evap}(t))T_{evap}^4(t)} \right)^{\frac{1}{2}} \qquad (4.1.3)$$

Equation (4.1.3) is derived from putting $T_{evap}(t)$ (computed from (4.1.2)) as the grain temperature in equation (3.5.8) with the optical depth due to circumstellar dust $\tau_\nu'(r) = 0$ and $H_* = 0$ (i.e. no background starlight). The parameters $L_*(t)$ and $T_e(t)$ are the supernova luminosity and effective temperature respectively at time t after outburst and the grains are spherical, of radius a_i, and composition i. The maximum value of $R_c'(t)$ considering evaporation only, gives the greatest distance from the centre of the supernova at which such grains evaporate, (other forces on the grains are considered below). This distance is taken to be the cavity radius R_c for such grains at all times after outburst in the dust models used to compute the flux received from such grains at any given time after outburst. The values of $R_c'(t)$ one day after outburst, the values of R_c and the times t after outburst at which $R_c'(t)$ reaches R_c have been computed for spherical, homogeneous grains of graphite around type I and type II supernovae and of silicate around type II supernovae. The grains are of radii ranging from 0.01μm to 0.25μm. Computations were also carried out for silican carbide-core graphite-mantle grains around type I supernovae and for corundum-core silicate-mantle grains around type II supernovae, as well as for the silicon carbide or corundum cores of these grains without their mantles. The radii of the core-mantle grains investigated were the same as those for the graphite and silicate grains, with the mantle:core ratio of 3.77 deduced in chapter 3. The results listed in table 5 show (by comparing R_c' with R_c) that for all the four grain types around type II supernovae the final cavity radius is approached sufficiently rapidly that its attainment can be regarded as instantaneous at outburst. However, for all the three grain types around type I supernovae, the expansion of the cavity in the first 20 days has to be taken into account in flux computations (using equation (3.5.5) with the cavity radius computed as a function of time).

TABLE 5

The cavity created by evaporation of pre-existing dust grains of radius a(μm) around a supernova; R_c' is the cavity radius one day after outburst; R_c is the final cavity radius due to evaporation; t is the time in days after the supernova outburst at which the final cavity radius due to evaporation is reached; the cavity radii R_c^{50} and R_c^{300} are the cavity radii values at 50 days and 300 days respectively after outburst, the cavity having expanded due to the forces acting on the grains. R_c', R_c, R_c^{50} and R_c^{300} are all written in units of 10^{13} m.

(i) GRAPHITE GRAINS AROUND A TYPE I SUPERNOVA

a (μm)	R_c' (m)	R_c (m)	t (Days)	R_c^{50} (m)	R_c^{300} (m)
0.010	6.847	26.70	20	34.44	73.46
0.015	6.986	27.29	20	35.47	75.97
0.020	7.077	27.74	20	36.66	79.18
0.025	7.055	27.81	20	37.68	82.26
0.030	6.917	27.46	20	38.27	84.42
0.035	6.725	26.90	20	38.50	85.59
0.040	6.524	26.27	20	38.51	86.14
0.050	6.112	24.89	20	38.14	86.04
0.060	5.661	23.26	20	37.38	84.71
0.070	5.201	21.49	20	36.32	82.49
0.080	4.782	19.82	20	35.11	79.88
0.100	4.105	17.00	20	32.66	74.47
0.125	3.531	14.52	20	29.96	68.40
0.150	3.170	12.93	20	27.80	63.48
0.200	2.786	11.20	20	24.72	56.41
0.250	2.617	10.42	20	22.68	51.68

(ii) SILICON CARBIDE GRAINS AROUND A TYPE I SUPERNOVA

a (μm)	R_c' (m)	R_c (m)	t (Days)	R_c^{50} (m)	R_c^{300} (m)
0.005	34.20	103.1	16	103.1	103.3
0.007	36.04	108.8	16	108.8	109.0
0.009	38.38	116.1	16	116.2	116.4
0.011	41.06	124.8	16	124.8	125.1
0.014	43.95	134.3	16	134.4	134.7
0.016	46.98	144.6	16	144.6	145.0
0.018	50.00	155.0	16	155.1	155.4
0.023	55.42	174.2	16	174.3	174.8
0.027	57.44	182.6	16	182.6	183.2
0.032	58.18	186.9	16	186.9	187.7
0.036	54.91	177.6	16	177.7	178.7
0.045	48.66	159.4	16	159.6	161.1
0.057	43.82	147.3	16	147.6	149.7
0.068	42.41	147.8	16	148.1	150.7
0.091	33.20	113.7	16	114.1	117.4
0.114	27.21	93.27	16	93.65	97.44

(iii) GRAPHITE-MANTLE SILICON-CARBIDE CORE GRAINS AROUND A TYPE I SUPERNOVA

a (μm)	R_c' (m)	R_c (m)	t (Days)	R_c^{50} (m)	R_c^{300} (m)
0.010	6.624	25.70	20	33.09	70.51
0.015	6.736	26.17	20	33.94	72.59
0.020	6.810	26.54	20	34.96	75.37
0.025	6.800	26.65	20	35.99	78.44
0.030	6.697	26.42	20	36.79	81.06
0.035	6.537	25.98	20	37.25	82.79
0.040	6.362	25.46	20	37.44	83.72
0.050	6.006	24.31	20	34.80	84.06
0.060	5.611	22.90	20	36.71	83.13
0.070	5.193	21.33	20	35.87	81.40
0.080	4.804	19.80	20	34.87	79.28
0.100	4.160	17.15	20	32.77	74.67
0.125	3.595	14.75	20	30.31	69.19
0.150	3.233	13.17	20	28.25	64.55
0.200	2.837	11.41	20	25.08	57.35
0.250	2.654	10.58	20	22.78	52.09

(iv) GRAPHITE GRAINS AROUND A TYPE II SUPERNOVA

a (μm)	R_c' (m)	R_c (m)	t (Days)	R_c^{50} (m)	R_c^{300} (m)
0.010	65.71	66.92	2.0	78.47	140.9
0.015	62.02	64.23	3.0	77.34	143.7
0.020	58.82	61.84	4.0	76.56	146.7
0.025	55.04	58.63	4.5	75.23	149.0
0.030	50.92	54.77	5.0	73.28	149.8
0.035	47.00	50.98	6.0	71.08	149.3
0.040	43.61	47.65	7.0	69.00	148.2
0.050	38.13	42.33	8.0	65.51	145.7
0.060	33.66	37.85	9.0	62.63	142.8
0.070	29.91	33.92	10.0	59.96	139.4
0.080	26.90	30.66	11.0	57.51	135.6
0.100	22.52	25.73	13.0	53.38	128.0
0.125	19.11	21.70	14.0	49.29	119.1
0.150	17.05	19.21	16.0	46.16	111.6
0.200	14.98	16.58	17.0	41.67	99.97
0.250	14.13	15.44	11.0	38.59	91.73

(v) SILICATE GRAINS AROUND A TYPE II SUPERNOVA

a (μm)	R_c' (m)	R_c (m)	t (Days)	R_c^{50} (m)	R_c^{300} (m)
0.010	634.5	634.5	1.0	634.5	634.7
0.015	613.4	613.4	1.0	613.5	613.7
0.020	584.6	585.9	1.5	585.9	586.2
0.025	555.6	558.0	1.5	558.0	558.3
0.030	525.6	528.8	1.5	528.8	529.2
0.035	495.7	499.3	1.5	499.3	499.7
0.040	469.7	473.6	1.5	473.7	474.1
0.050	423.7	428.4	2.0	428.5	429.0
0.060	387.9	393.4	2.0	393.4	394.0
0.070	356.7	362.4	2.0	362.5	363.1
0.080	331.2	337.2	2.0	337.3	338.0
0.100	290.0	296.4	2.5	296.5	297.4
0.125	250.8	257.6	2.5	257.7	258.8
0.150	220.8	227.6	2.5	227.8	229.1
0.200	176.2	183.0	3.0	183.2	185.0
0.250	146.8	153.3	3.5	153.5	155.9

(vi) CORUNDUM GRAINS AROUND TYPE II SUPERNOVAE

a (μm)	R_c (m)	t (Days)	R_c^{50} (m)	R_c^{300} (m)
0.0027	1330	0.5	1330	1330
0.0040	1339	0.5	1339	1339
0.0053	1345	0.5	1345	1345
0.0066	1347	0.5	1347	1347
0.0080	1343	0.5	1343	1343
0.0093	1334	0.5	1334	1334
0.0106	1319	0.5	1319	1319
0.0133	1280	0.5	1280	1280
0.0159	1234	0.5	1234	1234
0.0186	1188	0.5	1188	1188
0.0212	1143	0.5	1143	1143
0.0265	1042	0.5	1042	1042
0.0332	937.2	0.5	937.2	937.3
0.0398	857.5	0.5	857.5	857.6
0.0531	736.8	0.5	736.8	736.9
0.0663	652.0	0.5	652.0	655.2

(vii) SILICATE-MANTLE CORUNDUM-CORE GRAINS AROUND A TYPE II SUPERNOVA

a (μm)	R_c' (m)	R_c (m)	t (Days)	R_c^{50} (m)	R_c^{300} (m)
0.010	638.3	638.3	1.0	638.3	638.5
0.015	616.9	616.9	1.0	616.9	617.1
0.020	587.7	588.8	1.5	588.8	589.1
0.025	558.3	560.6	1.5	560.6	560.9
0.030	528.2	531.2	1.5	531.3	531.6
0.035	498.1	501.6	1.5	501.7	502.0
0.040	472.0	475.9	1.5	476.0	476.3
0.050	425.9	430.9	2.0	430.5	431.0
0.060	395.1	389.8	2.0	395.1	395.7
0.070	358.3	363.9	2.0	363.9	364.6
0.080	332.8	338.6	2.0	338.7	339.4
0.100	291.4	297.7	2.5	297.8	298.7
0.125	252.2	258.8	2.5	258.9	260.0
0.150	222.0	228.7	2.5	228.9	230.2
0.200	177.2	183.9	3.0	184.1	185.8
0.250	147.6	154.1	3.5	154.3	156.5

4.2 Forces Acting On Grains

The acceleration of a spherical grain, of radius a_i, velocity v, composition i, density s_i and Planck mean of radiation pressure efficiency $\overline{Q_{pr}}$ is considered. It is supposed that the grain is heated by a supernova of mass M_*, black-body radius R_*, luminosity L_*, and effective temperature T_e, from the centre of which the grain is at distance r. For a grain situated in a gas at temperature T, density ρ_g and atomic mass m, the forces on the grain due to the gravitational attraction of the supernova and the pressure of the supernova radiation are given by equations (4.2.1) and (4.2.3) respectively:

$$G_r = 4\pi a_i^3 s_i M_* G/3r^2 \qquad (4.2.1)$$

$$P_r = \pi a_i^2 \overline{Q_{pr}}(i,a_i,T_e)(R_*^2/r^2)\ (\sigma/c)T_e^4 \qquad (4.2.2)$$

so from (3.5.10) and (4.2.2)

$$P_r = \frac{a_i^2 \overline{Q_{pr}}(i,a_i,T_e)L_*}{4cr^2} \qquad (4.2.3)$$

The drag by the gas is given by equation (4.2.4)

$$D_r = 3a_i^2 v\rho_g\ (\pi KT/m)^{\frac{1}{2}} \qquad (4.2.4)$$

as the viscosity of the gas is given by equation (4.2.5)

$$\eta = a\rho_g\ (KT/\pi m)^{\frac{1}{2}} \qquad (4.2.5)$$

and

$$D_r = 6\pi\eta a_i v \qquad (4.2.6)$$

where v is the velocity of the grain relative to the gas. When the analysis was carried out initially, it was found that the velocity attained by graphite grains was of the order of c, and therefore it was necessary to include a relativistic correction in the equations. If the grain's rest mass is m_g,

$$m_g = \frac{4}{3}\pi a_i^3 s_i \qquad (4.2.7)$$

the grain's mass at velocity v is given by

$$m_g' = m_g (1-v^2/c^2)^{-\frac{1}{2}} \qquad (4.2.8)$$

from which

$$dm_g'/dt = (m_g v/c^2)(1-v^2/c^2)^{-\frac{3}{2}} dv/dt \qquad (4.2.9)$$

so the force on a grain, from equations (4.2.8) and (4.2.9) is given by

$$\frac{d}{dt}(m_g' v) = \frac{v dm_g'}{dt} + m_g' \frac{dv}{dt}$$

$$= m_g (1-v^2/c^2)^{-\frac{3}{2}} dv/dt \qquad (4.2.10)$$

Assuming the grain has zero velocity at time t=0

$$v(t) = \int_0^t \dot{v}(t)dt \qquad (4.2.11)$$

where the grain acceleration V(t) is given by, referring to equation (4.2.10)

$$v(t) = \frac{(P_r - G_r - D_r)\ (1-v^2/c^2)^{\frac{3}{2}}}{m_g} \qquad (4.2.12)$$

As the gas around grains around type II supernovae is mainly hydrogen, $\rho_g = mn_H$ where m is the mass of a hydrogen atom (1.67×10^{-27} kg) and n_H is the number density of hydrogen atoms. There is no hydrogen in the ejecta of type I supernovae (see chapter 2) and probably none in the gas around grains around them either so that the gas is probably mainly helium. Consequently, for the grains around type I supernovae, $\rho_g = mn_H$ where m is the mass of a helium atom (7.0×10^{-27} kg) and n_H is the number density of helium atoms. From substituting (4.2.1), (4.2.3), (4.2.4) and (4.2.7) in (4.2.12)

$$v(t) = (1-v^2/c^2)^{\frac{3}{2}}\ \frac{3\overline{Q_{pr}}\ (i,a_i,T_e)L_*(t)}{16\pi a_i s_i c r^2(t)}\ \frac{-M_* G}{r^2}\ \frac{-9vn_H\ (\pi mKT)^{\frac{1}{2}}}{4\pi a_i^2 s_i} \qquad (4.2.13)$$

For a grain of initial distance from the supernova r(0), as $v = \dot{r} > 0$, v(t), v(t) and r(t) can be computed as a function of time t after outburst, with the boundary conditions r(t=0)=r(0), v(t=0)=0.

By computing the distances r(t), for different grain types corresponding to a set of initial distances r(0) from the supernova greater than or equal to the final radius of the cavity created by grain evaporation, the cavity radius at time t, is determined. This is done by taking the minimum of all the distances r(t). The expansion of the cavity due to the forces on the grains is investigated for the same three sets of grains around type I supernovae and for the same four sets of grains around type II supernovae for which the evaporation of the cavity is investigated. The cavity radii after 50 days and after 300 days are given in table 5.

For the four types of grains around type II supernovae the ambient gas is assumed to be hydrogen with number density 10^7 m^{-3} and temperature of 100K. This will be realistic for interstellar graphite and silicate grains around type II supernovae. It will also give a lower limit to the viscosity of the gas for the silicate, corundum and silicate and silicate-corundum pre-existing circumstellar grains around type II supernovae (for which the grain and gas atom number densities are likely to be much higher). For circumstellar, corundum grains and silicate-mantle corundum-core grains and for circumstellar and interstellar silicate grains around type II supernovae, it can be seen that there is essentially no expansion of the cavity due to the forces on the grains. The expansion of the cavity of interstellar graphite grains around type II supernovae is significant and will be discussed in the chapter on the results of the interstellar flux computations (chapter 5).

The number density of the atoms in the gas surrounding the pre-existing circumstellar grains around type I supernovae is assumed to be 10^9 m^{-3}. As the cosmic helium:carbon mass abundance ratio is $10^{1.93}$ (Allen 1973) a helium gas density of 10^9 m^{-3} (or 7×10^{-18} kg m^{-3}) implies a carbon density of $\sim 8 \times 10^{-20}$ kg m^{-3}. If all of this were condensed into graphite grains, a circumstellar dust shell of typical cavity radius and thickness, both of 10^{14} m would have a mass of order $10^{-6} M_\odot$. It will be seen in chapter 6 that circumstellar dust shells around supernovae are at least an order of magnitude more massive than this. Consequently, this gas density (10^9 m^{-3}) gives a lower limit to the effect of the viscosity of the gas on the grains. The gas temperature is taken to be 100K.

There is no significant expansion of the cavity due to forces on the grains for silicon carbide grains around type I supernovae. For the graphite and the core-mantle grains around type I supernovae however, the forces on the grains cause significant expansion of the cavity and this effect should be taken into account for these grain types.

Sputtering of pre-existing circumstellar or interstellar grains is not considered to have any effect on the flux emitted by the grains. In the four out of the seven cases in which there is no expansion of the cavity after its initial evaporation, the minimum cavity radius is about 10^{15} m. With a velocity of 10^{7} ms^{-1}, the supernova shock front will take 3 years to reach the edge of the cavity and by that time the grains at the cavity edge will be cold and emitting negligible amounts of radiation. In the other three cases, the initial cavity radius due to evaporation is much smaller, but the cavity expands due to the forces on the grains. The smallest cavity radius due to evaporation is about 10^{14} m, which the shock front at 10^{7} ms^{-1} would reach in about 120 days. After 50 days however, this cavity has already expanded to 2.3×10^{14} m in radius and after 300 days, when the shock front will have covered 3×10^{14}m, the cavity radius has expanded to about 5.2×10^{14}m. A much higher gas density may brake the expansion of the cavity sufficiently to enable the shock front to reach the grains, but certainly not before 120 days after outburst and the grains at the cavity edges will no longer make such an important contribution to the dust flux at long times after outburst. Consequently, it is concluded that sputtering of pre-existing circumstellar or interstellar dust does not effect their radiation fluxes.

4.3 Condensation Of Grains

If the case of a condensing circumstellar dust shell around a supernova is to be considered, it is necessary to determine the time taken for the grains to condense. It is assumed, contrary to the assumption made in Clayton and Wickramasinghe (1976), that almost all of the grain forming material in the gas in which the grains form, condenses. This is justified by the observation that silicon, magnesium and iron are 90% to 100% depleted in interstellar gas (Whittet 1981). It is concluded that these

elements must be in interstellar silicate grains and a large fraction if not most of these grains probably condensed in supernova ejecta (Whittet 1981). It is shown in this section that if depletion is assumed to be important the grain condensation is in all realistic cases instantaneous.

Contrary to the assumption made in Clayton and Wickramasinghe (1976) the gas temperature is assumed to be constant rather than varying as the square root of the time after outburst, but this makes no essential difference to the argument. Its only effect is to slow down the rate of grain growth slightly from that which would be predicted by Clayton and Wickramasinghe because the rate of grain growth falls less rapidly with time (as t^{-2} rather than as $t^{-9/4}$).

The importance or otherwise of depletion of grain material from the ambient gas in grain condensation depends essentially on the number density of nucleation centres. In Clayton and Wickramasinghe (1976), the formation of nucleation centres is assumed to begin at the same time as condensation, and their final number density is assumed to be too low for depletion to be important. In this thesis, the number density of nucleation centres is assumed to be sufficient for depletion to be important. Furthermore, there is no reason why grain growth should begin concurrently with the formation of nucleation centres. In practice, the nucleation centres on which the grains condense must form before the beginning of condensation because the latter is found to be effectively instantaneous. Therefore no grains will condense on any nucleation centres forming after the beginning of grain condensation.

The condensation of grains is considered on nucleation centres of radius a_1 in a gas around a supernova, the ejecta of which are expanding with velocity V_{ej}. At a distance r_0 from the supernova condensation is assumed to begin at a time $t = 0$. For the condensed material at distance r_0 from the supernova the grain radius, total grain monomer number density in both grain and vapour states, and the number density of uncondensed grain

monomers at time t after the beginning of condensation, are denoted by $a(t)$, $n(t)$, and $n_v(t)$ respectively. Denoting the grain or nucleation centre number density at the beginning of condensation ($t = 0$) by N_{co},

$$n(t) = n(0)\left(\frac{r_o}{r_o + V_{ej}t}\right)^{\beta} \qquad \beta = 0 \text{ or } 2 \tag{4.3.1}$$

where,

$$n(0) = \frac{4\pi}{3} s_i/m \ (a_\infty^3 - a_1^3) N_{co} \tag{4.3.2}$$

(N.B. In this section $t = 0$ is the condensation time rather than the time of eruption). Equation (4.3.1) represents the time variation for the total monomer number density due to expansion.

Also

$$n_v(t) = n(t)\left(\frac{a_\infty^3 - a^3(t)}{a_\infty^3 - a_1^3}\right) \tag{4.3.3}$$

Equation (4.3.3) represents the time variation of the monomer number density in the gas due to expansion and depletion. In equation (4.3.2) s_i is the grain material density, m is the mass of the grain monomers and a_∞ is the grain radius when all of the grain monomers have condensed. From equations (4.3.1) and (4.3.2)

$$n(t) = \frac{4\pi s_i \ (a_\infty^3 - a_1^3) N_{co}}{3m \ (1 + (V_{ej}/r_o)t)^{\beta}} \tag{4.3.4}$$

Denoting the number of monomers in a single grain at time t by $n_m(t)$

$$n_m(t) = \frac{4\pi}{3} (s_i/m) (a^3(t) - a_1^3) \qquad (4.3.5)$$

Differentiating equation (4.3.5) with respect to t

$$\frac{dn_m(t)}{dt} = \frac{4\pi s_i a^2(t)}{m} \frac{da}{dt} \qquad (4.3.6)$$

But, from kinetic theory

$$\frac{dn_m(t)}{dt} = 4\pi a^2(t) \alpha n_v(t) \left(\frac{KT}{2\pi m}\right)^{\frac{1}{2}} \qquad (4.3.7)$$

where α in equation (4.2.7) is the probability that an uncondensed grain monomer will stick to a grain on colliding with it, and T is the temperature of the gas. Consequently from equations (4.3.3) and (4.3.7)

$$\frac{dn_m(t)}{dt} = \frac{4\pi\alpha (KT)^{\frac{1}{2}}}{(2\pi m)^{\frac{1}{2}}} a^2(t) n(t) \frac{a_\infty^3 - a^3(t)}{a_\infty^3 - a_1^3} \qquad (4.3.8)$$

from equations (4.3.6) and (4.3.8)

$$\frac{da}{dt} = \frac{\alpha}{s_i} \left(\frac{MKT}{2\pi}\right)^{\frac{1}{2}} n(t) \frac{a_\infty^3 - a^3(t)}{a_\infty^3 - a_1^3} \qquad (4.3.9)$$

This equation reduces to equation (10) in Clayton and Wickramasinghe (1976) if the depletion factor is removed from equation (4.3.9), i.e. if the term

$$\frac{a_\infty^3 - a^3(t)}{a_\infty^3 - a_1^3}$$ is removed.

From equations (4.3.4) and (4.3.9)

$$\frac{da}{dt} = \frac{2\alpha N_{CO}}{3}\left(\frac{2\pi KT}{m}\right)^{\frac{1}{2}} \frac{(a_\infty^3 - a^3(t))}{(1 + (V_{ej}/r_o)t)^\beta} \qquad \beta = 0,2 \qquad (4.3.10)$$

Integrating equation (4.2.10) as $a(0) = a_1$

$$\int_{a_1}^{a(t)} \frac{da}{(a_\infty^3 - a^3(t'))} = \frac{2\alpha N_{CO}}{3}\left(\frac{2\pi KT}{m}\right)^{\frac{1}{2}} I_\beta(t) \qquad (4.3.11)$$

where

$$I_\beta(t) = \int_0^t \frac{dt'}{(1 + (V_{ej}/r_o)t')^\beta}$$

$$= t \qquad \text{for } \beta=0$$

$$= \frac{t}{(1 + (V_{ej}/r_o)t} \qquad \text{for } \beta=2 \qquad (4.3.12)$$

Putting

$$x = a/a_\infty$$

$$x_T(t) = a(t)/a_\infty$$

$$\int_{a_1}^{a(t)} \frac{da}{(a_\infty^3 - a^3)} = a_\infty^{-2} \int_{x_1}^{x_T(t)} \frac{dx}{1 - x^3}$$

$$= \frac{1}{6a_\infty^2} \ln\left[\left(\frac{1 + x_T + x_T^2}{(1 - x_T)^2}\right) + 2\sqrt{3}\tan^{-1}\left(\frac{2x_T + 1}{\sqrt{3}}\right)\right]_{x_1}^{x}$$

(4.3.13)

It is convenient to define

$$J(x_T) = \ln(1 + x_T + x_T^2) - 2\ln(1 - x_T) + 2\sqrt{3} \tan^{-1}\left(\frac{2x_T + 1}{\sqrt{3}}\right) \tag{4.3.14}$$

From equations (4.3.11) (4.3.13) (4.3.14)

$$I_\beta(t) = \frac{1}{4\alpha N_{co} a_\infty^2}\left(\frac{m}{2\pi KT}\right)^{\frac{1}{2}} (J(x_T(t)) - J(x_1))$$

$$= \frac{1.20158 \times 10^8 \; m^{\frac{1}{2}} \; (J(x_T(t)) - J(x_1))}{(a_\infty/\mu m)^2 \; \alpha \; N_{co} \; r_o (T/1000K)^{\frac{1}{2}}} \tag{4.3.15}$$

where m is in units of the mass of one atom of ^{12}C because m is 12 atomic mass units for graphite and 25.49 atomic mass units for silicate, (the average mass of each atom in the material).

It should be noted that the question of growth of grains from polyatomic components (e.g. corundum or silicate) is not entirely understood. Preliminary work on this has been attempted by Donn (1978).

If the condensing circumstellar dust shell has total grain material mass M_g, inner radius R_c and outer radius R_1,

$$M_g = \frac{16\pi}{3}^2 (a_\infty^3 - a_1^3) s_i \int_{R_c}^{R_1} N_{co}\left(\frac{r}{ro}\right)^{-\beta} r^2 \, dr$$

$$= \frac{16\pi^2 a_\infty^3 s_i \; N_{co} r_o^\beta (1 - x_1^3)}{3}\left(\frac{R_1^{\,3-\beta} - R_c^{\,3-\beta}}{3 - \beta}\right) \tag{4.3.16}$$

From equation (4.3.16)

$$N_{co} = \frac{3(3 - \beta) \; M_g \; r_o^{-\beta}}{16\pi^2 \; a_\infty^3 \; s_i (1 - x_1^3) \; (R_1^{\,3-\beta} - R_c^{\,3-\beta})}$$

$$= \frac{3.78 \times 10^{46} \, (3 - \beta) \, (M_g/M_o) \, r_o^{-\beta}}{(a_\infty/\mu m)^3 \, s_i (1 - x_1^3)(R_1^{\,3-\beta} - R_c^{\,3-\beta})} \qquad (4.3.17)$$

From equation (4.3.15)

$$J(x(t)) = J(x_1) + \frac{\alpha \, N_{co} \, r_o \, (T/1000K)^{\frac{1}{2}} \, (a_\infty/\mu m)^2 \, I_\beta \, (t)}{1.20158 \, m^{\frac{1}{2}} \times 10^8} \qquad (4.3.18)$$

where N_{co} is obtained from (4.3.17). Equations (4.3.12) (4.3.14) and (4.3.18) enable the computation of the function $J(x_T)$ as a function of time t.

For an array of values of x_T, x_j, an array of values of $J(x_T)$, $J(x_j)$ is computed. The value of x_T corresponding to J(x) is then derived from linear interpolation of $J(x_j)$ and $J(x_{j+1})$ where $x_j < a/a_\infty < x_{j+1}$. The value of T is taken to be 1000K and the value of α is taken to be 0.2.

The time t_c' taken for silicate grains to condense from x = 0 (i.e. a = 0) to x = 0.99 has been computed for various values of N_{co} and r_o and the results are listed in table 6.

For β = 0 or 2 there is little difference in time for the same grain number density because the condensation times are too short for any significant reduction in the gas density to occur through expansion. Variations of the gas temperature T, the sticking probability α and the grain material will not change the order of magnitude of t_c. It can therefore be concluded that the condensation of grains and so of a circumstellar dust shell is essentially instantaneous in every realistic case. The condensation time is maximized by putting a_1 = 0 (as assumed here); assuming a_1 to be non zero would result in even shorter condensation times.

TABLE 6

Condensation times t_c of silicate dust grains of final radius a_∞ at distance from the supernova $r_o(m)$ where the grain number density is $N_{co}(m^{-3})$.

a_∞ (μm)	r_o (m)	N_{co} (m^{-3})	t_c (secs)	t_c (Days)
0.020	3×10^{13}	10^{-7}	8.828×10^{6}	1.022×10^{2}
0.020	3×10^{15}	10^{-7}	8.828×10^{4}	1.022×10^{0}
0.020	3×10^{13}	10^{-5}	8.828×10^{4}	1.022×10^{0}
0.020	3×10^{15}	10^{-5}	8.828×10^{2}	1.022×10^{-2}
0.020	3×10^{13}	10^{-3}	8.828×10^{2}	1.022×10^{-2}
0.020	3×10^{15}	10^{-3}	8.828×10^{0}	1.022×10^{-4}
0.020	3×10^{13}	10^{-1}	8.828×10^{0}	1.022×10^{-4}
0.020	3×10^{15}	10^{-1}	8.828×10^{-2}	1.022×10^{-6}
0.020	3×10^{13}	10^{+1}	8.828×10^{-2}	1.022×10^{-6}
0.020	3×10^{15}	10^{+1}	8.828×10^{-4}	1.022×10^{-8}
0.200	3×10^{13}	10^{-7}	8.828×10^{4}	1.022×10^{0}
0.200	3×10^{15}	10^{-7}	8.828×10^{2}	1.022×10^{-2}
0.200	3×10^{13}	10^{-5}	8.828×10^{2}	1.022×10^{-2}
0.200	3×10^{15}	10^{-5}	8.828×10^{0}	1.022×10^{-4}
0.200	3×10^{13}	10^{-3}	8.828×10^{0}	1.022×10^{-4}
0.200	3×10^{15}	10^{-3}	8.828×10^{-2}	1.022×10^{-6}
0.200	3×10^{13}	10^{-1}	8.828×10^{-2}	1.022×10^{-6}
0.200	3×10^{15}	10^{-1}	8.828×10^{-4}	1.022×10^{-8}
0.200	3×10^{13}	10^{+1}	8.828×10^{-4}	1.022×10^{-8}
0.200	3×10^{15}	10^{+1}	3.531×10^{-6}	1.022×10^{-10}

TABLE 6 (cont).

1.000	3×10^{13}	10^{-7}	3.531×10^{3}	4.087×10^{-2}
1.000	3×10^{15}	10^{-7}	3.531×10^{0}	4.087×10^{-2}
1.000	3×10^{13}	10^{-5}	3.531×10^{0}	4.087×10^{-4}
1.000	3×10^{15}	10^{-5}	3.531×10^{-1}	4.087×10^{-6}
1.000	3×10^{13}	10^{-3}	3.531×10^{-1}	4.087×10^{-6}
1.000	3×10^{15}	10^{-3}	3.531×10^{-3}	4.087×10^{-8}
1.000	3×10^{13}	10^{-1}	3.531×10^{-3}	4.087×10^{-8}
1.000	3×10^{15}	10^{-1}	3.531×10^{-5}	4.087×10^{-10}
1.000	3×10^{13}	10^{+1}	3.531×10^{-5}	4.087×10^{-10}
1.000	3×10^{15}	10^{+1}	3.531×10^{-7}	4.087×10^{-12}

4.4 CONCLUSION

At outburst the cavity of dust grains around the supernova is determined by the evaporation of the grains, as described by equation (4.1.2) from Draine and Salpeter (1979). For some grain types, the forces on the grains subsequently cause the cavity to expand.

In contrast to the formation of grains around novae (described in Clayton and Wickramasinghe (1976)), depletion of grain forming material from the surrounding gas is discovered to be important for supernovae. As a result, it is concluded that the condensation of grains in supernova ejecta is essentially instantaneous.

The results of this chapter are used in Chapters 5, 6 and 7.

CHAPTER FIVE

THE COMPUTATION OF THE RADIATION FLUX FROM INTERSTELLAR DUST GRAINS.

5.0 Introduction

In this chapter the heating of interstellar grains by supernova radiation is considered. It is assumed that there are two types of interstellar grains in a galaxy, graphite and silicate, and that all interstellar grains are spherical and homogeneous. The fractions by mass of graphite and silicate grains in the galaxy are denoted by Fg and Fs respectively; therefore Fg + Fs = 1. The fractions by grain number are denoted by fg and fs; therefore fg + fs = 1. All graphite grains are assumed to have the same radius a_g and all silicate grains the same radius a_s.

The interstellar grains are assumed to form a plane parallel slab, with a uniform (constant number density) distribution of both graphite and silicate grains. The number density of graphite grains is denoted by N_{og}, and the number density of silicate grains by N_{os}. The total grain number density is denoted by N_o ($N_o = N_{og} + N_{os}$). It is assumed that there are no grains outside the dust plane slab, (that is, outside the dust plane of the galaxy). The total mass density of grain material inside the infinite plane slab is denoted by d_{is} and

$$d_{is} = \frac{4\pi}{3} (a_s^3 s_s N_{as} + a_g^3 s_g N_{og}) \qquad (5.0.1)$$

where the density of graphite material s_g = 2250 kg m^{-3} and the density of silicate material s_s = 3320 kg m^{-3}.

Also, $N_{os} = 3f_o\, d_{is}/4\pi a_s^3\, s_s$ (5.0.2)

$N_{og} = 3f_g\, d_{is}/4\pi a_g^3\, s_g$ (5.0.3)

and $f_s = N_{os}/N_o$ (5.0.4)

$f_g = N_{og}/N_o$ (5.0.5)

All grains in the dust plane slab are assumed to have a constant radius and to always be in thermodynamic equilibrium with radiation from the supernova, that is, the grains are neither evaporating nor condensing. The cavity free of interstellar grains evaporated by the supernova in the galaxian dust plane is assumed to be spherical and centred on the supernova. (It is assumed that there are no grains inside the cavity). It is assumed that the dust plane slab is sufficiently optically thin to grain heating radiation from the supernova, and to infra-red radiation from the grains that grain heating by radiation emitted by other grains is negligible compared to grain heating by radiation emitted by the supernova. As the interstellar extinction at V in our Galaxy is about 1.9 magnitudes per kiloparsec in the vicinity of the sun (Allen 1973), this is a reasonable assumption because the galaxic dust plane is only hundreds of parsecs thick. The optical depth in the infra-red along one parsec of the interstellar dust plane is given by:

$$\text{optical depth/pc} = 1.587 \times 10^{-3} \times Q_{abs}\ \text{(graphite)} + 0.586 \times 10^{-3} \times Q_{abs}\ \text{(silicate)}$$

As the supernova is 100pc into the dust plane, path lengths of grain heating radiation will be of order 100pc. The optical depth at any wavelength is $\lesssim 0.2$. (See figure 20).

However the number density of grains is taken to be sufficient to ensure that the amount of radiation in any given frequency interval scattered out of a light path through the galaxian plane by grains is equal to the amount of radiation in the same frequency interval scattered into the same light path by grains, so the net extinction of radiation along a light path through the dust plane slab is the extinction due to absorption

by grains only.

If it is assumed that the interstellar medium consists of grains of a number of types, i, of identical spherical homogeneous grains, radius a_i, material density s_i, fraction by mass density of grain material F_i, fraction by number density, f_i total number density N_o, and total mass density d_{is}, putting

$$M_i = F_i\, d_{is} \text{ and } N_{oi} = f_i\, N_o$$

where M_i is the mass density of grain material of type i, and N_{oi} is the number density of grains of type i. Hence,

$$f_i = \frac{N_{oi}}{N_o} = \frac{M_i/\frac{4}{3}\pi a_i^3 s_i}{\sum_i M_i/\frac{4}{3}\pi a_i^3 s_i} = \frac{F_i/a_i^3 s_i}{\sum_i F_i/a_i^3 s_i} \qquad (5.0.6)$$

Consequently, the extinction in magnitudes, at frequency ν, due to absorption, scattering or extinction by interstellar grains is given by

$$\frac{A_\nu^{ext}}{E_{(B-V)}} = \frac{\sum_i N_{oi}\pi a_i^2 Q_{ext}(i,a_i,\nu)}{\sum_i N_{oi}\pi a_i^2 (Q_{ext}(i,a_i,B)-Q_{ext}(i,a_i,V))}$$

$$= \frac{\sum_i f_i a_i^2 Q_{ext}(i,a_i,\nu)}{\sum_i f_i a_i^2 (Q_{ext}(i,a_i,B)-Q_{ext}(i,a_i,V))} \qquad (5.0.7)$$

Two grain types are assumed silicate (i=s) and graphite (i=g), the total grain mass density is assumed to be 1.8×10^{-23} kg m^{-3} (Whittet 1981) and the fractions by mass of silicate and graphite grain material are assumed to be 0.7 and 0.3 respectively (Whittet 1981). The quantity $A_\nu^{ext}/E_{(B-V)}$ was plotted for various combinations of silicate and graphite grain radii and the plots compared with the three average interstellar grain extinction ($A_\nu^{ext} - A_\nu^{ext}/E_{(B-V)}$) curves (two of which are very similar and so appear as one in figures 6 to 10 inclusive) in Savage and Mathis (1979). It can be seen from figures 6 to 10 inclusive that a reasonably good resemblance to the interstellar extinction curve was given by 0.15μm silicate grains and

FIGURE 6. The variation of interstellar extinction with frequency for 0.035μm graphite grains and 0.100μm silicate grains compared with the observed interstellar extinction curves (broken lines).

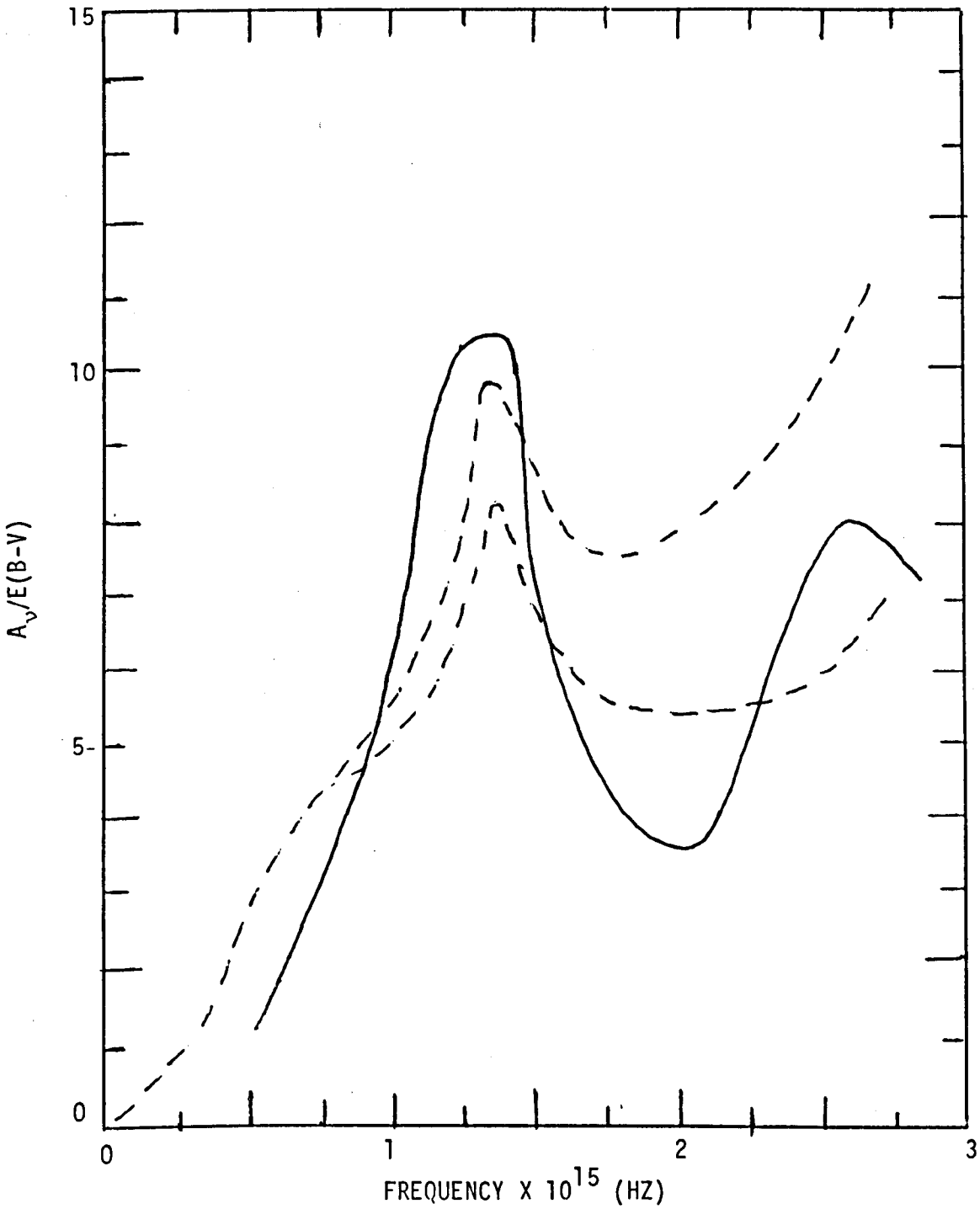
15
10
5
0
0
1
2
3
$A_v/E(B-V)$
FREQUENCY X 10^{15} (HZ)

FIGURE 7. The variation of interstellar extinction with frequency for 0.035μm graphite grains and 0.125μm silicate grains compared with the observed interstellar extinction curves (broken lines).

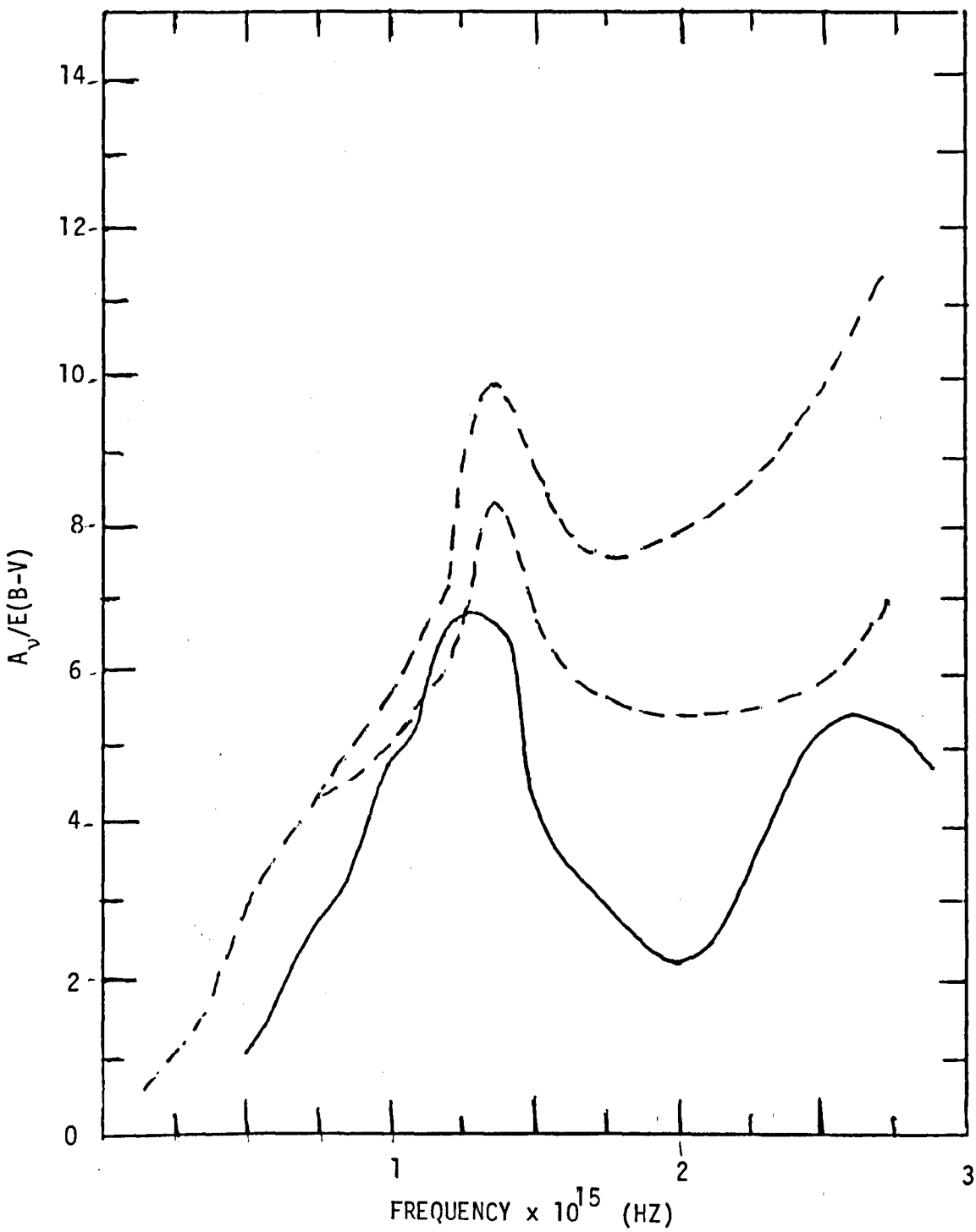
14
12
10
8
6
4
2
0
$A_v/E(B-V)$
1
2
3
FREQUENCY x 10^{15} (HZ)

FIGURE 8. The variation of interstellar extinction with frequency for 0.04μm graphite grains and 0.100μm silicate grains compared with the observed interstellar extinction curves (broken lines).

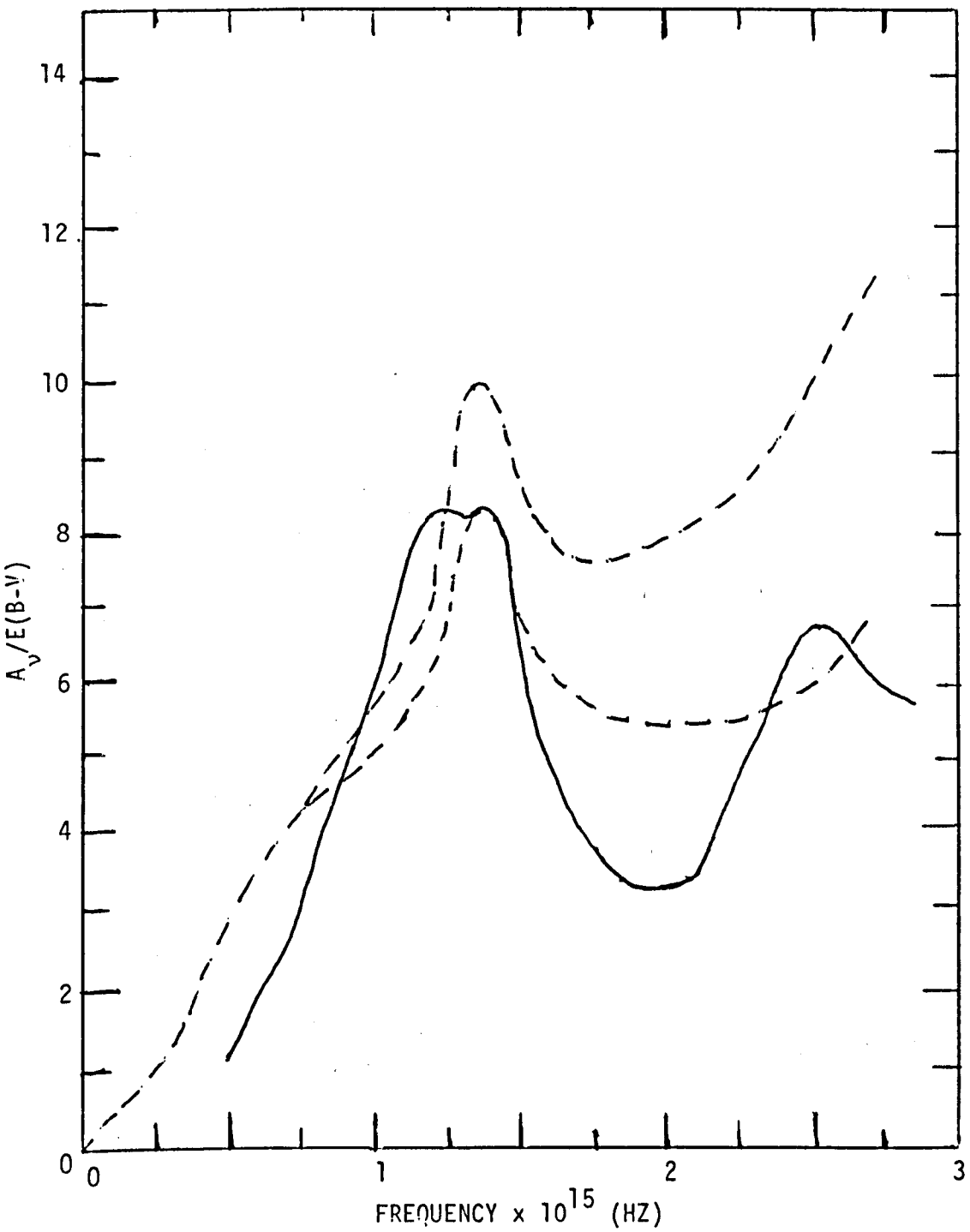
14
12
10
8
6
4
2
0
0
1
2
3
$A_v/E(B-V)$
FREQUENCY x 10^{15} (HZ)

FIGURE 9. The variation of interstellar extinction with frequency for 0.04μm graphite grains and 0.150μm silicate grains compared with the observed interstellar extinction curves (broken lines).

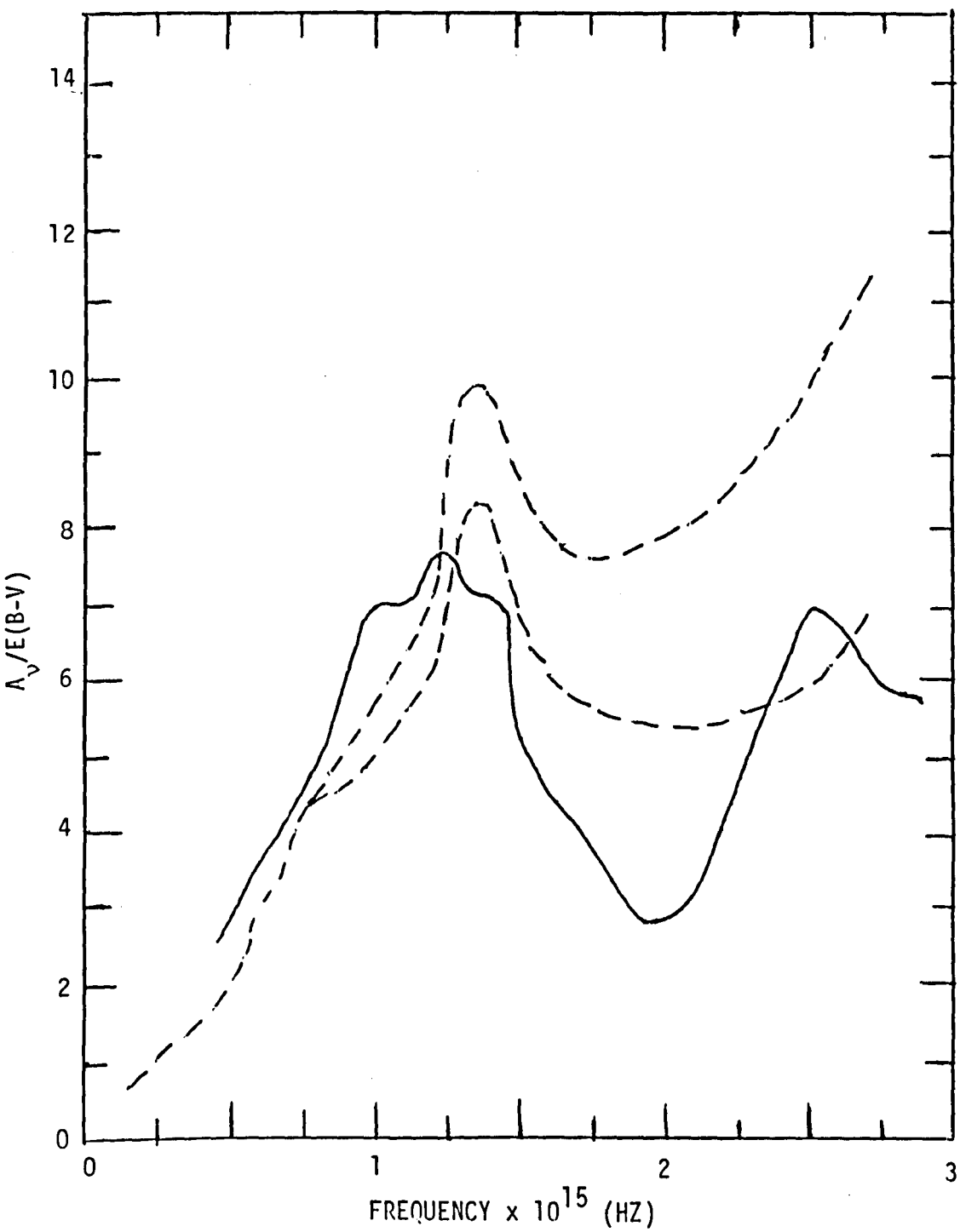
14
12
10
8
6
4
2
0
$A_v/E(B-V)$
0
1
2
3
FREQUENCY x 10^{15} (HZ)

FIGURE 10. The variation of interstellar extinction with frequency for 0.04μm graphite grains and 0.125μm silicate grains compared with the observed interstellar extinction curves (broken lines).

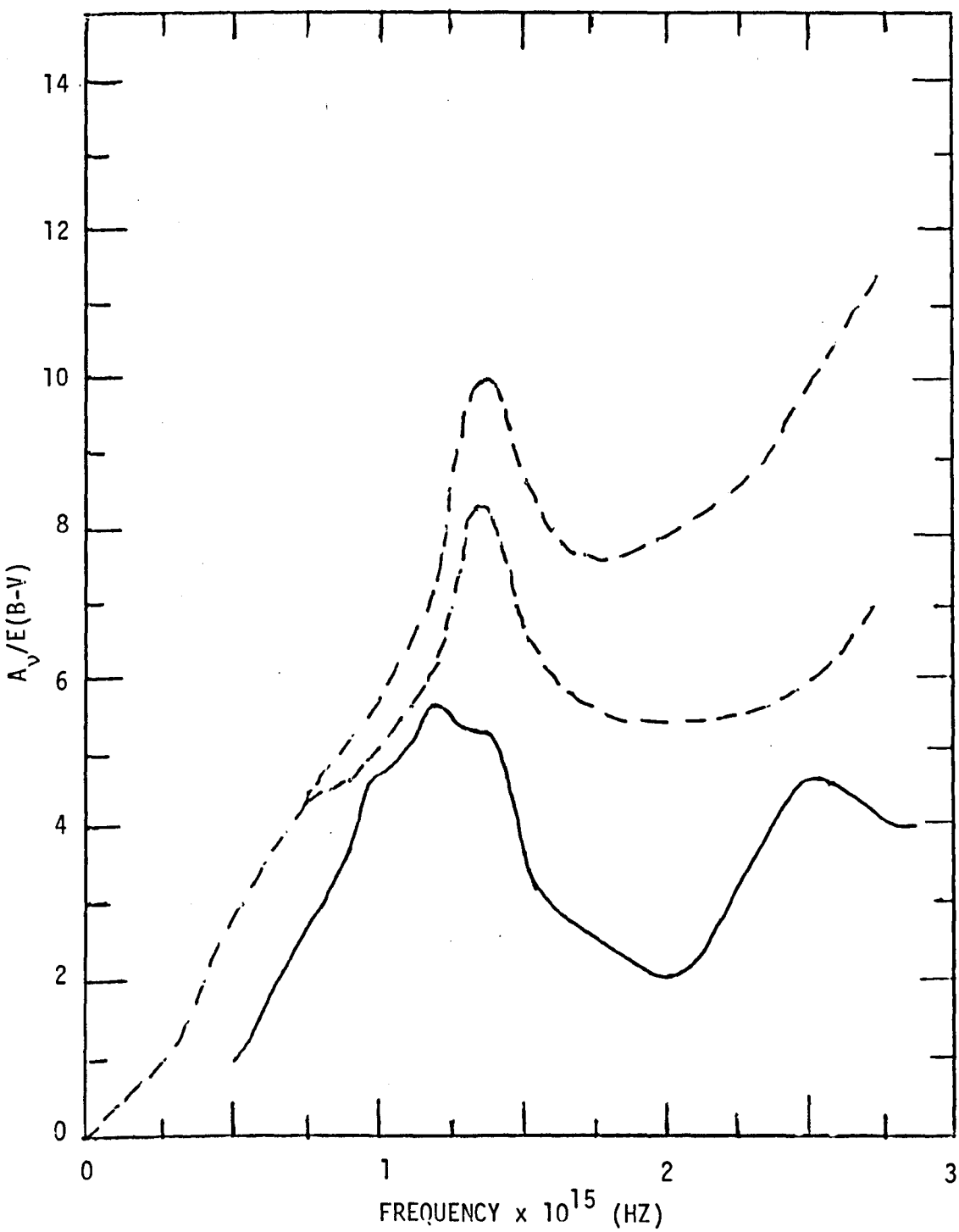
14
12
10
8
6
4
2
0
$A_v/E(B-V)$
0
1
2
3
FREQUENCY x 10^{15} (HZ)

0.035μm graphite grains so these grain radii were assumed for the interstellar grains used in the model.

The optical constants for the silicate and graphite are detailed in section 3.2.

5.1 The interstellar dust grain model

The interstellar dust plane model is illustrated in figure 11. The thickness of the plane parallel slab is denoted by Θ; the perpendicular distance of the supernova from the front of the plane by R; the radius of the spherical cavity of grains around the supernova by R_1, and the angle of inclination, of the plane parallel slab, forming the edge of the dust plane parallel slab, to the line of sight, by I. The coordinate system for the interstellar dust grain model is illustrated in figure 11, in which ρ is the perpendicular distance to any grain from the line of sight through the supernova, x is any distance parallel to the x-axis from the plane x=0. The supernova is situated at the origin of a cartesian system of coordinates with the x-axis towards the observer. The parameter $\underline{r}$ (also given by [x, y, z]) is the radius vector from the supernova to any grain. The perpendicular vector from the supernova to the front plane of the interstellar dust plane slab is represented by $\underline{R}$. As r and R are the distances corresponding to the vectors $\underline{r}$ and $\underline{R}$ respectively.

$$r = (\rho^2 = x^2)^{\frac{1}{2}} \qquad (5.1.1)$$

while $$y = -\rho \cos \gamma \qquad (5.1.2)$$

and $$z = -\rho \sin \gamma \qquad (5.1.3)$$

where γ is the angle measured clock-wise from the negative y direction in the plane perpendicular to the line of sight. From the standard equation of a plane, the front plane of the plane parallel dust slab is described by

$$\underline{r}.\underline{R} = R^2 \qquad (5.1.4)$$

FIGURE 11. The coordinate system for the interstellar case.

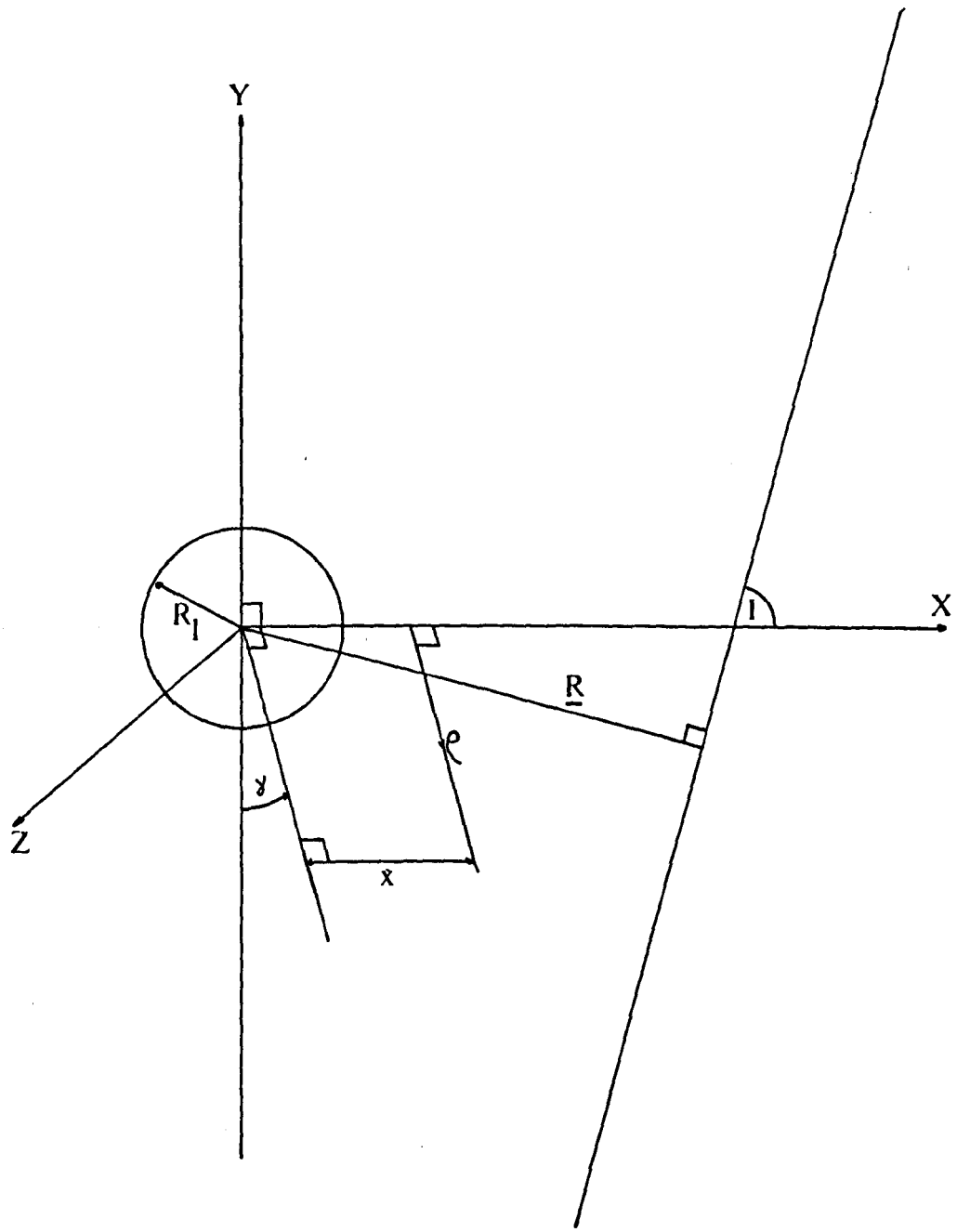
Y
X
Z
R_1
R
ρ
γ
x
l

so as the vector $\underline{R}$ is given by [Rsin I, -RcosI, 0], equation (5.1.4) yields

$$x = (R - \rho\cos\gamma\cos I)/\sin I \qquad (5.1.5)$$

Equation (5.1.5) gives the value of x as a function of ρ and γ at any point on the front plane (M in figure 12). At the edge of the cavity

$$x = \pm(R_1^2 - \rho^2)^{\frac{1}{2}} \qquad (5.1.6)$$

where the + and - signs refer to points F and B on figure 12 respectively. The parameters x(B) and x(F) are the negative and positive solutions of x as given by equation (5.1.6) and are illustrated in figure 12. At a point (U in figure 12) on the back plane of the plane parallel slab the following equation applies

$$x = (R - \Theta - \rho\cos\gamma\cos I)/\sin I \qquad (5.1.7)$$

As the supernova erupts at time t=0, and has essentially zero luminosity at all times $t < 0$, the region seen to be illuminated by supernova radiation at time t is within a paraboloid of revolution the edge of which is defined by

$$\tau(\rho, x)=0 \qquad (5.1.8)$$

where τ, the emission time of supernova radiation with which an observed grain is in thermodynamic equilibrium, is defined by equation (3.5.3) in section (3.5). From equations (3.5.3) and (5.1.8) on the edge of the paraboloid of revolution (point P in figure 13), the value of x is given by

$$x = (\rho^2 - c^2 t^2)/2ct \qquad (5.1.9)$$

It is useful to define the following equation:

$$N_{gs\nu} = N_{os}a_s^2 Q_{abs}(a_s,\nu) + N_{og}a_g^2 Q_{abs}(a_g,\nu) \qquad (5.1.10)$$

FIGURE 12. The interstellar dust plane slab.

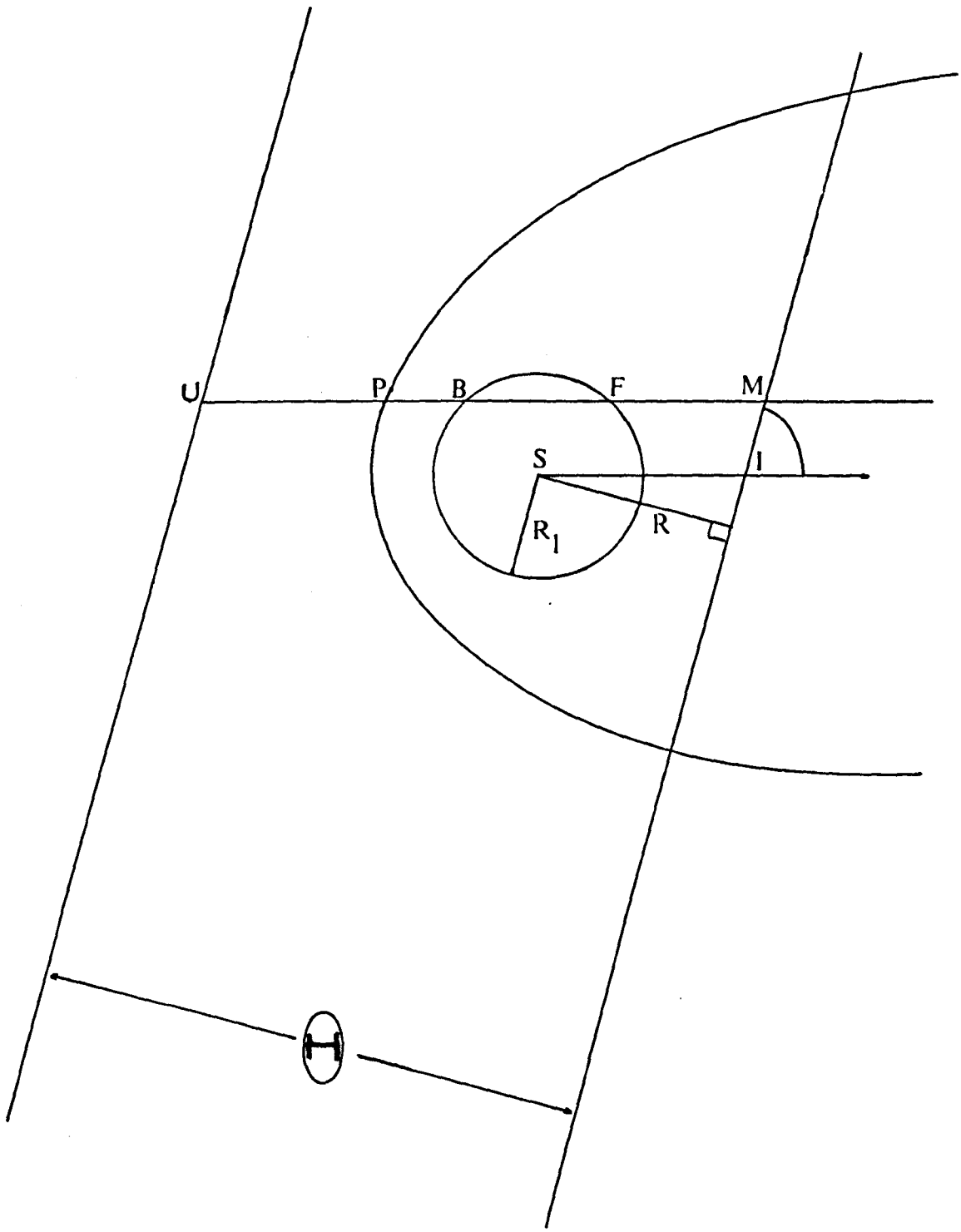
U
P
B
F
M
S
I
R
R_1

FIGURE 13. The circle of re-emission seen by the observer on the plane of the sky.

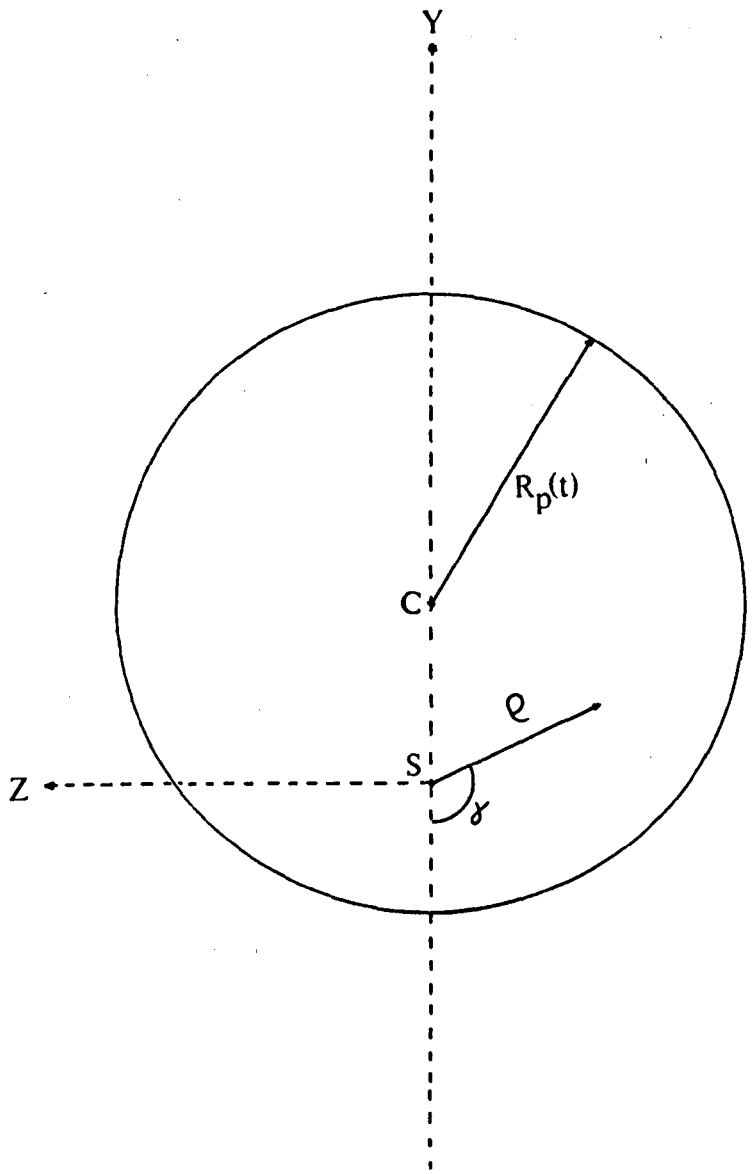
Y
$R_p(t)$
C
ϱ
S
Z
γ

The optical depth, at the observed frequency ν, to supernova radiation due to absorption by interstellar grains is given by

$$\tau_\nu^{is} = \pi N_{gs\nu} \ (R\,\mathrm{cosec}I - R_1) \qquad (5.1.11)$$

$\pi N_{gs\nu}$ is the extinction per unit length of radiation of frequency, ν in the interstellar dust plane parallel slab. The optical depth, τ_ν^{ic} at frequency ν from the nearside of the interstellar grain cavity to the nearside plane is given by

$$\tau_\nu^{ic}(\rho,\gamma) = N_{gs\nu}((R-\rho\cos\gamma\cos I)/\sin I-(R_1^2-\rho^2)^{\frac{1}{2}}) \qquad (5.1.12)$$

In figures 11 and 12 it can be seen that a line-of-sight is defined by the coordinates (ρ,γ). The values of coordinate x at points U,P,B,F, and M, are denoted by x(U), x(P), x(B), x(F) and x(M) respectively.

The perpendicular distance from the line of sight through the supernova to the line of sight through the point where the parabola intersects the front plane at angle γ is denoted by $\rho_c(\gamma)$, where $\rho_c(\gamma)$ is derived from equation (5.1.13), that is,

$$x(P) = x(M) \qquad (5.1.13)$$

From equations (5.1.5), (5.1.9) and (5.1.13)

$$\rho_c^2(\gamma)+2ct\rho_c(\gamma)\cos\gamma\cot I-(c^2t^2+2ctR\,\mathrm{cosec}I)=0 \qquad (5.1.14)$$

from which

$$\rho_c=-ct\cos\gamma\cot I+(c^2t^2\cos^2\gamma\cot^2 I+c^2t^2+2ctR\,\mathrm{cosec}I)^{\frac{1}{2}} \qquad (5.1.15)$$

from equations (5.1.2) (5.1.3) and (5.1.14)

$$(y-ctcotI)^2+z^2=cosec^2 I(2ctRsinI+c^2t^2) \qquad (5.1.16)$$

Equation (5.1.16) describes a circle of radius $R_p(t)$ given by figure 13

$$R_p(t) = cosecI\ (c^2t^2+2ctRsinI)^{\frac{1}{2}} \qquad (5.1.17)$$

From equation (5.1.16) it can be seen that $\rho = \rho_c(\gamma)$ forms a circle of radius $R_p(t)$ from the centre of which the line of sight through the supernova is displaced by distance ctcot(I) towards the γ=0 direction. (This is illustrated in figure 13).

The perpendicular distance from the line of sight through the supernova to the line of sight through a point where the parabola intersects the cavity is denoted by ρ_{cty} and ρ_{cty}, is derived from equation (5.1.18)

$$x^2(P) = R_1^2 - \rho_{cty}^2$$

$$x(P) \text{ can equal } + (R_1^2-\rho_{cty}^2)^{\frac{1}{2}} \text{ or } - (R_1^2-\rho_{cty}^2)^{\frac{1}{2}} \qquad (5.1.18)$$

depending on where the parabola crosses the cavity.

From equations (5.1.9) and (5.1.17)

$$\rho_{cty} = (2ctR_1-c^2t^2)^{\frac{1}{2}} \qquad \text{for } 0<ct<2R_1$$

$$= 0 \qquad \text{for } ct>2R_1 \qquad (5.1.19)$$

The equations derived in section (5.1), which describe the geometry of the interstellar dust grain model, are used in the computation of the radiation flux from interstellar dust grains, the method for which is described in section 5.2.

FIGURE 14. Intersection of the paraboloid with the cavity; case 1, $0<ct<R_1$.

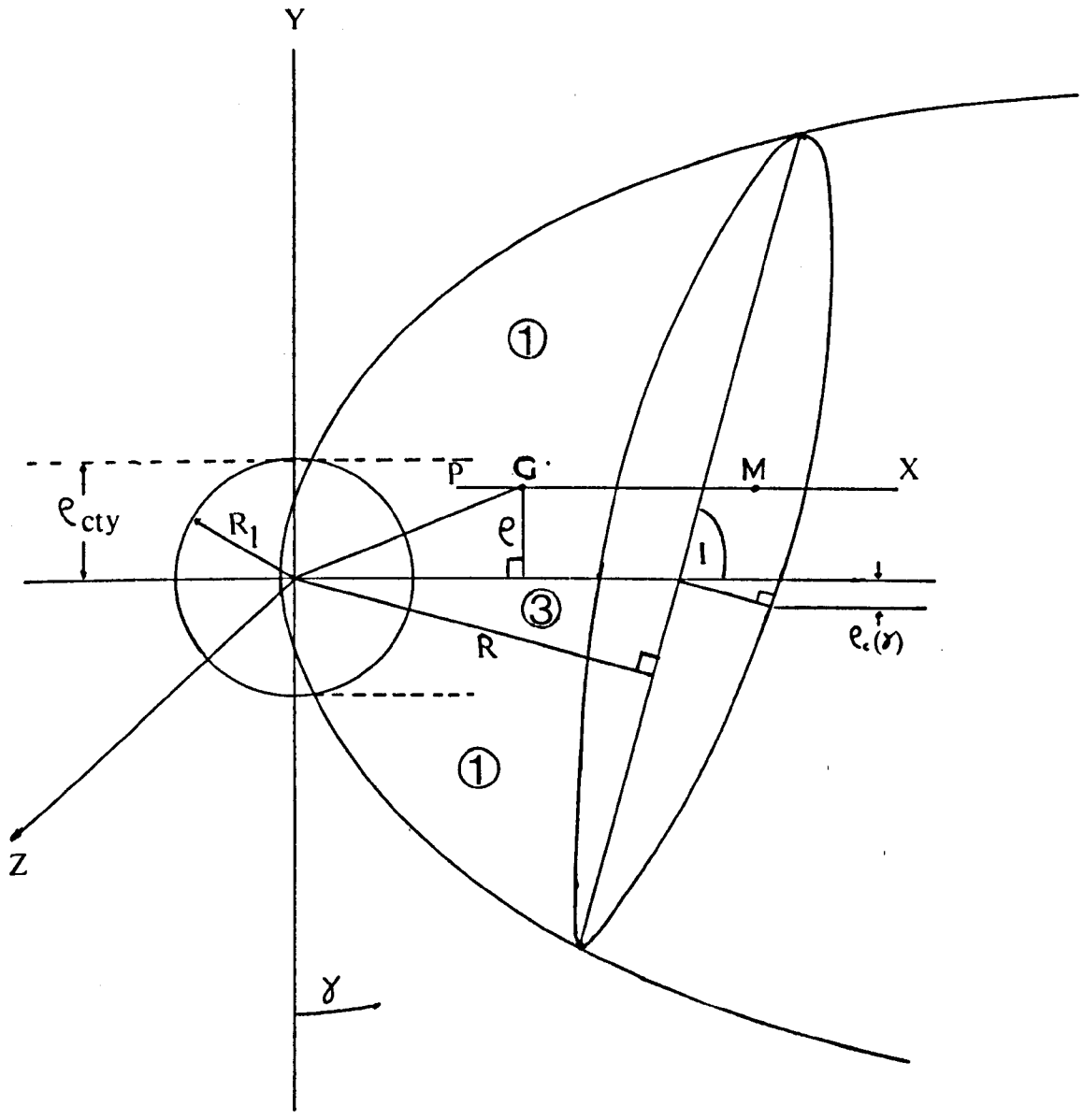
Y
①
P
G
M
X
ρ_{cty}
R_1
ρ
I
③
R
$\rho_c(\gamma)$
①
Z
γ

FIGURE 15. Intersection of the paraboloid with the cavity; case 2, $R_1 < ct < 2R_1$.

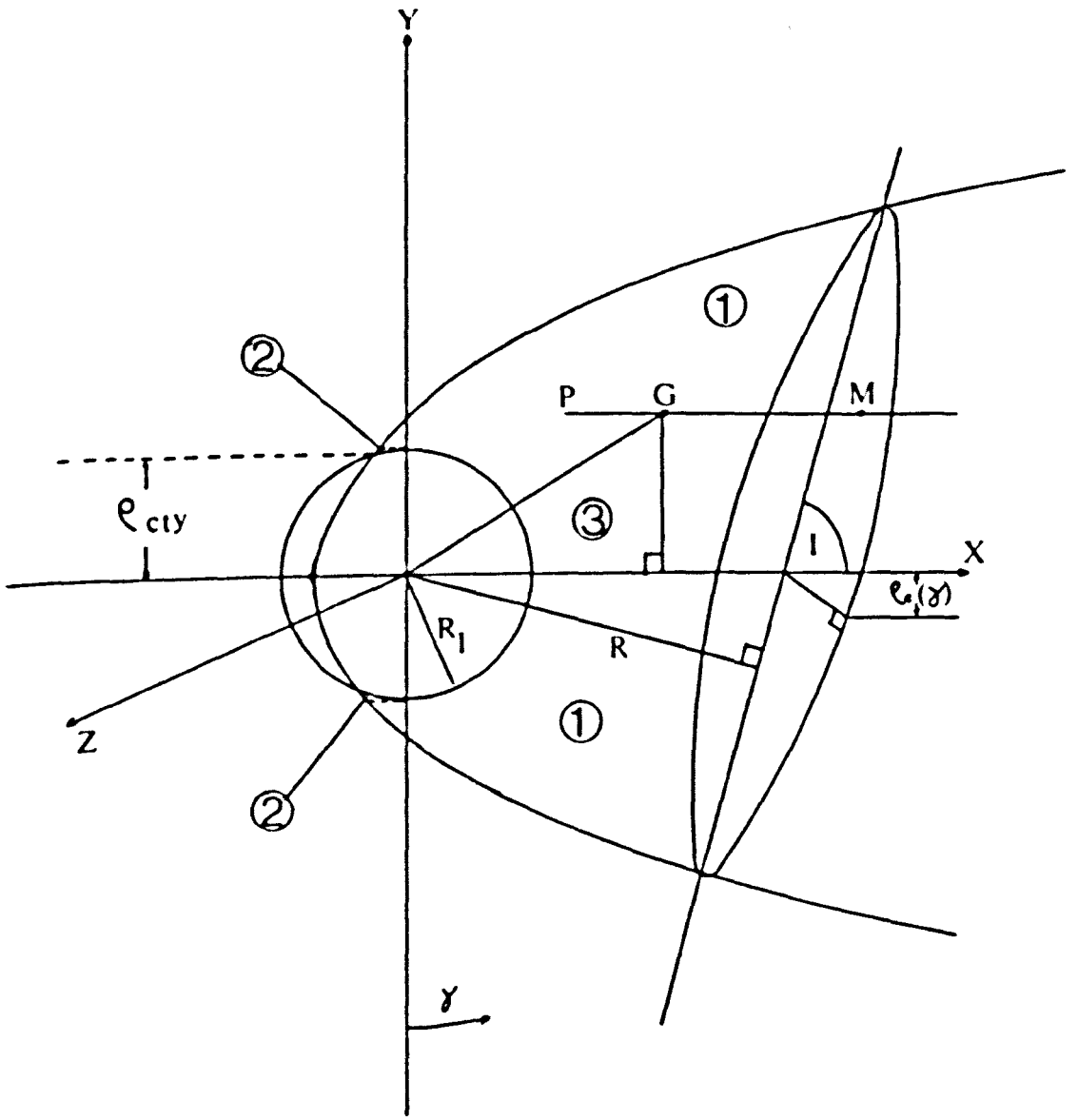
Y
X
Z
γ
P
G
M
I
①
②
③
ρ_{city}
R_1
R
$\rho_1(\gamma)$

FIGURE 16. Intersection of the paraboloid with the cavity; case 3, $\rho_{cty}=0$.

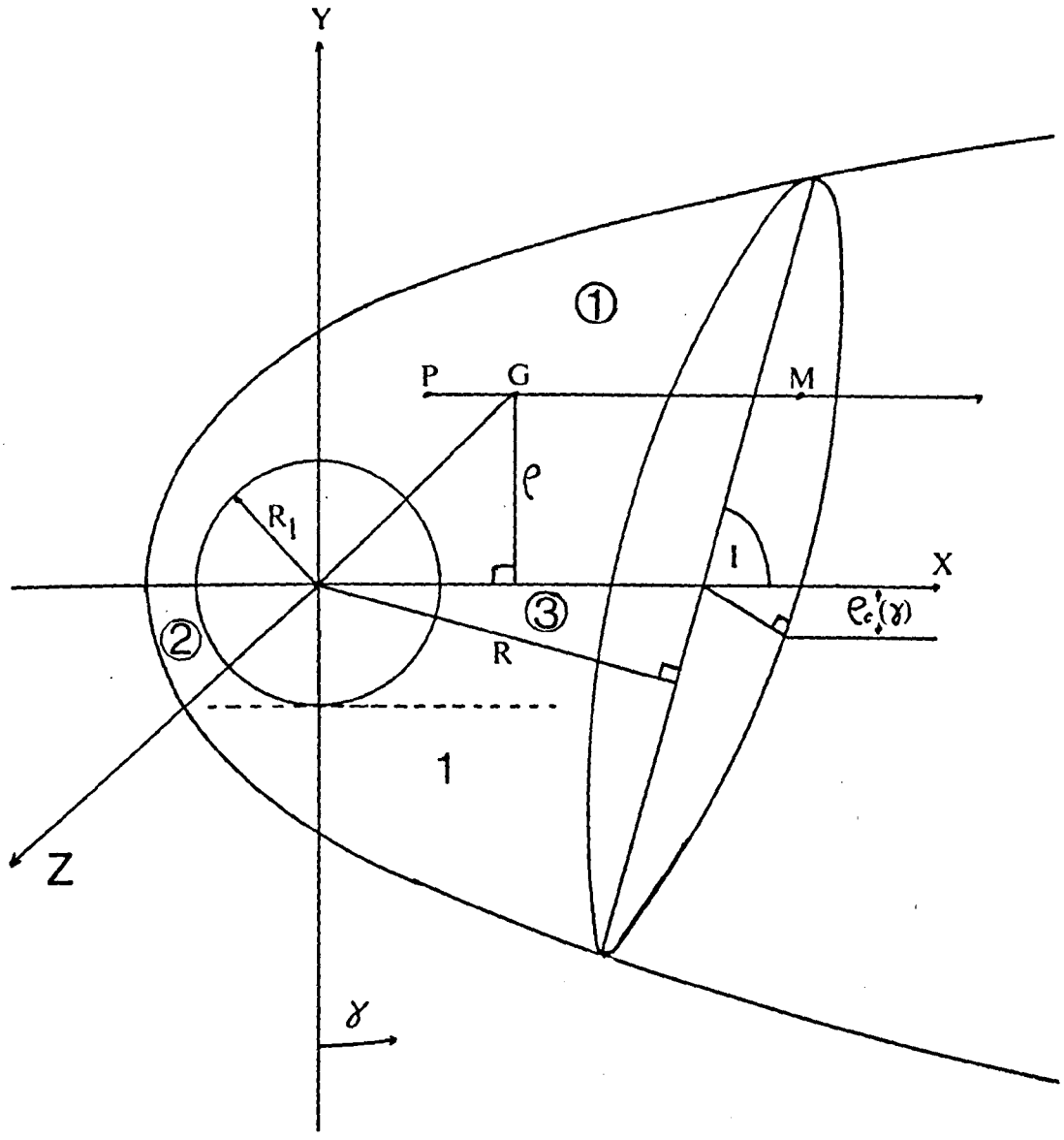
Y
①
P
G
M
ρ
R1
I
X
②
③
R
$e_c'(\gamma)$
1
Z
γ

5.2 Flux Computation

The flux seen by the observer per unit frequency interval at frequency ν at time t from a dust grain of type i at a position G (shown in figures 14 and 15 and 16) is given by

$$S_{\nu i}(x,\rho,\gamma,t) = (a_i^2/D^2)Q_{abs}(a_i,\nu)B_\nu(r,\tau(\rho,x,t)) \exp(-\pi N_{gs\nu}(x(M)-x+x_\xi(\rho))-\tau'_{\beta\nu}(\rho,x))$$

where i = g,s (5.2.1)

and x(M) -x is the path length of grain radiation through the interstellar dust plane and $\pi N_{gs\nu}(x(M)-x+x_\xi(\rho))$ is the optical depth to grain radiation at frequency ν.

The function $B_\nu(r,t)$ is defined in equation (3.5.2), $N_{gs\nu}$ is defined in equation (5.1.11), and $x_\xi(\rho)$ and $\tau'_{\beta\nu}(\rho,x)$ are defined as follows:

$$\tau'_{\beta\nu}(\rho,x) = \tau_{\beta\nu}(\rho) \quad \text{for } \rho<R_1 \quad \text{and } x\leq -(R_1^2-\rho^2)^{\frac{1}{2}}$$

$$= 0 \text{ otherwise} \qquad (5.2.2)$$

$\tau_{\beta\nu}$ is the optical depth to interstellar grain radiation from behind the cavity due to any circumstellar dust shell, whose outer radius is the interstellar dust cavity radius R_1. (see chapter 6). The function $x_\xi(\rho)$ in equation (5.2.1) is defined by

$$x_\zeta(\rho)=0 \quad \text{for } \rho>R_1 \text{ or } \rho<R_1 \text{ and } x>x(F). \qquad (5.2.3)$$

The term x_ζ removes the path length through the interstellar dust cavity from the path length through the interstellar dust plane in the optical depth expression in equation (5.2.1). The surface brightness at frequency ν, at time t, and at angular distance $\tan^{-1}(\rho/D)$ from the supernova image, and at angle γ clockwise from the -y axis, is given by

$$\sum_\nu(\rho,\gamma,t) = D^2 \int_{x(P)}^{x(M)} \zeta^{is}(\rho,x) \sum_{i=g,s} N_{0i}S_{\nu i}(x,\rho,\gamma,t)dx. \qquad (5.2.4)$$

as D^{-2} is the solid angle subtended by unit normal area of the dust plane. The term $\zeta^{is}(\rho,x)$, which ensures zero dust from the interstellar dust cavity, is defined by

$$\begin{aligned} \zeta^{is}(\rho,x) &= 0 && \text{for } r<R_1 \\ &= 1 && \text{for } r\geq R_1 \end{aligned} \qquad (5.2.5)$$

Substituting equation (5.2.1) into equation (5.2.4)

$$\sum_{\nu}(\rho,\gamma,t)=2\pi h\nu^3 c^{-2} \sum_{i=g,s} N_{oi} a_i^2 Q_{abs}(a_i,\nu)\sigma_{\nu i}(\rho,\gamma,t) \qquad (5.2.6)$$

where $\sigma_{\nu i}(\rho,\gamma,t)$ is defined as follows:

$$\sigma_{\nu i}(\rho,\gamma,t)= \int_{x(P)}^{x(M)} H_{\nu}(r,\tau(\rho,x))\zeta^{is}(\rho,x) \cdot\exp(-\pi N_{gs\nu}(x(M)-x+x_{\zeta}(\rho))-\tau'_{\beta\nu}(\rho,x))dx \qquad (5.2.7)$$

The function H_{ν}, which describes the emission of radiation by a grain at frequency ν is described in chapter 3. Substituting equations (5.2.2) (5.2.3) and (5.2.5) into equation (5.2.7) gives

$$\begin{aligned} \sigma_{\nu i}(\rho,\gamma,t) &= \int_{x(P)}^{x(M)} H_{\nu}(r,\tau(\rho,x,t))\exp(-\pi N_{gs\nu}(x(M)-x))dx \\ &\qquad \text{for } \rho_c(\gamma)>\rho\geq R_1 \\ &\qquad \rho_{cty}<\rho<R_1 \\ &\qquad \text{and } x(P))>0 \\ &= \int_{x(P)}^{x(M)} H_{\nu}(r,\tau(\rho,x,t))\exp(-\pi N_{gs\nu}(x(B)-x+x(M)-x(F))-\tau_{\beta\nu}(\rho)dx \\ &+ \int_{x(P)}^{x(M)} H_{\nu}(r,\tau(\rho,x,t))\exp(-\pi N_{gs\nu}(x(M)-x))dx \\ &\qquad \text{for } \rho_{cty}<\rho<R_1 \; x(P)<0 \\ &= \int_{x(P)}^{x(M)} H_{\nu}(r,\tau(\rho,x,t))\exp(-\pi N_{gs\nu}(x(M)-x))dx \\ &\qquad \text{for } 0<\rho<\rho_{cty} \end{aligned} \qquad (5.2.8)$$

where ρ_{cty} is given by equation (5.1.19)

Therefore

$$\sigma_{\nu i}(\rho,\gamma,t) = \int_{(\rho^2-c^2t^2)/2ct}^{(R-\rho\cos\gamma\cos I)/\sin I} H_\nu(r,\tau(\rho,x,t))\exp(\pi N_{gs\nu}(x-(R-\rho\cos\gamma\cos I)/\sin I))dx$$

for $R_1<\rho<\rho_c(\gamma)$ if $ct > R_1$ and for $\rho_{cty}<\rho<\rho_c(\gamma)$ if $0<ct<R_1$

$$= \int_{(\rho^2-c^2t^2)/2ct}^{-(R_1^2-\rho^2)^{\frac{1}{2}}} H_\nu(r,\tau(\rho,x,t))\exp(\pi N_{gs\nu}(x+2(R_1^2-\rho^2)^{\frac{1}{2}} -(R-\rho\cos\gamma\cos I)/\sin I)-\tau_{\beta\nu}(\rho))dx$$

$$+ \int_{(R_1^2-\rho^2)^{\frac{1}{2}}}^{(R-\rho\cos\gamma\cos I)/\sin I} H_\nu(r,\tau(\rho,x,t))\exp(\pi N_{gs\nu}(x-(R-\rho\cos\gamma\cos I)/\sin I))dx.$$

for $\rho_{cty}<\rho<R_1$ if $ct>R_1$

$$= \int_{(R_1^2-\rho^2)^{\frac{1}{2}}}^{(R-\rho\cos\gamma\cos I)/\sin I} H_\nu(r,\tau(\rho,x,t)\exp(\pi N_{gs\nu}(x-(R-\rho\cos\gamma\cos I)/\sin I))dx.$$

for $0<\rho<\rho_{cty}$

$$= 0 \qquad \text{for } \rho>\rho_c(\gamma) \qquad (5.2.9)$$

where the term $(R-\rho\cos\gamma\cos I/\sin I)$ represents the condition where the line of sight crosses the front plane of the interstellar dust plane; $x=(\rho^2-c^2t^2)/2ct$ is the equation of the paraboloid of revolution, the term $-(R_1^2-\rho^2)^{\frac{1}{2}}$ represents the point where the line of sight through the supernova intersects with the farside of the cavity; and the term $\exp(\pi N_{gs\nu}(x-(R-\rho\cos\gamma\cos I)/\sin I))$ represents the optical depth along a line of sight. Equations (5.2.8) and (5.2.9) define a set of conditions for the position of the parabola relative to the cavity. If $0<ct<R_1$ the parabola is inside the cavity, (see figure 14). For the condition $R_1<ct<2R_1$ the parabola is also inside the cavity but interstellar grains defined by region (2) on figure 15 are also being heated, which is not the case for figure 14. For the condition illustrated by figure 16, the parabola is

completely behind the cavity. So far only radiation from interstellar grains heated by the supernova has been considered. It is necessary especially for observations in the far infra-red region of the spectrum to consider radiation from grains behind (as seen by the observer) the paraboloid of revolution that defines the region where grains are heated by supernova radiation. The temperature T'_{gi} of the grains of type i heated by background starlight only is obtained from

$$Q'_{gi} = \sum_{j=1,2,3} W_j \overline{Q_{abs}}(a_i, T_j) T_j^4 \qquad (5.2.10)$$

where W_1, W_2, W_3, T_1, T_2, and T_3 are given in section 3.4. The parameter T'_{gi} is derived from Q'_{gi} using the method of deriving the temperature T_{gi} from $Q_{gi}(r,t)$, which is given by equation (3.5.9). The flux per unit frequency interval, at frequency ν, from a grain of type i at position (x,ρ,γ) is given by

$$S_{\nu i}(x,\rho,\gamma) = (a_i^2/D^2) B(\nu, T'_{gi}) Q_{abs}(a_i,\nu)$$

$$\cdot \exp(-\pi N_{gs\nu}[x(M)-x] - \tau_{\beta\nu}(\rho) + \tau_{cav}(\rho)) \qquad (5.2.11)$$

where

$$\tau_{cav}(\rho) = 2\pi N_{gs\nu}(R_1^2-\rho^2)^{\frac{1}{2}} \quad \text{for } \rho < R_1$$

$$= 0 \quad \text{for } \rho > R_1 \qquad (5.2.12)$$

The contribution from grains heated by starlight only to the surface brightness at frequency ν is given by

$$\sum_{\nu}(\rho,\gamma,t) = \sum_{i=g,s} N_{oi} D^2 \left(\int_{x(u)}^{x(BP)} S_{\nu i}(x,\rho,\gamma)dx + I_{\nu i}(\rho,\gamma,t) \right) \qquad (5.2.13)$$

where

$$x(BP) = x(P) \qquad \text{for } \rho > R_1$$
$$= \min[x(P),x(B)] \qquad \text{for } \rho < R_1 \qquad (5.2.14)$$

and the contribution from any grains in front of the cavity (at times t, for which $ct<R_1$). Behind the paraboloid of revolution the contribution from grains heated by starlight only is given by

$$I_{\nu i}(\rho,\gamma,t) = \int_{x(F)}^{x(PM)} (a_i^2/D^2) B(\nu,T'_{gi}) Q_{abs}(a_i,\nu) \exp(-\pi N_{gs\nu}(x(M)-x))dx$$

$$\text{if } x(F)<x(PM),$$

$$ct<R_1 \text{ and } \rho, R_1$$

$$= 0 \qquad \text{otherwise.} \qquad (5.2.15)$$

where

$$x(PM) = \min[x(P),x(M)] \qquad (5.2.16)$$

substituting equations (5.2.11) and (5.2.14) into equation (5.2.13)

$$\sum_{\nu}(\rho,\gamma,t) = \frac{2\pi h\nu^3}{c^2} \left(\exp(-\pi N_{gs\nu}x(M)-\tau_{\beta\nu}(\rho)+\tau_{cav}(\rho))\right.$$

$$\left.\cdot(\pi N_{gs\nu})^{-1} \left(\exp(\pi N_{gs\nu}x(BP))-\exp(\pi N_{gs\nu}x(u))\right)+\sigma_{\nu i}(\rho,\gamma,t)\right)$$

$$\cdot \sum_{i=g,s} \frac{N_{oi}a_i^2 Q_{abs}(a_i,\nu)}{e^{h\nu/KT'_{gi}}-1} \qquad (5.2.17)$$

where $B(\nu,T'_{gi})$ is the Planck function; the term $Q_{abs}(a_i,\nu)$ represents the absorption efficiency of the grains; the term $\exp(-\pi N_{gs\nu}(x(M)-x))$ is the optical depth term, and $\sigma_{\nu i}$ is defined by:

$$\sigma_{\nu i}(\rho,\gamma,t) = (\pi N_{gs\nu})^{-1} \exp(-\pi N_{gs\nu}x(M))$$
$$(\exp(\pi N_{gs\nu}x(PM))-\exp(\pi N_{gs\nu}x(F))) \qquad (5.2.18)$$

The surface brightness from the dust plane slab for $\rho(\gamma,t)>\rho_c(\gamma,t)$ is given by

$$\sum_\nu(\rho,\gamma) = \frac{2\pi h\nu^3}{c^2} \sum_{i=g,s} \frac{N_{oi}a_i^2 Q_{abs}(a_i,\nu)}{e^{h\nu/KT'_{gi}}-1} \int_{x(L)}^{x(M)} \exp(\pi N_{gs\nu}(x-x(M)))dx$$

$$= \frac{2\pi h\nu^3}{c^2} \sum_{i=g,s} \frac{N_{oi}a_i^2 Q_{abs}(a_i,\nu)}{e^{h\nu/KT'_{gi}}-1} \frac{1-e^{-\pi N_{gs}\nu/\sin I}}{\pi N_{gs\nu}} \qquad (5.2.19)$$

The flux per unit frequency interval from the part of the dust plane slab within angular distance $\tan^{-1}(\rho_o/D)$ from the supernova is given by

$$f_\nu(t) = 2D^{-2}\int_o^\pi \int_o^{\rho o} \sum_\nu(\rho,\gamma,t)\rho d\rho d\gamma \qquad (5.2.20)$$

while the flux per unit frequency interval observed from the circle of re-emission as seen on the plane of the sky is given by

$$f_\nu(t) = 2D^{-2}\int_o^\pi \int_o^{\rho c(\gamma)} \sum_\nu(\rho,\gamma,t)\rho d\rho d\gamma \qquad (5.2.21)$$

Equation (5.2.21) is then used to compute the dust flux. The results of these flux computations are described in section (5.3).

5.3 Interpretation of Results

In this section the infra-red flux emitted from interstellar grains heated by a supernova is investigated when various physical parameters such as the inclination (I) of the galaxy to the observer's line of sight, the depth (R) of the supernova into the galaxy and the radius (R_1) of the cavity are varied. The infra-red fluxes are computed using equation (5.2.21), and the corresponding spectra and light curves are produced. The distance of the galaxy is taken to be 10Mpc and the thickness of the dust

plane is taken to be 1Kpc. These values of 10Mpc and 1Kpc are chosen because supernovae have been observed in galaxies at distances typically of the order of 10Mpc. Also 1Kpc is a typical value for the thickness of a galactic dust plane. With the instrumentation which may be available in the near future, infra-red fluxes from interstellar grains heated by supernovae in galaxies at such distances could be detected.

Obviously grains close to the supernova will not survive the eruption, which will sweep out a spherical cavity centred on the supernova. In view of the differing optical and the thermodynamic properties of the two types of grain, each grain type will give rise to cavities of different dimensions. These are evaluated from

$$R_1 = \left(\frac{L_*(t)\overline{Q_{abs}}(a_i, T_e^{(t)})}{16\pi\sigma\overline{Q_{abs}}(a_i, T_{evap}^{(t)})T_{evap}^4(t)} \right)^{\frac{1}{2}} \qquad (5.3.1)$$

where $T_{evap}(t)$ is given by equation (4.0.1). The final cavity size reached by evaporation is 4.7×10^{14}m for graphite and 2.2×10^{15}m for silicate, and these final radii are reached about a day after outburst. However, while the forces on the grains have little effect on the cavity radius for silicate grains, they subsequently cause the cavity radius for graphite grains to expand as described in figure 17.

The graph of the infra-red flux variation with the angle of inclination I of the galaxy to the line-of-sight (figure 18), shows that as the angle I decreases, the dust flux increases. This can also be seen from figure 19 which shows the dust spectrum at 100 days after outburst for $I=65^0$ and $I=10^0$, (R=100pc in both cases). This occurs because we are looking at more dust heated by the supernova and more dust in the background. The supernova flux decreases because the optical depth of the interstellar dust grains to supernova radiation increases. If the grain number density were sufficiently large as the angle of inclination of the galaxy is decreased the dust flux at short wavelengths would eventually

FIGURE 17. The graphite cavity radius $\underline{V}$ time for the interstellar grains.

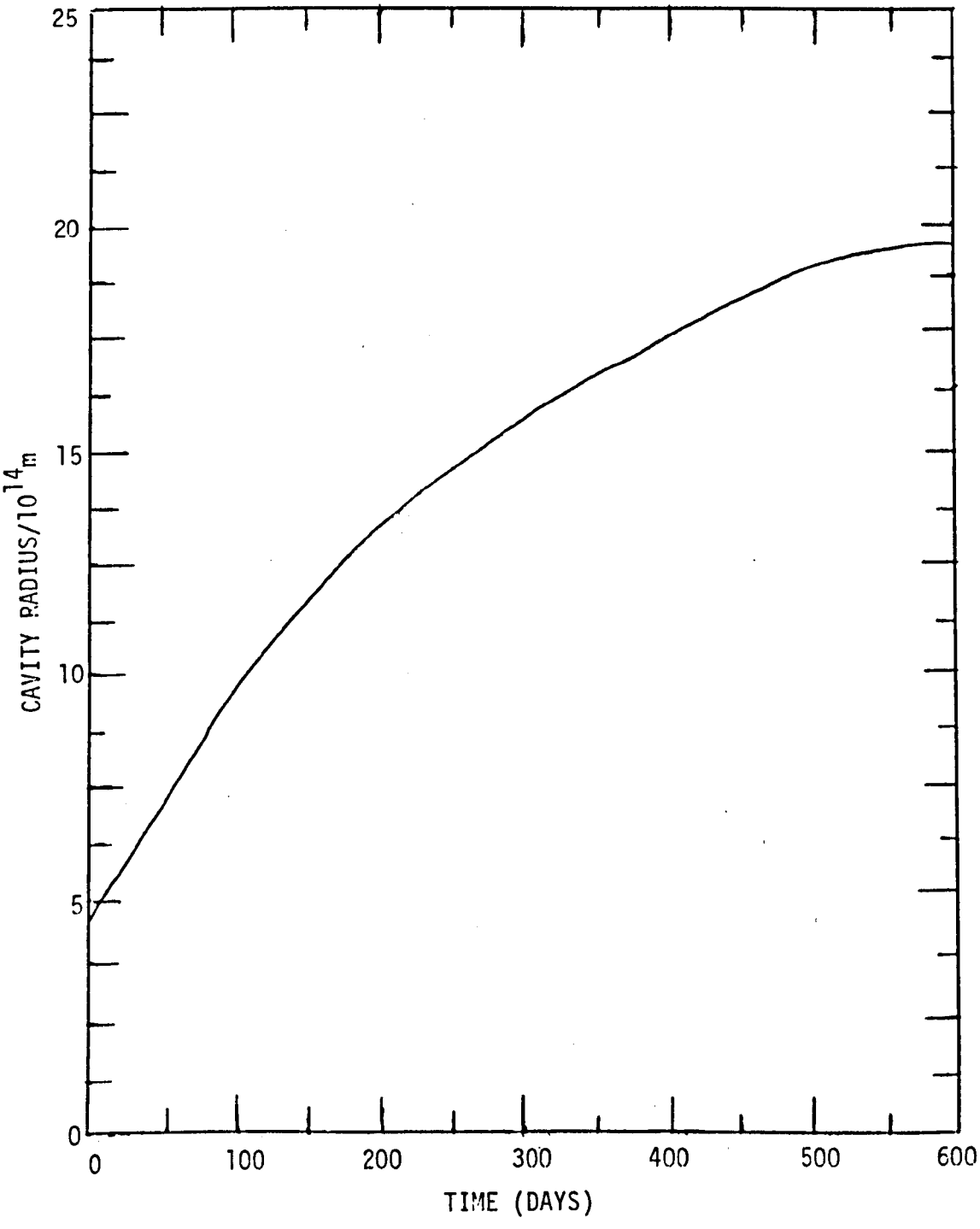
25
20
15
10
5
0
CAVITY RADIUS/10^{14}m
0
100
200
300
400
500
600
TIME (DAYS)

FIGURE 18. Dependence of infra-red flux distribution on angle of inclination of galaxy. Curves are labelled by wavelength, in μm. R=100pc, t=360 days, silicate:graphite ratio = 70:30.

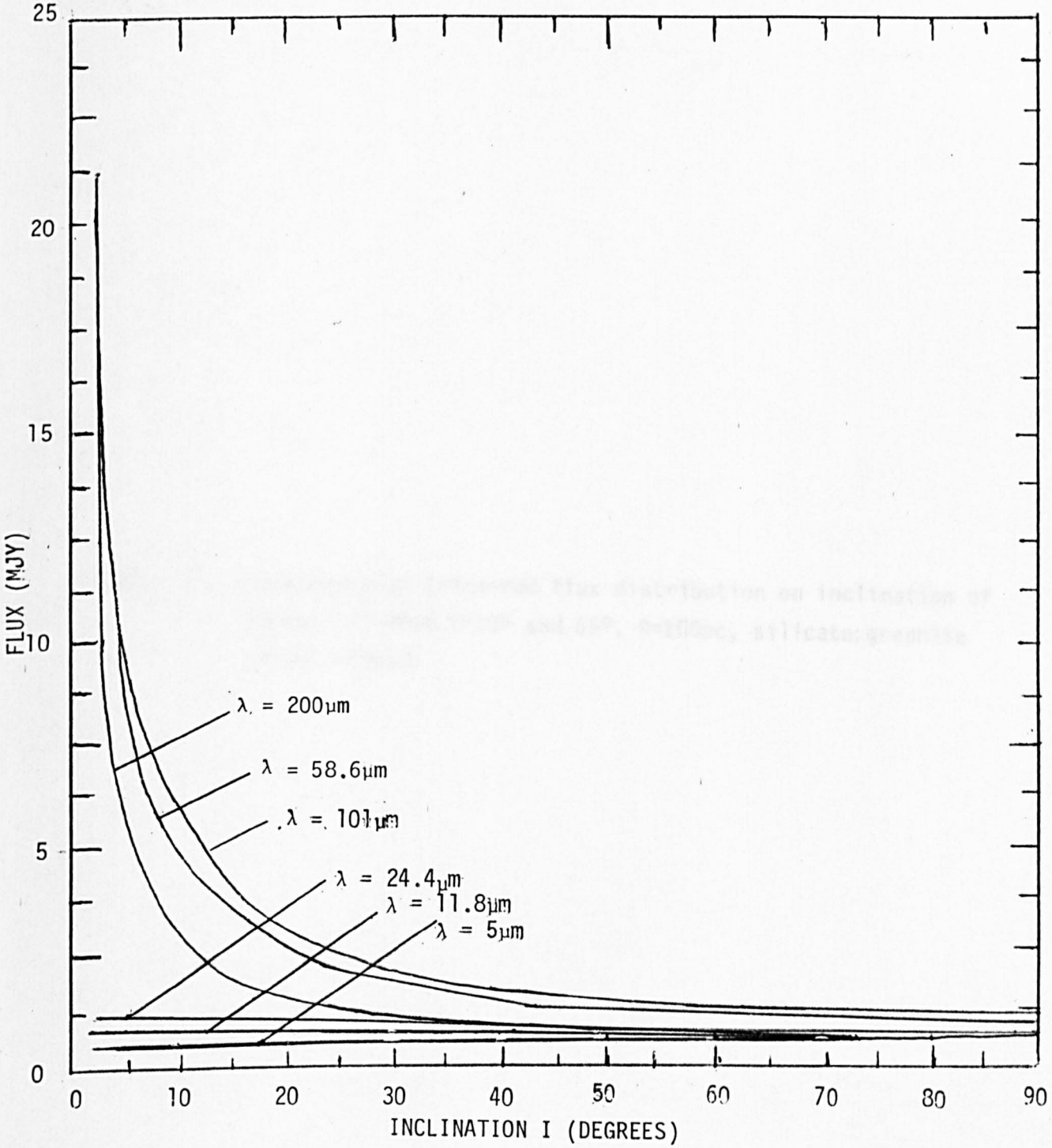
25
20
15
10
5
0
FLUX (MJY)
λ = 200μm
λ = 58.6μm
λ = 10.1μm
λ = 24.4μm
λ = 11.8μm
λ = 5μm
0
10
20
30
40
50
60
70
80
90
INCLINATION I (DEGREES)

FIGURE 19. Dependence of infra-red flux distribution on inclination of galaxy (I) when I=10^{o} and 65^{o}. R=100pc, silicate:graphite ratio = 70:30.

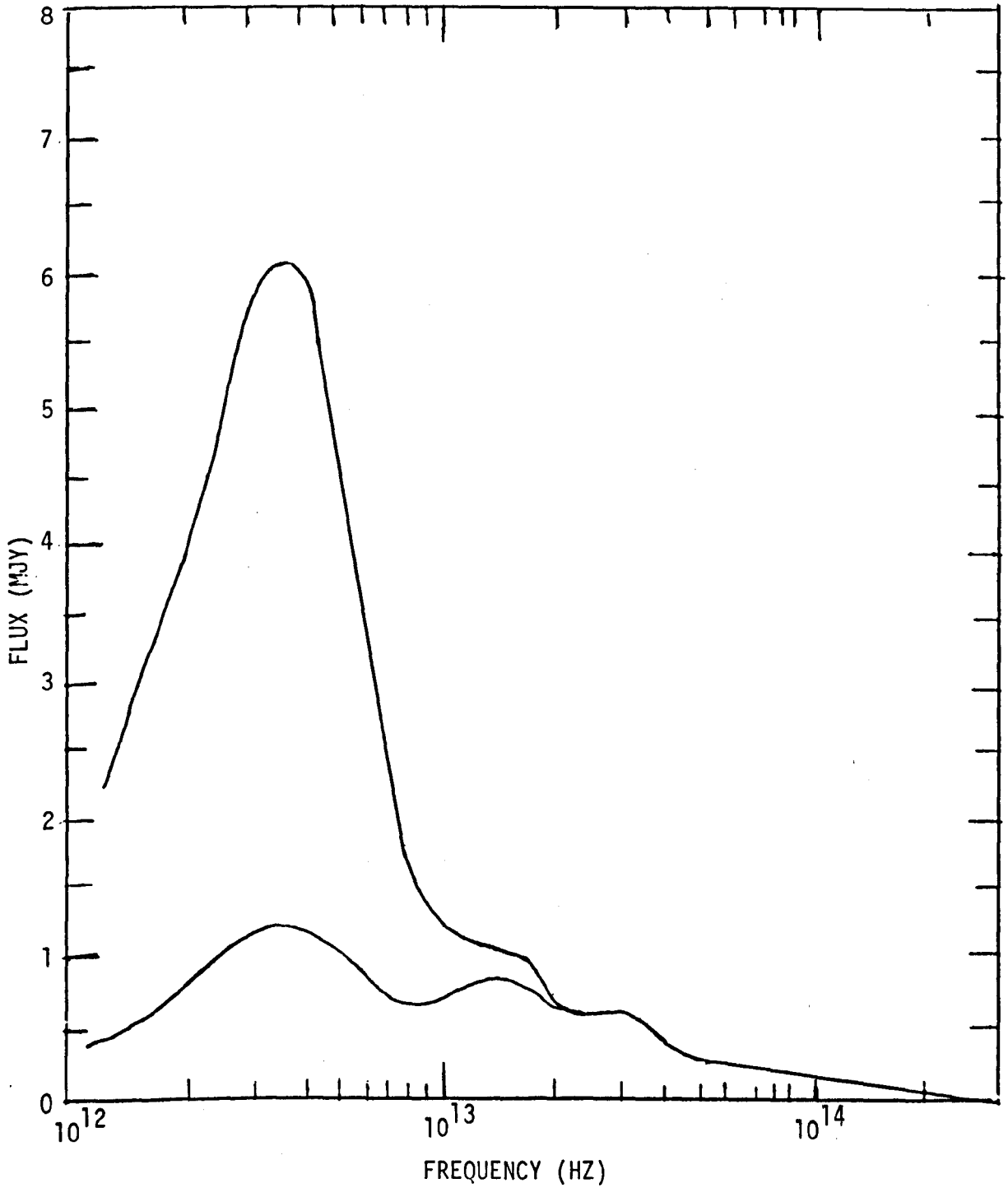
8
7
6
5
4
3
2
1
0
FLUX (MJY)
10^{12}
10^{13}
10^{14}
FREQUENCY (HZ)

FIGURE 20. Q_{abs} V wavelength/frequency for graphite and silicate interstellar grains.

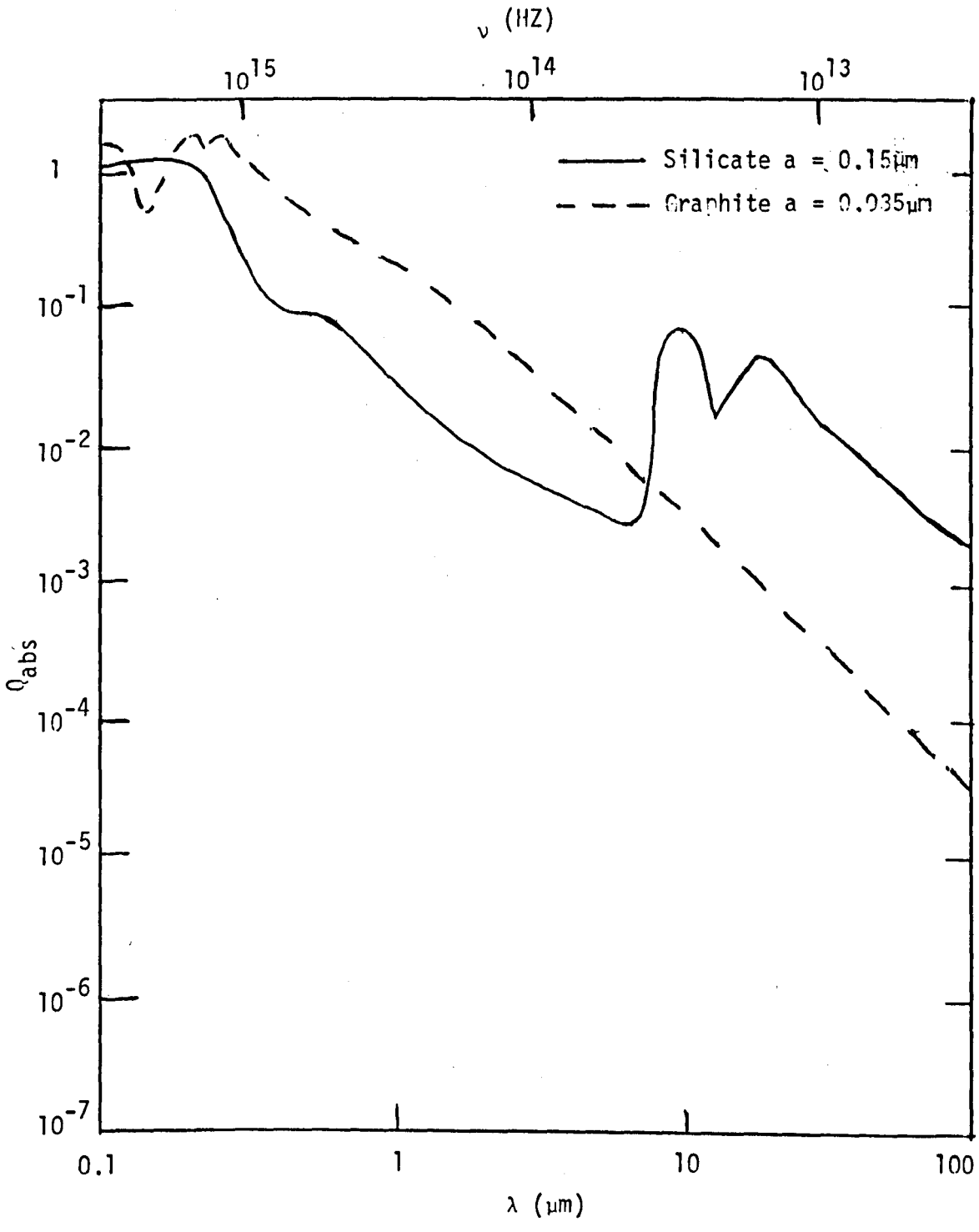
ν (HZ)
10^15
10^14
10^13
Silicate a = 0.15μm
Graphite a = 0.035μm
1
10^-1
10^-2
10^-3
10^-4
10^-5
10^-6
10^-7
Q_abs
0.1
1
10
100
λ (μm)

decrease after reaching a maximum. This would occur because the optical depth to the supernova through the observed dust grains would become large, so the temperatures of the observed grains would fall. However the optical depth of the interstellar dust is too small for this effect to occur in the dust being heated by the supernova.

A comparison of the spectra from dust heated by starlight only for $I=65^{o}$ and for $I=10^{o}$ (figures 21 and 23 respectively), shows that there is less flux at all wavelengths at least up to 300μm for galactic inclination $I=65^{o}$. This is because a far greater number of grains are being observed for $I=10^{o}$, and is inspite of the fact that they are being observed at much greater optical depths than is the case for $I=65^{o}$. Because the assumed thickness of the dust plane is 1Kpc the dust at the nearside of the dust plane obscures radiation from dust at the farside of the dust plane. Extinction is much greater for 10^{o} than for 65^{o} because of the much longer path length. When the supernova is included then as the angle I decreases there is also a spectral shift to longer wavelengths, (figure 19). This shift to longer wavelengths occurs because a greater number of grains are being observed and they are observed at much greater distances from the supernova. The extra grains being seen are all at a lower temperature than those already seen at longer wavelengths.

From the light curves in figure 24, the dust flux (following the first ~ 100 days after outburst) remains more or less constant to all infra-red wavelengths ranging from 5μm to 200μm for ~2000 days after outburst. While most of the flux in the far infra-red (i.e. ~ 100μm) is due to grains heated by background starlight only, (and so would be expected to remain more or less constant) the flux at wavelengths shortwards of 30μm is entirely due to grains heated by supernova radiation (see figures 21 to 23 inclusive).

This would seem to indicate that the heating of grains by the supernova continues for many years after outburst. Reference to figures 25,

FIGURE 21. Infra-red flux distribution for interstellar grains heated by background starlight only. I=65^{o}, R=100pc, silicate:graphite ratio = 30:70.

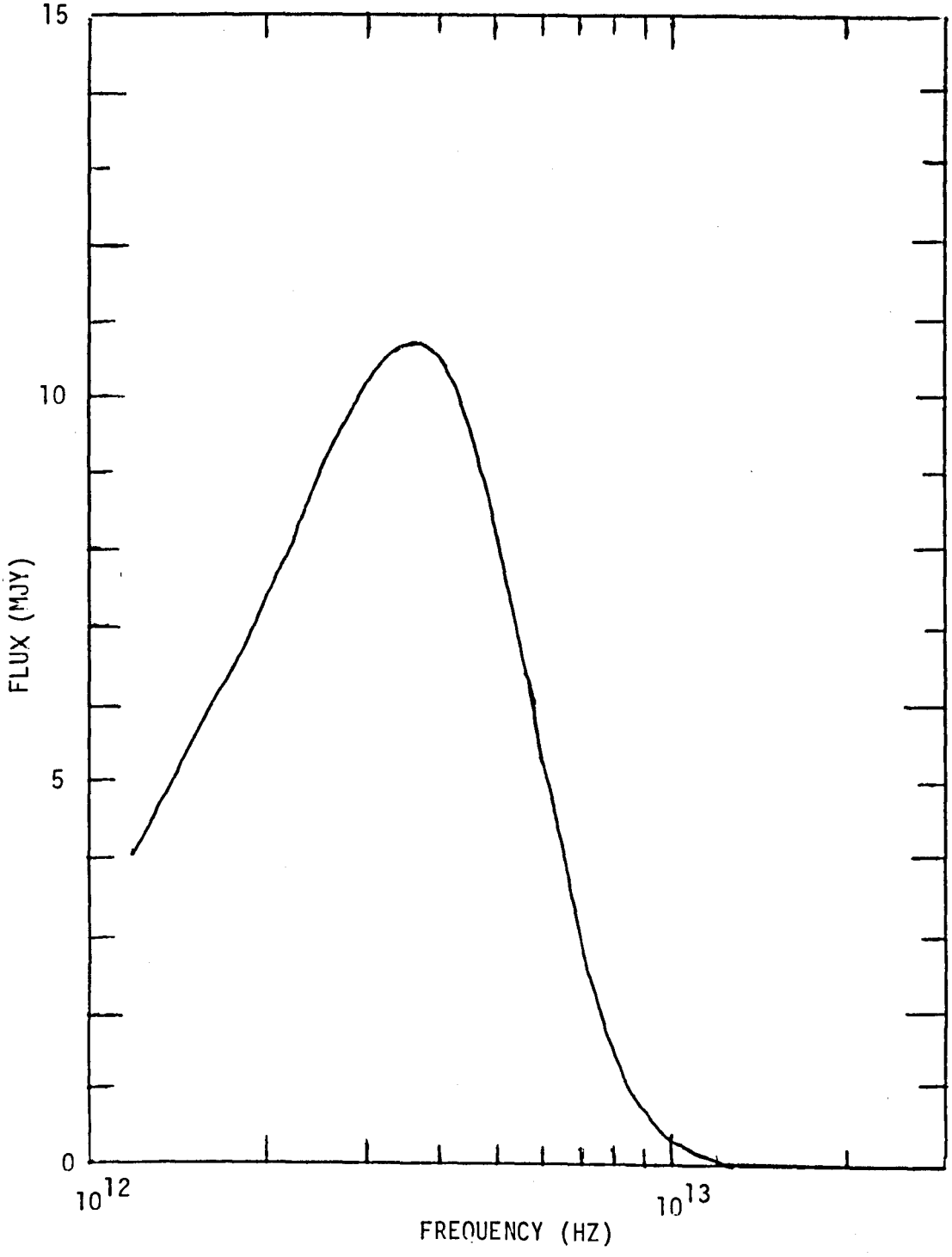
15
10
5
0
FLUX (MJY)
10^{12}
10^{13}
FREQUENCY (HZ)

FIGURE 22. Infra-red flux distribution due to interstellar grains heated by background starlight only. I=65°, R=100pc, silicate:graphite ratio = 50:50.

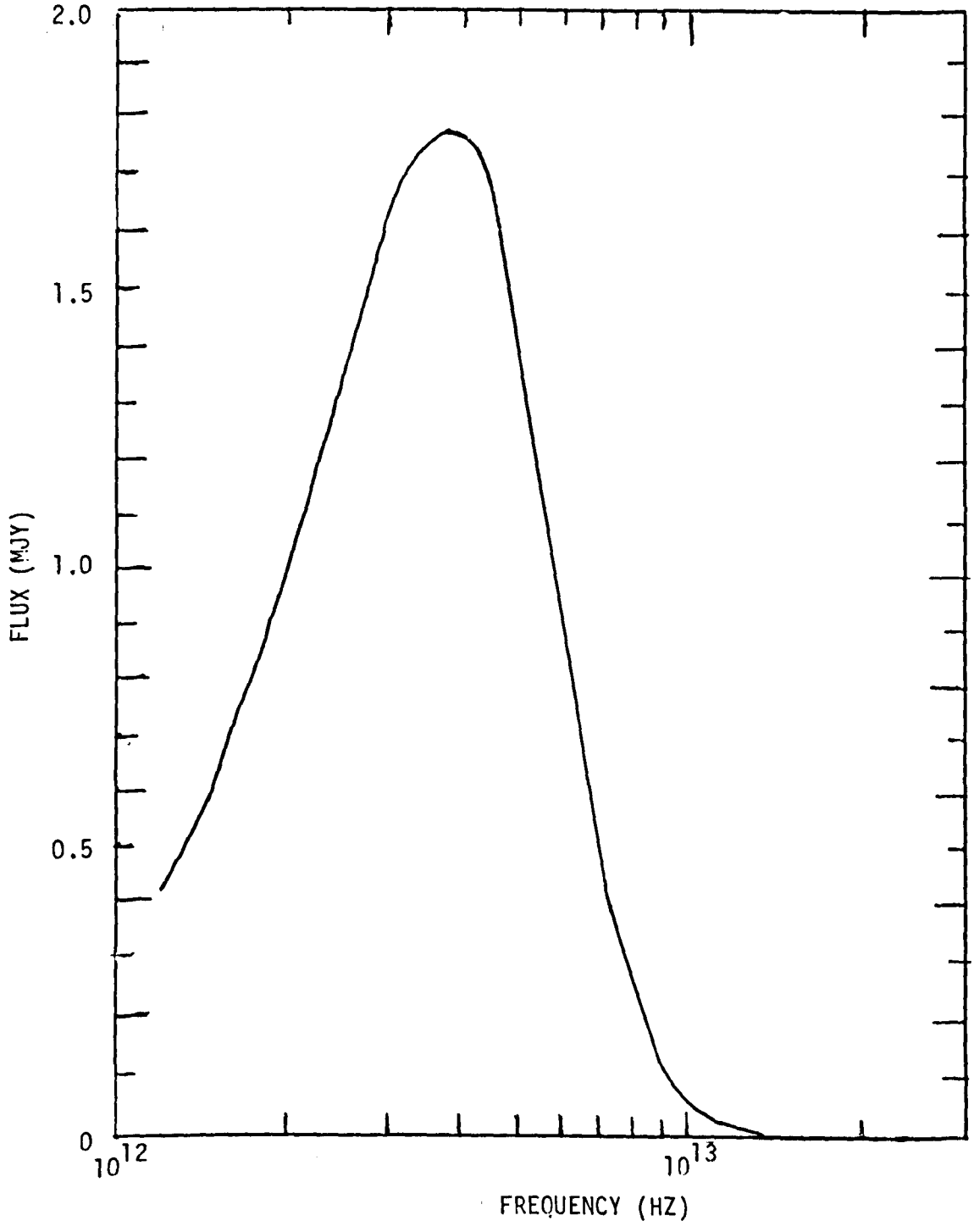
2.0
1.5
1.0
0.5
0
FLUX (MJY)
10^{12}
10^{13}
FREQUENCY (HZ)

FIGURE 23. Infra-red flux distribution due to interstellar grains heated by background starlight only. I=10^{o}, R=100pc, silicate:graphite ratio = 70:30.

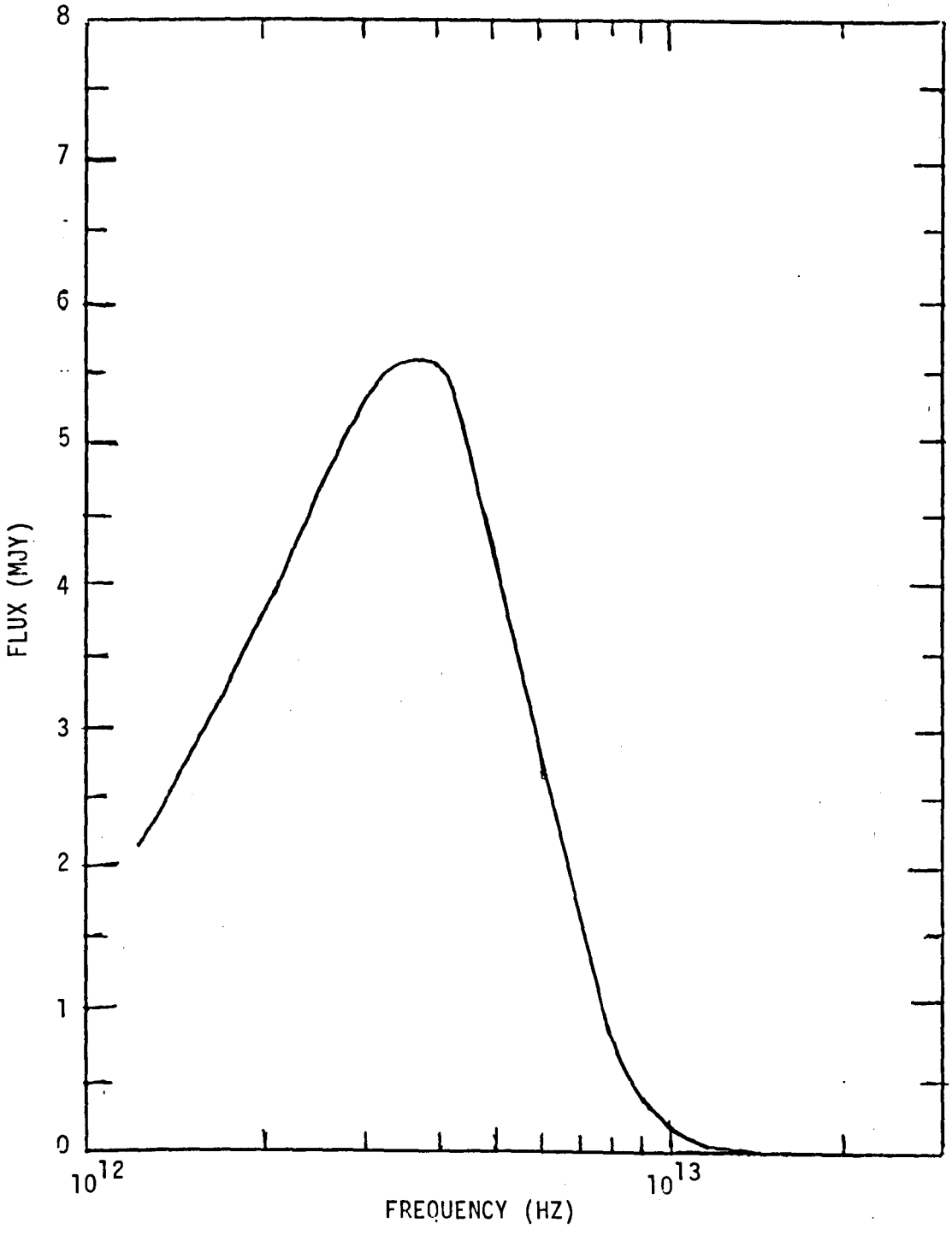
8
7
6
5
4
3
2
1
0
FLUX (MJY)
10^{12}
10^{13}
FREQUENCY (HZ)

FIGURE 24. Infra-red light curves for parameters R=100pc, I=65°, silicate:graphite ratio = 70:30. Curves are labelled by wavelength.

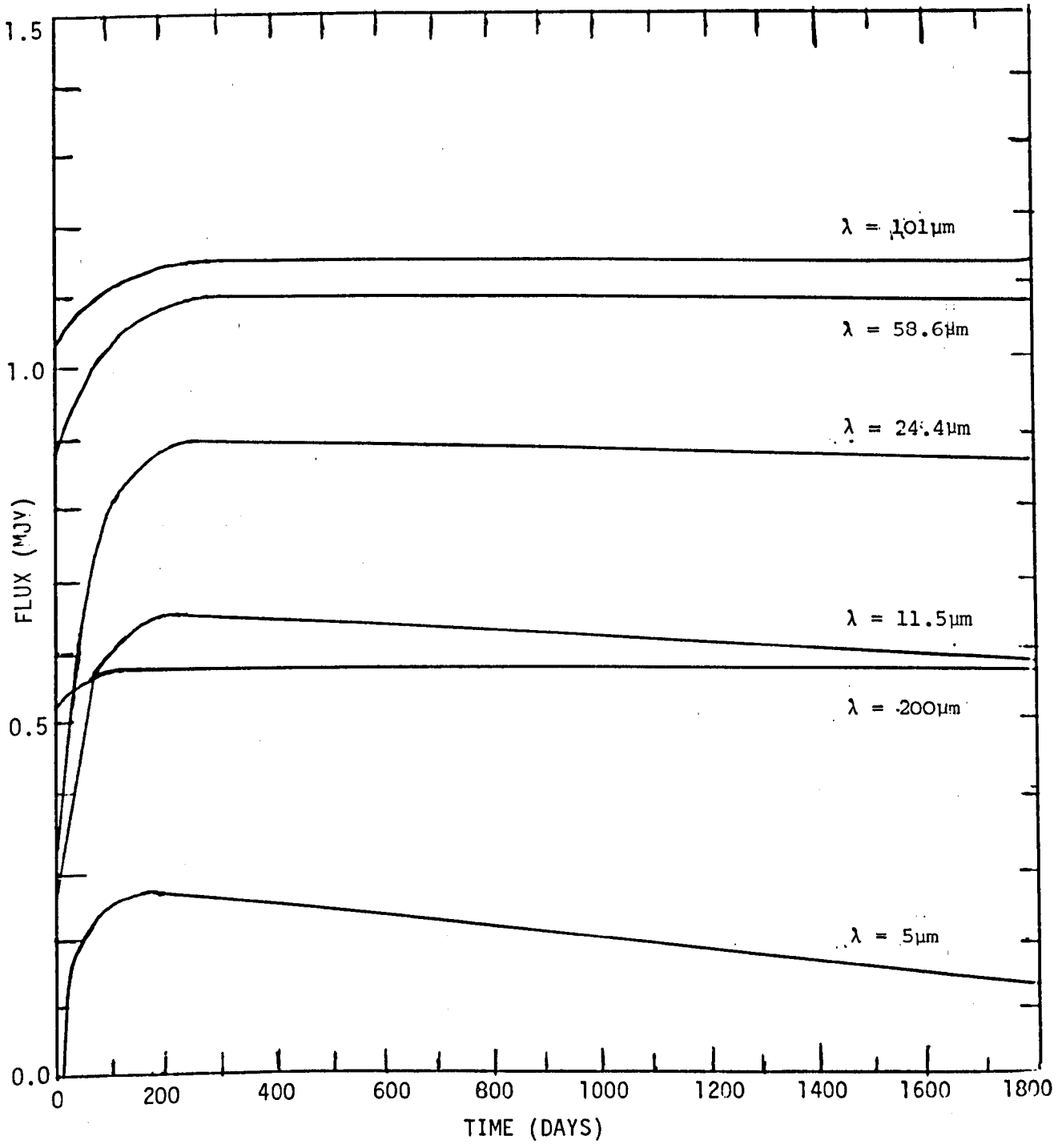
1.5
1.0
0.5
0.0
FLUX (MJY)
λ = 101μm
λ = 58.6μm
λ = 24.4μm
λ = 11.5μm
λ = 200μm
λ = 5μm
0
200
400
600
800
1000
1200
1400
1600
1800
TIME (DAYS)

FIGURE 25. Infra-red flux distribution at 100 days after outburst. I=65^{o}, R=100pc. Silicate:graphite ratio = 70:30. (Dust flux only).

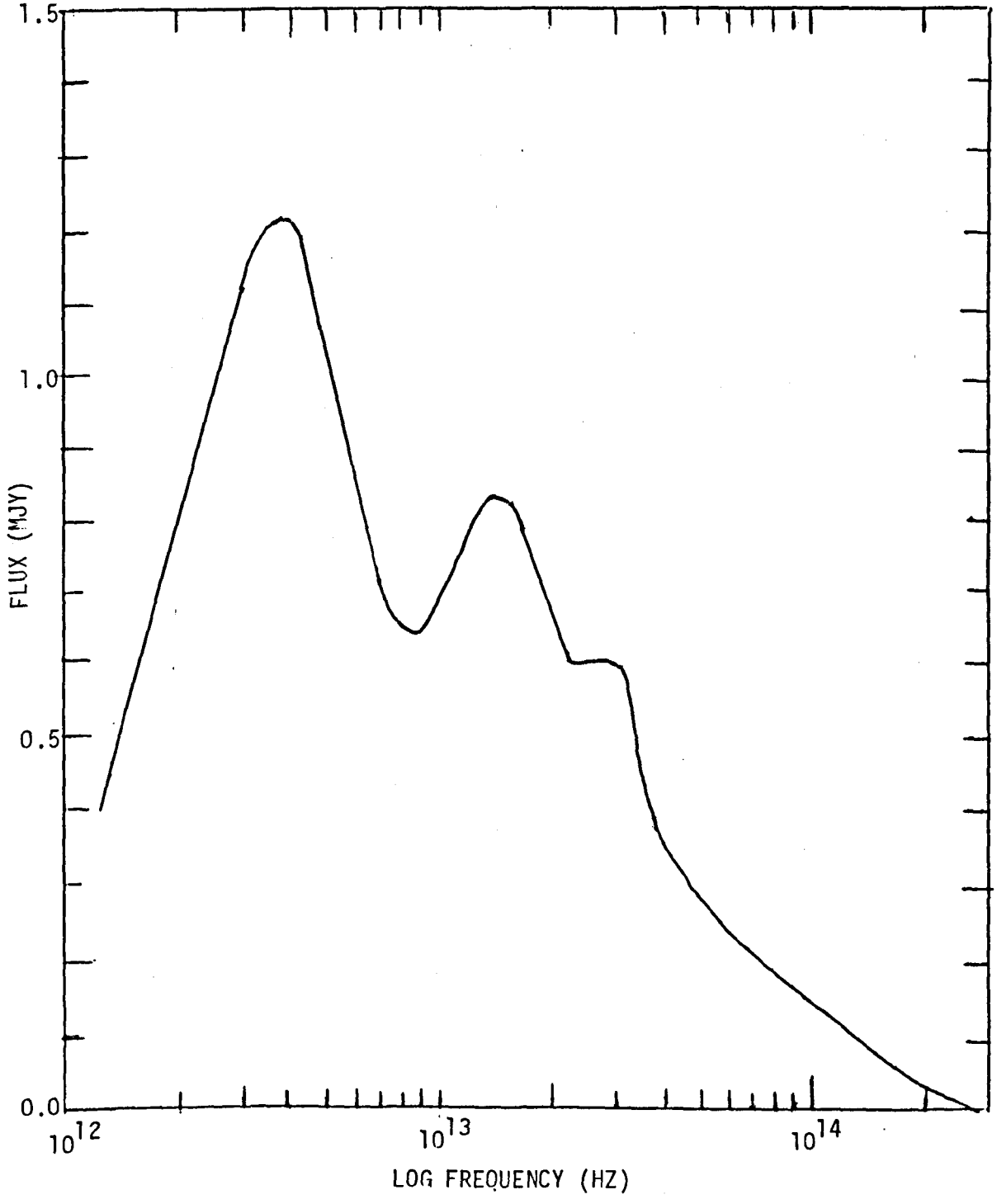
1.5
1.0
0.5
0.0
FLUX (MJY)
10^{12}
10^{13}
10^{14}
LOG FREQUENCY (HZ)

26 and 27 (dust, supernova, and total flux respectively at 100 days) and comparing them with figures 28, 29 and 30 (dust, supernova, and total flux respectively at 360 days) shows that the supernova flux dominates the near infra-red at 100 days almost as far as the 10μm feature, whereas at 360 days the supernova flux does not become dominant until about 3μm. At 750 days it has in effect completely disappeared. By contrast there is of order 1mJy of dust flux at 750 days, 1800 days, and 3600 days after outburst as can be seen from figures 31, 32 and 33 respectively, in the mid and far infra-red (that is between 5μm and ~300μm).

At 10 years after outburst a comparison of figures 21 and 33 shows that the dust flux is still much greater than that which would be expected from heating due to ambient starlight only. While this dust heated by ambient starlight only, radiates very little at wavelengths short of 30μm, peaks at about 100μm, and radiates mostly in the 30 to 300μm range, the dust flux at 10 years after outburst, while also peaking at about 100μm, has another peak at about 20μm. The latter is due to the effect of supernova radiation. Furthermore in addition to radiating strongly in the 30μm to 300μm range, the interstellar dust 10 years after outburst begins to radiate substantially at about 5μm and produces significant amounts of radiation in the 5μm to 30μm region.

The dust spectrum just described exists with very little change from 100 days to 10 years. However, at earlier times there is also a 10μm feature which can be clearly seen in the dust spectrum after 100 days and after 360 days. It is still visible but starting to disappear at 750 days and at this and later times exists only as a lessening of the downward gradient of flux towards shorter wavelengths. This 10μm feature and the 20μm peak are undoubtedly due to the optical properties of the silicate dust whereas the 100μm peak is the peak intensity of the radiation of the large mass of cooler dust grains heated by starlight only and also those within the paraboloid of revolution that have comparatively little

FIGURE 26. Supernova flux distribution at 100 days after outburst. I=65°, R=100pc.

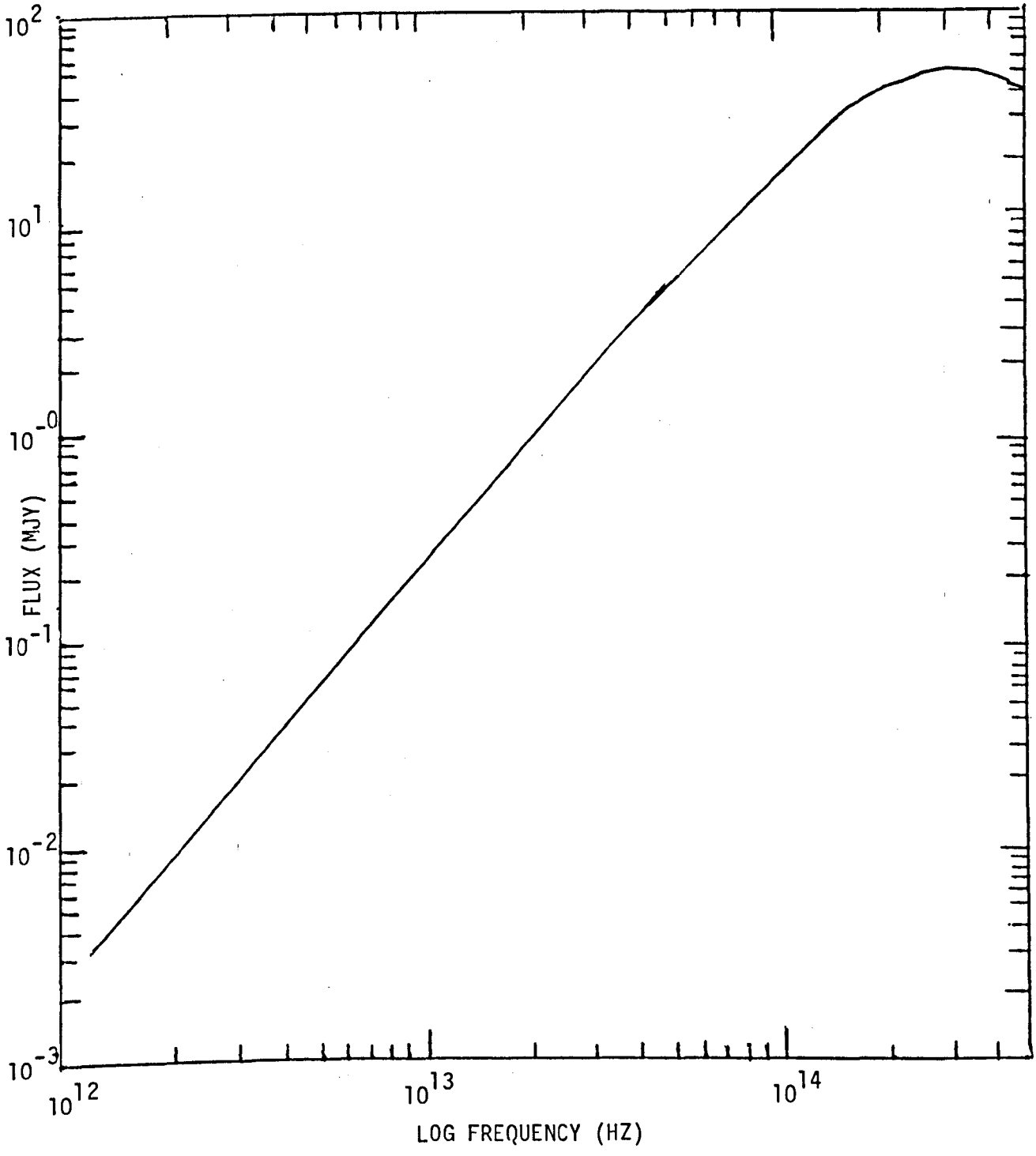
10^{2}
10^{1}
10^{-0}
10^{-1}
10^{-2}
10^{-3}
FLUX (MJY)
10^{12}
10^{13}
10^{14}
LOG FREQUENCY (HZ)

FIGURE 27. Infra-red flux distribution at 100 days after outburst. I=65°, R=100pc, silicate:graphite ratio = 70:30. (Total flux = supernova flux + dust flux)

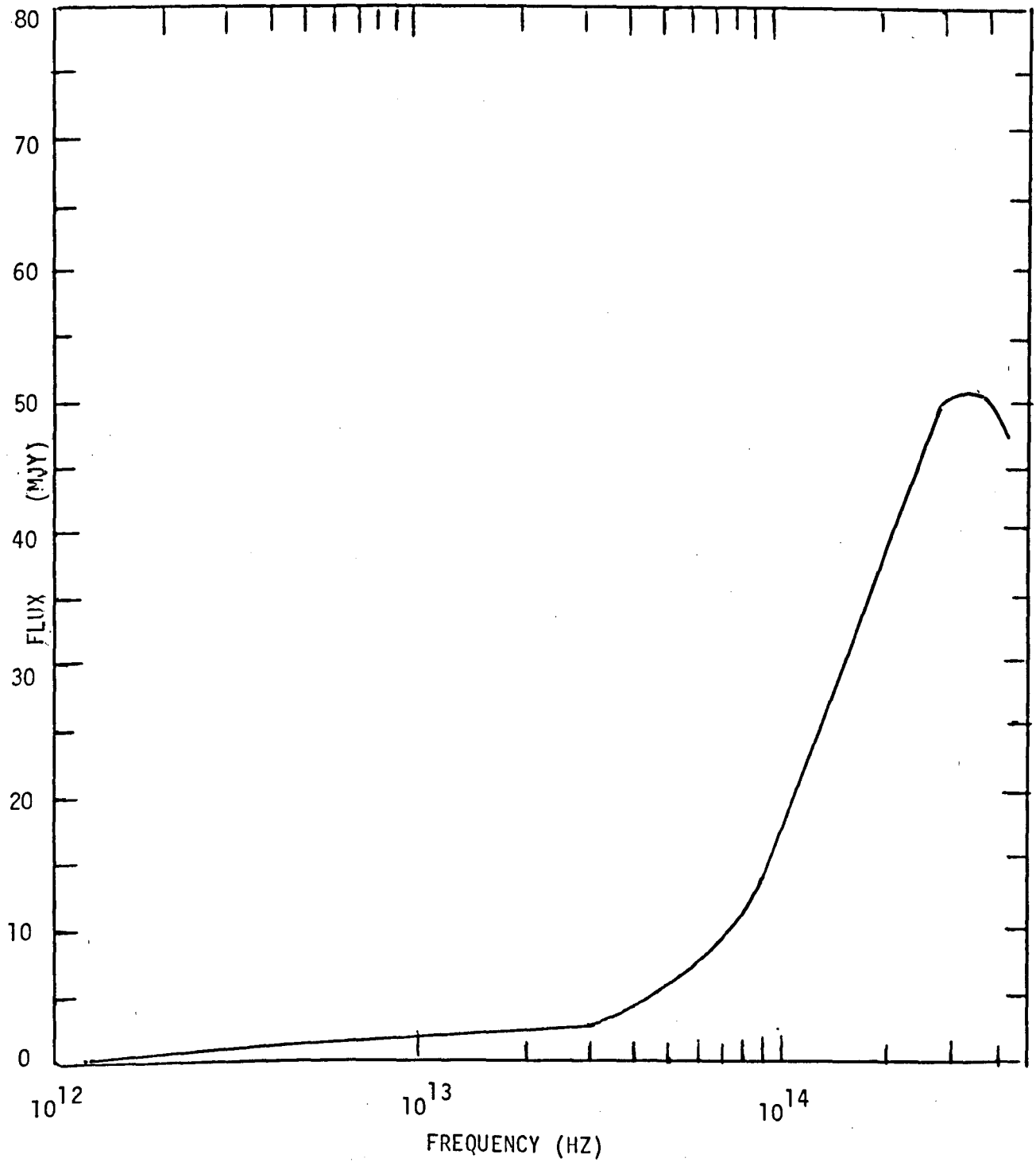
80
70
60
50
40
30
20
10
0
FLUX (MJY)
10^{12}
10^{13}
10^{14}
FREQUENCY (HZ)

FIGURE 28. Infra-red flux distribution at 360 days after outburst. I=65°, R=100pc, silicate:graphite ratio = 70:30. (Dust flux only).

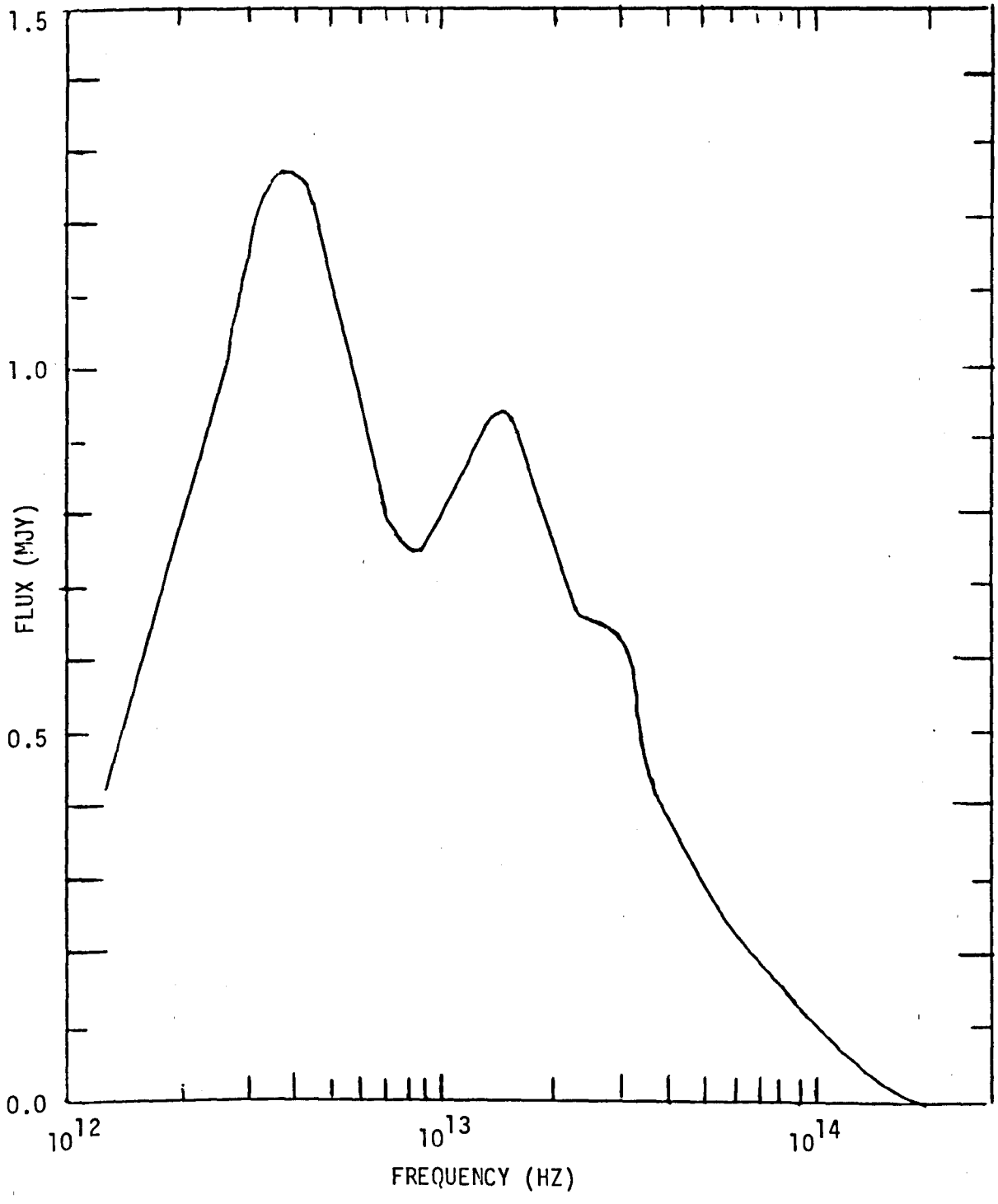
1.5
1.0
0.5
0.0
FLUX (MJY)
10^{12}
10^{13}
10^{14}
FREQUENCY (HZ)

FIGURE 29. Supernova flux distribution at 360 days after outburst.

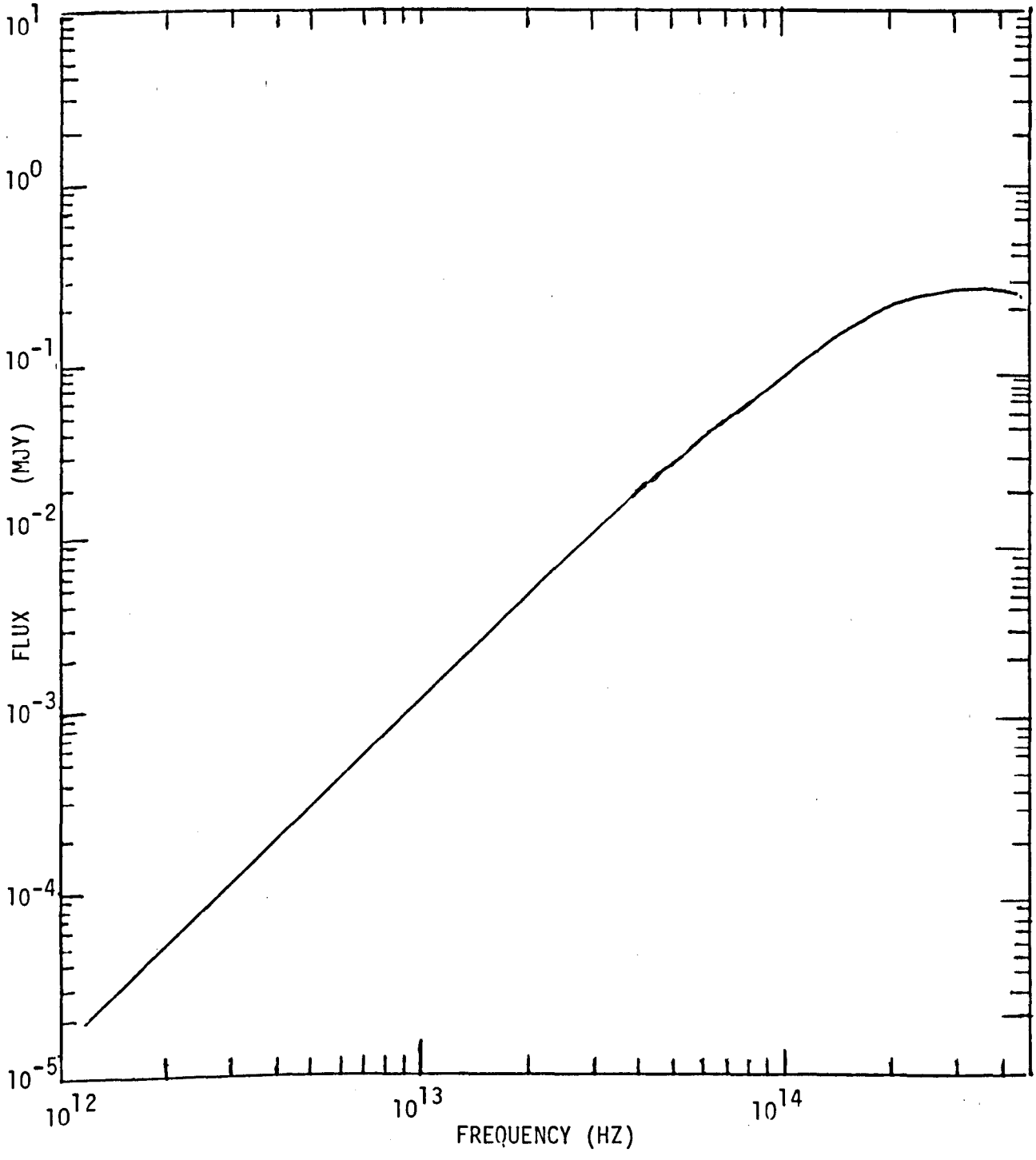
10^{1}
10^{0}
10^{-1}
10^{-2}
10^{-3}
10^{-4}
10^{-5}
FLUX (MJY)
10^{12}
10^{13}
10^{14}
FREQUENCY (HZ)

FIGURE 30. Infra-red flux distribution at 360 days after outburst. I=65°, R=100pc, silicate:graphite ratio = 70:30. (Total flux = supernova flux + dust flux).

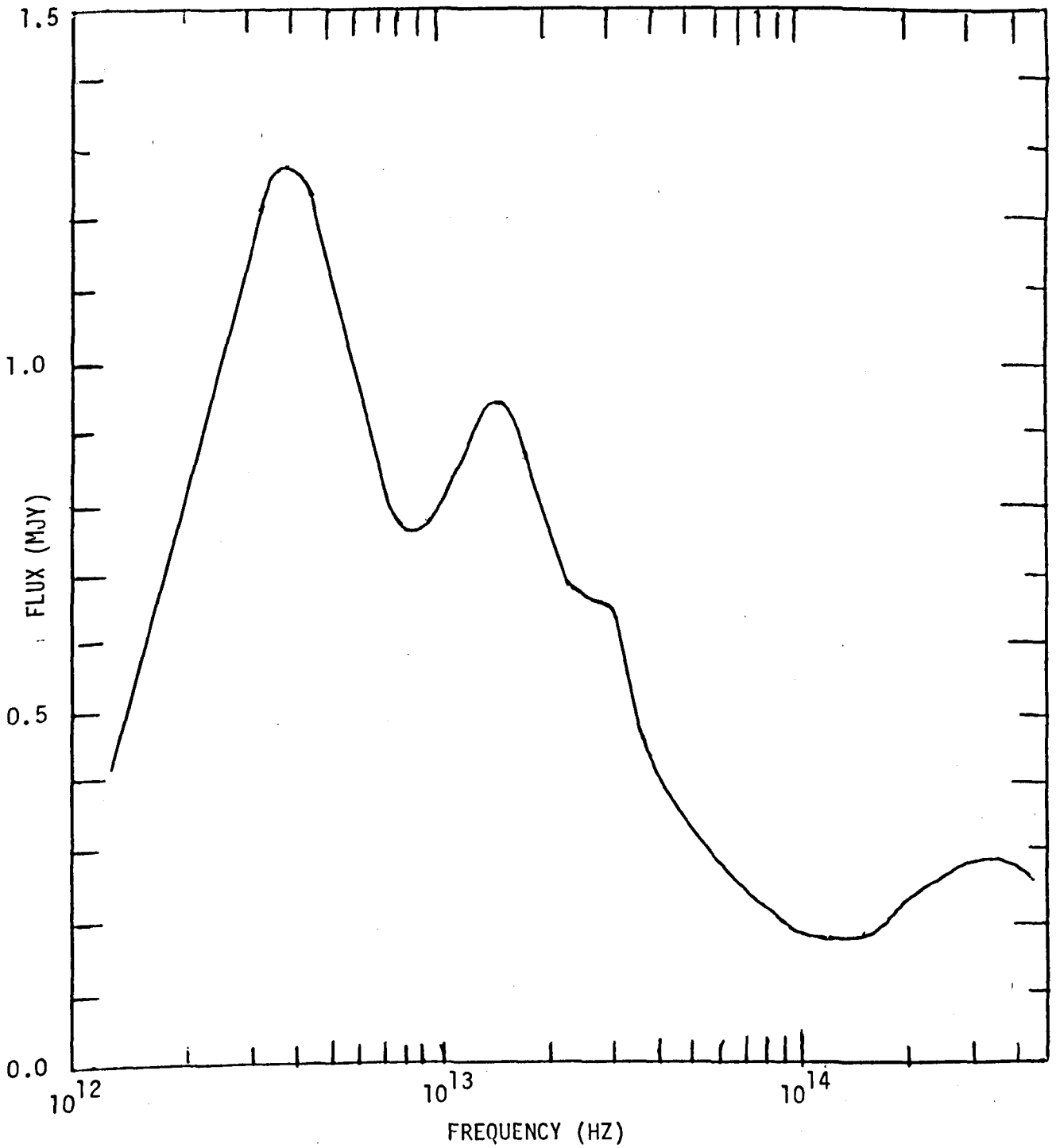
1.5
1.0
0.5
0.0
FLUX (MJY)
10^{12}
10^{13}
10^{14}
FREQUENCY (HZ)

FIGURE 31. Infra-red flux distribution at 750 days after outburst. I=65°, R=100pc, silicate:graphite ratio = 70:30. (Dust flux only).

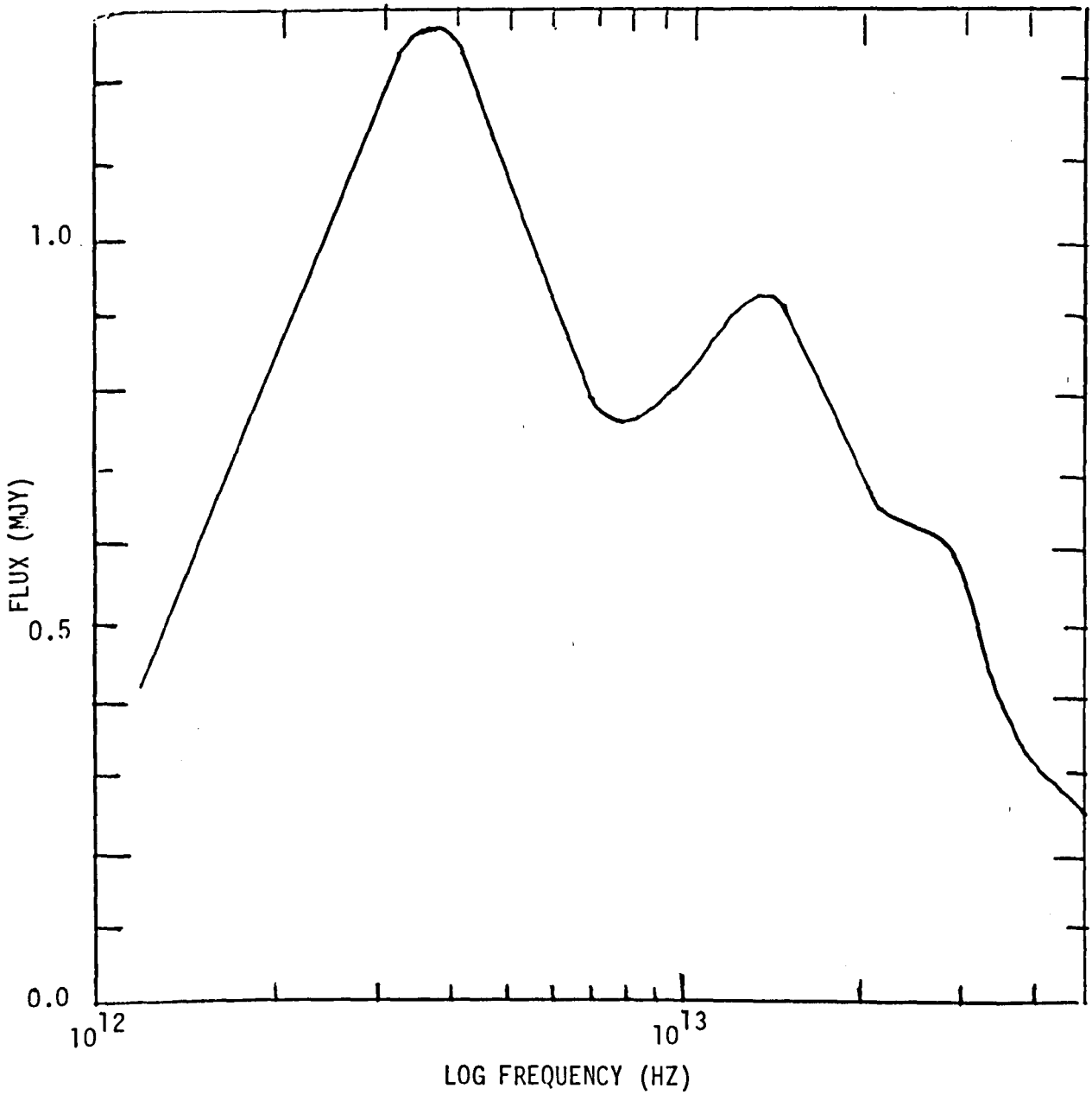
1.0
0.5
0.0
FLUX (MJY)
10^{12}
10^{13}
LOG FREQUENCY (HZ)

FIGURE 32. Infra-red flux distribution at 1800 days after outburst. $I=65^{o}$, R=100pc, silicate:graphite ratio = 70:30. (Dust flux only).

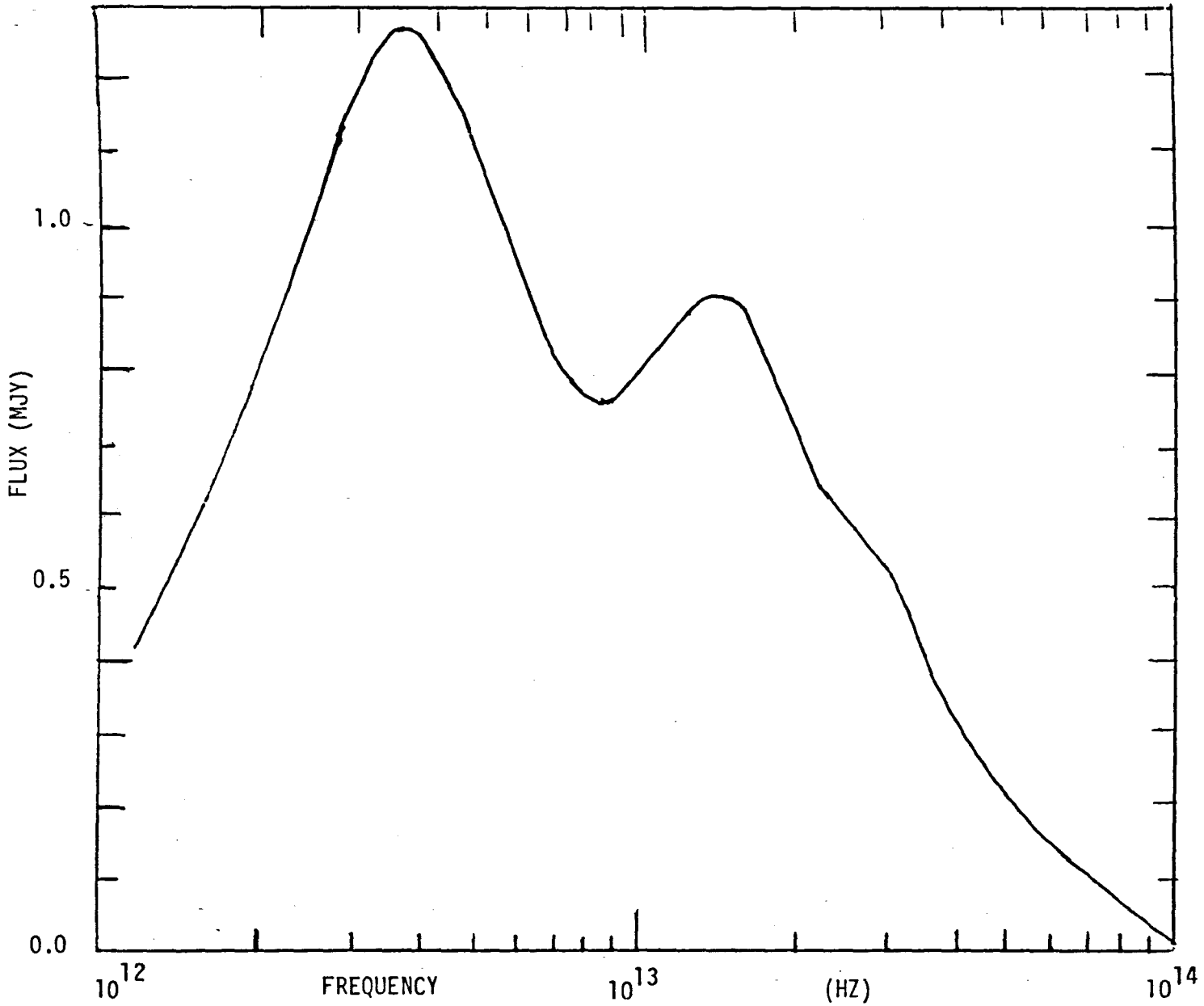
1.0
0.5
0.0
FLUX (MJY)
10^{12}
FREQUENCY
10^{13}
(HZ)
10^{14}

FIGURE 33. Infra-red flux distribution at 3600 days after outburst. $I=65^{o}$, R=100pc, silicate:graphite ratio = 70:30. (Dust flux only).

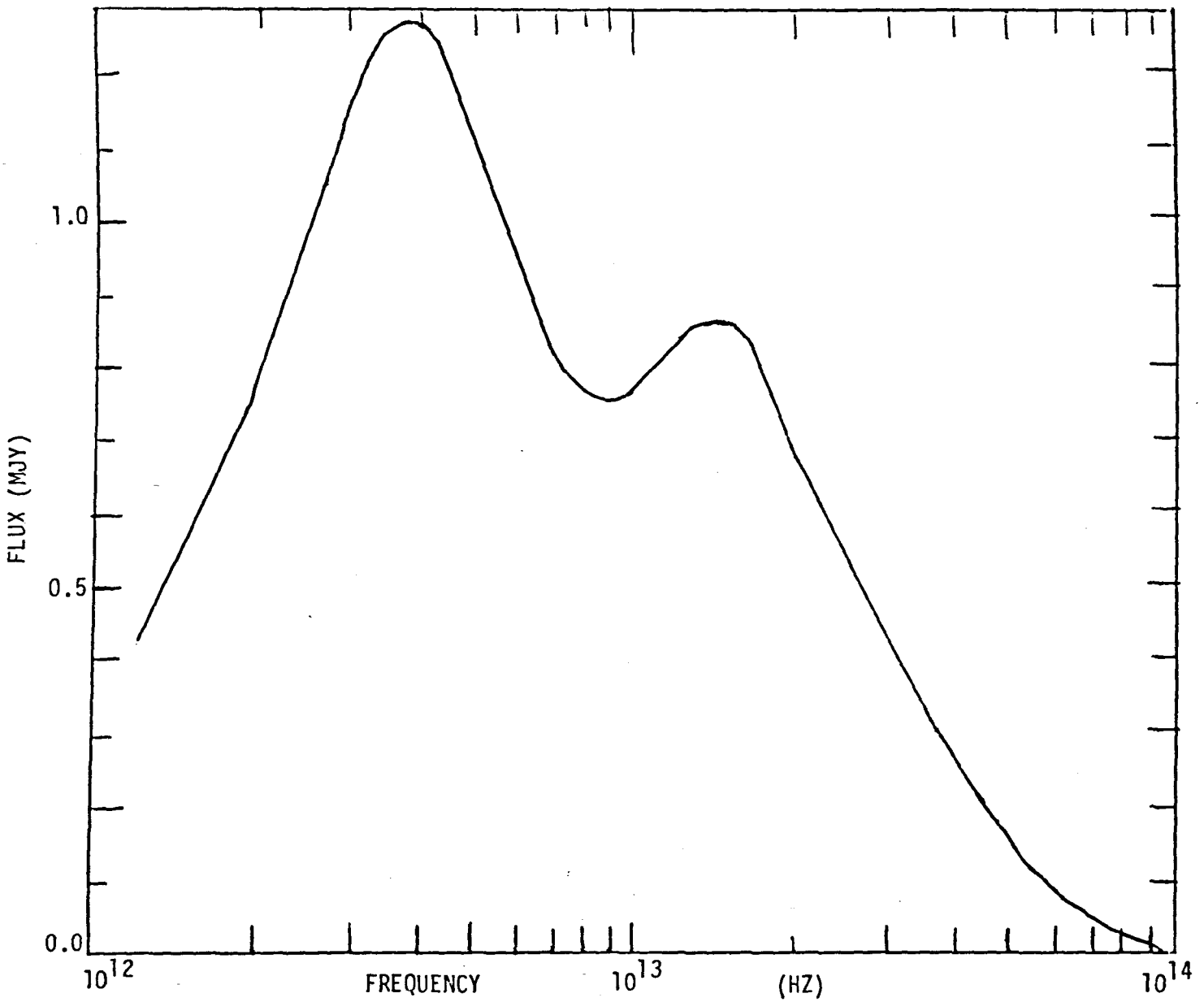
1.0
0.5
0.0
FLUX (MJY)
10^{12}
FREQUENCY
10^{13}
(HZ)
10^{14}

supernova radiation heating.

Comparison of the dust spectrum after 100 days for R=100pc and R=25pc (figure 34) shows that the 100μm peak, while differing between the two, is essentially present in both with similar flux. The difference is due to the difference in the contribution of radiation from grains heated by the supernova at these frequencies. The spectra at wavelengths short of the 10μm peak are the same suggesting that this spectrum is part of the spectrum due to hotter grains near to the cavity. The 9.8μm feature is much more clearly visible for R=25pc because the 20μm feature is very much less intense than for R=100pc. This shows that the 20μm feature must be due to the grains near the parabola which are considerably hotter than the other interstellar grains because they are heated by supernova radiation near the peak of its luminosity. These hotter grains are far fewer in number for R=25pc than for R=100pc. The 10μm feature does not suffer such a dramatic drop in intensity, but decays over time so probably comes from grains at the point where the line of sight through the supernova intersects with the paraboloid of revolution, where the maximum supernova luminosity has its greatest heating effect. The grains at this point will be the same in number for R=25pc and R=100pc but their temperatures will fall with time as the paraboloid of revolution gets further from the supernova.

A comparison of the spectra for 70:30 (70% silicate by mass and 30% graphite by mass)(figure 35) and 50:50 grain ratios shows that the flux for the 50:50 case is greater than that for the 70:30 ratio throughout the spectrum. Also the 9.8μm silicate feature is much less prominent in the 50:50 spectrum. From figure 35, it can be seen that the flux at all wavelengths >3μm is very much greater for the 50:50 silicate:graphite mass ratio than for the 70:30 silicate:graphite mass ratio. The increase is greatest for the 100μm peak at which the flux is more than 50% greater for the 50:50 silicate:graphite mass ratio. Furthermore the 9.8μm silicate feature, while recognizable for the 70:30 silicate:graphite mass ratio is

FIGURE 34. Infra-red flux distribution at 100 days after outburst for R=100pc and R=25pc. I=65^{o}, silicate:graphite ratio = 70:30. (Dust flux only).

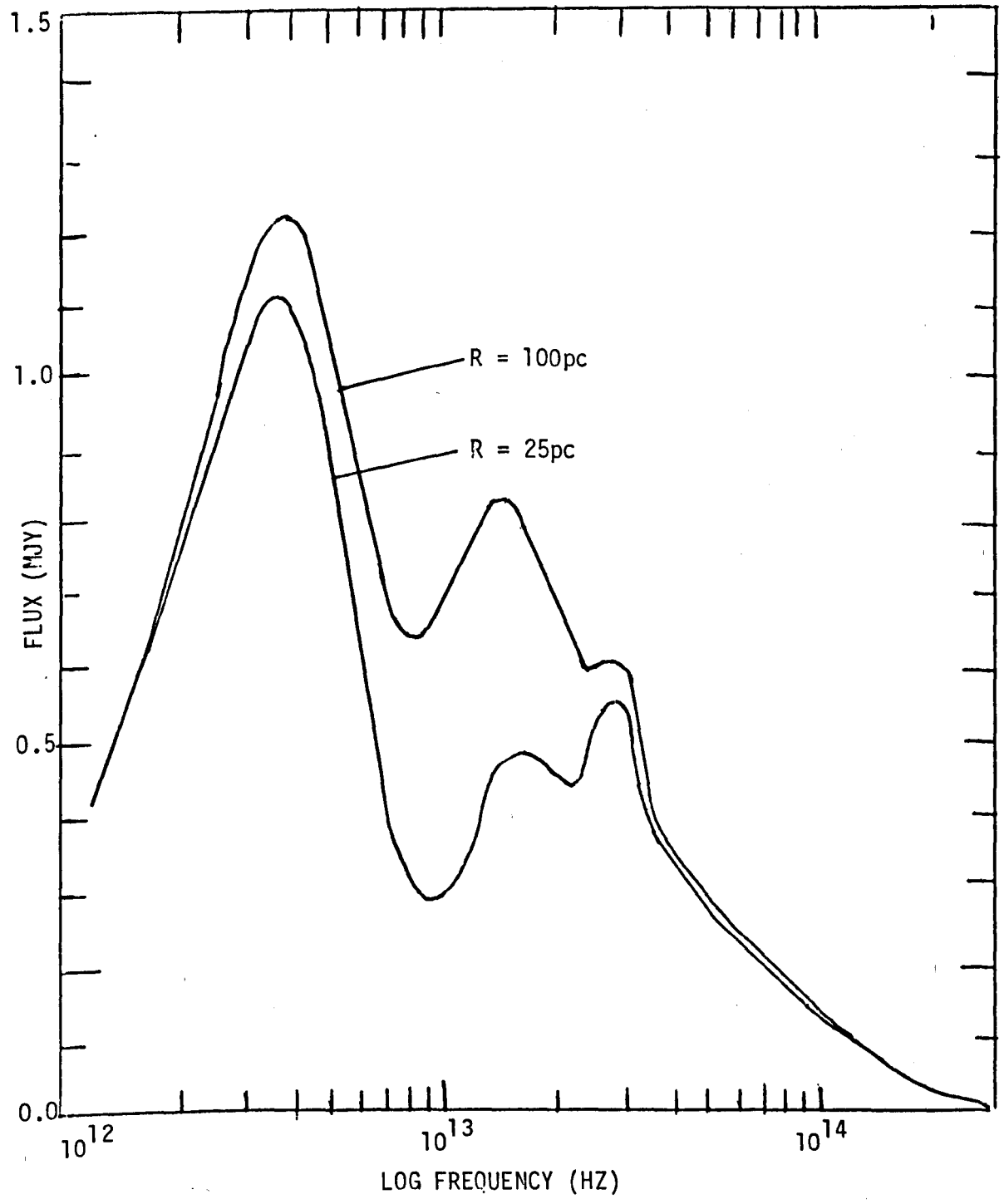
1.5
1.0
0.5
0.0
FLUX (MJY)
R = 100pc
R = 25pc
10^{12}
10^{13}
10^{14}
LOG FREQUENCY (HZ)

FIGURE 35. Infra-red flux distribution at 100 days after outburst, for 70:30 and 50:50 silicate:graphite ratios. I=65^{o}, R=100pc. (Dust flux only).

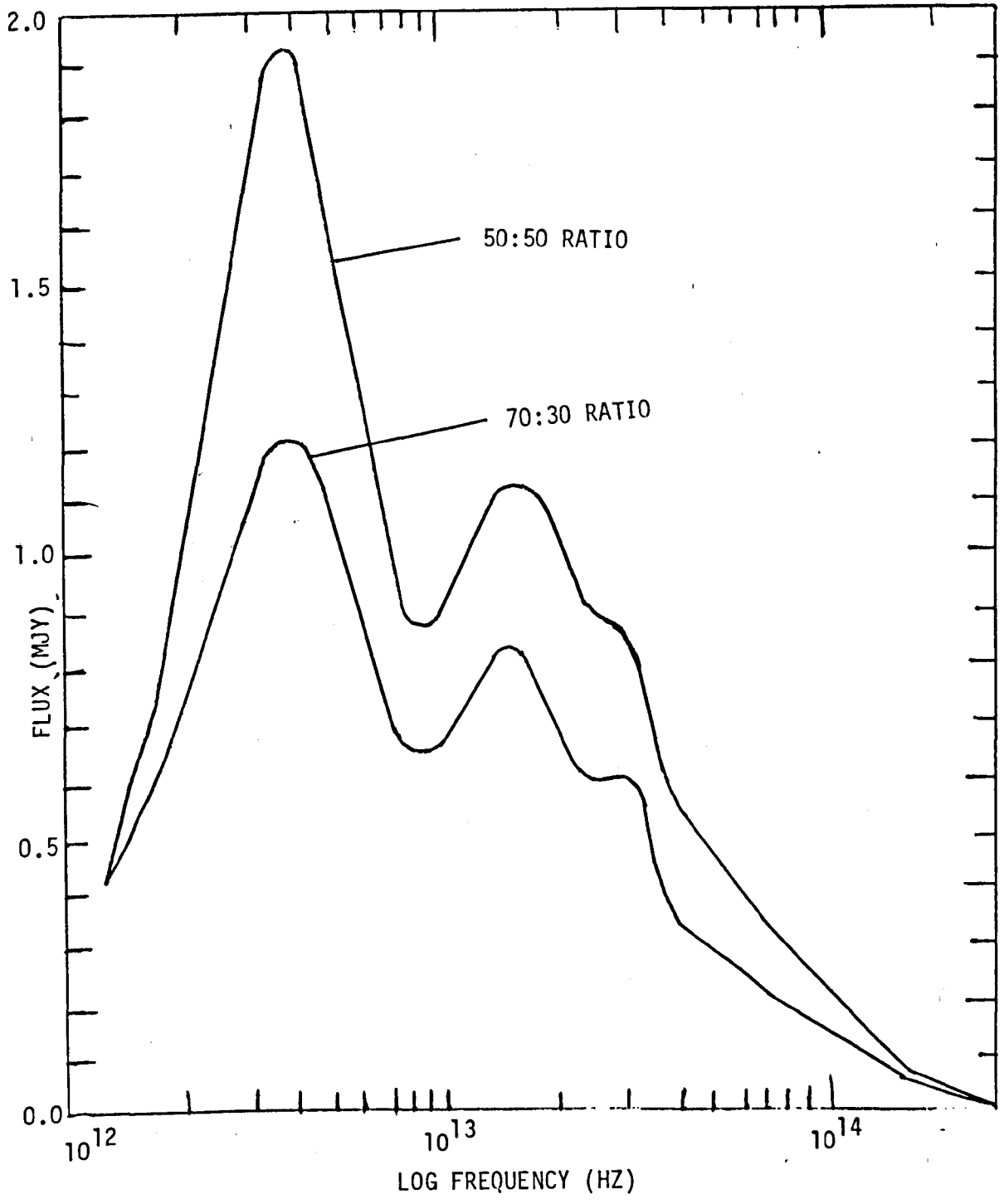
2.0
1.5
1.0
0.5
0.0
FLUX (MJY)
50:50 RATIO
70:30 RATIO
10^{12}
10^{13}
10^{14}
LOG FREQUENCY (HZ)

almost indiscernible for the 50:50 silicate:graphite mass ratio. The spectacular increase of about 50% in the flux at longer wavelengths illustrates that the graphite grains heated by ambient starlight radiate far more strongly than do silicate grains. This is not suprising for whereas the silicate grain temperature outside the paraboloid of revolution is about 14K the graph ite grain temperature outside the paraboloid of revolution is about 35K. The different optical properties of the graphite grains enable them to absorb ambient starlight much more efficiently than do the silicate grains. Inspite of the fact that the mass density of silicate grains is more than twice that of graphite grains the far infra-red radiation, peaking at about 10μm, from grains heated by ambient starlight is almost entirely all graphite grain radiation. Graphite grains make a significant contribution at all wavelenghts but the 10μm and 20μm features are obviously due to the optical properties of the silicate grains with graphite grain radiation simply moving the whole feature upwards in flux almost independently of wavelength across each feature.

A comparison of the spectra at 100 days after outburst for the cavity radii already assumed for graphite and silicate grains (see equation 5.3.1) and cavity radii that are ten times greater in each case is given in figure 36. This reveals the contribution to the spectrum of grains near the edge of the cavity. In particular these grains can be seen to make a significant contribution to the dust flux at 9.8μm. The 9.8μm silicate feature has almost disappeared in the spectrum of the increased cavity radii. As expected it has no effect on the spectrum on wavelengths longer than 30μm, and very little effect on the 20μm feature, which is probably due to the grains at all parts of the paraboloid rather than those specifically at the point where the line of sight through the supernova intersects with the paraboloid of revolution near to the edge of the cavity.

Figure 37 shows a comparison of the heating due to background starlight only compared to the heating of interstellar grains by the

FIGURE 36. Infra-red flux distribution at 100 days after outburst, for cavity radii 1 x initial value and 10 x initial value. I=65°, R=100pc, silicate:graphite ratio = 70:30. (Dust flux only).

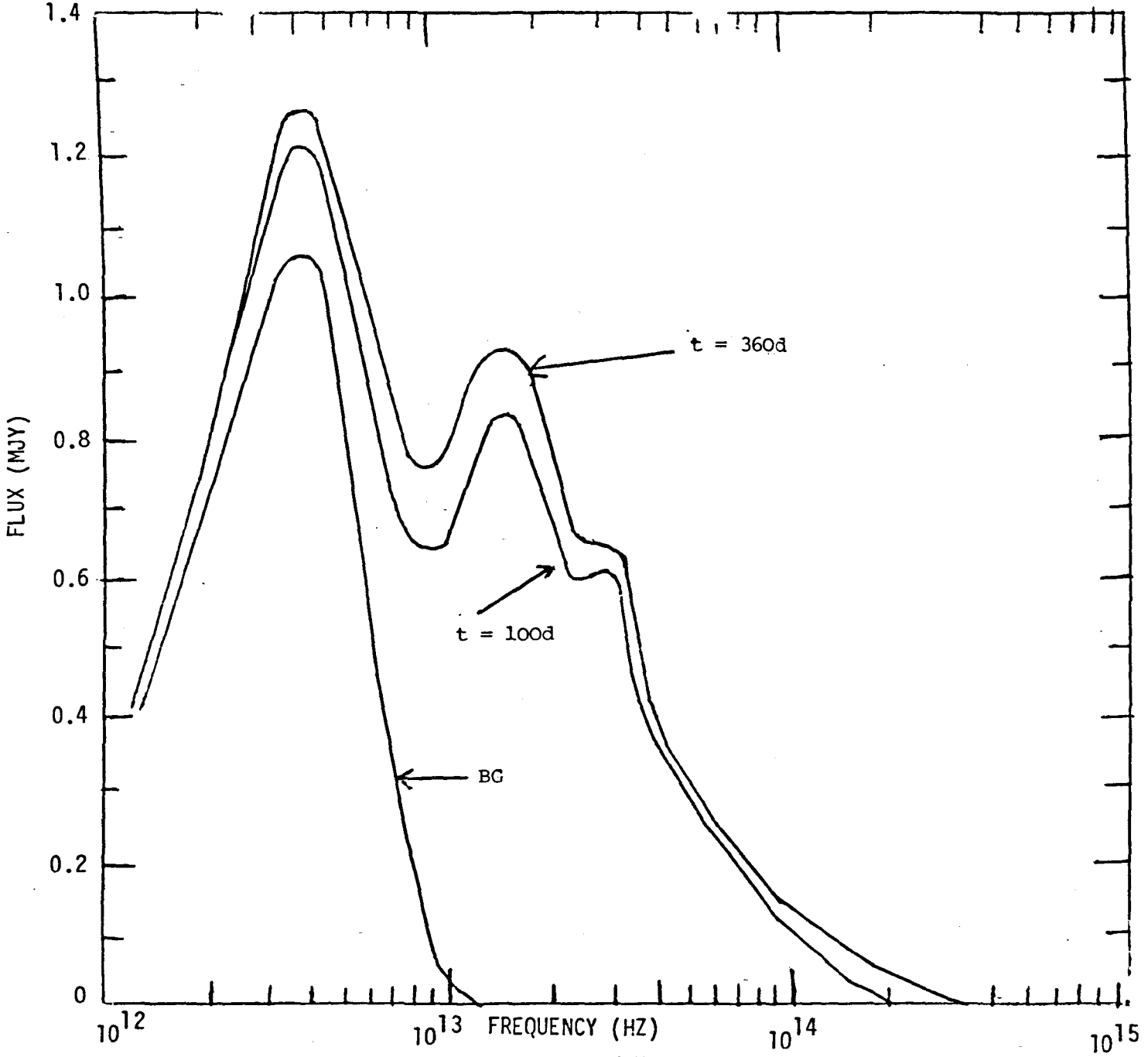
1.4
1.2
1.0
0.8
0.6
0.4
0.2
0
FLUX (MJY)
t = 360d
t = 100d
BG
10^{12}
10^{13}
FREQUENCY (HZ)
10^{14}
10^{15}

FIGURE 37. Infra-red dust flux distribution at 100 days and 360 days after outburst compared with the infra-red flux distribution of dust heated by background starlight only. $I=65^{o}$, R=100pc.

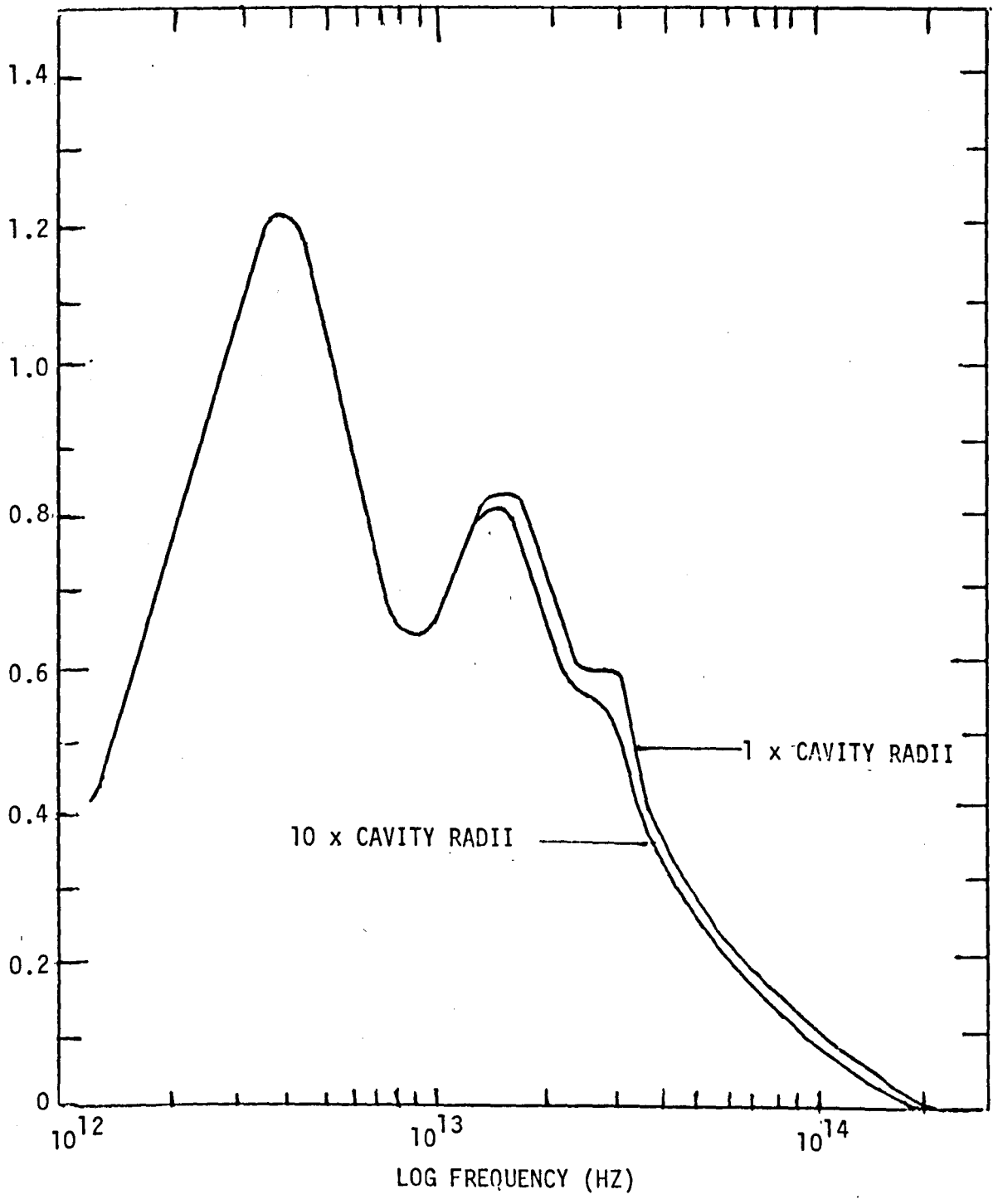
1.4
1.2
1.0
0.8
0.6
0.4
0.2
0
10^{12}
10^{13}
10^{14}
LOG FREQUENCY (HZ)
1 x CAVITY RADII
10 x CAVITY RADII

supernova (plus background heating by starlight at t=100 days and t=360 days after outburst).

Figure 38 shows the flux emitted at 5μm from the supernova itself as a function of time. By comparing these two figures (figures 37 and 38) it can be seen that only at relatively late times (t~4 years after outburst) would the background flux (due to heating by starlight of interstellar grains) become comparable to the heating of the interstellar grains by the supernova, since the supernova radiation would provide negligible heating effect at ~3 to 4 years after outburst.

5.4 Conclusion

In this chapter the effect of heating interstellar grains by an erupting supernova and background starlight has been considered. It is concluded that the infra-red flux emitted from grains at far infra-red wavelengths (λ~100μm) is due primarily to the heating of the grains by background starlight. The infra-red emission from grains at relatively near infra-red wavelengths (λ~5μm to 24μm) is due to heating of grains by the erupting supernova. To-date no such far infra-red observations have been recorded, and so a direct comparison of observations with the model described in chapter 5 is not yet possible. The effects of various background radiations are not serious, provided observations are made away from the galactic plane and the ecliptic, so that the diffuse emission of interstellar and interplanetary dust is avoided. Such observations could be undertaken with, for example, the Shuttle Infra-Red Telescope Facility. Therefore, it would be worthwhile observing recent supernovae up to ten years after outburst at far infra-red wavelengths.

FIGURE 38. Supernova flux distribution at 5μm.

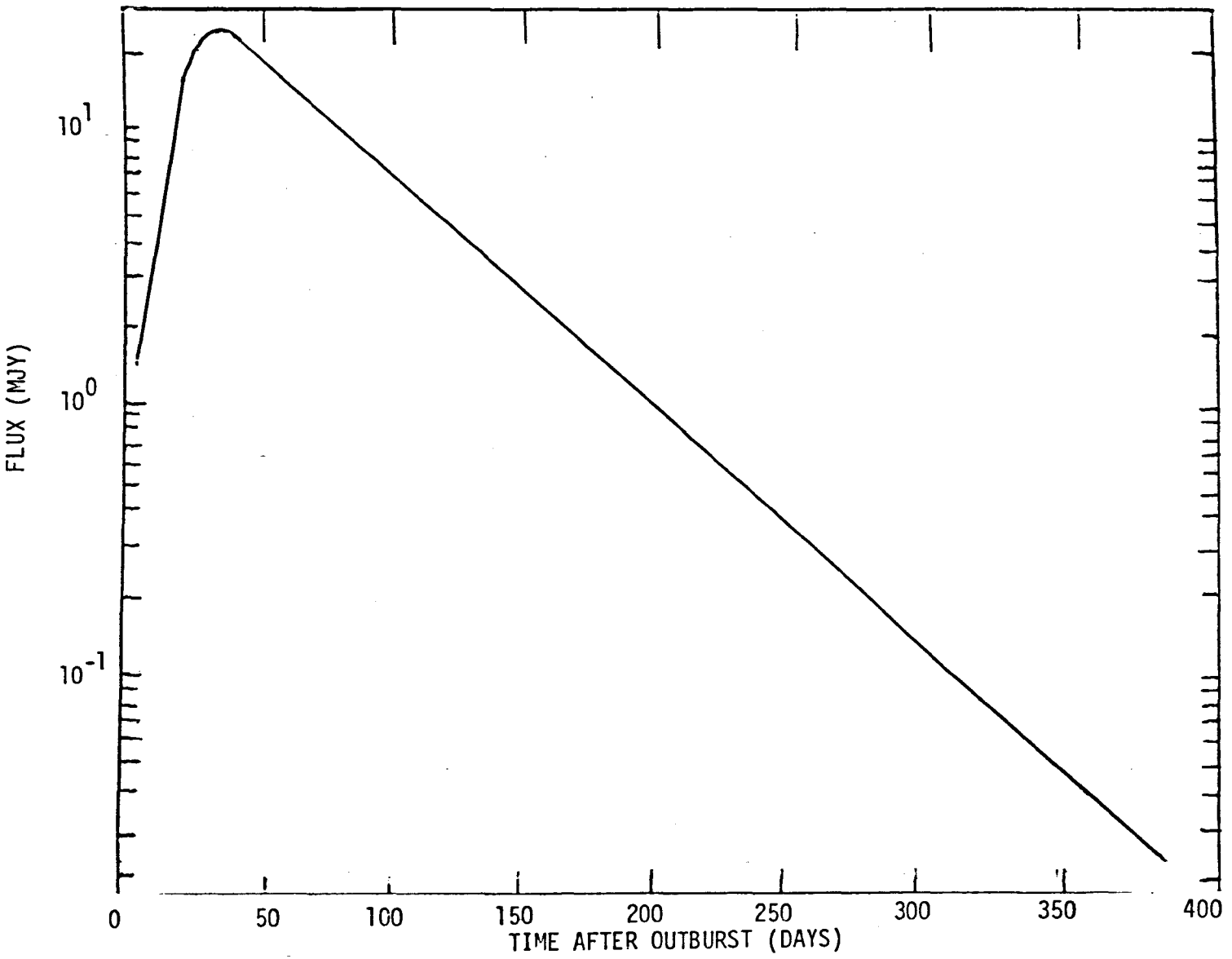
FLUX (MJY)
10^1
10^0
10^{-1}
0
50
100
150
200
250
300
350
400
TIME AFTER OUTBURST (DAYS)

CHAPTER 6

THE COMPUTATION OF EMISSION FROM CIRCUMSTELLAR DUST GRAINS.

6.0 Introduction.

The radiation from the supernovae SN1979c (Merrill, 1980) and SN1980k (Dwek et al. 1983) have been found to show an infra-red excess at times later than ~ 200 days after outburst. It is thought that this infra-red excess is due to radiation from circumstellar dust grains. A model is therefore set up to compute the flux from a circumstellar dust shell around a supernova in order to determine some characteristics of the circumstellar dust shells around these two supernovae. The model parameters giving the closest approximation to the observational data from these supernovae will be taken as giving the best description of their respective circumstellar dust shells.

6.1 The Circumstellar Dust Grain Population.

It is assumed that all grains in the circumstellar shell are spherical, homogeneous, of the same radius, a_c, and are of the same composition and density s_c.

The circumstellar grains are assumed to form a spherical shell, the cavity radius being R_c (the inner radius of the dust shell), and outer radius R_1 (if interstellar grains are to be considered along with circumstellar grains, the outer radius should be put equal to the cavity radius of the interstellar dust plane slab), centred on the supernova. The number density of the circumstellar dust grains is given by:-

$$N_c(r)=N_{oc}r^{-\beta} \qquad R_c<r<R_1$$
$$=0 \qquad \text{otherwise} \qquad (6.1.1)$$

where $\beta=0$, 1 or 2. A value of $\beta=0$ corresponds to a constant grain number density throughout the dust shell, while $\beta=2$ corresponds to an equal number of grains in any thin spherical shell whatever its distance from the supernova. The case of $\beta=2$ would occur if a shell condensed from uniformly outflowing material, while lower values of β would correspond to more material near the outer edges of the shell. Assuming that the circumstellar shell has a total mass M_g

$$M_g = \int_{R_c}^{R_1} N_c(r)\frac{4\pi}{3}a_c^3 s_c 4\pi r^2 dr \qquad (6.1.2)$$

Substituting equation (6.1.1) into equation (6.1.2) yields equation (6.1.3) which expresses N_{oc} in terms M_g, R_1, and R_c.

$$N_{oc}= \frac{3(3-\beta)M_g}{16\pi^2 a_c^3 s_c (R_1^{3-\beta} - R_c^{3-\beta})} \qquad (6.1.3)$$

It is assumed that all the grains in the circumstellar shell are always in thermodynamic equilibrium with radiation from the supernova. It is also assumed that all grains in the circumstellar dust shell are of constant radius, that is, grains are neither evaporating nor growing.

It is further assumed that the circumstellar dust shell was sufficiently optically thin to grain heating radiation from the supernova and to infra-red radiation from the grains that heating of grains due to radiation emitted by other grains is negligible compared to heating of grains due to radiation emitted by the supernova. For the models to be discussed below the infra-red optical depth is negligible. It can be seen from figure 57 that the optical depth in the infra-red is less than unity, except at around the 10μm and 20μm peaks. However it is assumed that the

number density of grains is sufficient to ensure that the amount of radiation in any given frequency interval scattered out of a light path through the circumstellar dust shell by grains, is equal to the amount of radiation in the same frequency interval scattered into the same light path by grains. Consequently the net extinction of radiation along a light path through the circumstellar dust shell is the extinction due to absorption (by grains) only.

The parameter $N_{c\nu}$ is defined as follows:-

$$N_{c\nu}=N_{oc}\pi a_c^2 Q_{abs}(a_c,\nu) \qquad (6.1.4)$$

to simplify the coefficient in equation (6.1.6) below. The optical depth to any interstellar grain radiation from behind the circumstellar dust shell due to absorption by circumstellar dust grains is likely to be negligible but is included for completeness. It is given by:-

$$\tau_{\beta\nu}(\rho)=\pi a_c^2 Q_{abs}(a_c,\nu) \int_{-(R_1^2-\rho^2)^{\frac{1}{2}}}^{(R_1^2-\rho^2)^{\frac{1}{2}}} N_c(\rho,x)dx \qquad (6.1.5)$$

susbstituting equation (6.1.4) into equation (6.1.5)

$$\tau_{\beta\nu}(\rho)=N_{c\nu} \int_{-(R_1^2-\rho^2)^{\frac{1}{2}}}^{(R_1^2-\rho^2)^{\frac{1}{2}}} (\rho^2+x^2)^{-\beta/2}\, dx \qquad \text{for } R_c\leq\rho<R_1$$

$$=2N_{c\nu}(R_1^2-\rho^2)^{\frac{1}{2}} \qquad \text{for } \beta=0.$$

$$=2N_{c\nu}\ln(((R_1^2-\rho^2)^{\frac{1}{2}}+R_1)/(-(R_1^2-\rho^2)^{\frac{1}{2}}+R_1)) \qquad \text{for } \beta=1.$$

$$\text{for } R_c\leq\rho<R_1$$

$$=2N_{c\nu}\rho^{-1}\tan^{-1}((R_1^2-\rho^2)^{\frac{1}{2}}/\rho) \qquad \text{for } \beta=2.$$

$$=N_{c\nu}\left(\int_{-(R_1^2-\rho^2)^{\frac{1}{2}}}^{-(R_c^2-\rho^2)^{\frac{1}{2}}} (\rho^2+x^2)^{-\beta/2}dx + \int_{(R_c^2-\rho^2)^{\frac{1}{2}}}^{(R_1^2-\rho^2)^{\frac{1}{2}}} (\rho^2+x^2)^{-\beta/2}dx\right)$$

$$=2N_{c\nu}((R_1^2-\rho^2)^{\frac{1}{2}}-(R_c^2-\rho^2)^{\frac{1}{2}}) \qquad \text{for } \beta=0.$$

$$\text{for } 0\leq\rho<R_c$$

FIGURE 39. The coordinate system for circumstellar dust grains.

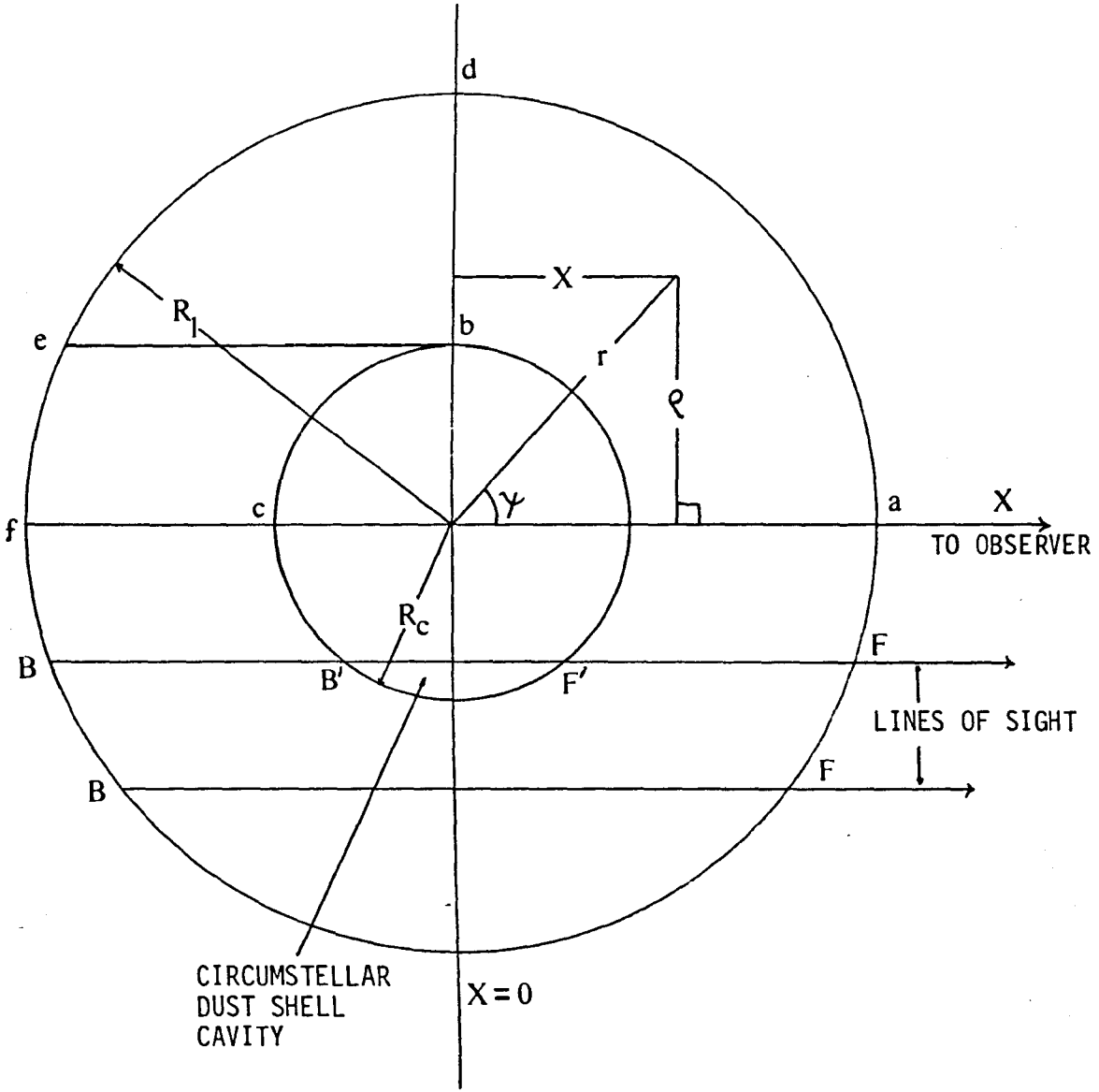
d
X
R_1
e
b
r
ϱ
c
ψ
a
X
f
TO OBSERVER
R_c
F
B
B'
F'
LINES OF SIGHT
F
B
CIRCUMSTELLAR
DUST SHELL
CAVITY
X=0

$$= N_{C\nu}\left(\ln\left(\left((R_1^2-\rho^2)^{\frac{1}{2}}+R_1\right)/\left((R_C-\rho^2)^{\frac{1}{2}}+R_C\right)\right)\right. \qquad \text{for } \beta=1.$$
$$\left.+\ln\left((-R_C^2-\rho^2)^{\frac{1}{2}}+R_C\right)/\left(-(R_1^2-\rho^2)^{\frac{1}{2}}+R_1\right)\right)$$
$$=2N_{C\nu}\rho^{-1}\left(\tan^{-1}\left((R_1^2-\rho^2)^{\frac{1}{2}}/\rho\right)-\tan^{-1}\left((R_C^2-\rho^2)^{\frac{1}{2}}/\rho\right)\right) \qquad \text{for } \beta=2.$$
$$=0 \qquad \text{for } \rho>R_1$$
(6.1.6)

Equations (6.1.5) and (6.1.6) represent the expressions for the optical depth to interstellar grain radiation from behind the circumstellar dust due to absorption by circumstellar dust grains.

6.2 The Flux Computation.

A different coordinate system is used to the interstellar case. Instead of x the variable ψ is used and is defined by (see figure 39)

$$x=\rho\cot\psi \qquad (6.2.1)$$

or $$r=\rho\,\mathrm{cosec}\psi \qquad (6.2.2)$$

Differentiating equation (6.2.2) gives

$$\left(\frac{\partial r}{\partial \psi}\right)_\rho = -\rho\cot\psi\,\mathrm{cosec}\psi \qquad (6.2.3)$$

As

$$dx = -\left(r^2+\left(\frac{\partial r}{\partial \psi}\right)_\rho^2\right)d\psi \qquad (6.2.4)$$

substit uting (6.2.4) and (6.2.3) into (6.2.4)

$$dx = -\rho\,\mathrm{cosec}^2\psi\,d\psi \qquad (6.2.5)$$

From substitiuting equation (6.2.4) in (3.5.3)

$$\tau(\rho,\psi,t) = t+\left(\frac{\rho}{c}\right)(\cot\psi-\mathrm{cosec}\psi) \qquad (6.2.6)$$

where the second term in the expression represents the light travel time across the dust shell. From equations (3.5.6), (3.5.7) and (6.2.2) the

function f_β used in the optical depth expressions is given by

$$\begin{aligned} f_\beta(R_c,r) &= \rho\,\mathrm{cosec}\psi - R_c && \text{for } \beta=0 \\ &= \ln(\rho/R_c\sin\psi) && \text{for } \beta=1 \\ &= R_c^{-1} - \rho^{-1}\sin\psi && \text{for } \beta=2 \end{aligned} \qquad (6.2.7)$$

Defining the values of ψ as a function of ρ and t at points P, F, F', B and B' in figure 39 as $\psi(P)$, $\psi(F)$, $\psi(F')$, $\psi(B)$ and $\psi(B')$ respectively

$$\begin{aligned} \psi(P) &= \tan^{-1}\,(2ct\rho/(\rho^2-c^2t^2)) && \text{for } \rho>ct \\ &= \pi/2 && \text{for } \rho=ct \\ &= \pi-\tan^{-1}\,(2ct\rho/(\rho^2-c^2t^2)) && \text{for } \rho<ct \end{aligned} \qquad (6.2.8)$$

$$\psi(F) = \tan^{-1}\,(\rho/(R_1^2-\rho^2)^{\frac{1}{2}}) \qquad (6.2.9)$$

$$\psi(F') = \tan^{-1}\,(\rho/(R_c^2-\rho^2)^{\frac{1}{2}}) \qquad (6.2.10)$$

$$\psi(B) = \pi-\tan^{-1}\,(\rho/(R_1^2-\rho^2)^{\frac{1}{2}}) \qquad (6.2.11)$$

$$\psi(B') = \pi-\tan^{-1}\,(\rho/(R_c^2-\rho^2)^{\frac{1}{2}}) \qquad (6.2.12)$$

Equation (6.2.8) is derived from substituting equation (6.2.1) into the paraboloid equation (5.1.9) while (6.2.9) to (6.2.12) inclusive are derived from equation (6.2.1) and from the following equations

$$x(F) = (R_1^2-\rho^2)^{\frac{1}{2}} \qquad (6.2.13)$$

$$x(F') = (R_c^2-\rho^2)^{\frac{1}{2}} \qquad (6.2.14)$$

$$x(B) = -(R_1^2-\rho^2)^{\frac{1}{2}} \qquad (6.2.15)$$

and

$$x(B') = -(R_c^2-\rho^2)^{\frac{1}{2}} \qquad (6.2.16)$$

Where the paraboloid crosses the cavity surface of the circumstellar dust shell, from equation (5.1.19)

$$\rho = (2ctR_c - c^2t^2)^{\frac{1}{2}} \qquad (6.2.17)$$

Similarly where the paraboloid crosses the outer surface of the circumstellar dust shell.

$$\rho = (2ctR_1 - c^2t^2)^{\frac{1}{2}} \qquad (6.2.18)$$

In figure 39 the paraboloid crosses point a at time ct=0, b at time $ct=R_c$, c at time $ct=2R_c$, d at time $ct=R_1$, e at time $ct=R_1+(R_1^2-R_c^2)^{\frac{1}{2}}$ (as $\rho=R_c$ and $\rho=(2ctR_1-c^2t^2)^{\frac{1}{2}}$ so $c^2t^2-2ctR_1+R_c^2=0$), and f at time $ct=2R_1$.

The order in which the paraboloid crosses the different points varies according to the thickness of the dust shell. Denoting the times at which the paraboloid crosses points a, b, c, d, e and f respectively by t(a), t(b), t(c), t(d), t(e) and t(f), we have the following conditions.

If
$$R_1 > 2R_c, \quad t(a)<t(b)<t(c)<t(d)<t(e)<t(f).$$
If
$$t(c)<t(e), \quad 2R_c<R_1+(R_1^2-R_c^2)^{\frac{1}{2}}$$
So
$$R_1 > \frac{5R_c}{4}.$$

Consequently, if

$$\frac{5R_c}{4}<R_1<2R_c, \quad t(a)<t(b)<t(d)<t(c)<t(e)<t(f)$$

but if

$$R_c<R_1<\frac{5R_c}{4}, \quad t(a)<t(b)<t(d)<t(e)<t(c)<t(f).$$

There are a total of eight possible cases for the position of the paraboloid of revolution relative to the circumstellar dust shell, involving a total of twelve sets of limits on ρ and ψ for the regions of the circumstellar dust shell observed to be illuminated by the supernova. The eight cases are illustrated in figures 40 to 47 inclusive and the conditions in terms of R_c, R_1 and ct under which they apply are given in the captions to the figures. The regions of integration in each case are

FIGURE 40. The circumstellar dust shell, case 1 : $ct < R_c$.

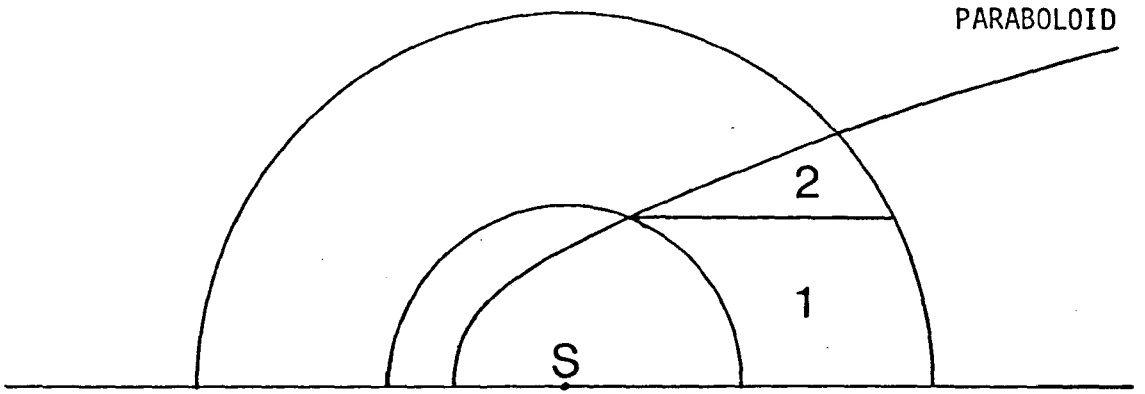
PARABOLOID
2
1
S

FIGURE 41. The circumstellar dust shell, case 2 : $R_c < ct < R_1$ and $R_1 < 2R_c$, or $R_c < ct < 2R_c$ and $R_1 > 2R_c$

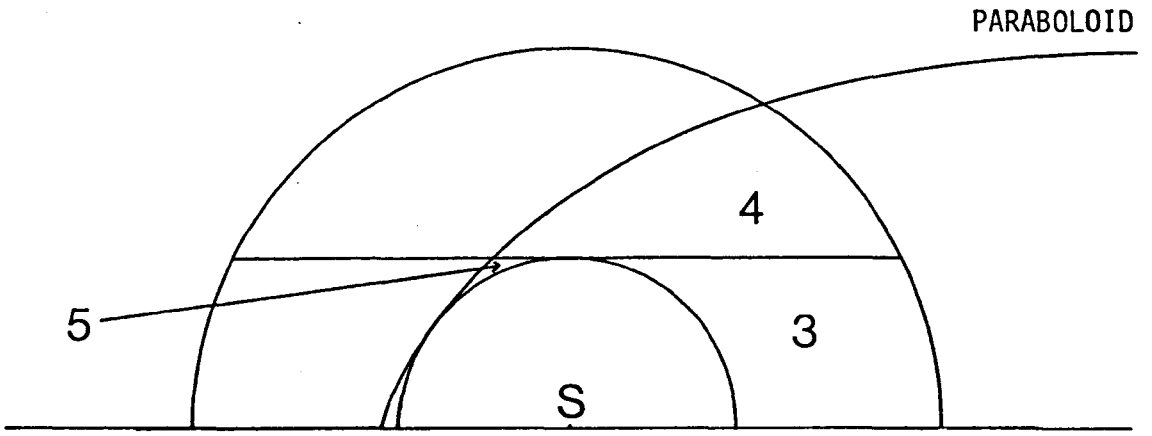
PARABOLOID
4
5
3
S

FIGURE 42. The circumstellar dust shell, case 3 : $2R_c < ct < R_1$ and $R_1 > 2R_c$.

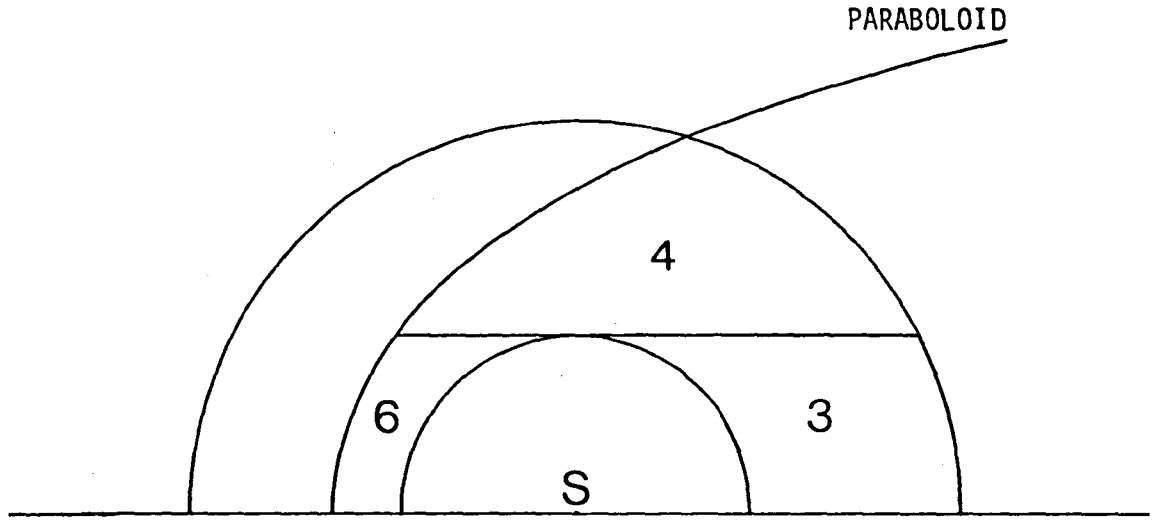
PARABOLOID
4
6
3
S

FIGURE 43. The circumstellar dust shell case 4 : $2R_1 < ct < 2R_c$ and $1.25R_c < R_1 < 2R_c$ or $R_1 < ct < R_1 + (R_1^2 - R_c^2)$ and $R_c < R_1 < 1.25R_c$.

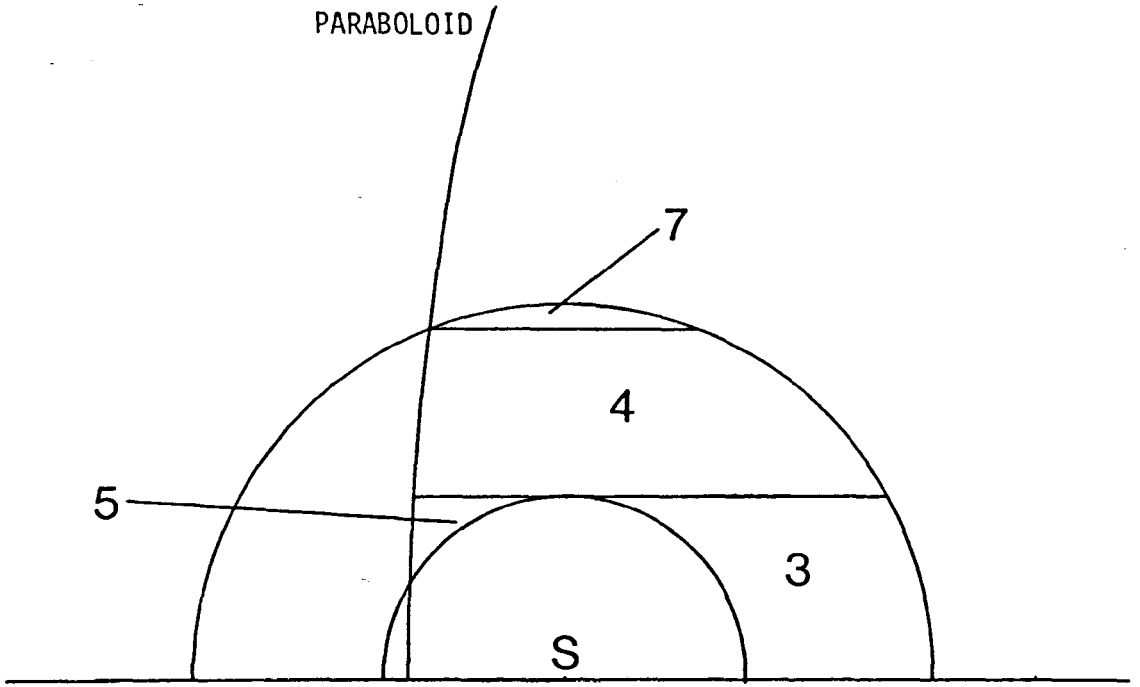
PARABOLOID
7
4
5
3
S

FIGURE 44. The circumstellar dust shell, case 5 : $R_1 < ct < R_1 + (R_1^2 - R_c^2)$ and $R_1 > 2R_c$ or $2R_c < ct < R_1 + (R_1^2 - R_c^2)$ and $1.25R_c < R_1 < 2R_c$.

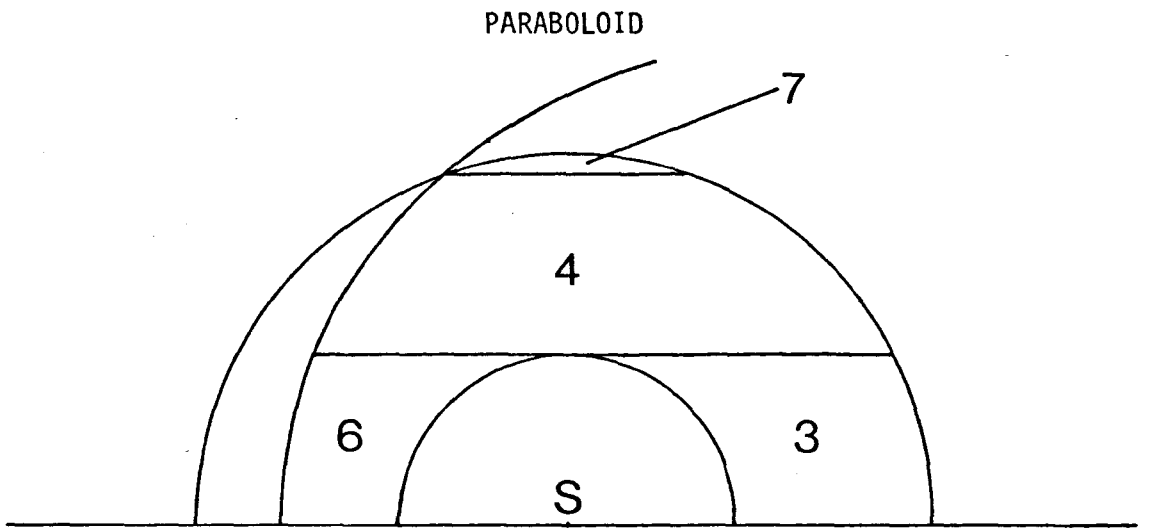
PARABOLOID
7
4
6
3
S

FIGURE 45. The circumstellar dust shell, case 6 : $R_1 + (R_1^2 - R_c^2) < ct < 2R_c$ and $R_c < R_1 < 1.25R_c$.

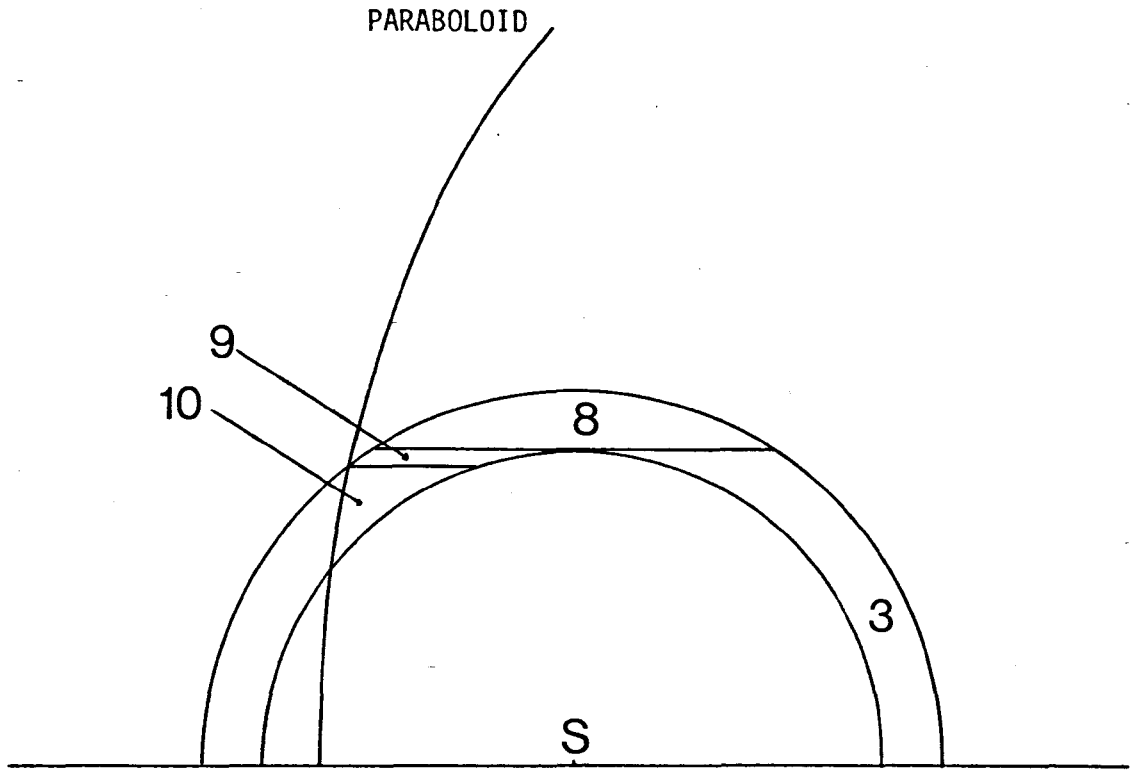
PARABOLOID
9
10
8
3
S

FIGURE 46. The circumstellar dust shell, case 7 : $R_1 + (R_1^2 - R_c^2) < ct <$ $2R_1$ and $R_1 > R_c$ or $2R_c < ct < 2R_1$ and $R_c < R_1 < 1.25R_c$.

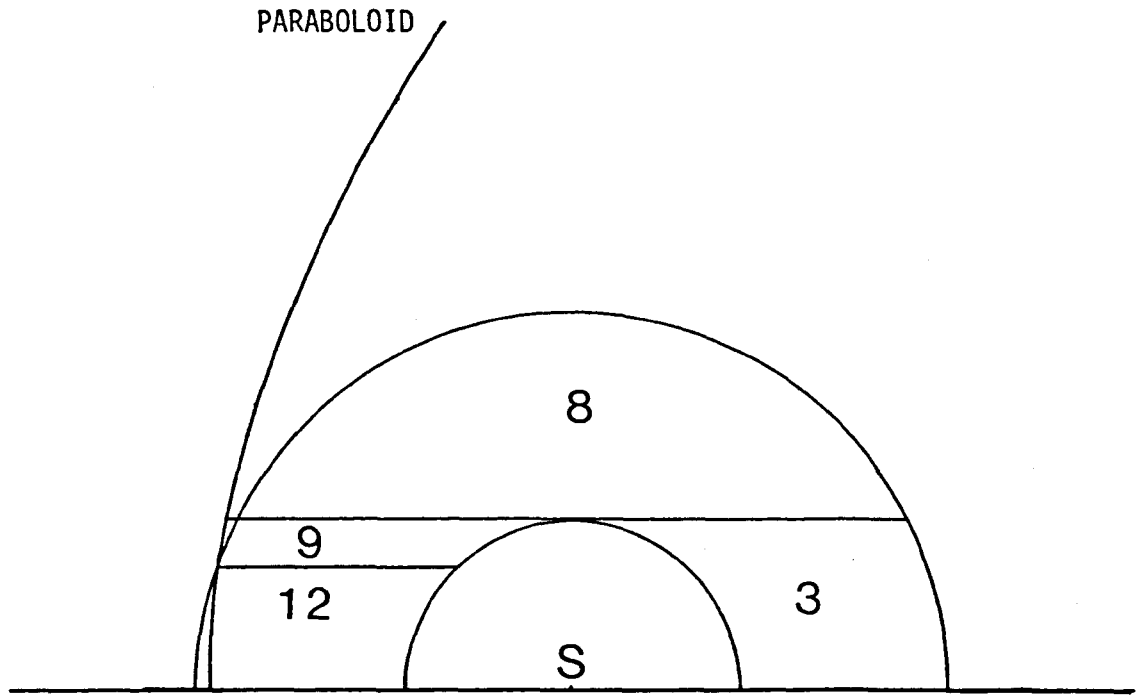
PARABOLOID
8
9
12
3
S

FIGURE 47. The circumstellar dust shell, case 8 : $ct > 2R_1$.

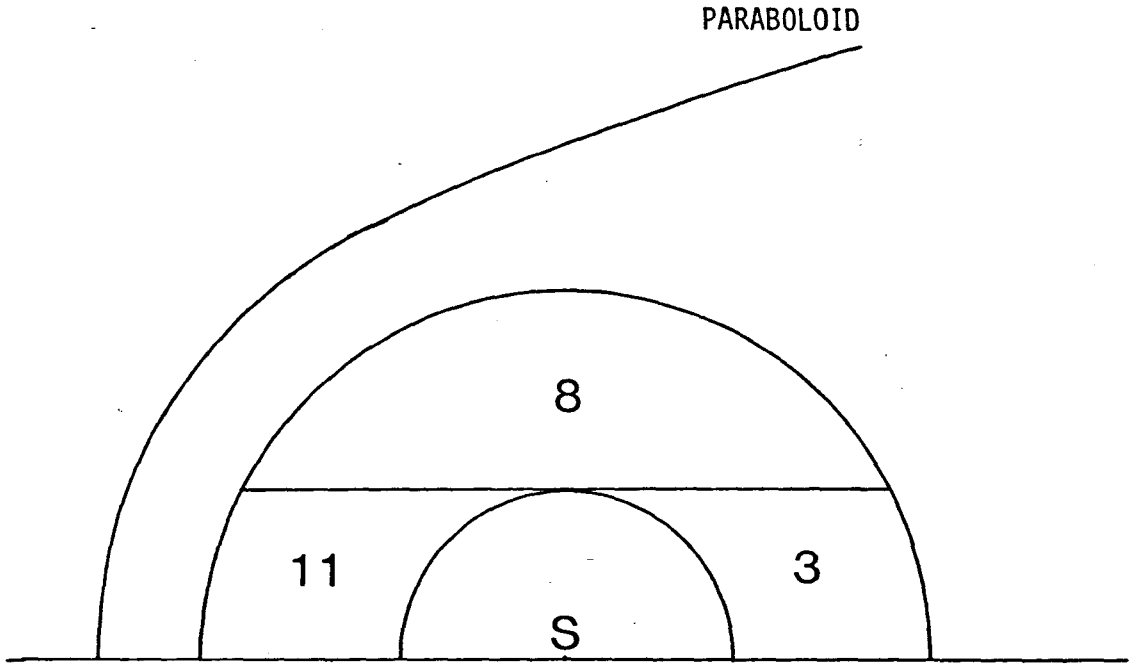
PARABOLOID
8
11
3
S

numbered. The integration limits on ρ and ψ in the flux integral for the twelve regions of integration are given below. (See figures 40 to 47 inclusive).

INTEGRATIONS LIMITS

REGION

(1) $0<\rho<(2ctR_c-c^2t^2)^{\frac{1}{2}}$; $\tan^{-1}(\rho/(R_1^2-\rho^2)^{\frac{1}{2}})<\psi<\tan^{-1}(\rho/(R_c^2-\rho^2)^{\frac{1}{2}})$

(2) $(2ctR_c-c^2t^2)^{\frac{1}{2}}<\rho<(2ctR_1-c^2t^2)^{\frac{1}{2}}$; $\tan^{-1}(\rho/(R_1^2-\rho^2)^{\frac{1}{2}})<\psi<\psi(P)$

(3) $0<\rho<R_c$; $\tan^{-1}(\rho/(R_1^2-\rho^2)^{\frac{1}{2}})<\psi<\tan^{-1}(\rho/(R_c^2-\rho^2)^{\frac{1}{2}})$

(4) $R_c<\rho(2ctR_1-c^2t^2)^{\frac{1}{2}}$; $\tan^{-1}(\rho/(R_1^2-\rho^2)^{\frac{1}{2}})<\psi<\psi(P)$

(5) $(2ctR_c-c^2t^2)^{\frac{1}{2}}<\rho<R_c$; $\pi-\tan^{-1}(\rho/(R_c^2-\rho^2)^{\frac{1}{2}})<\psi<\psi(P)$

(6) $0<\rho<R_c$; $\pi-\tan^{-1}(\rho/(R_c^2-\rho^2)^{\frac{1}{2}})<\psi<\psi(P)$

(7) $(2ctR_1-c^2t^2)^{\frac{1}{2}}<\rho<R_1$; $\tan^{-1}(\rho/(R_1^2-\rho^2)^{\frac{1}{2}})<\psi<\pi-\tan^{-1}((\rho/(R_1^2-\rho^2)^{\frac{1}{2}})$

(8) $R_c<\rho<R_1$; $\tan^{-1}(\rho/(R_1^2-\rho'^2)^{\frac{1}{2}})<\psi<\pi-\tan^{-1}(\rho/(R_1^2-\rho^2)^{\frac{1}{2}})$

(9) $(2ctR_1-c^2t^2)^{\frac{1}{2}}<\rho<R_c$; $\pi-\tan^{-1}(\rho/(R_c^2-\rho^2)^{\frac{1}{2}})<\psi<\pi-\tan^{-1}(\rho/(R_1^2-\rho^2)^{\frac{1}{2}})$

(10) $(2ctR_c-c^2t^2)^{\frac{1}{2}}\leq\rho\leq(2ctR_1-c^2t^2)^{\frac{1}{2}}$; $\pi-\tan^{-1}(\rho/(R_\psi^2-\rho^2)^{\frac{1}{2}})<\psi<\psi(P)$

(11) $0<\rho<R_c$; $\pi-\tan^{-1}(\rho/(R_c^2-\rho^2)^{\frac{1}{2}})<\psi<\pi-\tan^{-1}(\rho/(R_1^2-\rho^2)^{\frac{1}{2}})$

(12) $0<\rho(2ctR_1-c^2t^2)^{\frac{1}{2}}$; $\pi-\tan^{-1}(\rho/(R_c^2-\rho^2)^{\frac{1}{2}})<\psi<\psi(P)$

The flux seen by the observer per unit frequency interval at frequency ν at time t, from a circumstellar dust grain at position $\underline{r}$ is given by

$$S_\nu(\psi,\rho,\gamma,t) = (a_c^2/D^2)Q_{abs}(a_c,\nu)B_\nu(r,\tau(\rho,\psi,t)) \cdot \exp\left(-\int_{\psi'=\psi}^{\psi'=\psi(F)} N_c(r')\zeta'(\rho,\psi')dx' - \tau_\nu^{ic}(\rho,\gamma)\right) \qquad (6.2.19)$$

where τ_ν^{ic} is the extinction of circumstellar dust radiation by interstellar dust grains in the parent galaxy of the supernova, and is defined in chapter 5. The grain absorption cross-section ζ' is given by

$$\zeta'(\rho,\psi')=0 \qquad \text{for } \rho\,\mathrm{cosec}\psi' < R_c$$

$$\zeta'(\rho,\psi')=\pi a_c^2 Q_{abs}(a_c,\nu) \qquad \text{for } \rho\,\mathrm{cosec}\psi' > R_c$$

and from equation (6.2.2)

$$r'=\rho\,\mathrm{cosec}\psi' \tag{6.2.21}$$

and from equation (6.2.5)

$$dx'=-\rho\,\mathrm{cosec}^2\psi'\,d\psi' \tag{6.2.22}$$

To simplify the expression for optical depth in equation (6.2.28) the function $\phi_\beta(\rho,\psi)$ is defined by

$$\tau_\nu^{cs}=N_{c\nu}\rho^{1-\beta}\phi_\beta(\rho,\psi)=\int_{\psi'=\psi}^{\psi'=\psi(F)} N_c(r')\zeta'(\rho,\psi')dx' \tag{6.2.23}$$

This gives the optical depth τ_ν^{cs} at the observer to grain radiation from the circumstellar dust shell. Substituting equations (6.1.1), (6.1.4), (6.2.21) and (6.2.22) into equation (6.2.23) yields

$$\phi_\beta(\rho,\psi)=\int_{\psi}^{\psi(F)} \frac{\zeta'(\rho,\psi')\sin^{\beta-2}\psi'\,d\psi'}{\pi a_c^2 Q_{abs}(a_c,\nu)} \tag{6.2.24}$$

susbstituting equation (6.2.20) into equation (6.2.24)

$$\phi_\beta(\rho,\psi) = \int_{\psi}^{\psi(F)} \sin^{\beta-2}\psi' \, d\psi' \qquad \text{for } \rho \geq R_c \text{ or } \rho < R_c,\ \psi < \psi(F')$$

$$= \int_{\psi}^{\psi(B')} \sin^{\beta-2}\psi' \, d\psi' + \int_{\psi(F')}^{\psi(F)} \sin^{\beta-2}\psi' \, d\psi' \qquad \text{for } \rho < R_c,\ \psi > \psi(B') \tag{6.2.25}$$

The integrals in equation (6.2.25) have the following solutions

$$\int_x^y \sin^{\beta-2}\psi' \, d\psi' = \cot x - \cot y \qquad \text{for } \beta = 0.$$

$$= \ln\left(\tan\frac{y}{2}\cot\frac{x}{2}\right) \qquad \text{for } \beta = 1.$$

$$= y - x \qquad \text{for } \beta = 2. \tag{6.2.26}$$

Substituting equations (6.2.9), (6.2.10), (6.2.11), (6.2.12) and (6.2.26) into equation (6.2.25) yields the following solutions

$$\phi_\beta(\rho,\psi) = \cot\psi - (R_1^2-\rho^2)^{\frac{1}{2}}/\rho \qquad \text{for } \beta = 0.$$

$$= \ln\left(\tan\tfrac{1}{2}(\tan^{-1}(\rho/(R_1^2-\rho^2)^{\frac{1}{2}}))\cot\tfrac{1}{2}\psi\right) \qquad \text{for } \beta = 1.$$

$$= \tan^{-1}(\rho/(R_1^2-\rho^2)^{\frac{1}{2}}) - \psi \qquad \text{for } \beta = 2. \qquad \left.\right\} \rho \geq R_c \text{ or } \rho < R_c,\ \psi \leq \psi(F')$$

$$= \cot\psi - ((R_1^2-\rho^2)^{\frac{1}{2}}/\rho) - 2((R_c^2-\rho^2)^{\frac{1}{2}}/\rho) \qquad \text{for } \beta = 0.$$

$$= \ln\left(\tan\tfrac{1}{2}(\tan^{-1}(\rho/(R_1^2-\rho^2)^{\frac{1}{2}}))\cot^2\tfrac{1}{2}\psi\cot^2\tfrac{1}{2}(\tan^{-1}(\rho/(R_c^2-\rho^2)^{\frac{1}{2}}))\right)$$

$$\text{for } \beta = 1$$

$$= \tan^{-1}(\rho/(R_1^2-\rho^2)^{\frac{1}{2}}) - \psi - 2\tan^{-1}(\rho/(R_c^2-\rho^2)^{\frac{1}{2}}) + \pi$$

$$\text{for } \beta = 2. \qquad \left.\right\} \rho < R_c,\ \psi > \psi(B') \tag{6.2.27}$$

substituting equations (3.5.2) and (6.2.23) into equation (6.2.19) gives

$$S_\nu(\psi,\rho,\gamma,t) = \frac{2\pi h\nu^3 a_c^2}{c^2 D^2} Q_{abs}(a_c,\nu) H_\nu(r,\tau(\rho,\psi t)) \cdot \exp(N_{c\nu}\rho^{1-\beta}\phi_\beta(\rho,\psi) - \tau_\nu^{ic}(\rho,\gamma))$$

(6.2.28)

where H_ν is defined in chapter 3. The surface brightness, that is, the flux seen by the observer per unit frequency interval at frequency ν at time, t, from unit solid angle at angles $\tan^{-1}(\rho/D)$ and γ (see figure 113) to the observer from the supernova is given by

$$\sum_\nu(\rho,\gamma,t) = D^2 \int_{\psi=\min(\psi(B);\psi(P))}^{\psi=\psi(F)} N_c(r) S_\nu(\psi,\rho,\gamma,t)dx \qquad (6.2.29)$$

substituting equations (6.1.1), (6.2.1), (6.2.4) and (6.2.28) into equation (6.2.29)

$$\sum_\nu(\rho,\gamma,t) = \pi 2h\nu^3 c^{-2} N_{c\nu} \sigma'_\nu(\rho,\gamma,t) \qquad (6.2.30)$$

where

$$\sigma'_\nu(\rho,\gamma,t) = \delta(a) \int_{\tan^{-1}(\rho/(R_1^2-\rho^2)^{\frac{1}{2}})}^{\tan^{-1}(\rho/(R_C^2-\rho^2)^{\frac{1}{2}})} H_\nu(r,\tau(\rho,\psi,t)\rho^{1-\beta}\sin^{\beta-2}\psi\exp(N_{c\nu}\rho^{1-\beta}\phi_\beta(\rho,\psi) - \tau_\nu^{ic}(\rho,\gamma))d\psi$$

$$+\delta(b) \int_{\tan^{-1}(\rho/(R_1^2-\rho^2)^{\frac{1}{2}})}^{\tan^{-1}(2ct\rho/(\rho^2-c^2t^2))} \rho^{1-\beta}\sin^{\beta-2}\psi\exp(N_{c\nu}\rho^{1-\beta}\phi_\beta(\rho,\psi) - \tau_\nu^{ic}(\rho,\gamma))d\psi H_\nu(\rho,\tau(\rho,\psi,t))$$

$$+\delta(c) \int_{\pi-\tan^{-1}(\rho/(R_C^2-\rho^2)^{\frac{1}{2}})}^{\tan^{-1}(2ct\rho/(\rho^2-c^2t^2))} \rho^{1-\beta}\sin^{\beta-2}\psi\exp(N_{c\nu}\rho^{1-\beta}\phi_\beta(\rho,\psi) - \tau_\nu^{ic}(\rho,\gamma))d\psi H_\nu(\rho,\tau(\rho,\psi,t))$$

$$+\delta(d) \int_{\tan^{-1}(\rho/(R_1^2-\rho^2)^{\frac{1}{2}})}^{\pi-\tan^{-1}(\rho/(R_1^2-\rho^2)^{\frac{1}{2}})} \rho^{1-\beta}\sin^{\beta-2}\psi\exp(N_{c\nu}\rho^{1-\beta}\phi_\beta(\rho,\psi) - \tau_\nu^{ic}(\rho,\gamma))d\psi H_\nu(\rho,\tau(\rho,\psi,t))$$

$$+\delta(e) \int_{\pi-\tan^{-1}(\rho/(R_C^2-\rho^2)^{\frac{1}{2}})}^{\pi-\tan^{-1}(\rho/(R_1^2-\rho^2)^{\frac{1}{2}})} \rho^{1-\beta}\sin^{\beta-2}\psi\exp(N_{c\nu}\rho^{1-\beta}\phi_\beta(\rho,\psi) - \tau_\nu^{ic}(\rho,\gamma))d\psi H_\nu(\rho,\tau(\rho,\psi,t))$$

(6.2.31)

$\delta(a)$, $\delta(b)$, $\delta(c)$, $\delta(d)$ and $\delta(e)$ determine whether or not their respective integrals contribute to the circumstellar dust surface brightness.

For
$\delta(a)=1$ $0<ct<R_c$
and
$0<\rho<(2ctR_c-c^2t^2)^{\frac{1}{2}}$
or
$ct>R_c$
and
$0<\rho<R_c$
otherwise
$\delta(a)=0.$

So the corresponding integral is from the front of the dust shell to the front of the cavity.

For
$\delta(b)=1$ $0<ct<R_c$
and
$(2ctR_c-c^2t^2)^{\frac{1}{2}} <\rho<(2ctR_1-c^2t^2)^{\frac{1}{2}}$
or
$R_c<ct<R_1+(R_1^2-R_c^2)^{\frac{1}{2}}$
and
$R_c<\rho<(2ctR_1-c^2t^2)^{\frac{1}{2}}$

So this integration is from the farside of the dust shell to the parabola;

otherwise
$\delta(b)=0$

For
$\delta(c)=1$ $R_c<ct<2R_c$
and
$R_1>\frac{5}{4}R_c$
and
$(2ctR_c-c^2t^2)^{\frac{1}{2}} <\rho<R_c$
or
$R_c<ct<R_1+(R_1^2-R_c^2)^{\frac{1}{2}}$
and
$R_1<\frac{5}{4}R_c$
and
$(2ctR_c-c^2t^2)^{\frac{1}{2}} <\rho<R_c$
or
$2R_c<ct<R_1+(R_1^2-R_c^2)^{\frac{1}{2}}$
and
$R_1>\frac{5}{4}R_c$
and
$0<\rho<R_c$
or
$R_1+(R_1^2-R_c^2)^{\frac{1}{2}} <ct<2R_c$

and $R_1 < \frac{5}{4}R_c$

and $(2ctR_c - c^2t^2)^{\frac{1}{2}} < \rho < (2ctR_1 - c^2t^2)^{\frac{1}{2}}$

or $R_1 + (R_1^2 - R_c^2)^{\frac{1}{2}} < ct < 2R_1$

and $R_1 > \frac{5}{4}R_c$

and $0 < \rho < (2ctR_1 - c^2t^2)^{\frac{1}{2}}$

or $2R_c < ct < 2R_1$

and $R_1 < \frac{5}{4}R_c$

and $0 < \rho < (2ctR_1 - c^2t^2)^{\frac{1}{2}}$

otherwise $\delta(c) = 0$

so this integration is from the farside of the cavity to the parabola

For $\delta(d) = 1$ $R_1 < ct < R_1 + (R_1^2 - R_c^2)^{\frac{1}{2}}$

and $R_1 > \rho > (2ctR_1 - c^2t^2)^{\frac{1}{2}}$

or $ct > R_1 + (R_1^2 - R_c^2)^{\frac{1}{2}}$

and $R_c < \rho < R_1$

otherwise $\delta(d) = 0$

so the corresponding integral is from the front of the dust shell to the back of the dust shell.

For $\delta(e) = 1$ $R_1 + (R_1^2 - R_c^2)^{\frac{1}{2}} < ct < 2R_1$

and $(2ctR_1 - c^2t^2)^{\frac{1}{2}} < \rho < R_c$

or $ct > 2R_1$

and $0 < \rho < R_c$

otherwise $\delta(e) = 0$

so this integration is from the farside of the cavity to the back of the dust shell.

The flux per unit frequency interval from the circumstellar at time t is given by

$$f_\nu(t)=2D^{-2}\int_0^{\pi}\int_0^{R_1}\Sigma_\nu(\rho,\gamma,t)\rho d\rho d\gamma \qquad \text{for } (\tau_\nu^{ic}(\rho,\gamma)\neq 0) \quad (6.2.32)$$

or

$$f_\nu(t)=2\pi D^{-2}\int_0^{R_1}\Sigma_\nu(\rho,t)\rho d\rho \qquad \text{for } (\tau_\nu^{ic}(\rho,\gamma)=0) \quad (6.2.33)$$

where the first version occurs if there is an interstellar dust plane slab, and the second version occurs if there is no interstellar dust plane slab. It is necessary to add the flux from circumstellar dust grains heated by starlight only as it may make a significant contribution to the circumstellar dust flux in the far infra-red. If such grains have temperature T_{gc} in the integrands of the surface brightness ($\Sigma_\nu(\rho,\gamma,t)$) integrals, the following transformation is made

$$H_\nu(\rho,\tau(\rho,\psi,t)) \rightarrow H_\nu(\rho,\tau(\rho,\psi,t)) - \frac{1}{e^{h\nu/KT_{gc}}-1} \qquad (6.2.34)$$

This essentially subtracts the flux that would be produced if the grains were heated by starlight only from the flux emitted by grains heated by both the supenova and the background starlight. The infra-red flux that would arise from the circumstellar shell in the absence of the supernova, that is due to background starlight only, is given by:-

$$f_\nu = 2\int_0^{\pi}d\gamma\int_{R_c}^{R_1}\rho d\rho\int_{-(R_1^2-\rho^2)^{\frac{1}{2}}}^{(R_1^2-\rho^2)^{\frac{1}{2}}}N_c(\rho,x)\frac{2\pi h\nu^3}{c^2}Q_{abs}(a_c,\nu)\frac{a_c^2}{D^2}$$

$$\cdot\frac{\exp(N_{c\nu}\rho^{1-\beta}\phi_\beta(\rho,\psi)-\tau_\nu^{ic}(\rho,\gamma))dx}{e^{h\nu/KT_{gc}}-1}$$

$$+\int_0^{R_c}\rho d\rho\int_{-(R_1^2-\rho^2)^{\frac{1}{2}}}^{-(R_c^2-\rho^2)^{\frac{1}{2}}}N_c(\rho,x)\frac{2\pi h\nu^3}{c^2}Q_{abs}(a_i,\nu)\frac{a_c^2}{D^2}$$

$$\cdot\frac{\exp(N_{c\nu}\rho^{1-\beta}\phi_\beta(\rho,\psi)-\tau_\nu^{ic}(\rho,\gamma))dx}{e^{h\nu/KT_{gc}}-1}$$

$$+\int_0^{R_c}\rho d\rho\int_{(R_c^2-\rho^2)^{\frac{1}{2}}}^{(R_1^2-\rho^2)^{\frac{1}{2}}}N_c(\rho,x)\frac{2\pi h\nu^3}{c^2}Q_{abs}(a_i,\nu)\frac{a_c^2}{D^2}$$

$$\cdot\frac{\exp(N_{c\nu}\rho^{1-\beta}\phi_\beta(\rho,\psi)-\tau_\nu^{ic}(\rho,\gamma))dx}{e^{h\nu/KT_{gc}}-1}$$

$$=\frac{4\pi h\nu^3}{c^2D^2}\frac{a_c^2\,N_cQ_{abs}(a_i,\nu)}{(e^{h\nu/KT_{gc}}-1)}\int_0^{\pi}d\gamma\int_{R_c}^{R_1}\rho d\rho\int_{-(R_1^2-\rho^2)^{\frac{1}{2}}}^{(R_1^2-\rho^2)^{\frac{1}{2}}}(\rho^2+x^2)^{-\beta/2}$$

$$\cdot\exp(N_{c\nu}\rho^{1-\beta}\phi_\beta(\rho,\psi)-\tau_\nu^{ic}(\rho,\dot{\psi}))dx$$

$$+\int_0^{R_c}\rho d\rho\int_{-(R_1^2-\rho^2)^{\frac{1}{2}}}^{-(R_c^2-\rho^2)^{\frac{1}{2}}}(\rho^2+x^2)^{-\beta/2}\exp(N_{c\nu}\rho^{1-\beta}\phi_\beta(\rho,\psi)-\tau_\nu^{ic}(\rho,\gamma))dx$$

$$+\int_0^{R_c}\rho d\rho\int_{(R_c^2-\rho^2)^{\frac{1}{2}}}^{(R_1^2-\rho^2)^{\frac{1}{2}}}(\rho^2+x^2)^{-\beta/2}\exp(N_{c\nu}\rho^{1-\beta}\phi_\beta(\rho,\psi)-\tau_\nu^{ic}(\rho,\gamma))dx \qquad (6.2.35)$$

Using equations (6.2.32) or (6.2.33) the total flux can be calculated. Equation (6.2.35) can be used to subtract out any heating due to background starlight.

6.3 The application of the circumstellar dust model to SN1980k.

The supernova SN1980k erupted in NGC6946; (a galaxy at a distance of 5.5Mpc) on October 28th 1980. An infra-red excess was first observed at 215 days after outburst. (Dwek et al. 1983).

The U, B and V data for SN1980k are taken from Buta (1982), while data

at J, H, K, L and 3.8μm are taken from Dwek et al. (1983). The date of outburst is assumed to be October 28.0 1980 U.T. The U, B, V data for SN1980k (uncorrected for interstellar extinction in this Galaxy) are listed in table 7 and plotted in figures 48, 49 and 50 respectively. The J, H, K, L and 3.8μm data (corrected for interstellar extinction in this Galaxy) are listed in table 8 and the J, H, K and L data are plotted in figures 51, 52, 53 and 54 respectively. The errors in the data up to 52 days after outburst are $\leq \pm 0.15$ magnitudes while the errors in the data taken 215 days after outburst and later, are listed with the data. The zero magnitude fluxes for U, B, V, J, H, K and L are listed in Appendix I and that for 3.8μm is taken to be the same as for 3.4μm. The following variations (also shown on figures 48 to 54 respectively) were assumed for U, B, V, J, H, K and L for the purposes of determining the supernova luminosity and effective temperature for any time t(days) after outburst by means of a black body fit to the photospheric magnitudes:-

$$
\begin{aligned}
U &= 10.50 + 0.09\ t && 0 < t < 50 \\
&= 15.00 + 0.04\ (t-50) && 50 < t < 170 \\
&= 19.80 + 0.01\ (t-170) && t > 170 \qquad (6.3.1)
\end{aligned}
$$

$$
\begin{aligned}
B &= 11.30 + 0.06\ t && 0 < t < 50 \\
&= 14.30 + 0.038(t-50) && 50 < t < 170 \\
&= 18.86 + 0.01\ (t-170) && t > 170 \qquad (6.3.2)
\end{aligned}
$$

$$
\begin{aligned}
V &= 11.00 + 0.045t && 0 < t < 50 \\
&= 13.25 + 0.0375(t-50) && 50 < t < 170 \\
&= 17.75 + 0.01\ (t-170) && t > 170 \qquad (6.3.3)
\end{aligned}
$$

$$
\begin{aligned}
J &= 10.20 + 0.025t && 0 < t < 170 \\
&= 11.95 + 0.036(t-70) && 70 < t < 170 \\
&= 15.55 + 0.01\ (t-170) && t > 170 \qquad (6.3.4)
\end{aligned}
$$

$$
\begin{aligned}
H &= 10.10 + 0.025t && 0 < t < 70 \\
&= 11.85 + 0.036(t-70) && 70 < t < 170 \\
&= 15.45 + 0.01\ (t-170) && t > 170 \qquad (6.3.5)
\end{aligned}
$$

$$
\begin{aligned}
K &= 9.90 + 0.02t && 0 < t < 70 \\
&= 11.30 + 0.036(t-70) && 70 < t < 170 \\
&= 14.90 + 0.01\ (t-170) && t > 170 \qquad (6.3.6)
\end{aligned}
$$

$$
\begin{aligned}
L &= 9.55 + t/70 && 0 < t < 70 \\
&= 10.55 + 0.03\ (t-70) && 70 < t < 170 \\
&= 13.55 + 0.01\ (t-170) && t > 170 \qquad (6.3.7)
\end{aligned}
$$

FIGURE 48. SN1980k in NGC6946 : Magnitude U, for the first 200 days after outburst. The solid line is a fit to the observed data used in the black body fit. The dotted line is predicted by the black-body fit. The crosses are the observed data points.

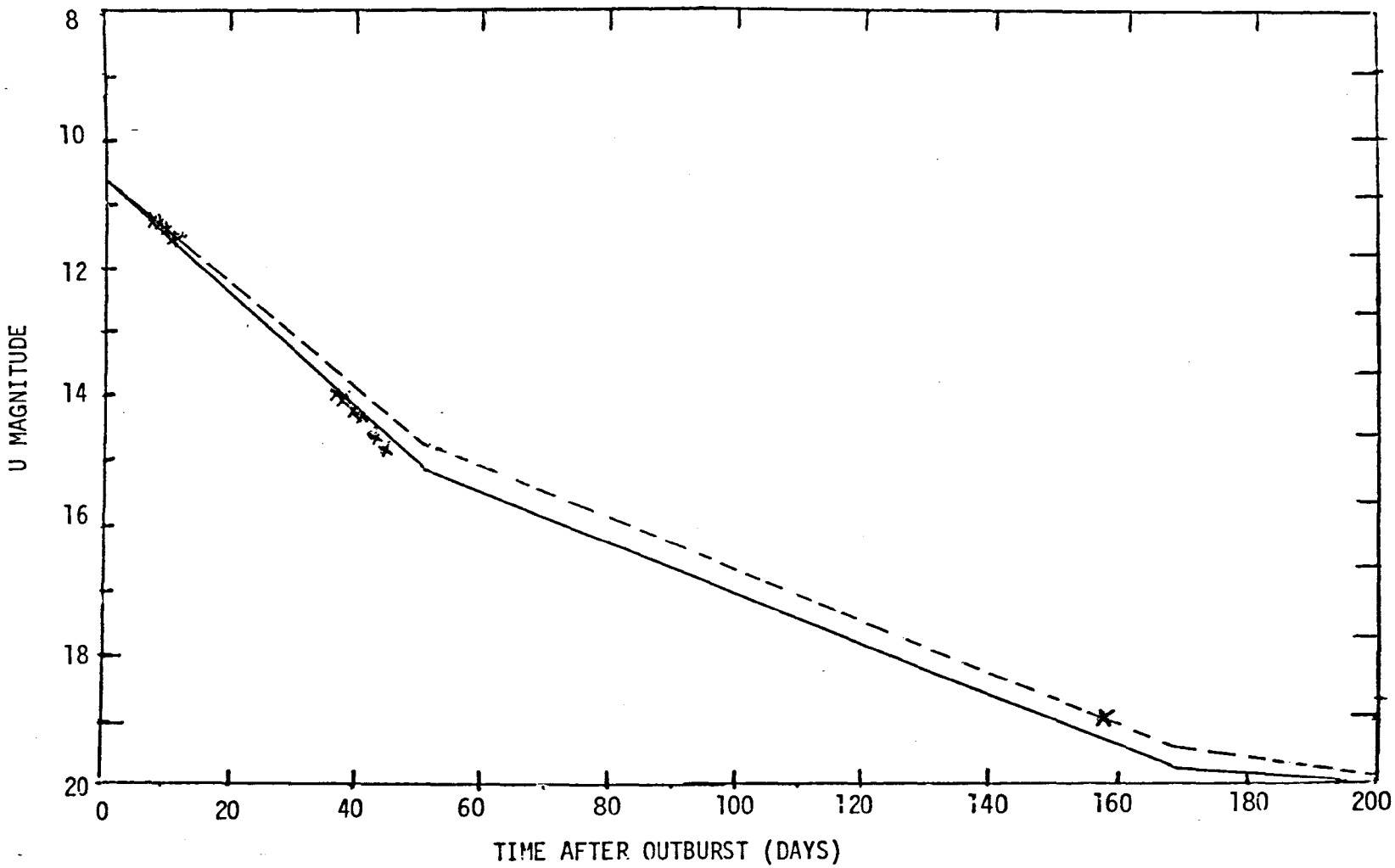
8
10
12
14
16
18
20
U MAGNITUDE
0
20
40
60
80
100
120
140
160
180
200
TIME AFTER OUTBURST (DAYS)

FIGURE 49. SN1980k in NGC6946 : Magnitude B, for the first 200 days after outburst. The solid line is a fit to the observed data used in the black body fit. The dotted line is predicted by the black-body fit. The crosses are the observed data points.

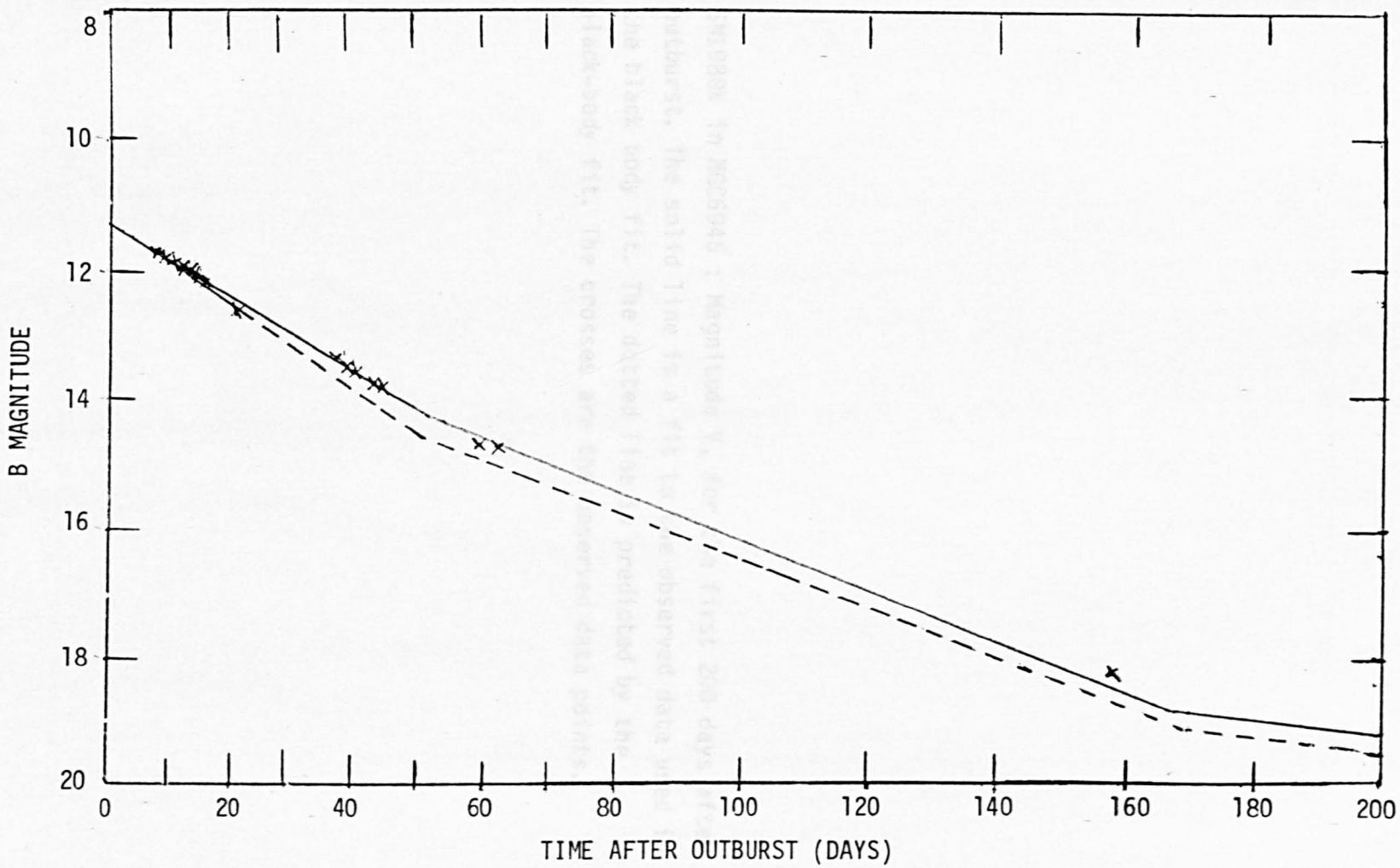
8
10
12
14
16
18
20
B MAGNITUDE
0
20
40
60
80
100
120
140
160
180
200
TIME AFTER OUTBURST (DAYS)

FIGURE 50. SN1980k in NGC6946 : Magnitude V, for the first 200 days after outburst. The solid line is a fit to the observed data used in the black body fit. The dotted line is predicted by the black-body fit. The crosses are the observed data points.

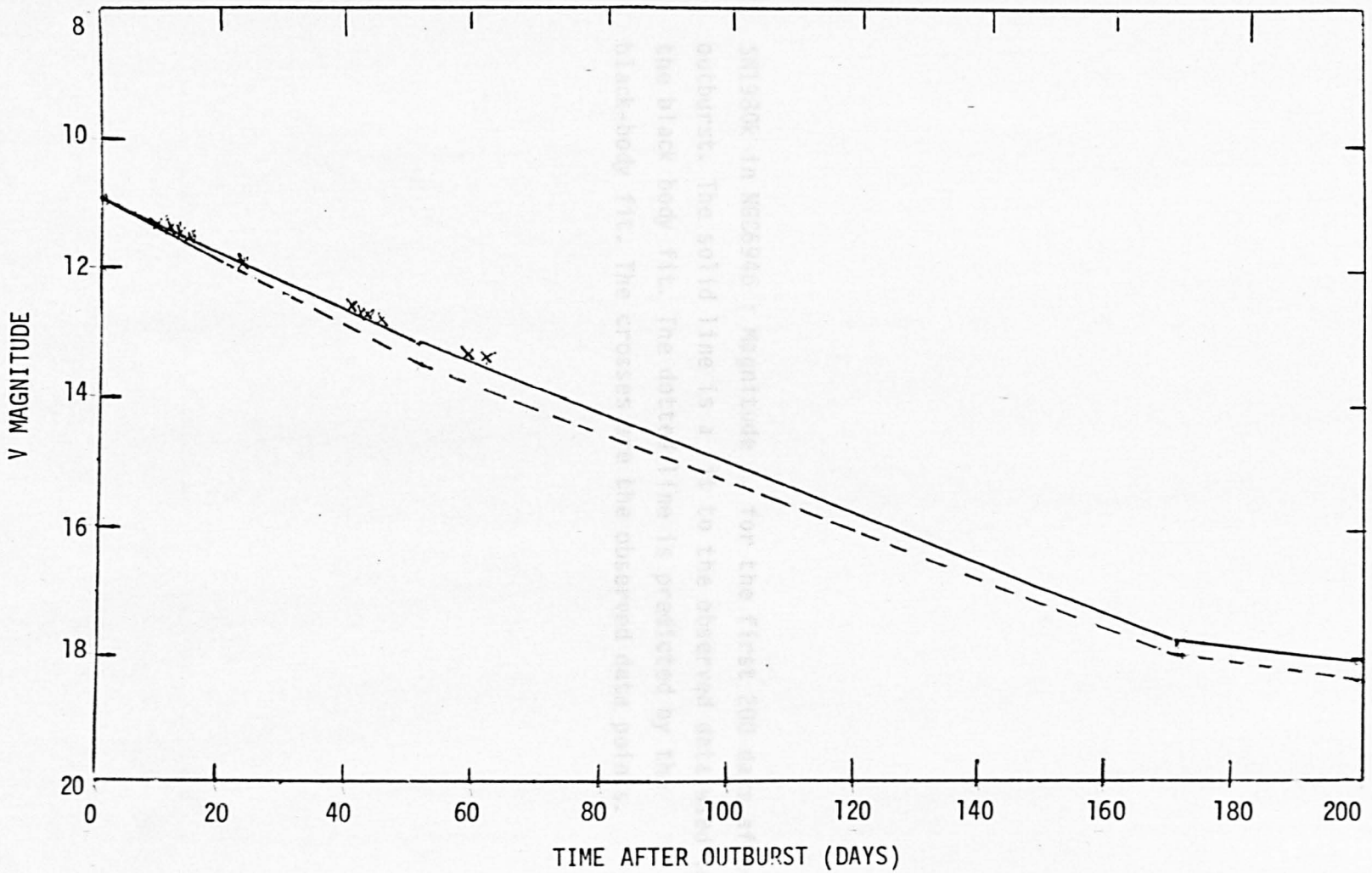
8
10
12
14
16
18
20
V MAGNITUDE
0
20
40
60
80
100
120
140
160
180
200
TIME AFTER OUTBURST (DAYS)

FIGURE 51. SN1980k in NGC6946 : Magnitude J, for the first 200 days after outburst. The solid line is a fit to the observed data used in the black body fit. The dotted line is predicted by the black-body fit. The crosses are the observed data points.

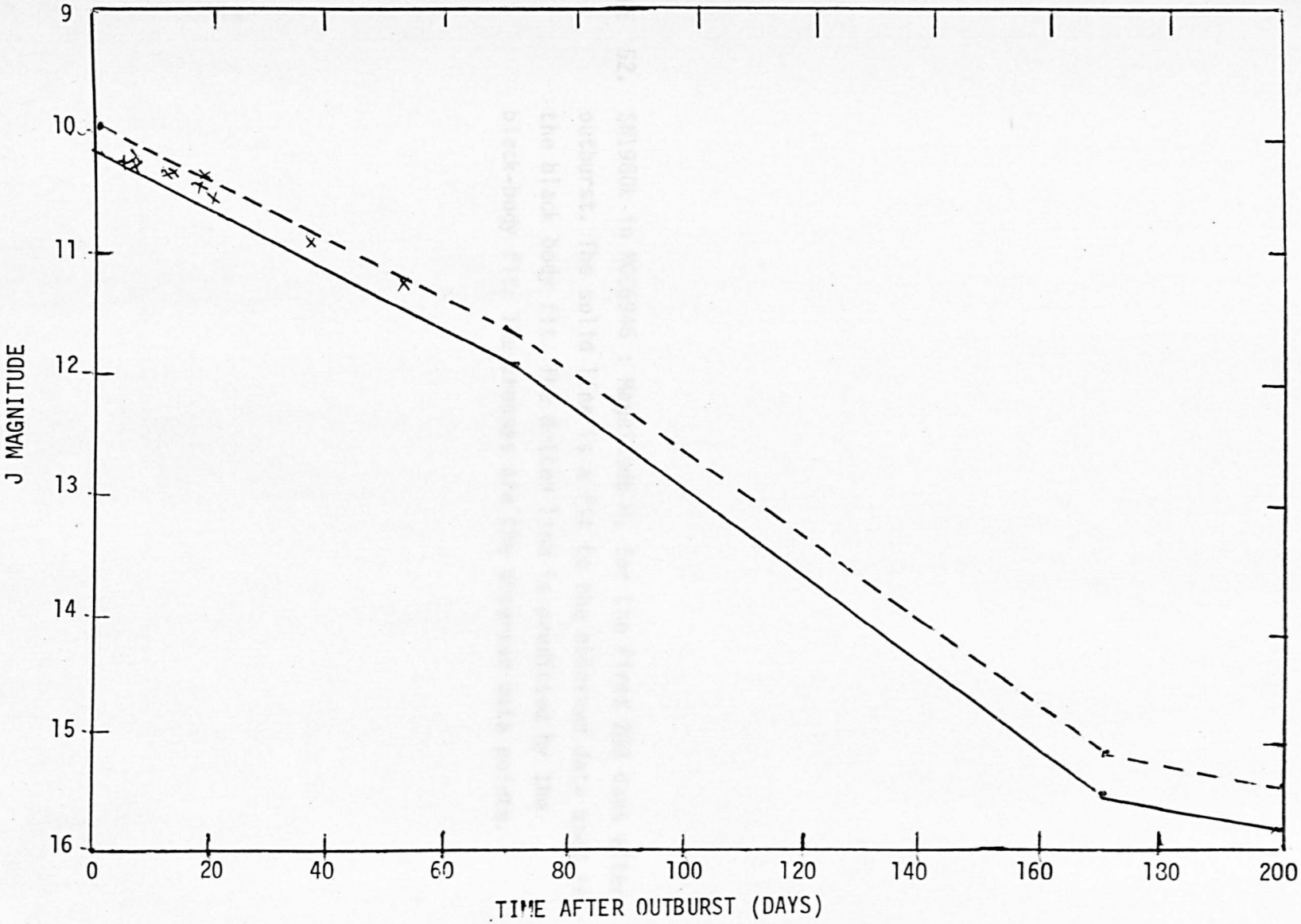
9
10
11
12
13
14
15
16
J MAGNITUDE
0
20
40
60
80
100
120
140
160
180
200
TIME AFTER OUTBURST (DAYS)

FIGURE 52. SN1980k in NGC6946 : Magnitude H, for the first 200 days after outburst. The solid line is a fit to the observed data used in the black body fit. The dotted line is predicted by the black-body fit. The crosses are the observed data points.

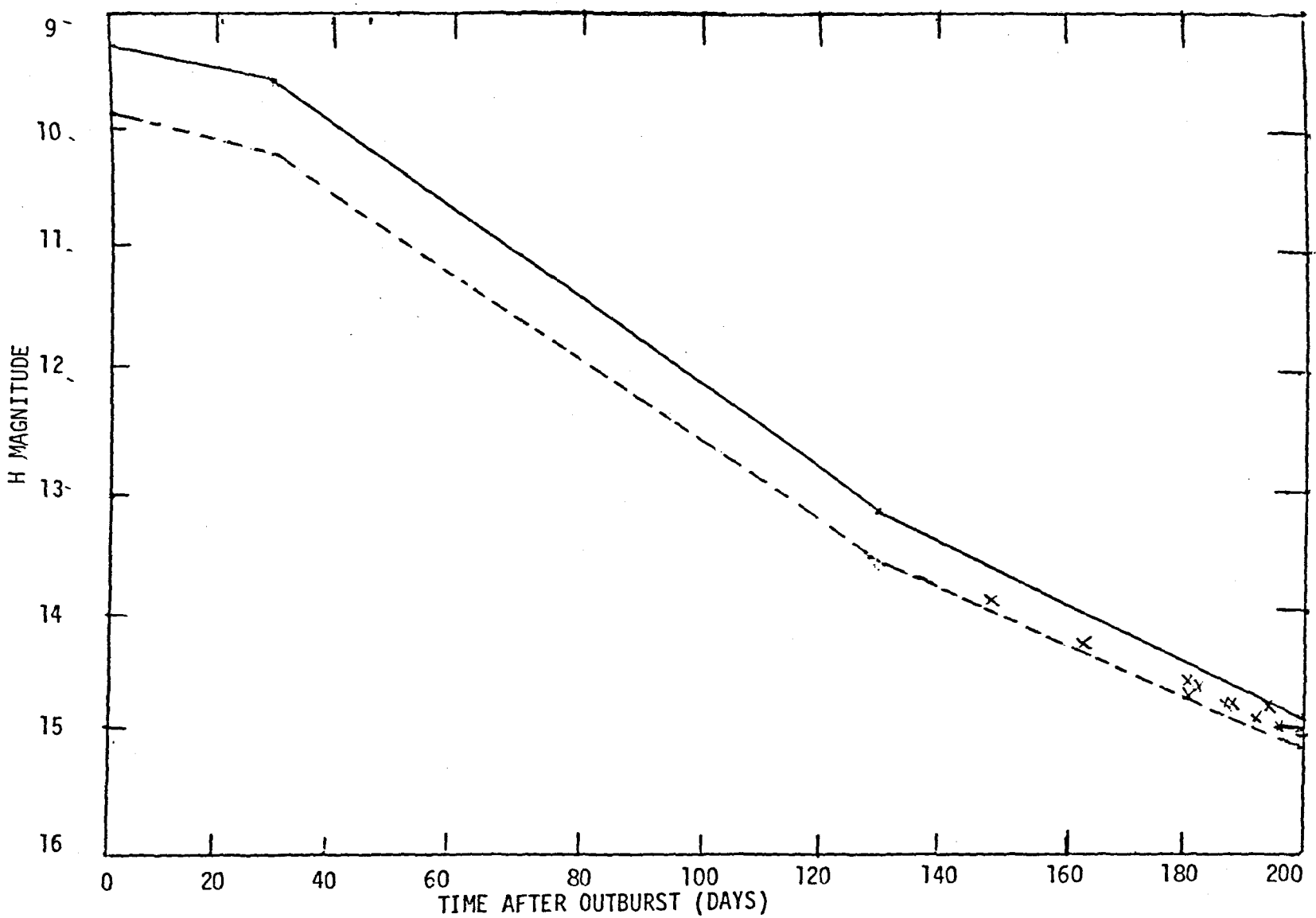
9
10
11
12
13
14
15
16
H MAGNITUDE
0
20
40
60
80
100
120
140
160
180
200
TIME AFTER OUTBURST (DAYS)

FIGURE 53. SN1980k in NGC6946 : Magnitude K, for the first 200 days after outburst. The solid line is a fit to the observed data used in the black body fit. The dotted line is predicted by the black-body fit. The crosses are the observed data points.

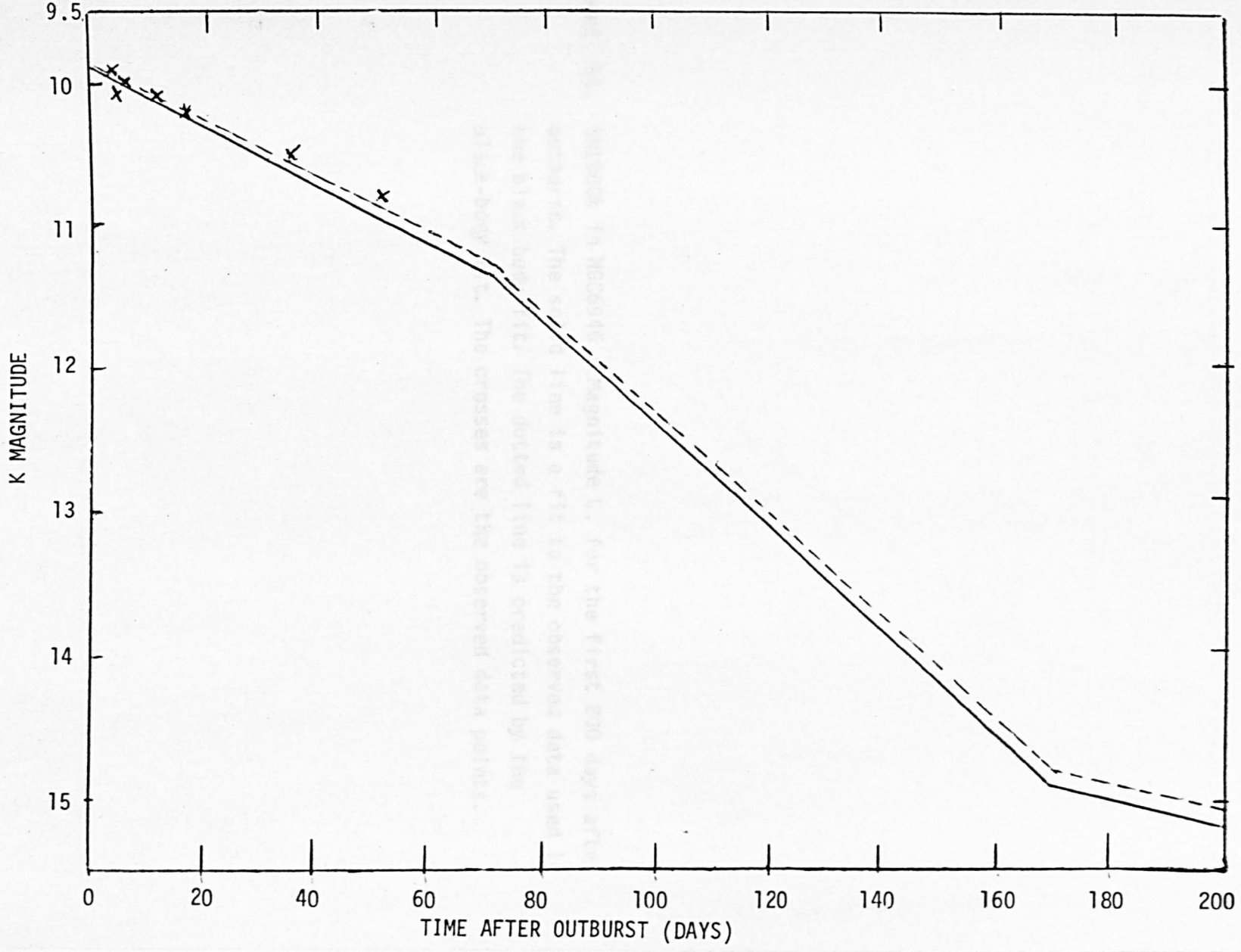
9.5
10
11
12
13
14
15
K MAGNITUDE
0
20
40
60
80
100
120
140
160
180
200
TIME AFTER OUTBURST (DAYS)

FIGURE 54. SN1980k in NGC6946 : Magnitude L, for the first 200 days after outburst. The solid line is a fit to the observed data used in the black body fit. The dotted line is predicted by the black-body fit. The crosses are the observed data points.

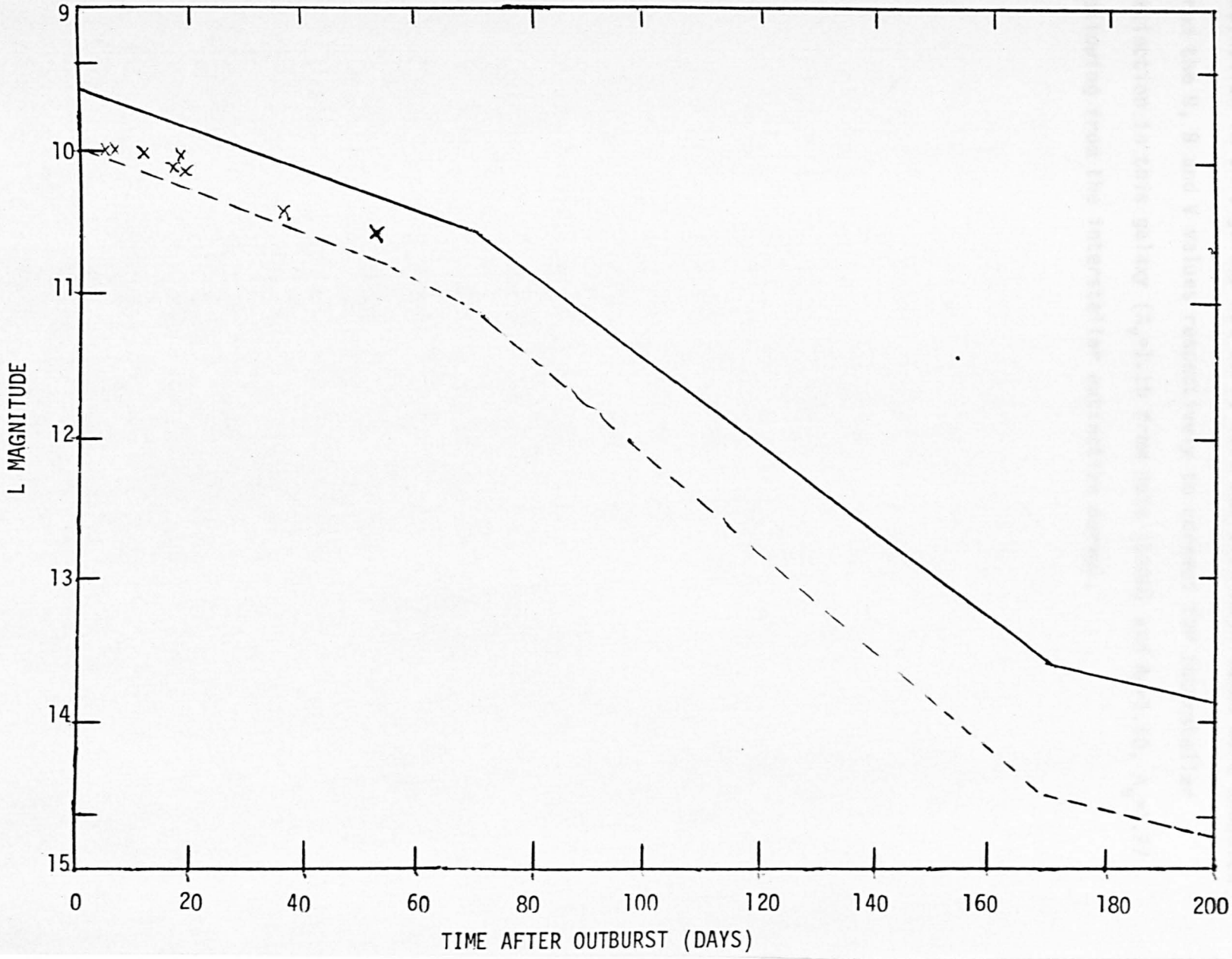
9
10
11
12
13
14
15
L MAGNITUDE
0
20
40
60
80
100
120
140
160
180
200
TIME AFTER OUTBURST (DAYS)

The J, H, K and L data are already corrected for interstellar extinction in this galaxy but 1.77, 1.50 and 1.15 magnitudes were deducted from the U, B and V values respectively to correct for interstellar extinction in this galaxy (A_V=1.15 from Buta (1980) and A_B=1.50, A_U=1.77 following from the interstellar extinction curve).

TABLE 7

THE U, B, V DATA FOR SN1980k.

TIME AFTER OUTBURST. (Days)	V	B	U
7.15	11.39	11.79	11.22
8.11	11.41	11.81	11.27
9.10	11.43	11.85	11.33
10.11	11.46	11.89	11.39
11.10	11.51	11.96	11.50
11.10	11.50	11.91	11.40
12.09	11.54	12.00	11.54
12.11	11.56	11.98	11.51
13.10	11.59	12.06	11.64
13.12	11.58	12.05	11.65
14.14	11.63	12.11	11.74
15.12	11.68	12.18	11.85
22.07	12.03	12.66	
36.10	12.60	13.46	14.02
37.10	12.63	13.51	14.06
38.10	12.67	13.59	14.21
39.11	12.71	13.64	14.29
42.14	12.82	13.80	14.60
43.10	12.84	13.83	14.65
44.06	12.87	13.88	14.73
58.07	13.41	14.70	

TABLE 7 (cont).

61.08	13.50	14.79	
158.42	17.25	18.24	19.03

FIGURE 55. SN1980k in NGC6946 : Luminosity for the first 200 days after outburst. The effect of increased luminosity is shown by the dotted line. See text for details.

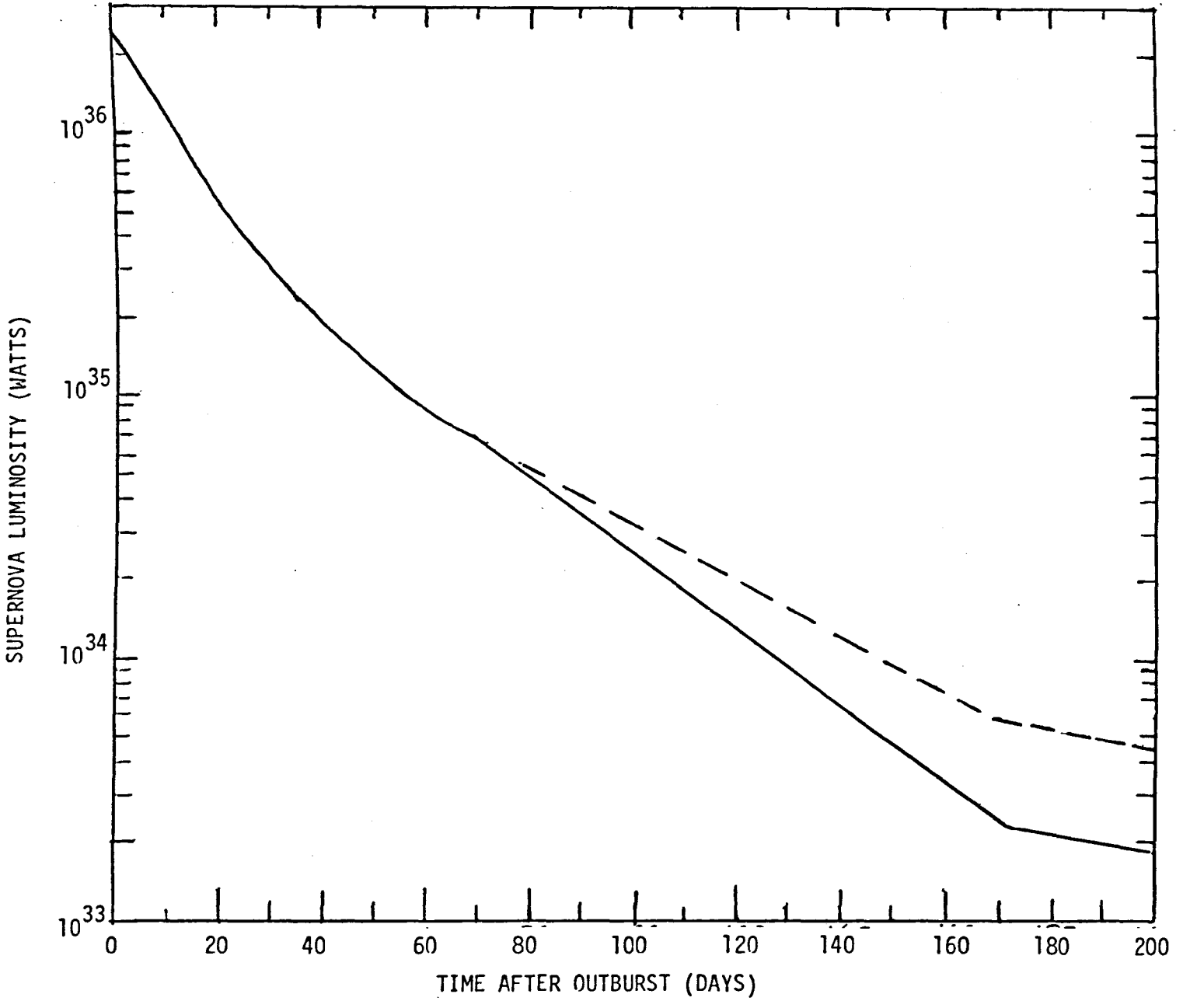
SUPERNOVA LUMINOSITY (WATTS)
10^{36}
10^{35}
10^{34}
10^{33}
0
20
40
60
80
100
120
140
160
180
200
TIME AFTER OUTBURST (DAYS)

FIGURE 56. SN1980k in NGC6946 : Effective temperature for the first 200 days after outburst.

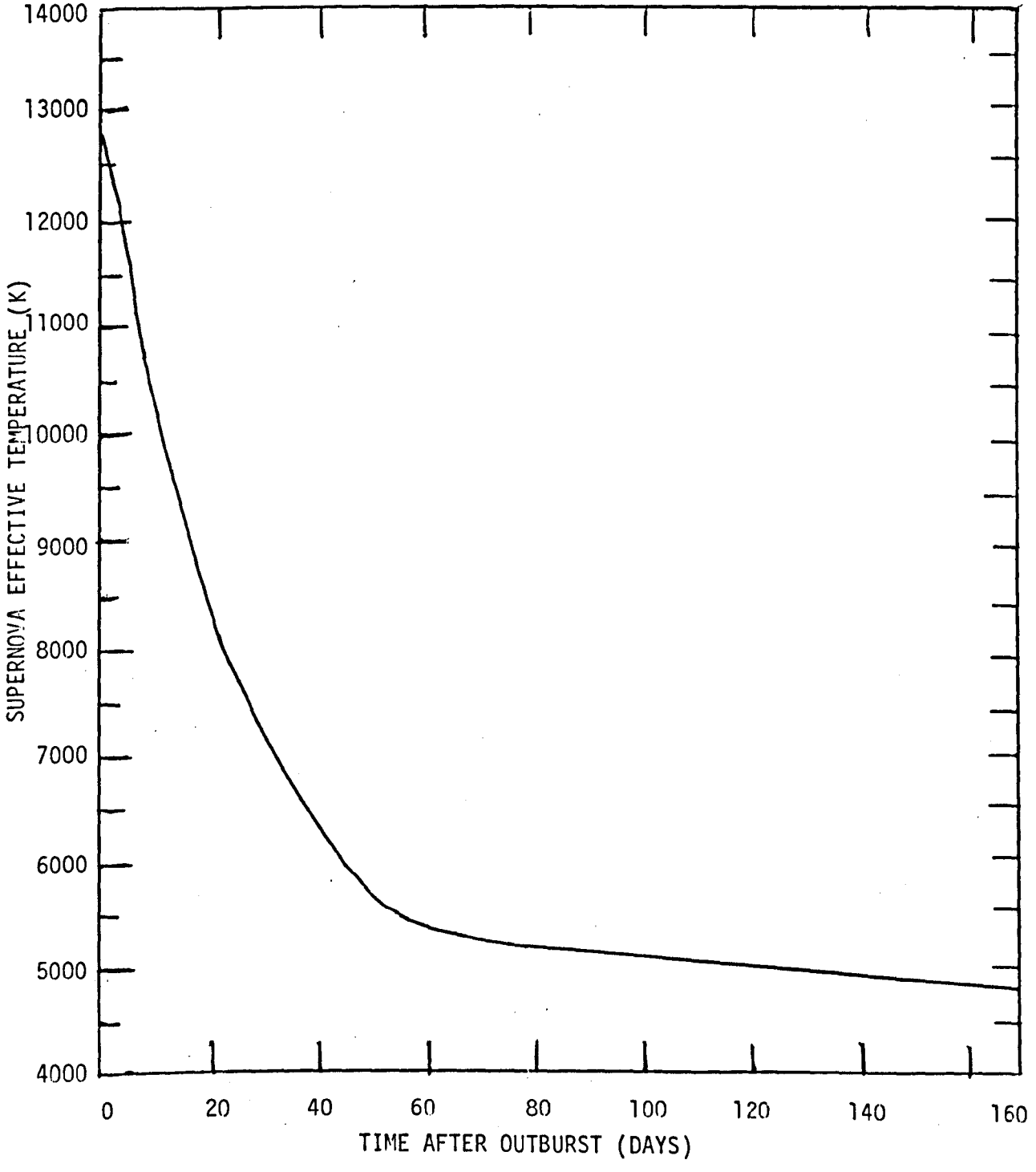
14000
13000
12000
11000
10000
9000
8000
7000
6000
5000
4000
SUPERNOVA EFFECTIVE TEMPERATURE (K)
0
20
40
60
80
100
120
140
160
TIME AFTER OUTBURST (DAYS)

The values of U, B, V, J, H, K and L for the black-body used to model the supernova are computed for the first 200 days after outburst, and shown with the observational data in figures 48, 49, 50, 51, 52, 53 and 54 respectively. The variations with time of the luminosity and effective temperature of this black-body are shown for the first 200 days after outburst in figures 55 and 56 respectively.

The first time at which an infra-red excess due to circumstellar dust radiation is observed is 215 days after outburst. Infra-red data up to 52 days can be explained entirely by supernova photosphere radiation. The circumstellar dust shell is assumed to condense in the way described in chapter 3. In other words each grain condenses when it is in thermodynamic equilibrium with supernova radiation emitted at time t_c and attains its final radius immediately. The condensation time t_c is taken to be 200 days after outburst as this is around the time at which material ejected by the supernova reaches the distance from the centre of the supernova at which the dust shell condenses. The time of condensation is not however of critical importance because the light travel time across the circumstellar dust shell turns out to be a few days at most. As the earliest times at which infra-red excesses are observed are 215 days after outburst in the case of SN1980k and 259 days in the case of SN1979c, the parabola $\tau=t_c$ will be entirely outside the dust shell for all relevant times. The dust grains are assumed to be 0.2μm radius spherical, homogeneous silicate grains. The radius assumed is typical of interstellar and circumstellar grains and silicate is assumed because oxygen has a greater abundance numerically than carbon in the supernova ejecta.

The coefficient c_T of Q_{abs} in the expression for the optical depth of the circumstellar dust shell (that is $\tau_v^{cs}=c_T Q_{abs}$), the inner radius R_c of the circumstellar dust shell and the ratio R_1/R_c of the shell's outer radius to its inner radius are the parameters varied in the modelling of the infra-red excess of SN1980k by a circumstellar dust shell. The flux

predicted by the model is computed at J, H, K, L and 3.8μm for 215 days, 234 days, 323 days, 340 days and 357 days after outburst for comparison with the observed fluxes listed in table 8. The deviations of the common logarithms of the computed fluxes from the common logarithms of the observed fluxes are computed for each of the 16 observed fluxes. Then the mean deviation (Δf_ν) and the standard deviations δf_ν are found, as follows

$$\Delta f_\nu = \frac{1}{N} \sum (\log_{10}(f_\nu^{cal}/f_\nu^{obs})) \qquad (6.3.8)$$

$$\delta f_\nu = \left(\frac{1}{N} \sum (\log_{10}(f_\nu^{cal}/f_\nu^{obs}))^2 \right)^{\frac{1}{2}} \qquad (6.3.9)$$

where f_ν^{cal} is the computed flux, f_ν^{obs} the corresponding observed flux and N the number of observed fluxes being compared. A similar procedure for comparing the 42 observed fluxes up to 52 days after outburst (for which there is no infra-red excess and all the infra-red flux is photospheric) gives $\Delta f_\nu = 0.011$ and $\delta f_\nu = 0.0555$, which shows that the time variations assumed for U, B, V, J, H, K and L in equations (6.3.1) to (6.3.7) inclusive are reasonably appropriate.

If R_1/R_c is kept constant, for a given value of c_T, Δf_ν is found to decrease monotonically as R_c is increased, the value of R_c for which $\Delta f_\nu = 0$ being denoted by R_{cm}. The quantity δf_ν has a minimum value at one particular value of R_c denoted by R_{cs}. It is found that $R_{cs} = R_{cm}$ at a particular value of c_T.

For each value of R_1/R_c, the values of c_T and R_c for the circumstellar dust shell that best fit the observational data are the values for which $R_{cm} = R_{cs}$. The values of Δf_ν and δf_ν are computed for many different values of c_T and R_c for a number of different values of R_1/R_c to obtain the best fitting values of c_T and R_c for each value of R_1/R_c. The circumstellar dust shell parameters considered to give the best overall fit to the observational data are those of the best fit which has the lowest

TABLE 8

THE J, H, K, L AND 3.8μm DATA FOR SN1980k.

TIME AFTER OUTBURST (Days)	J	H	K	L	3.8μm
4	10.290	10.097	9.935		9.896
5	10.324	10.264	10.055	9.962	10.274
7	10.233	10.142	9.968	9.929	10.147
11	10.414	10.290	10.110	10.032	
12	10.386	10.277	10.091	9.929	
17	10.543	10.417	10.210	10.107	
18	10.433	10.387	10.189	10.032	
19	10.619	10.510	10.275	10.188	
36	10.962	10.785	10.495	10.419	
52	11.306	11.154	10.844	10.587	
215	16.205	15.705	14.367	12.651	
234	16.205	15.806	14.591		
323	17.499	17.377	16.560		
340	17.499		16.362		
357	18.075	17.472	16.362		

TABLE 8 (cont).

FLUXES IN mJy.

Days after outburst	J	H	K	L	3.8μm
215	0.56±0.06	0.56±0.09	1.13±0.15	2.69±0.40	
234	0.56±0.06	0.51±0.05	0.92±0.10		
323	0.17±0.03	0.12±0.03	0.15±0.03		
340	0.17±0.03		0.18±0.03		
357	0.10±0.03	0.11±0.02	0.18±0.03		1.05±0.22

value of δf_ν. Approximately one thousand computer runs were performed to determine the best fit for the data. (The same number of computer runs were undertaken to fit the data for SN1979c also).

The best fit was found to occur for c_T=24.00. The values of Δf_ν for the following values of R_c and R_1/R_c are tabulated below:

		R_c		
		2.6×10^{13}(m)	2.7×10^{13}(m)	2.8×10^{13}(m)
R_1/R_c	1.3	0.020(.212)	0.013(.210)	0.005(.209)
	1.6	0.010(.213)	0.003(.212)	-0.004(.211)
	1.8	0.008(.213)	0.001(.213)	-0.006(.212)
	2.0	0.007(.214)	-0.001(.214)	-0.008(.213)
	2.2	0.006(.215)	-0.001(.214)	-0.008(.214)
	2.5	0.006(.216)	-0.001(.215)	-0.008(.215)

It can be seen that the observations do not give any indication of the thickness of the dust shell. The computation errors correspond to a difference of 0.008 in the logarithm of the flux. For $R_1/R_c > 1.6$ the best fitting dust shell inner radius (R_c) as indicated by the value for which Δf_ν is closest to zero is 2.7×10^{13}m. Spectra and light curves were then computed for three values of R_1/R_c; 1.6, 2.0 and 2.5. Three values were chosen to investigate the possibility that observations further into the infra-red than L would give further information on the thickness of the circumstellar dust shell. For R_1/R_c=1.6, the dust shell mass is $1.57 \times 10^{-4} M_\odot$ and the optical depth is shown as a function of wavelengths between 0.1μm and 100μm in figure 57. For R_1/R_c=2.0 and 2.5, the dust shell mass is $1.96 \times 10^{-4} M_\odot$ and $2.45 \times 10^{-4} M_\odot$ respectively and the optical depths are the same as for R_1/R_c = 1.6.

The dust and total flux spectra at 215 days after outburst are shown along with the observed fluxes taken from table 8, for R_1/R_c = 1.6, 2.0 and

FIGURE 57. The optical depths of the circumstellar dust shells around SN1979c (lower line) and SN1980k (upper line).

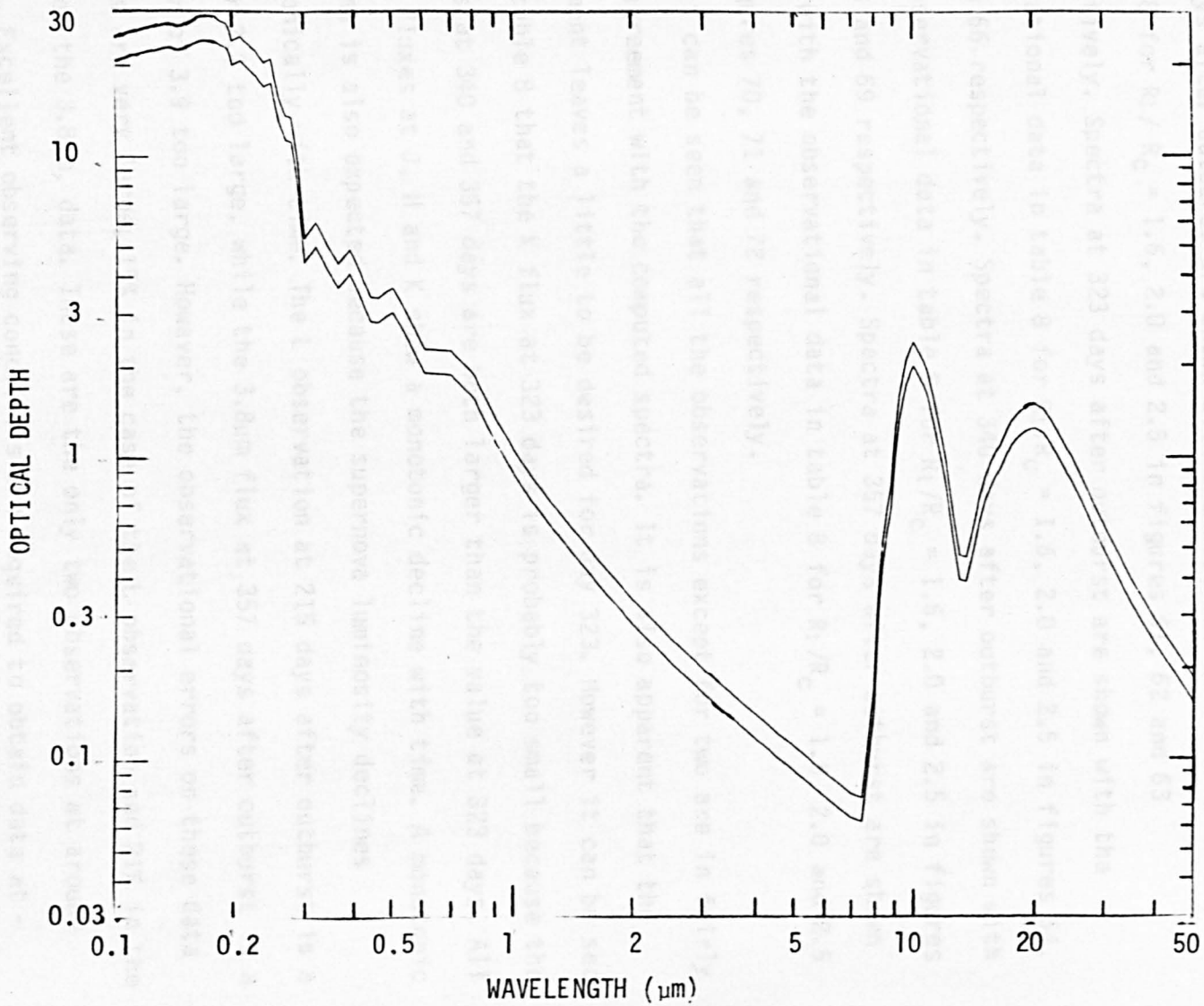
30
10
3
1
0.3
0.1
0.03
OPTICAL DEPTH
0.1
0.2
0.5
1
2
5
10
20
50
WAVELENGTH (μm)

2.5 in figures 58, 59 and 60 respectively. The dust and total flux spectra are also computed at 234 days, 323 days, 340 days and 357 days after outburst. The 10μm peak due to silicate is clearly visible. The spectra at 234 days after outburst are shown with the observational data taken from table 8 for R_1 / R_c = 1.6, 2.0 and 2.5 in figures 61, 62 and 63 respectively. Spectra at 323 days after outburst are shown with the observational data in table 8 for R_1/R_c = 1.6, 2.0 and 2.5 in figures 64, 65 and 66 respectively. Spectra at 340 days after outburst are shown with the observational data in table 8 for R_1/R_c = 1.6, 2.0 and 2.5 in figures 67, 68 and 69 respectively. Spectra at 357 days after outburst are shown along with the observational data in table 8 for R_1/R_c = 1.6, 2.0 and 2.5 in figures 70, 71 and 72 respectively.

It can be seen that all the observations except for two are in fairly good agreement with the computed spectra. It is also apparent that the agreement leaves a little to be desired for day 323. However it can be seen from table 8 that the K flux at 323 days is probably too small because the values at 340 and 357 days are both larger than the value at 323 days. All other fluxes at J, H and K show a monotonic decline with time. A monotonic decline is also expected because the supernova luminosity declines monotonically with time. The L observation at 215 days after outburst is a factor 2.2 too large, while the 3.8μm flux at 357 days after outburst is a factor of 3.9 too large. However, the observational errors on these data points are very large; 15% in the case of the L observation and 21% in the case of the 3.8μm, data. These are the only two observations at around 3.5μm. Excellent observing conditions are required to obtain data at ~ 3.5μm. Consequently it is quite possible that the observational errors are much bigger than indicated, and this could account for the discrepancy. Other possible reasons for the discrepancy are discussed later on in the chapter.

It is interesting to compare the approach here with that of Dwek

FIGURE 58. The computed dust and total infra-red spectra of SN1980k for R_1/R_c = 1.6 compared with the observational data at 215 days after outburst.

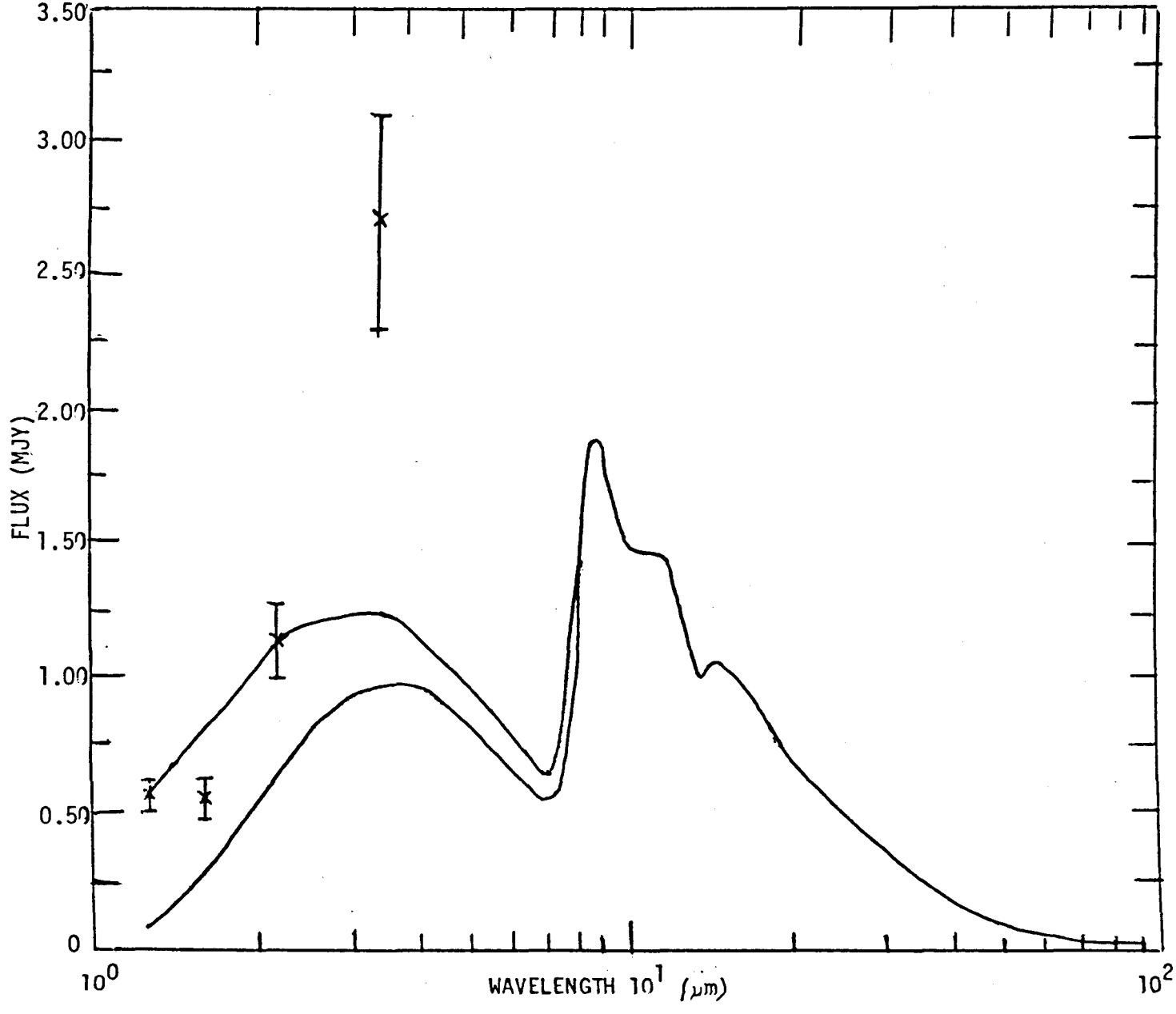
3.50
3.00
2.50
2.00
1.50
1.00
0.50
0
FLUX (MJY)
10^0
10^1
10^2
WAVELENGTH 10^1 (μm)

FIGURE 59. The computed dust and total flux infra-red spectra of SN1980k for R_1/R_c = 2.0 compared with the observational data at 215 days after outburst.

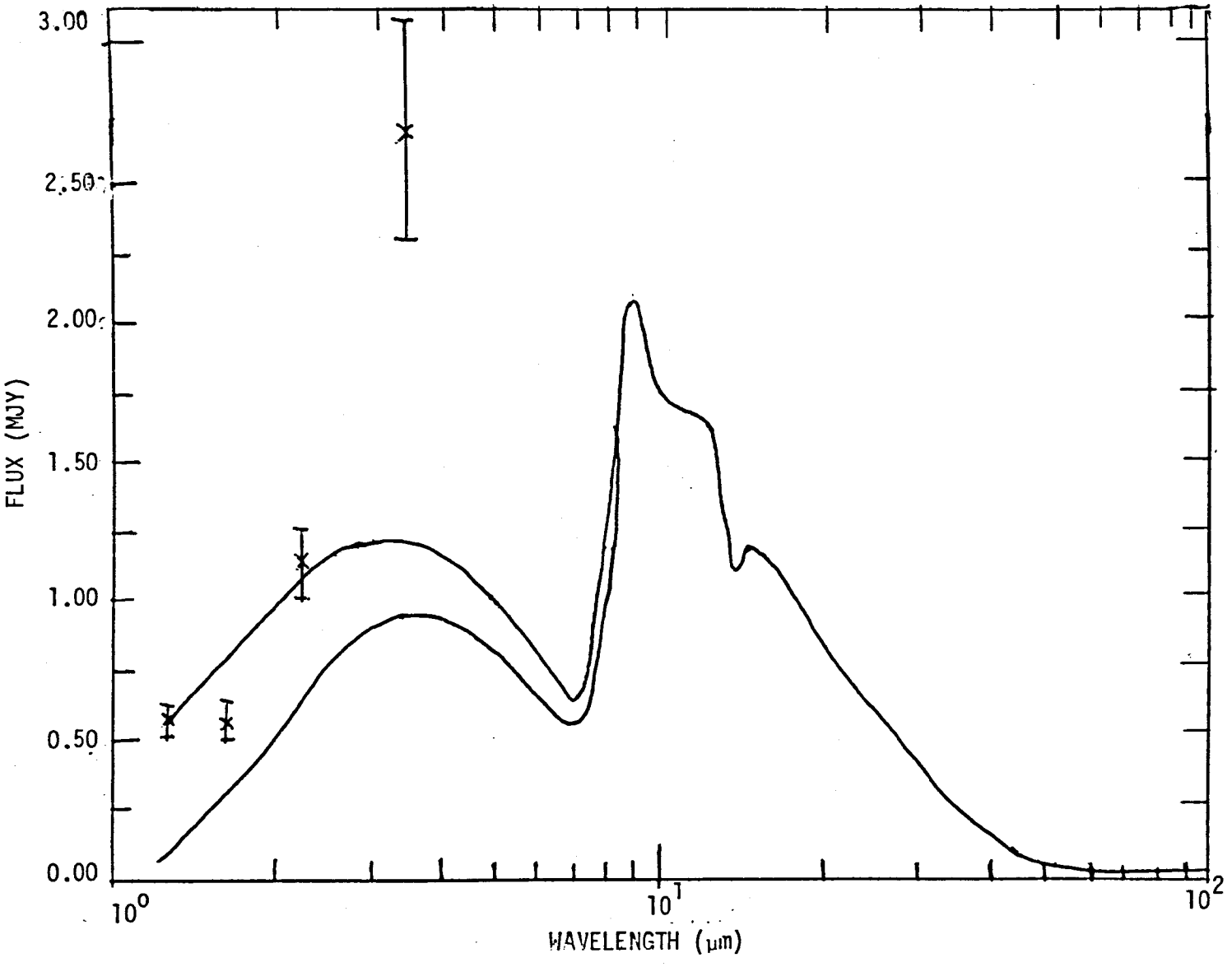
3.00
2.50
2.00
1.50
1.00
0.50
0.00
FLUX (MJY)
10^0
10^1
10^2
WAVELENGTH (μm)

FIGURE 60. The computed dust and total flux infra-red spectra of SN1980k for $R1/R_C$ = 2.5 compared with the observational data at 215 days after outburst.

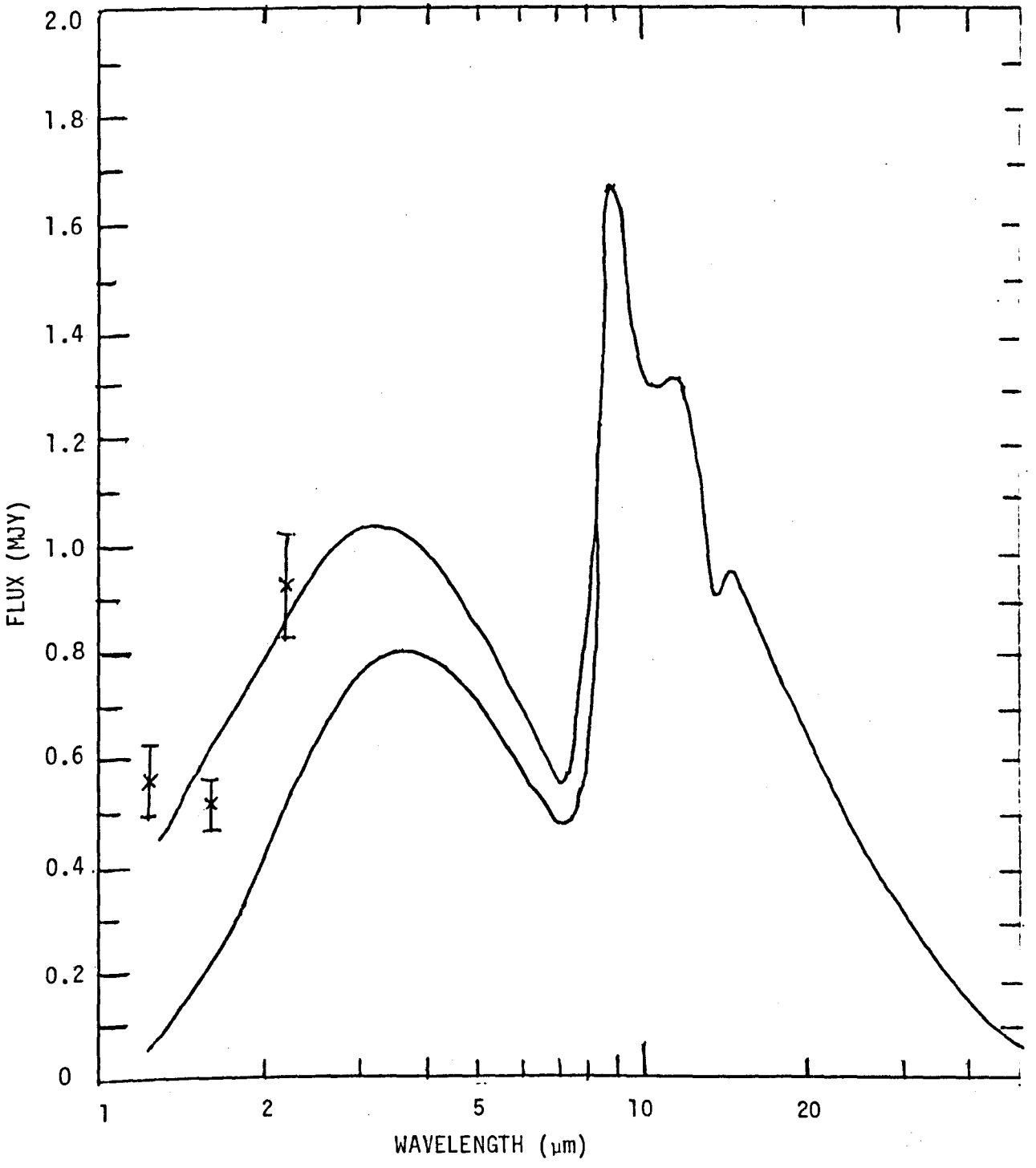
2.0
1.8
1.6
1.4
1.2
1.0
0.8
0.6
0.4
0.2
0
FLUX (MJY)
1
2
5
10
20
WAVELENGTH (μm)

FIGURE 61. The computed dust and total flux infra-red spectra of SN1980k for R_1/R_c = 1.6 compared with the observational data at 234 days after outburst.

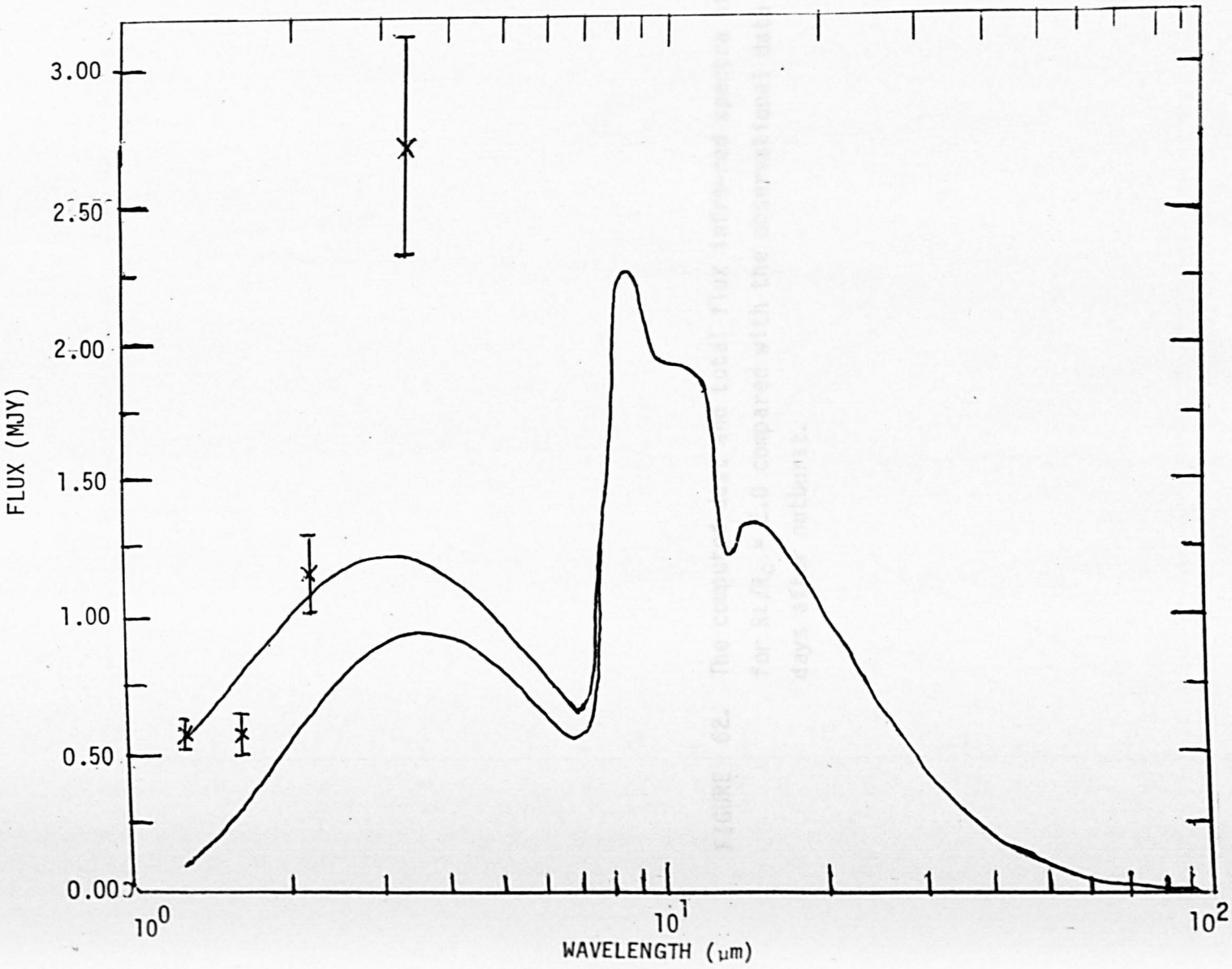
3.00
2.50
2.00
1.50
1.00
0.50
0.00
FLUX (MJY)
10^0
10^1
10^2
WAVELENGTH (μm)

FIGURE 62. The computed dust and total flux infra-red spectra of SN1980k for R_1/R_c = 2.0 compared with the observational data at 234 days after outburst.

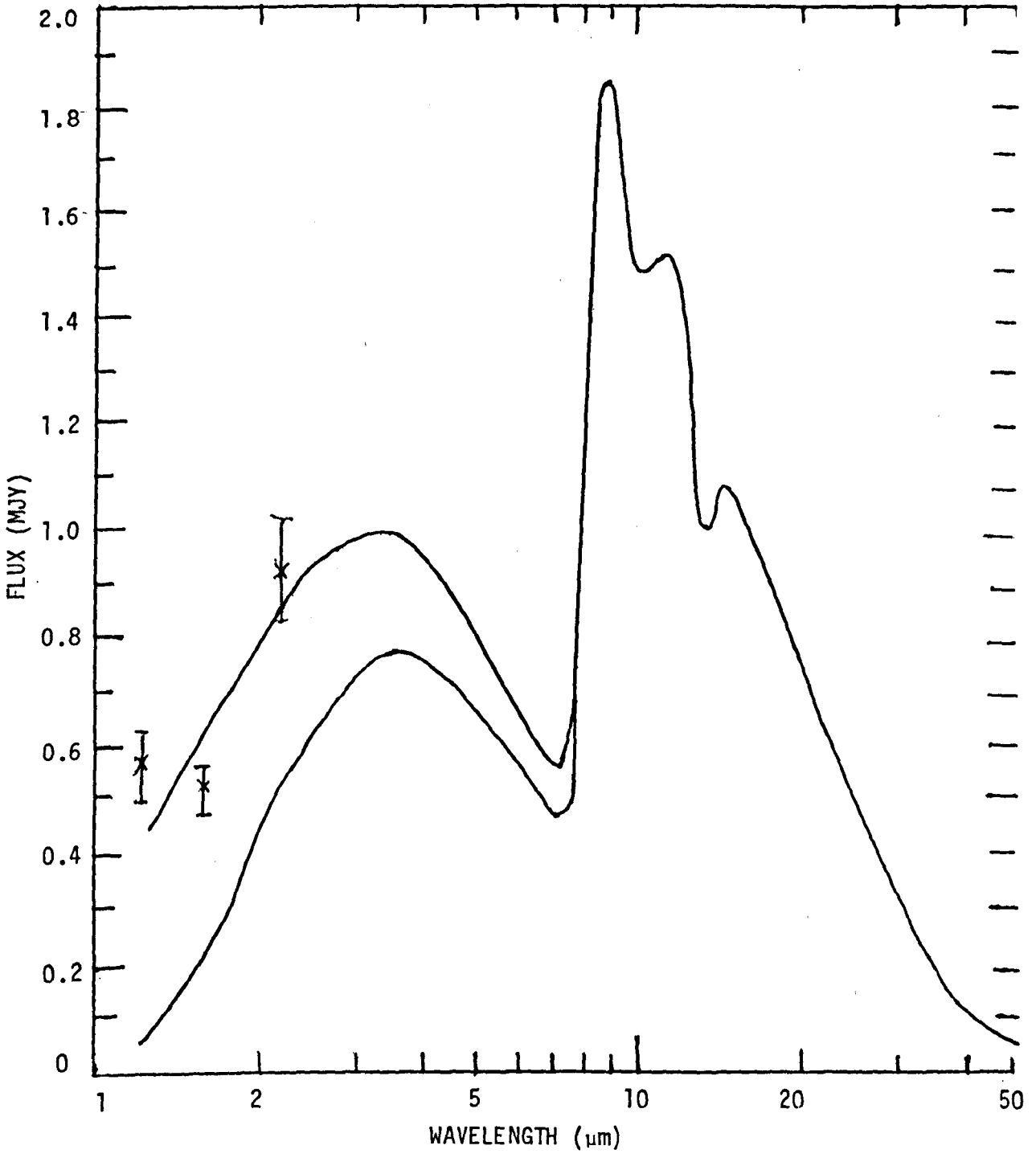
2.0
1.8
1.6
1.4
1.2
1.0
0.8
0.6
0.4
0.2
0
FLUX (MJY)
1
2
5
10
20
50
WAVELENGTH (μm)

FIGURE 63. The computed dust and total flux infra-red spectra of SN1980k for R_1/R_c = 2.5 compared with the observational data at 234 days after outburst.

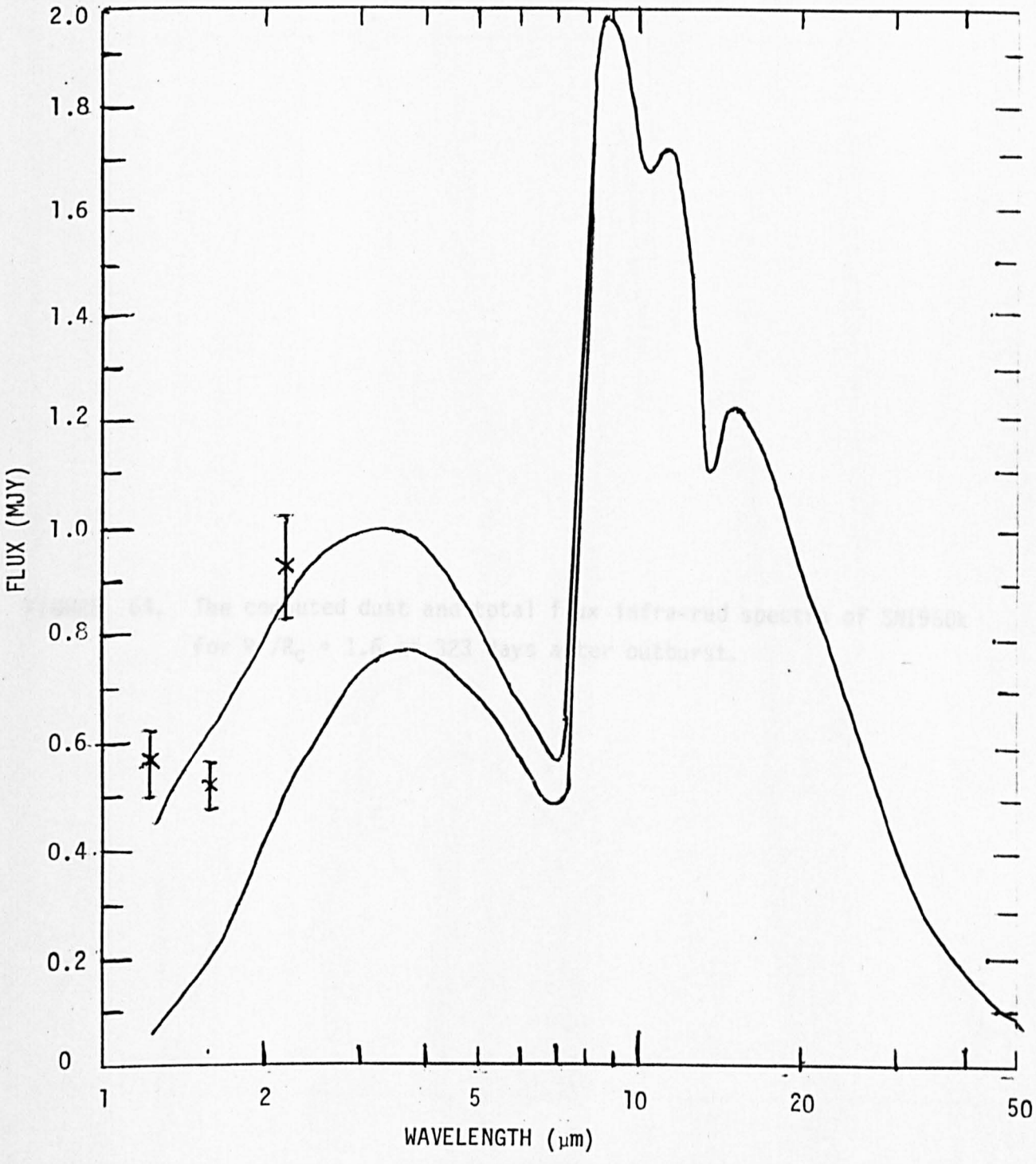
2.0
1.8
1.6
1.4
1.2
1.0
0.8
0.6
0.4
0.2
0
FLUX (MJY)
1
2
5
10
20
50
WAVELENGTH (μm)

FIGURE 64. The computed dust and total flux infra-red spectra of SN1980k for R_1/R_c = 1.6 at 323 days after outburst.

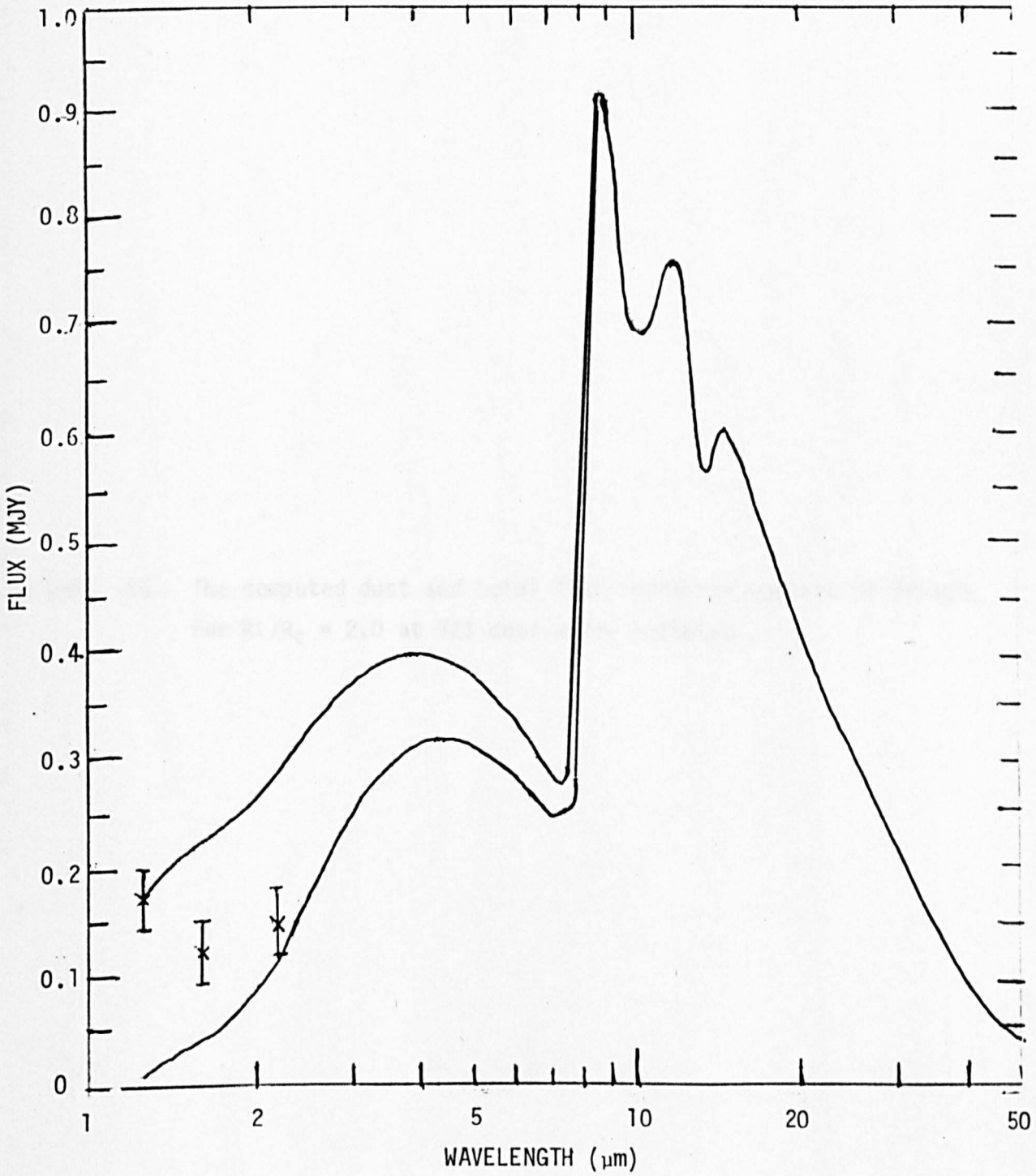
1.0
0.9
0.8
0.7
0.6
0.5
0.4
0.3
0.2
0.1
0
FLUX (MJY)
1
2
5
10
20
50
WAVELENGTH (μm)

FIGURE 65. The computed dust and total flux infra-red spectra of SN1980k for R_1/R_c = 2.0 at 323 days after outburst.

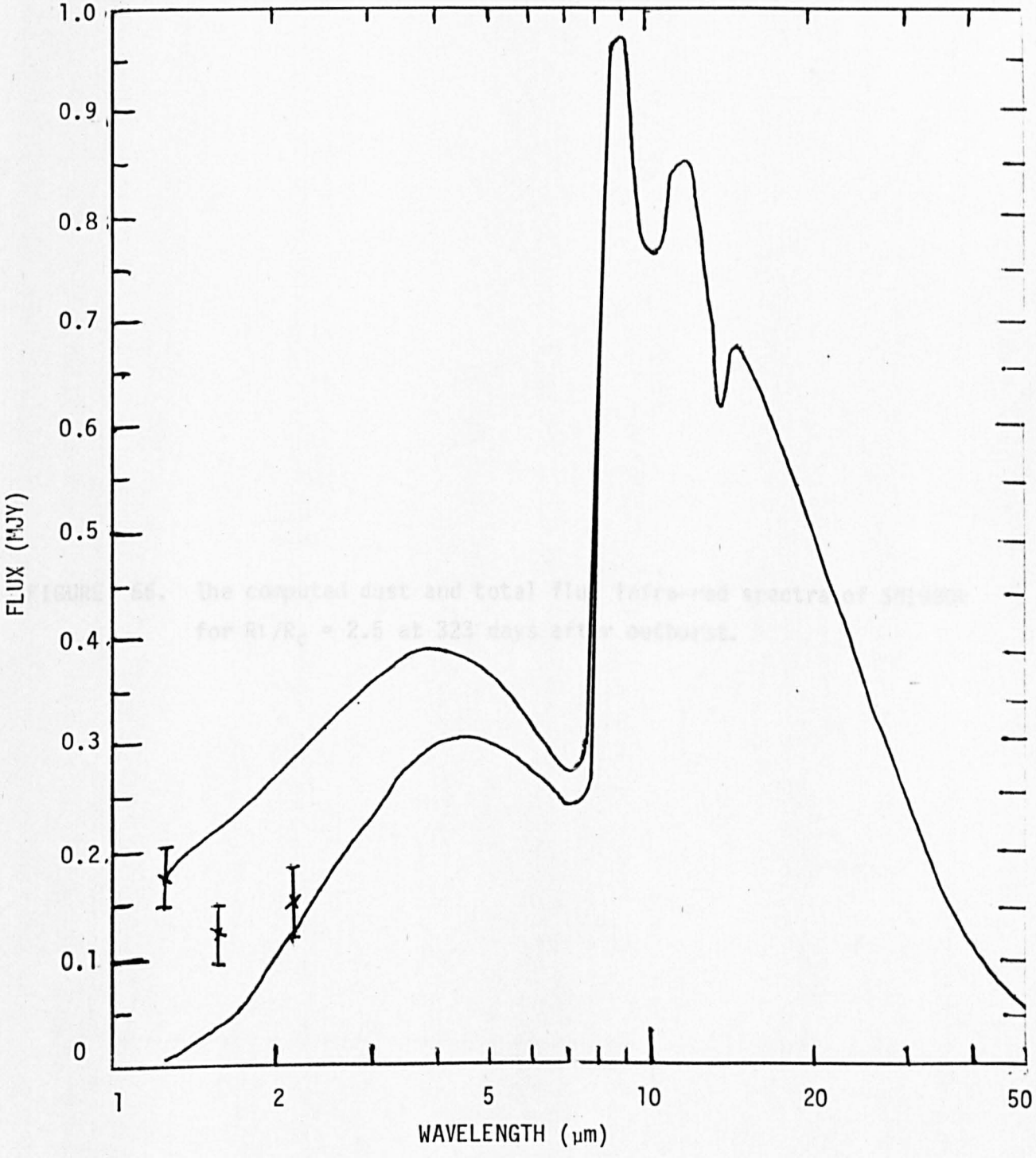
1.0
0.9
0.8
0.7
0.6
0.5
0.4
0.3
0.2
0.1
0
FLUX (MJY)
1
2
5
10
20
50
WAVELENGTH (μm)

FIGURE 66. The computed dust and total flux infra-red spectra of SN1980k for $R1/R_C$ = 2.5 at 323 days after outburst.

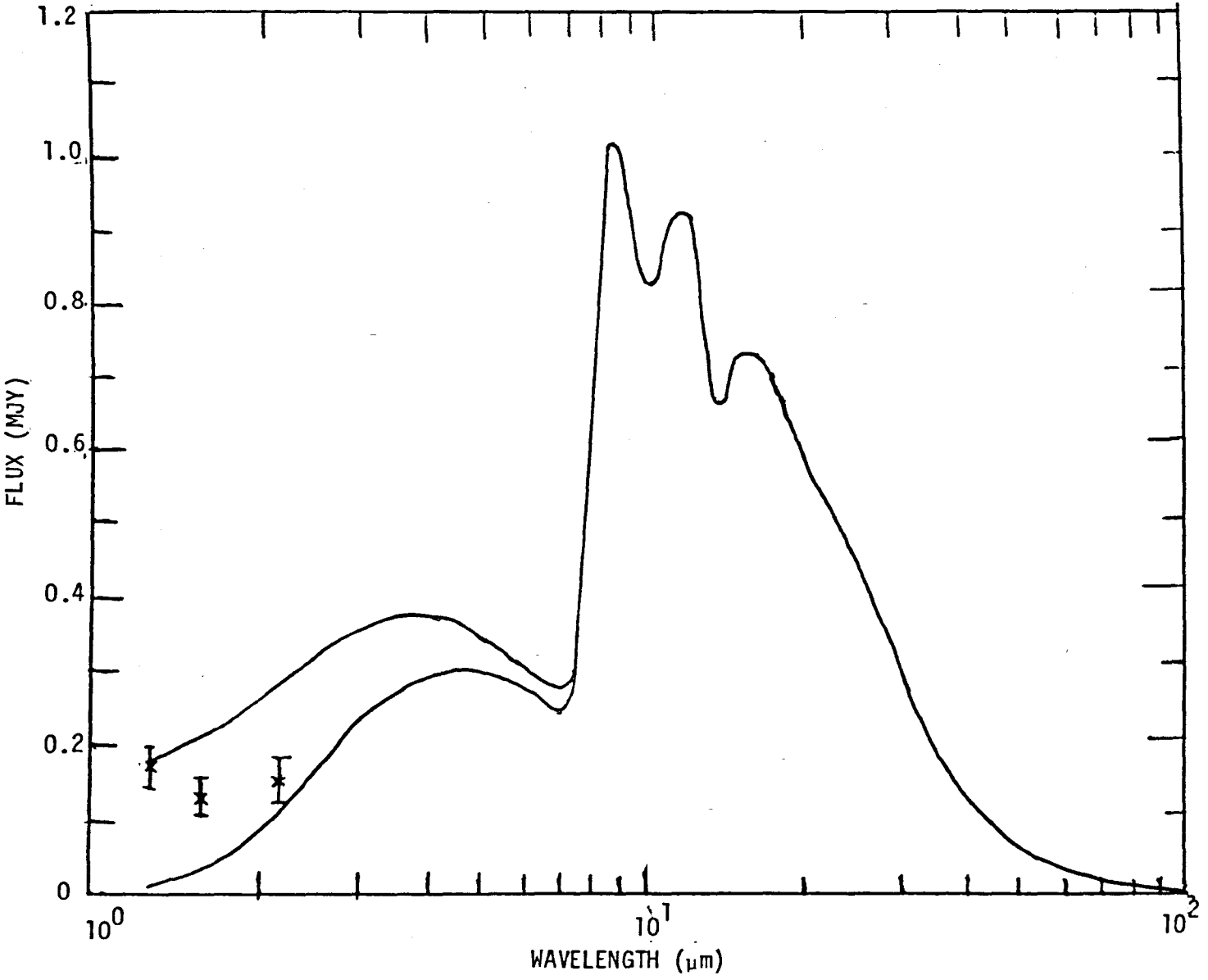
1.2
1.0
0.8
0.6
0.4
0.2
0
FLUX (MJY)
10^0
10^1
10^2
WAVELENGTH (μm)

FIGURE 67. The computed dust and total flux infra-red spectra of SN1980k for R_1/R_c = 1.6 at 340 days after outburst.

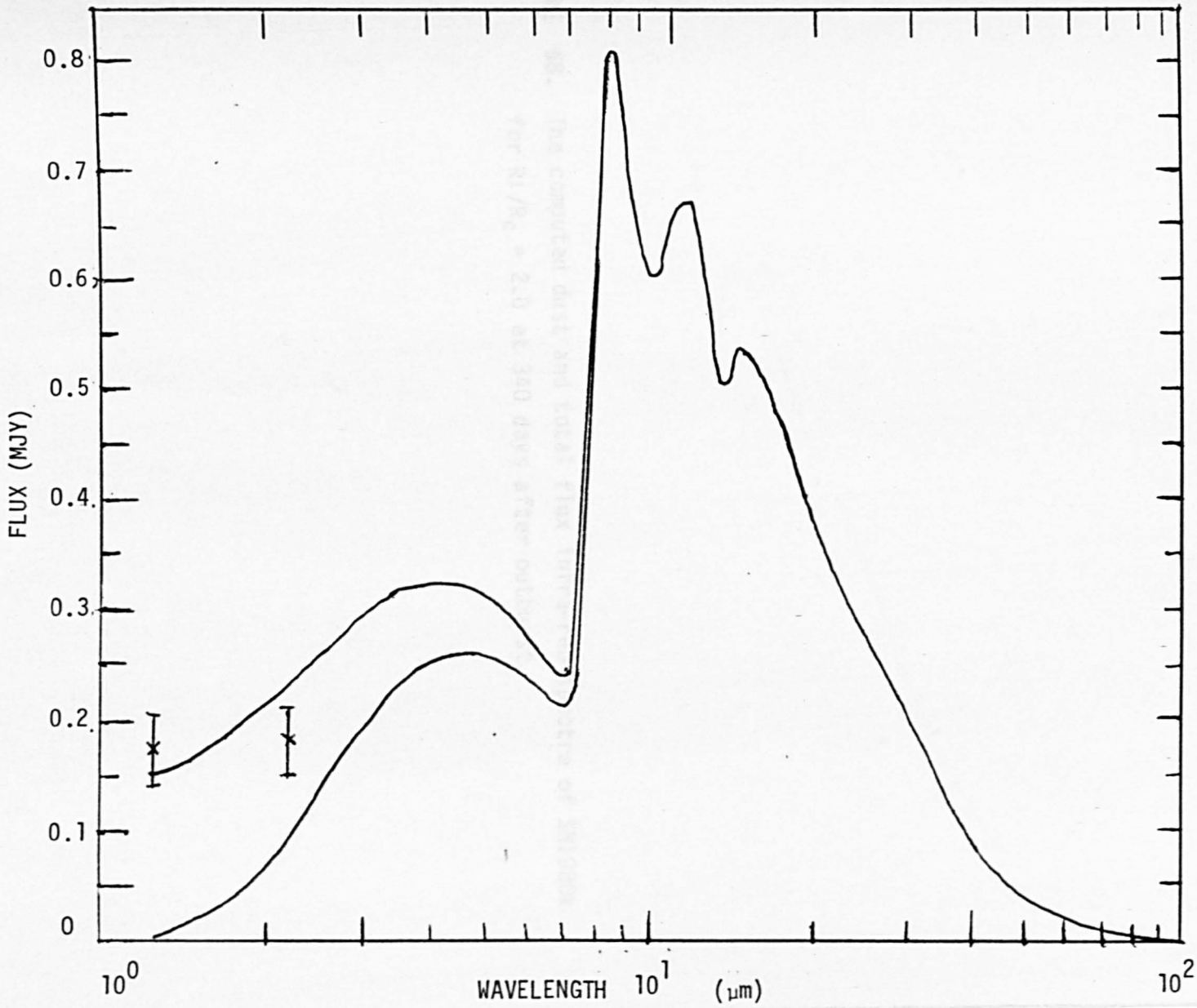
0.8
0.7
0.6
0.5
0.4
0.3
0.2
0.1
0
FLUX (MJY)
10^0
10^1
10^2
WAVELENGTH (μm)

FIGURE 68. The computed dust and total flux infra-red spectra of SN1980k for R_1/R_c = 2.0 at 340 days after outburst.

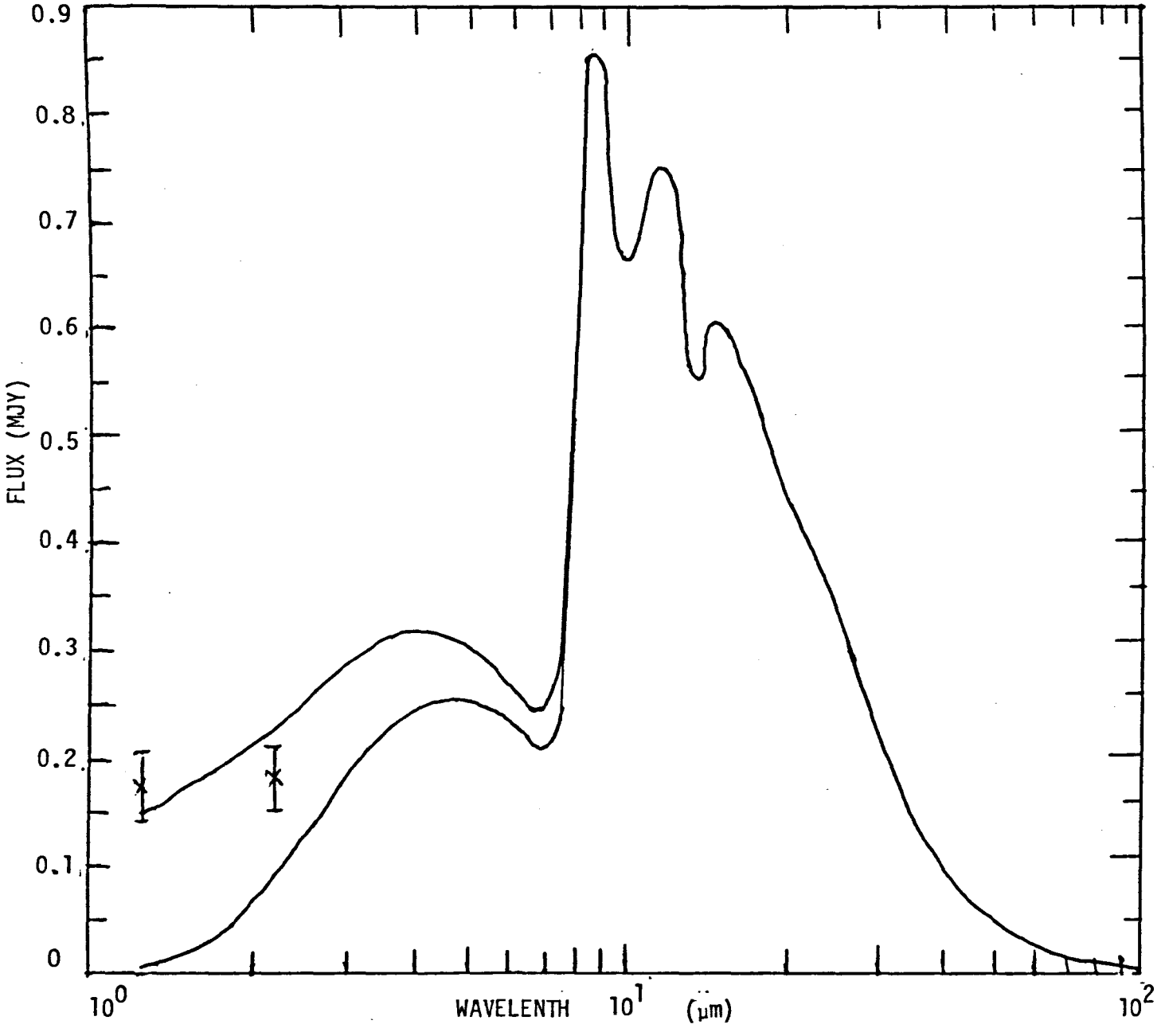
0.9
0.8
0.7
0.6
0.5
0.4
0.3
0.2
0.1
0
FLUX (MJY)
10^0
WAVELENTH
10^1
(μm)
10^2

FIGURE 69. The computed dust and total flux infra-red spectra of SN1980k for R_1/R_c = 2.5 at 340 days after outburst.

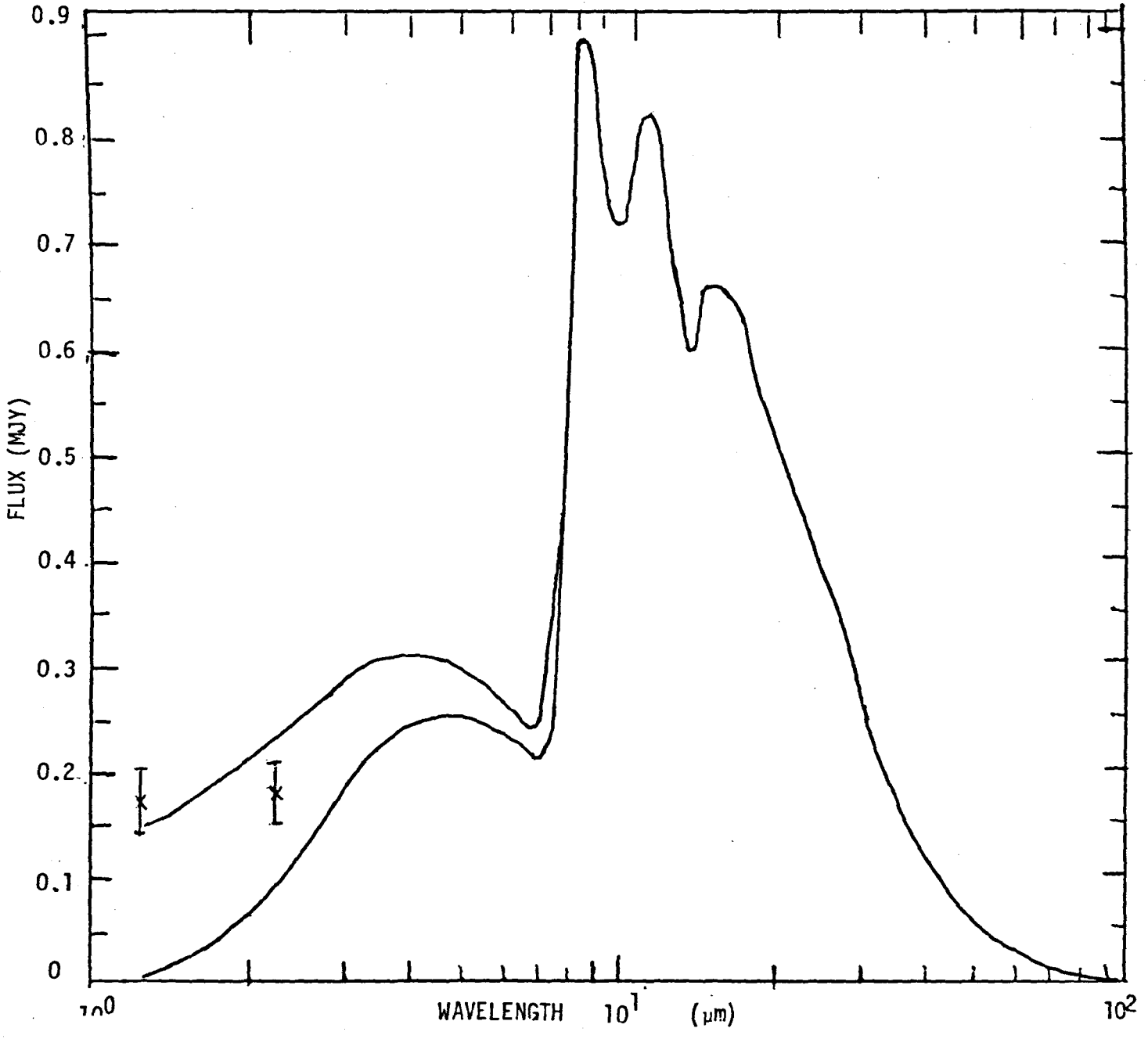
0.9
0.8
0.7
0.6
0.5
0.4
0.3
0.2
0.1
0
FLUX (MJY)
10^0
WAVELENGTH 10^1 (μm)
10^2

FIGURE 70. The computed dust and total flux infra-red spectra of SN1980k for R_1/R_c = 1.6 at 357 days after outburst.

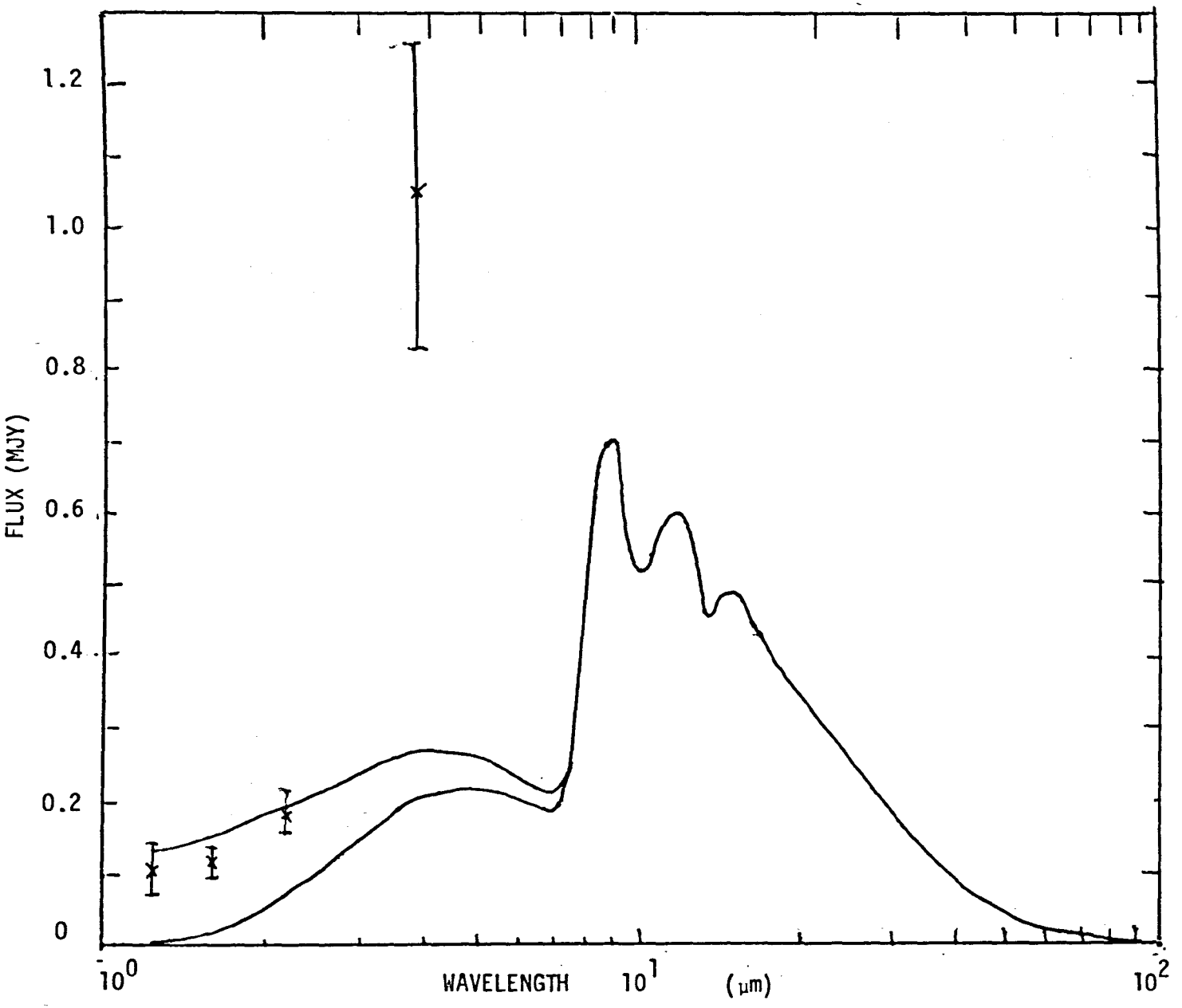
1.2
1.0
0.8
0.6
0.4
0.2
0
FLUX (MJY)
10^0
WAVELENGTH
10^1
(μm)
10^2

FIGURE 71. The computed dust and total flux infra-red spectra of SN1980k for R_1/R_c = 2.0 at 357 days after outburst.

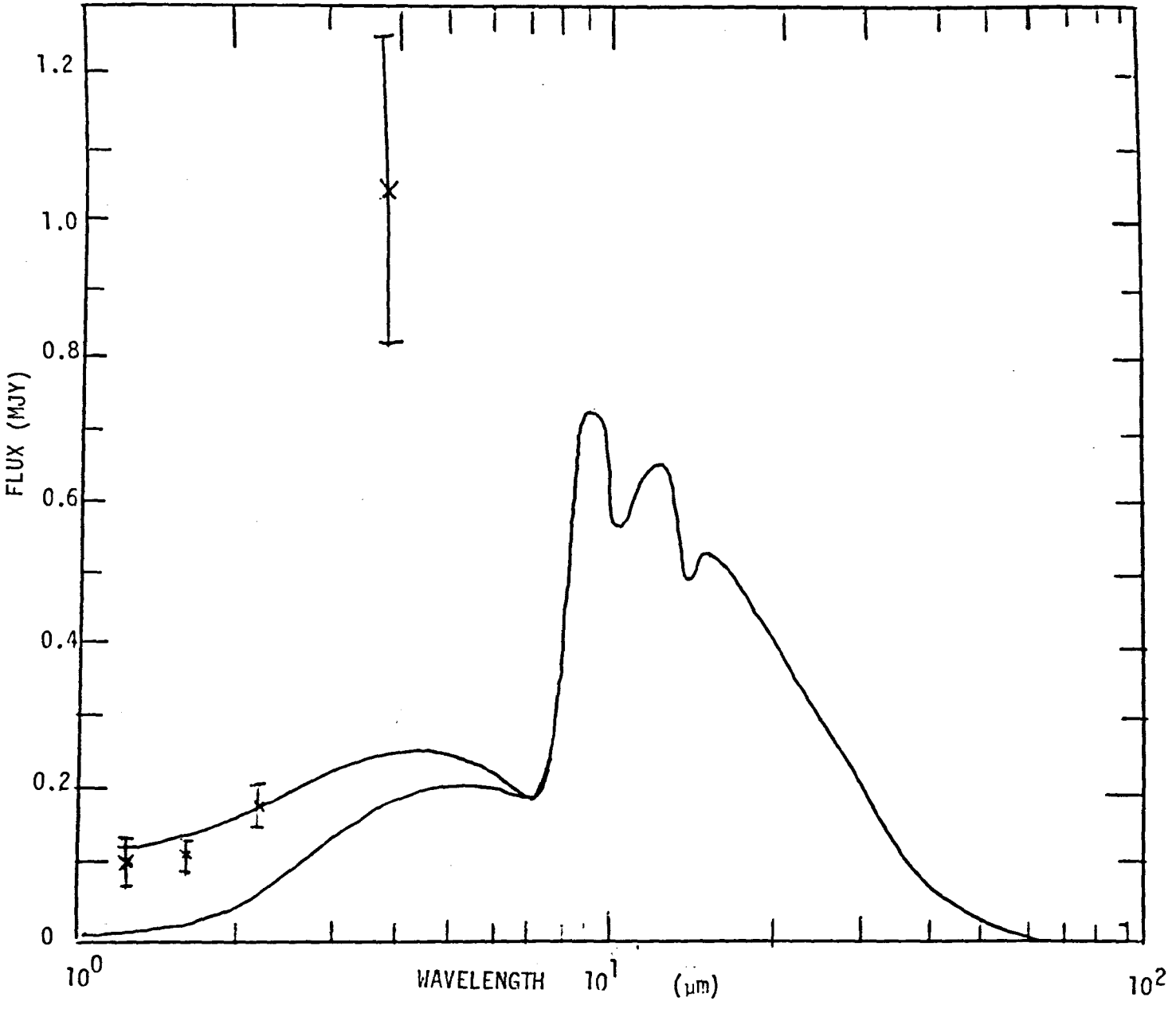
1.2
1.0
0.8
0.6
0.4
0.2
0
FLUX (MJY)
10^0
WAVELENGTH
10^1
(μm)
10^2

FIGURE 72. The computed dust and total flux infra-red spectra of SN1980k for $R1/R_c$ = 2.5 at 357 days after outburst.

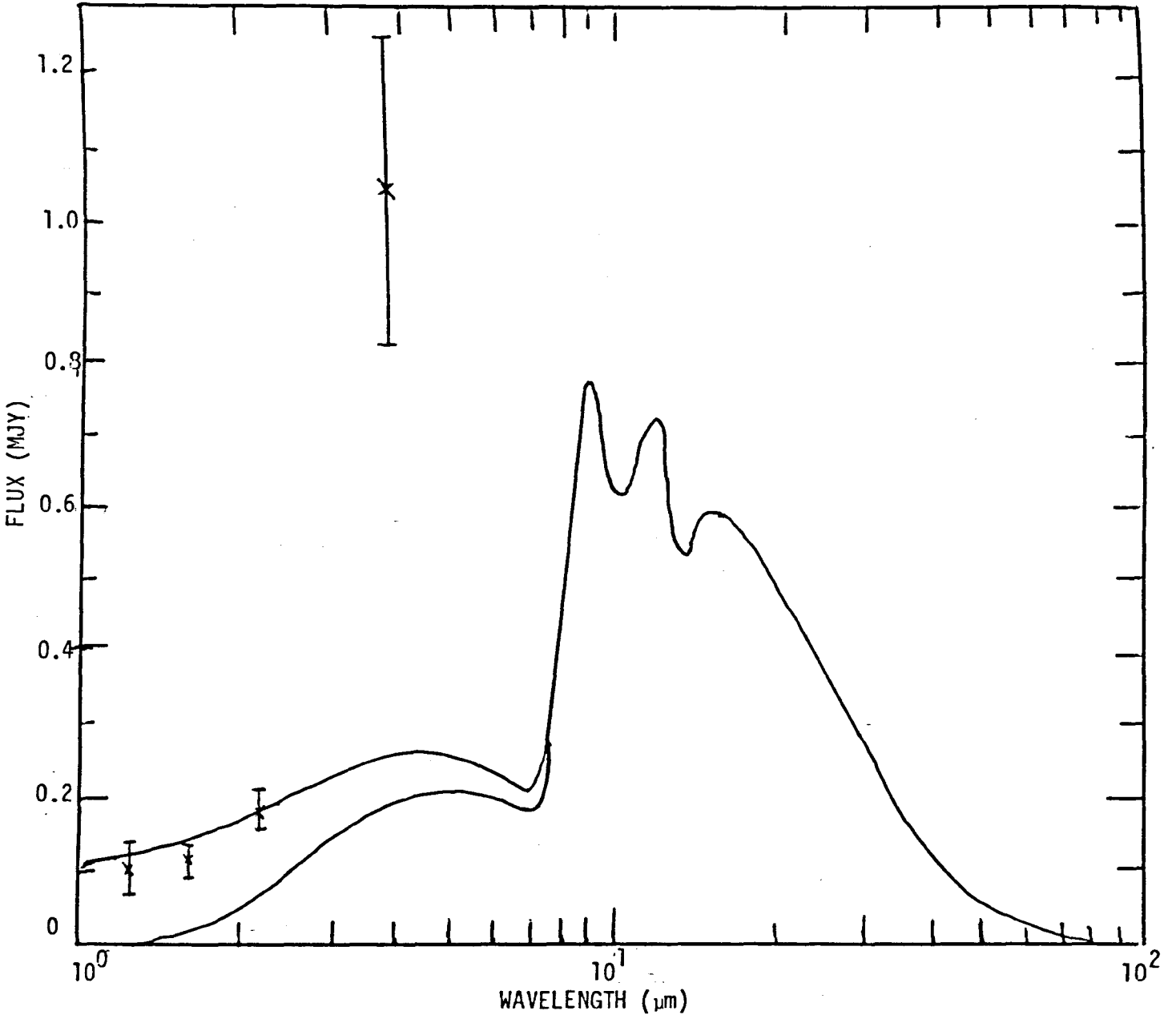
1.2
1.0
0.8
0.6
0.4
0.2
0
FLUX (MJY)
10^0
10^1
10^2
WAVELENGTH (μm)

(1983). The model by Dwek used to solve the equation of transfer contain certain questionable assumptions. One assumption made is

$$\int_0^\infty Q_{abs}(\nu)e^{-\tau'_\nu(r)}B(\nu,T_e)d\nu=\overline{Q_{abs}}(T_e)e^{-\tau_*(r)}\sigma\ T_e^4 \qquad (6.3.10)$$

where $\tau_*(r)$ is given by the expression for $\tau'_\nu(r)$ with $Q_{abs}(\nu)$ replaced by $\overline{Q_{abs}}(T_e)$; this equality only applies under certain conditions. It is also assumed by Dwek that $\overline{Q_{abs}}(T_e) = 1$. This is not the case for silicate grains at the temperatures of supernovae, (Gilman, 1974), silicate grains being the most likely to occur around type II supernovae. The grains are also assumed to be conducting which as discussed is unlikely to be the case. As a result of these assumptions the validity of the computed spectra is questionable. The J and H fluxes are between three and twenty times greater than the predicated dust fluxes at those wavelengths, and no attempt is made to investigate whether these can be fitted by the supernova flux. The approach here is much more rigorous. The K fluxes do not agree quite as well as they do with the fluxes computed in this thesis, (as shown in figures 58, 59, 60, 70, 71 and 72) and while the fluxes at 3.4μm and 3.8μm at 215 days and 357 days respectively are in better agreement, it has been pointed out that there are likely to be large observational errors on these points.

The flux from the supernova photosphere as a function of time for the first 800 days after outburst is shown at 3.4μm, 9μm and 20μm in figures 73, 74 and 75 respectively. The dust and total flux for case R_1/R_c = 1.6 at 3.4μm, 9μm and 20μm are shown as a function of time for the first 800 days after outburst in figures 76, 77 and 78 respectively. The dust flux for the three cases R_1/R_c = 1.6, 2.0 and 2.5 is shown as a function of time for the first 800 days after outburst at 3.4μm, 9μm and 20μm in figures 79, 80 and 81 respectively. The light curves at 3.4μm represent the typical time variation of the dust flux in the near infra-red region of the spectrum,

FIGURE 73. SN1980k : The computed light curve at 3.4μm.

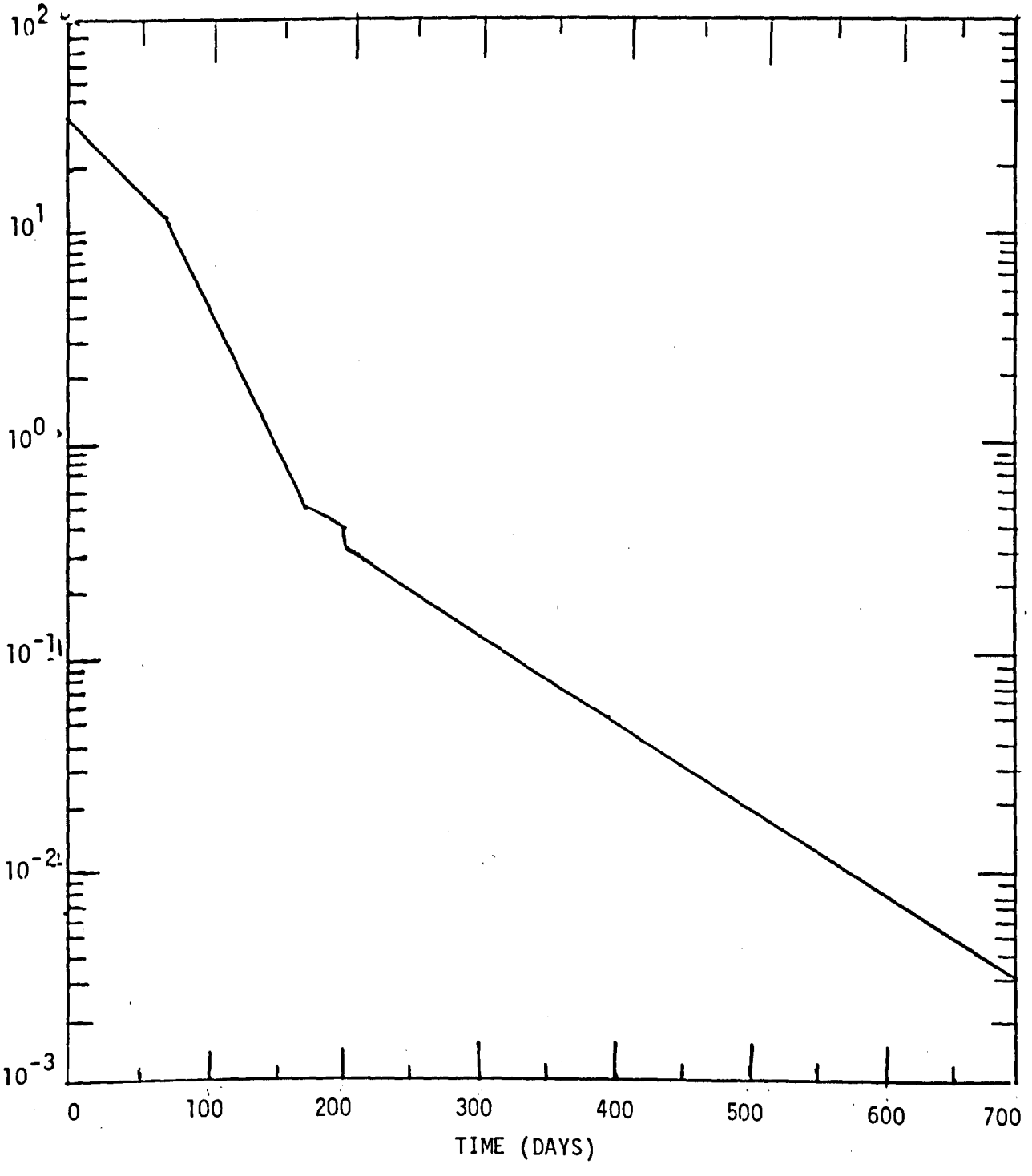
10^2
10^1
10^0
10^{-1}
10^{-2}
10^{-3}
0
100
200
300
400
500
600
700
TIME (DAYS)

FIGURE 74. SN1980k : The computed light curve at 9μm.

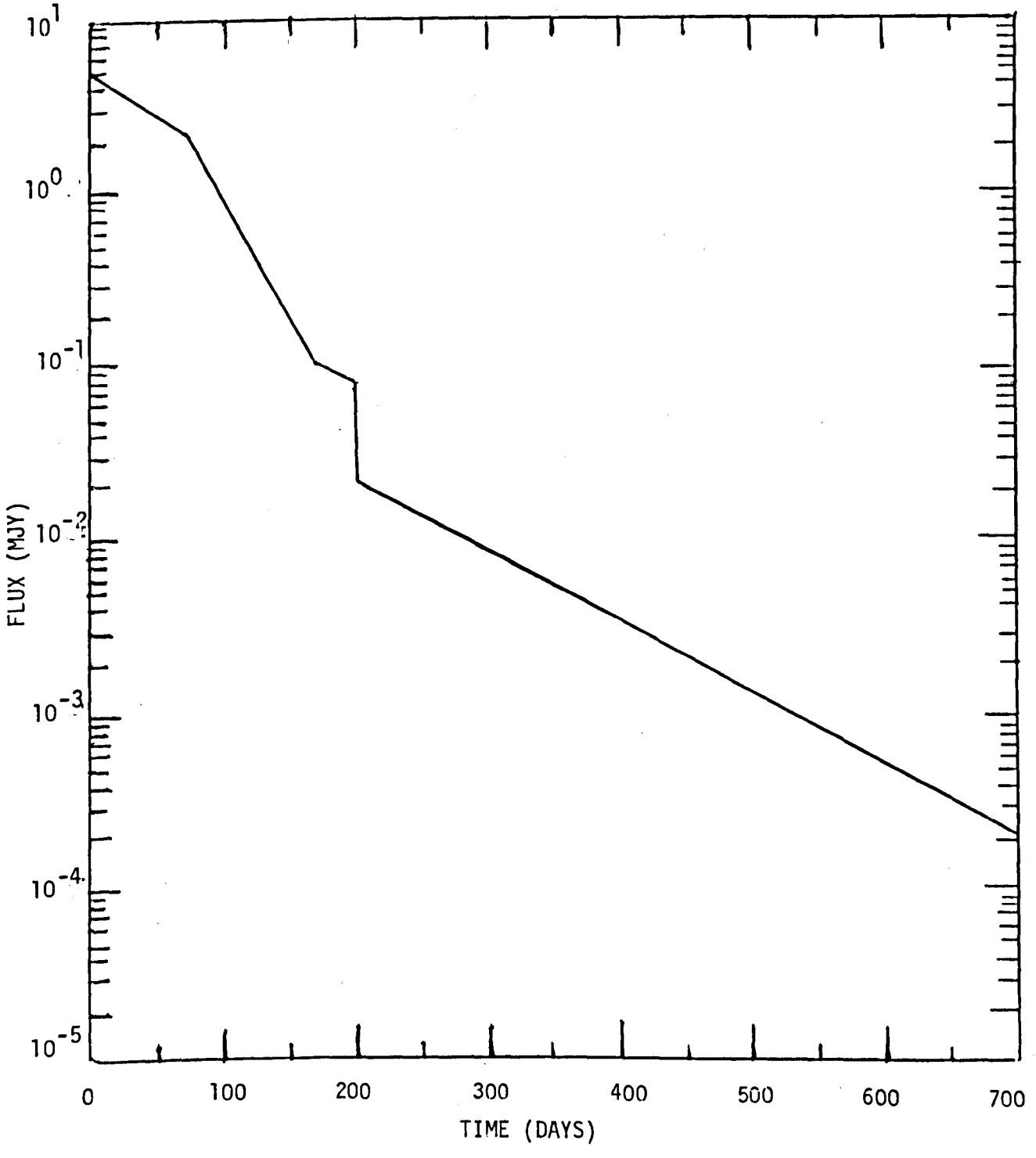
10^{1}
10^{0}
10^{-1}
10^{-2}
10^{-3}
10^{-4}
10^{-5}
FLUX (MJY)
0
100
200
300
400
500
600
700
TIME (DAYS)

FIGURE 75. SN1980k : The computed light curve at 20μm.

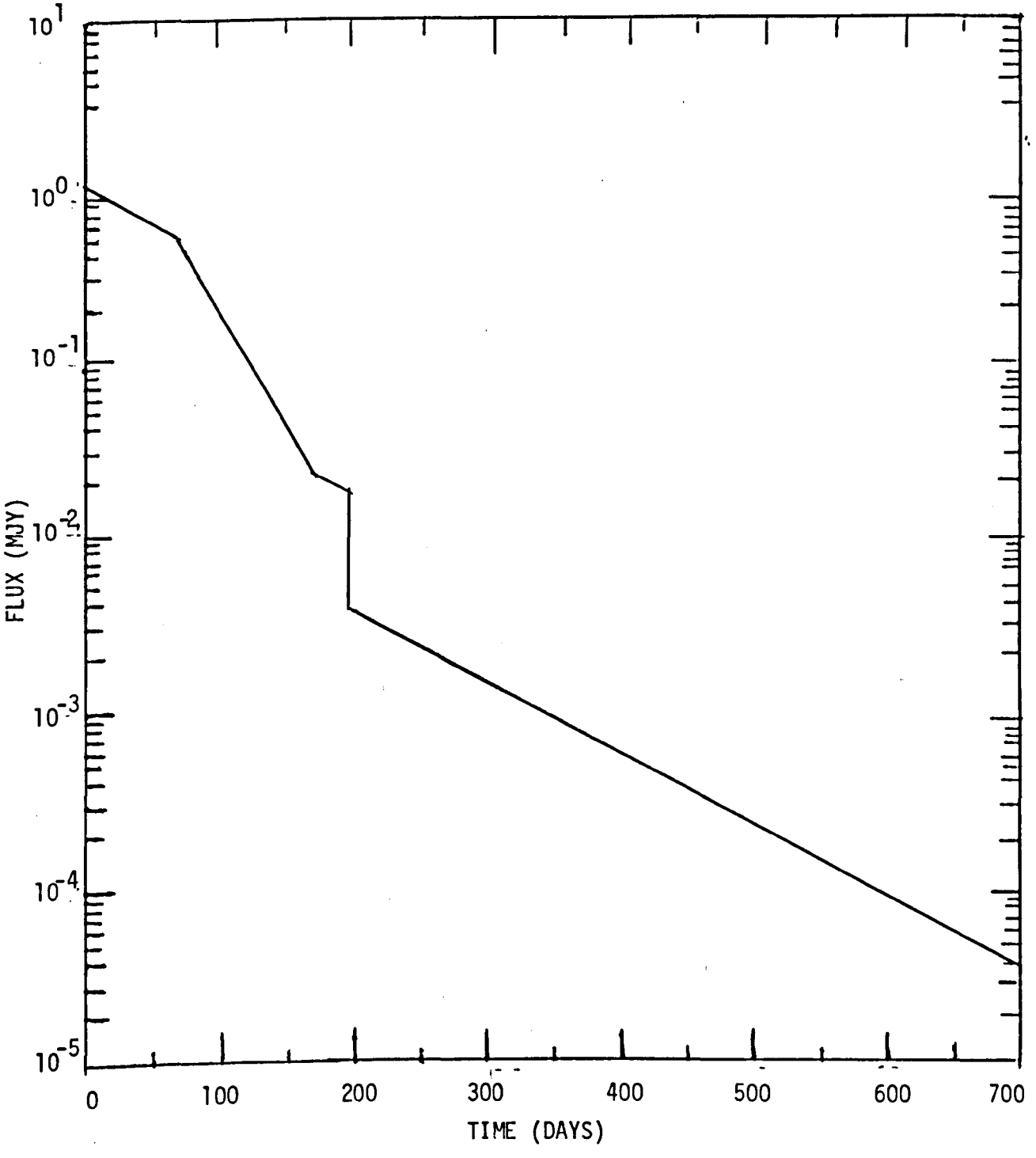
10^{1}
10^{0}
10^{-1}
10^{-2}
10^{-3}
10^{-4}
10^{-5}
FLUX (MJY)
0
100
200
300
400
500
600
700
TIME (DAYS)

FIGURE 76. SN1980k : The computed dust and total flux as a function of time for $R1/R_C$ = 1.6 at 3.4μm. (The two curves are virtually indistinguishable).

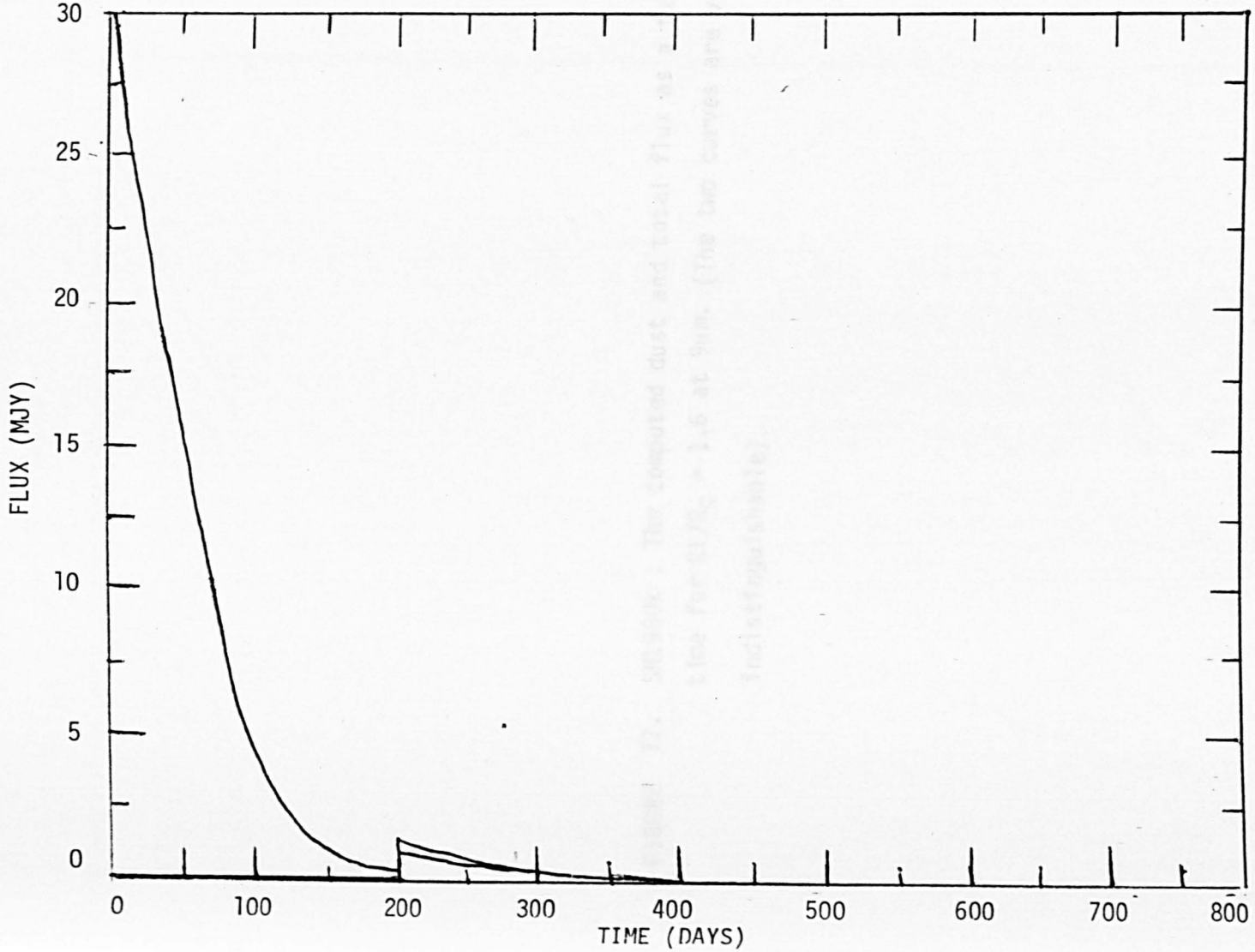
30
25
20
15
10
5
0
FLUX (MJY)
0
100
200
300
400
500
600
700
800
TIME (DAYS)

FIGURE 77. SN1980k : The computed dust and total flux as a function of time for R_1/R_C = 1.6 at 9μm. (The two curves are virtually indistinguishable).

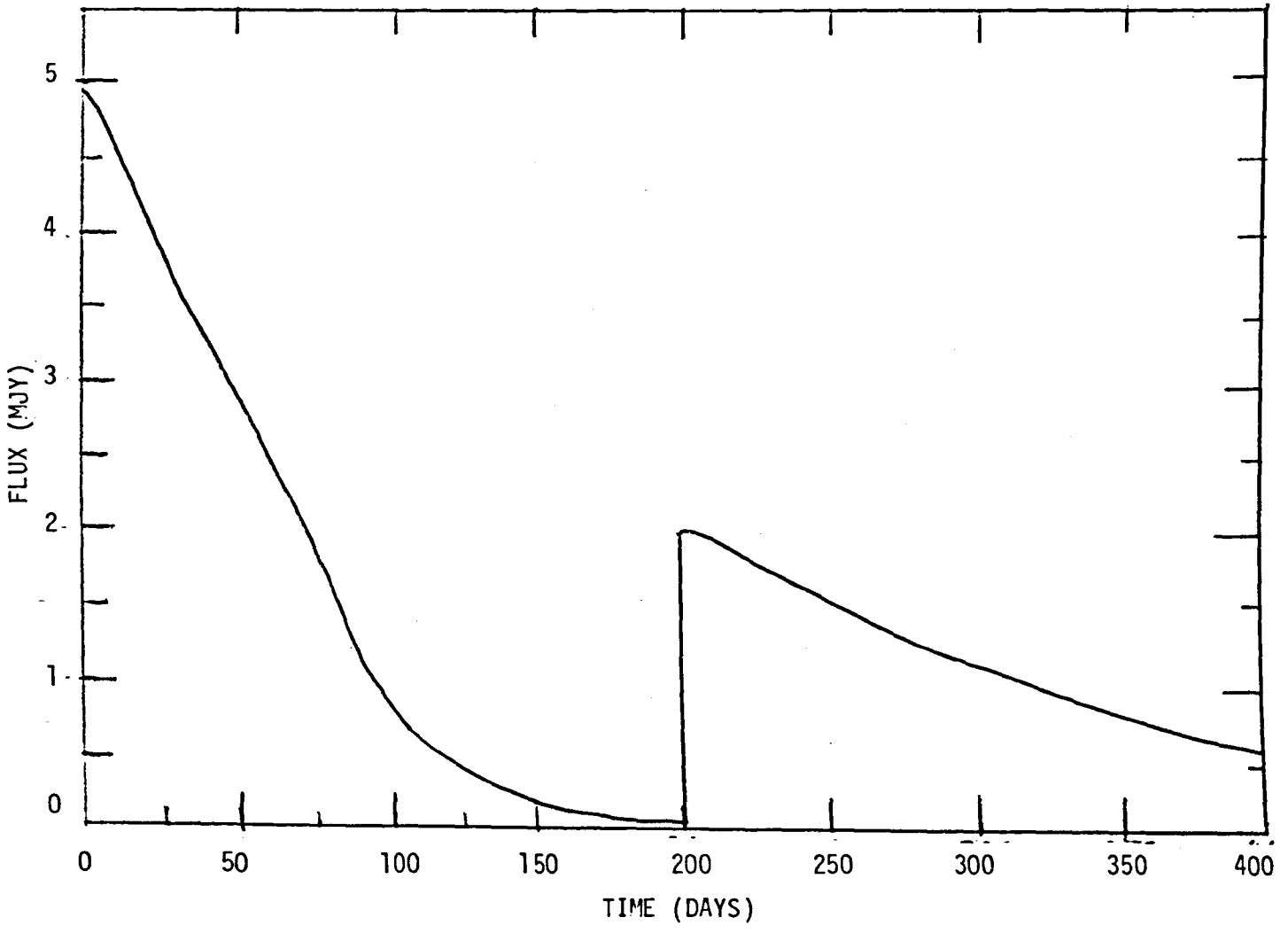
5
4
3
2
1
0
FLUX (MJY)
0
50
100
150
200
250
300
350
400
TIME (DAYS)

FIGURE 78. SN1980k : The computed dust and total flux as a function of time for R_1/R_C = 1.6 at 20μm. (The two curves are virtually indistinguishable).

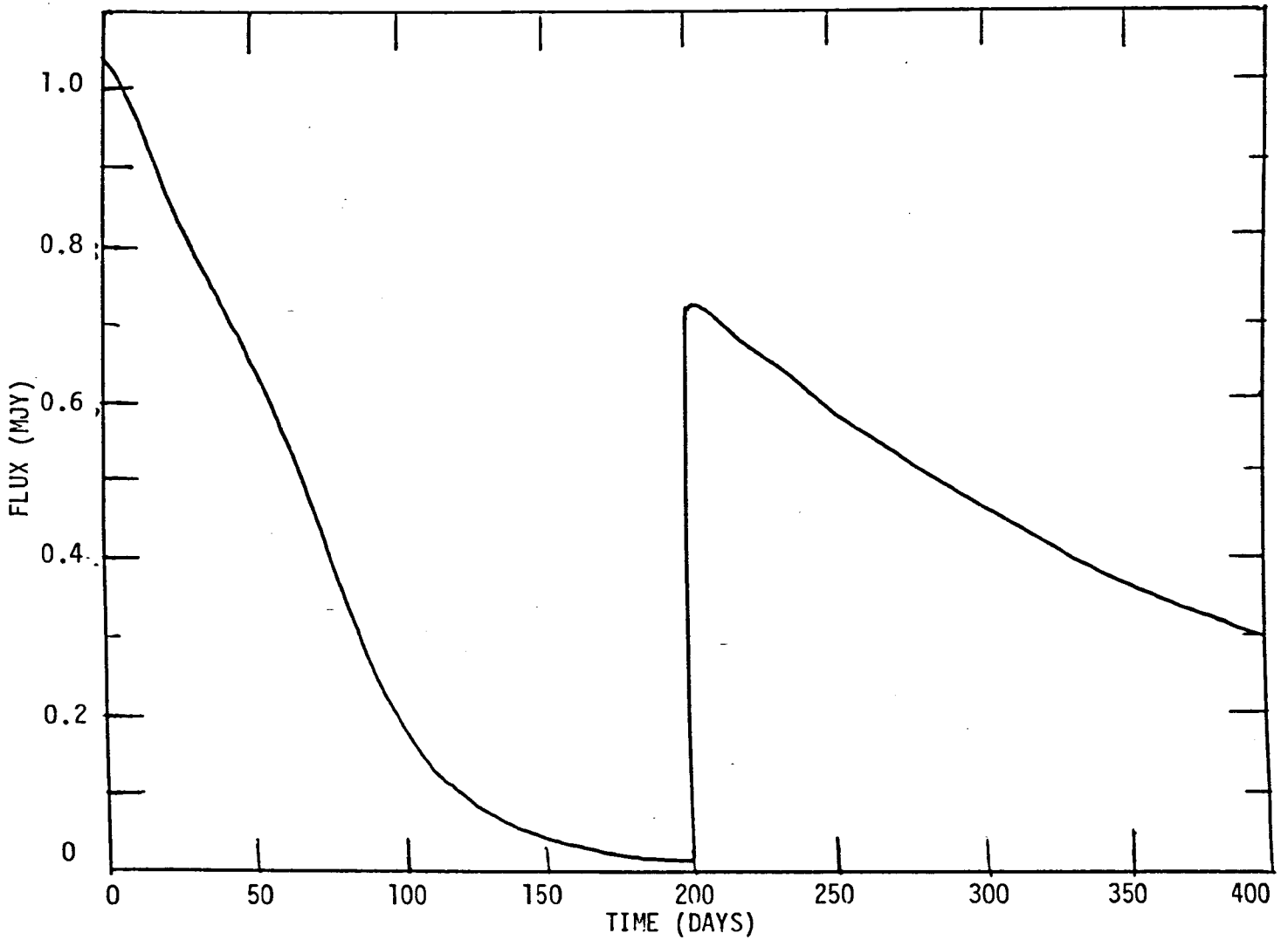
1.0
0.8
0.6
0.4
0.2
0
FLUX (MJY)
0
50
100
150
200
250
300
350
400
TIME (DAYS)

FIGURE 79. SN1980k : The computed infra-red dust flux as a function of time for R_1/R_C = 1.6 and 2.5 at 3.4μm. NB. The three curves are indistinguishable.

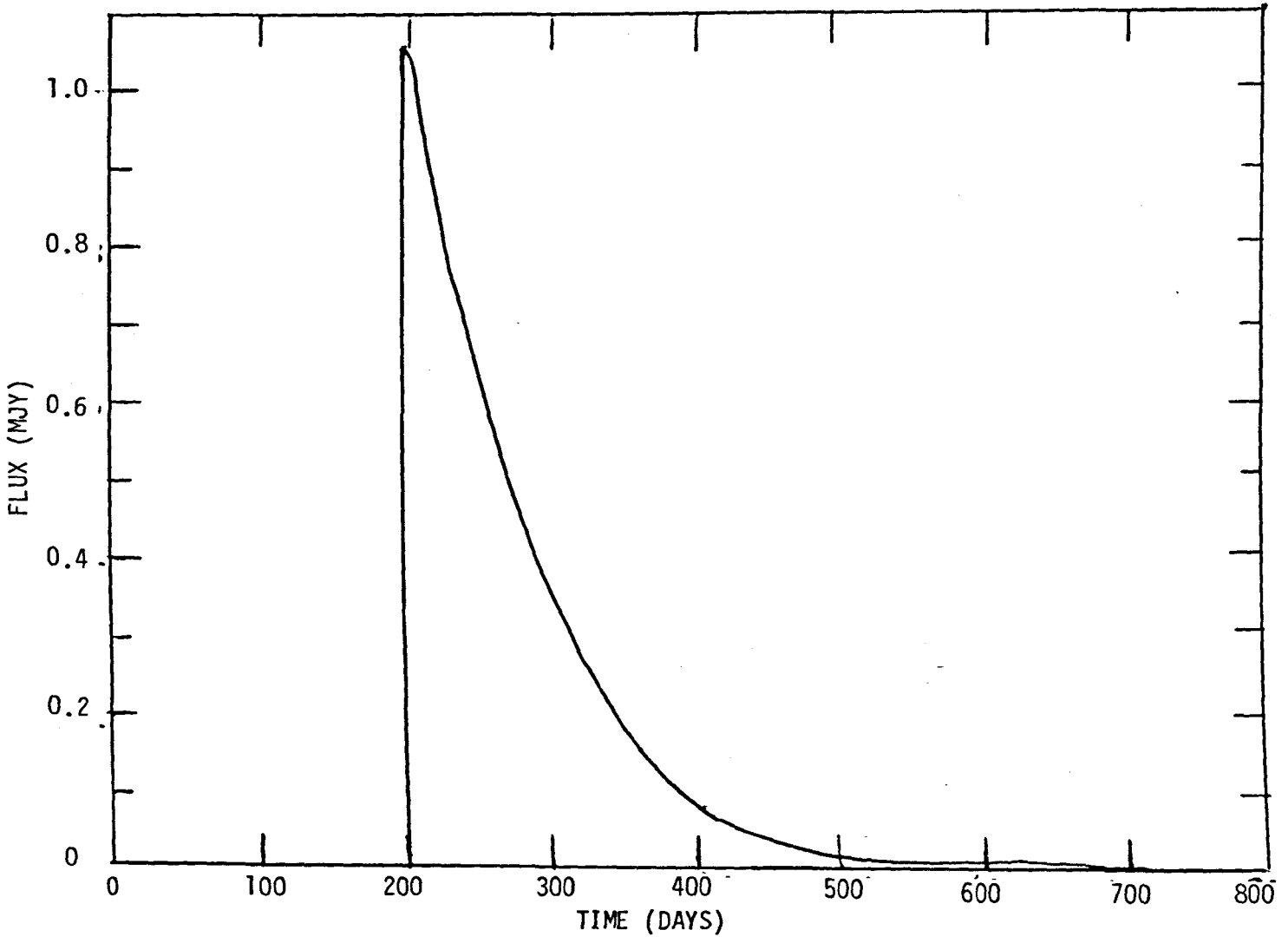
1.0
0.8
0.6
0.4
0.2
0
FLUX (MJY)
0
100
200
300
400
500
600
700
800
TIME (DAYS)

FIGURE 80. SN1980k : The computed infra-red dust flux as a function of time for $R1/R_c$ = 1.6 (lower curve), 2.0 (middle curve) and 2.5 (upper curve) at 9μm.

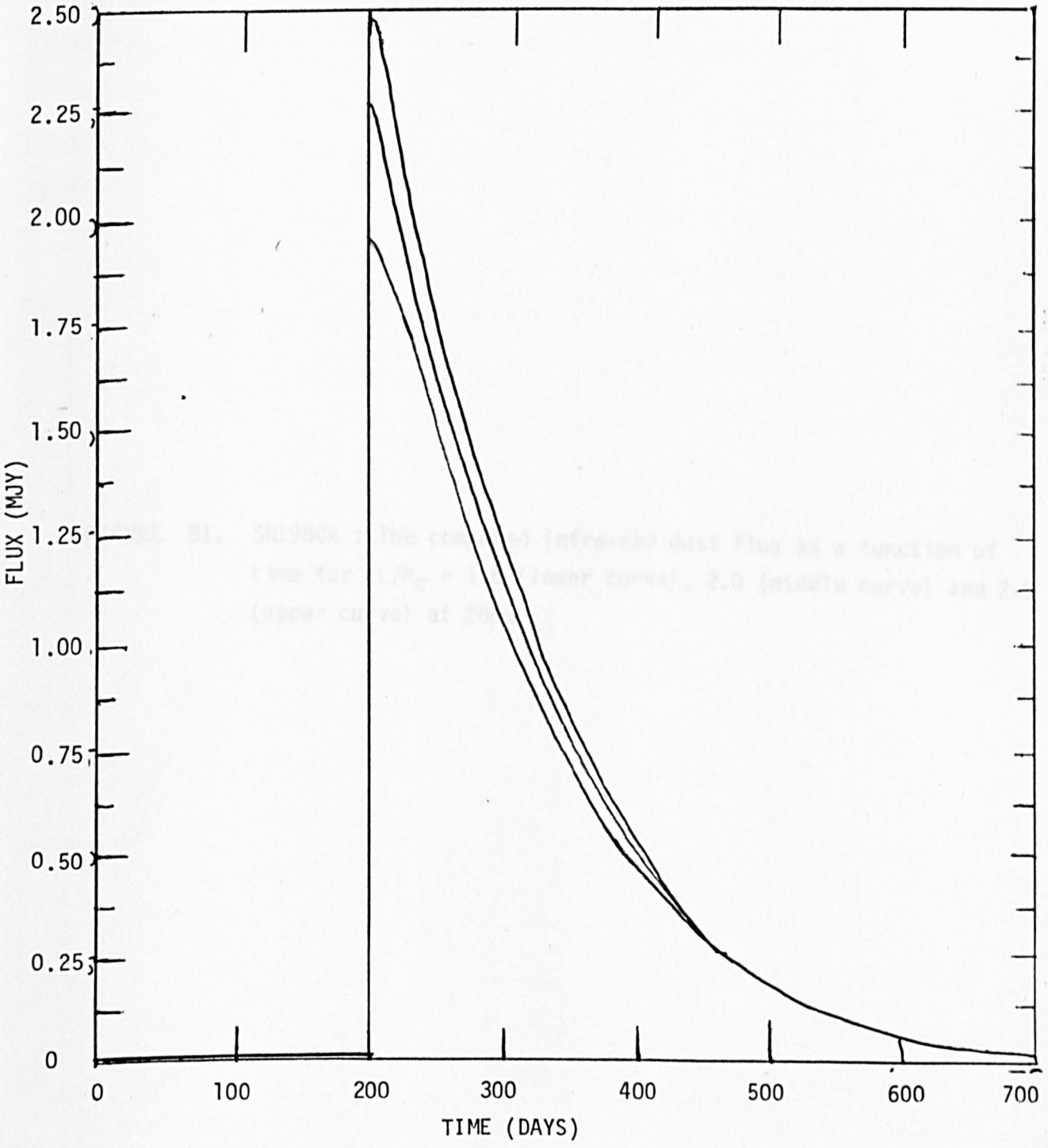
2.50
2.25
2.00
1.75
1.50
1.25
1.00
0.75
0.50
0.25
0
FLUX (MJY)
0
100
200
300
400
500
600
700
TIME (DAYS)

FIGURE 81. SN1980k : The computed infra-red dust flux as a function of time for R_1/R_c = 1.6 (lower curve), 2.0 (middle curve) and 2.5 (upper curve) at 20μm.

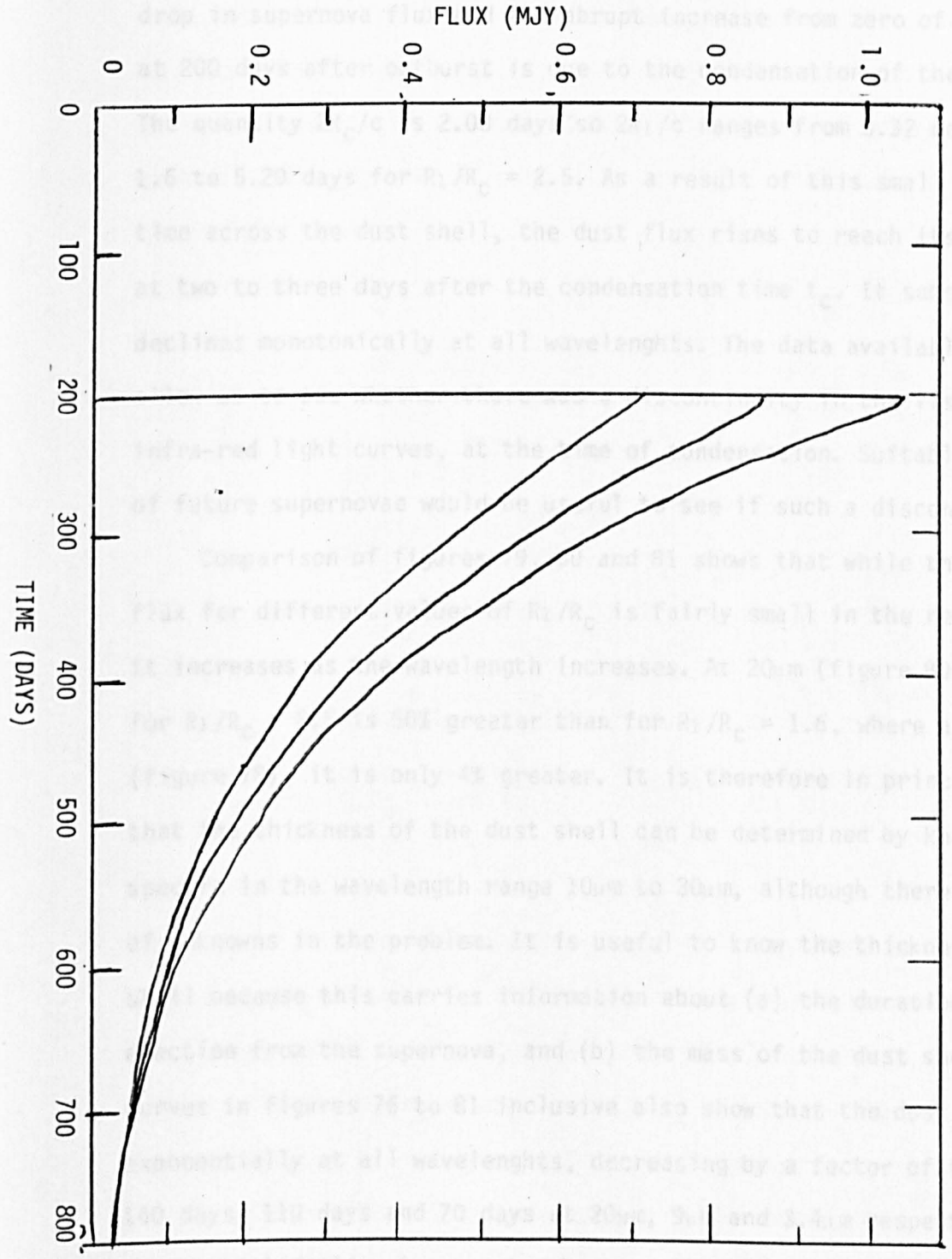
FLUX (MJY)
0
0.2
0.4
0.6
0.8
1.0
TIME (DAYS)
0
100
200
300
400
500
600
700
800

while light curves at 20μm represent the typical time variation of the dust flux in the far infra-red region of the spectrum. The time variation of the flux at 9μm describes the flux variation of the silicate peak. The abrupt drop in supernova flux and the abrupt increase from zero of the dust flux at 200 days after outburst is due to the condensation of the dust shell. The quantity $2R_c/c$ is 2.08 days so $2R_1/c$ ranges from 3.32 days for R_1/R_c = 1.6 to 5.20 days for R_1/R_c = 2.5. As a result of this small light travel time across the dust shell, the dust flux rises to reach its maximum value at two to three days after the condensation time t_c. It subsequently declines monotonically at all wavelenghts. The data available does not allow us to see whether there was a discontinuity in the visual and infra-red light curves, at the time of condensation. Suitable observations of future supernovae would be useful to see if such a discontinuity occurs.

Comparison of figures 79, 80 and 81 shows that while the difference in flux for different values of R_1/R_c is fairly small in the near infra-red, it increases as the wavelength increases. At 20μm (figure 80) the dust flux for R_1/R_c = 2.5 is 50% greater than for R_1/R_c = 1.6, where as at 3.4μm (figure 78), it is only 4% greater. It is therefore in principle possible that the thickness of the dust shell can be determined by knowledge of the spectra in the wavelength range 10μm to 30μm, although there are a number of unknowns in the problem. It is useful to know the thickness of the dust shell because this carries information about (a) the duration of the mass ejection from the supernova, and (b) the mass of the dust shell. The light curves in figures 76 to 81 inclusive also show that the dust flux declines exponentially at all wavelenghts, decreasing by a factor of two in about 140 days, 110 days and 70 days at 20μm, 9μm and 3.4μm respectively. The exponential decline is expected because the light travel time across the dust shell is only a few days and the supernova luminosity declines exponentially with time. The decline becomes steeper than exponential at ~ 400 days after outburst and at 800 days after outburst the dust flux at

20μm is 0.02mJy while it is an order of magnitude less than this at 9μm and negligible at 3.4μm.

In an attempt to improve the fit to the two observational data points at 3.4μm at 215 days after outburst and at 3.8μm at 357 days after outburst, the assumed U, B, V, J, K and L variations with time were altered to the following at more than 70 days after outburst (they were left unchanged for up to 70 days after outburst).

$$
\begin{aligned}
U &= 15.8 + 0.03\,(t-70) && 70 < t < 170\\
&= 18.8 + 0.01\,(t-170) && t > 170\\
B &= 15.06 + 0.028(t-70) && 70 < t < 170\\
&= 17.86 + 0.01\,(t-170) && t > 170\\
V &= 14.0 + 0.0275(t-70) && 70 < t < 170\\
&= 16.75 + 0.01\,(t-170) && t > 170\\
J &= 11.95 + 0.026(t-70) && 70 < t < 170\\
&= 14.55 + 0.01\,(t-170) && t > 170\\
H &= 11.85 + 0.026(t-70) && 70 < t < 170\\
&= 14.45 + 0.01\,(t-170) && t > 170\\
K &= 11.3 + 0.026(t-70) && 70 < t < 170\\
&= 13.9 + 0.01\,(t-170) && t > 170\\
L &= 10.55 + 0.02\,(t-70) && 70 < t < 170\\
&= 12.55 + 0.01\,(t-170) && t > 170
\end{aligned}
$$

The rate of decrease in brightness was reduced by 0.01 magnitude per day in all wavebands between 70 and 170 days after outburst so that the supernova was assumed to be one magnitude brighter in all wavebands at all times greater than 170 days after outburst. The effective temperature of the supernova was of course unchanged by this alteration but the luminosity at $t > 70$ days after outburst was increased. The variation with time of the altered luminosity is shown as a broken line in figure 55. The optical depth of the circumstellar dust shell was left unchanged and R_c was increased by a factor $1.59 \times 10m^{13}$ to $4.28 \times 10m^{13}$. This factor is the square root of the factor by which the supernova luminosity was increased.

The effect of these alterations should be to leave the distribution of grain temperatures across the dust shell unchanged for thermodynamic equilibrium with supernova radiation emitted at any given time after outburst but to increase the mass of the dust shell by a factor 2.51. The value of R_1/R_c was taken to be 1.6. The total flux spectrum and dust spectrum were computed for these new parameters and were compared with the observational data for 215, 234, 323, 340 and 357 days after outburst in figures 82, 83, 84, 85 and 86 respectively. The spectra are essentially the same as those in figures 58, 61, 64, 67 and 70 with all the fluxes approximately increased by a factor of 2.5. However, increasing the size of the dust shell causes the grains to be heated by supernova radiation emitted at earlier times. This ensures that the change in flux is not exactly an increase of one magnitude in every waveband. It can be seen that while the observational data at 3.4μm and 3.8μm are fitted much better by these parameters, the fits to the much more accurate J, H and K data are far worse so it can be assumed that the original parameters are much more likely to be more appropriate.

FIGURE 82. The computed dust and total infra-red spectra of SN1980k for R_1/R_c = 1.6 for the increased supernova luminosity compared with the observational data at 215 days after outburst.

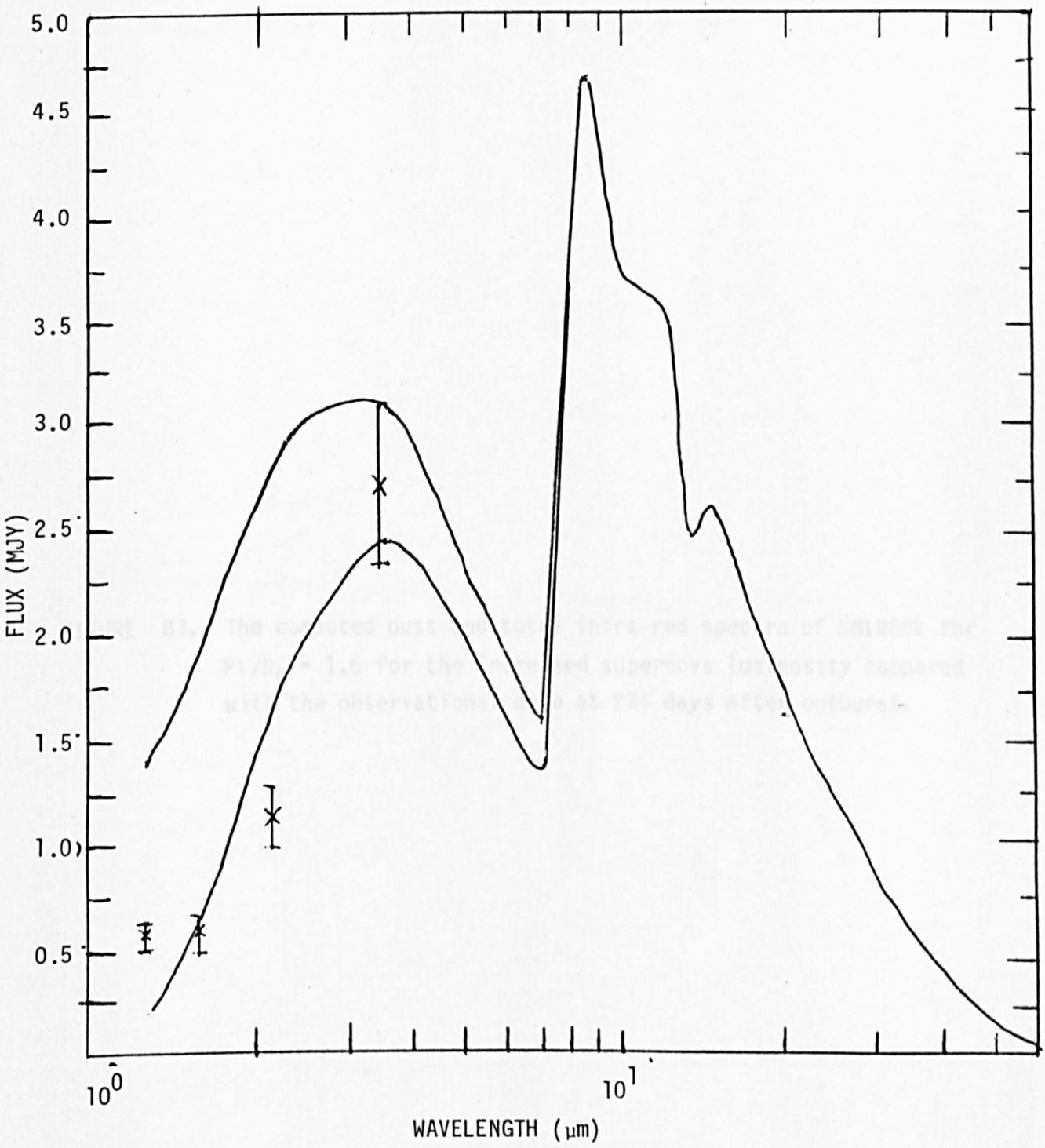
5.0
4.5
4.0
3.5
3.0
2.5
2.0
1.5
1.0
0.5
FLUX (MJY)
10^0
10^1
WAVELENGTH (μm)

FIGURE 83. The computed dust and total infra-red spectra of SN1980k for $R1/R_c$ = 1.6 for the increased supernova luminosity compared with the observational data at 234 days after outburst.

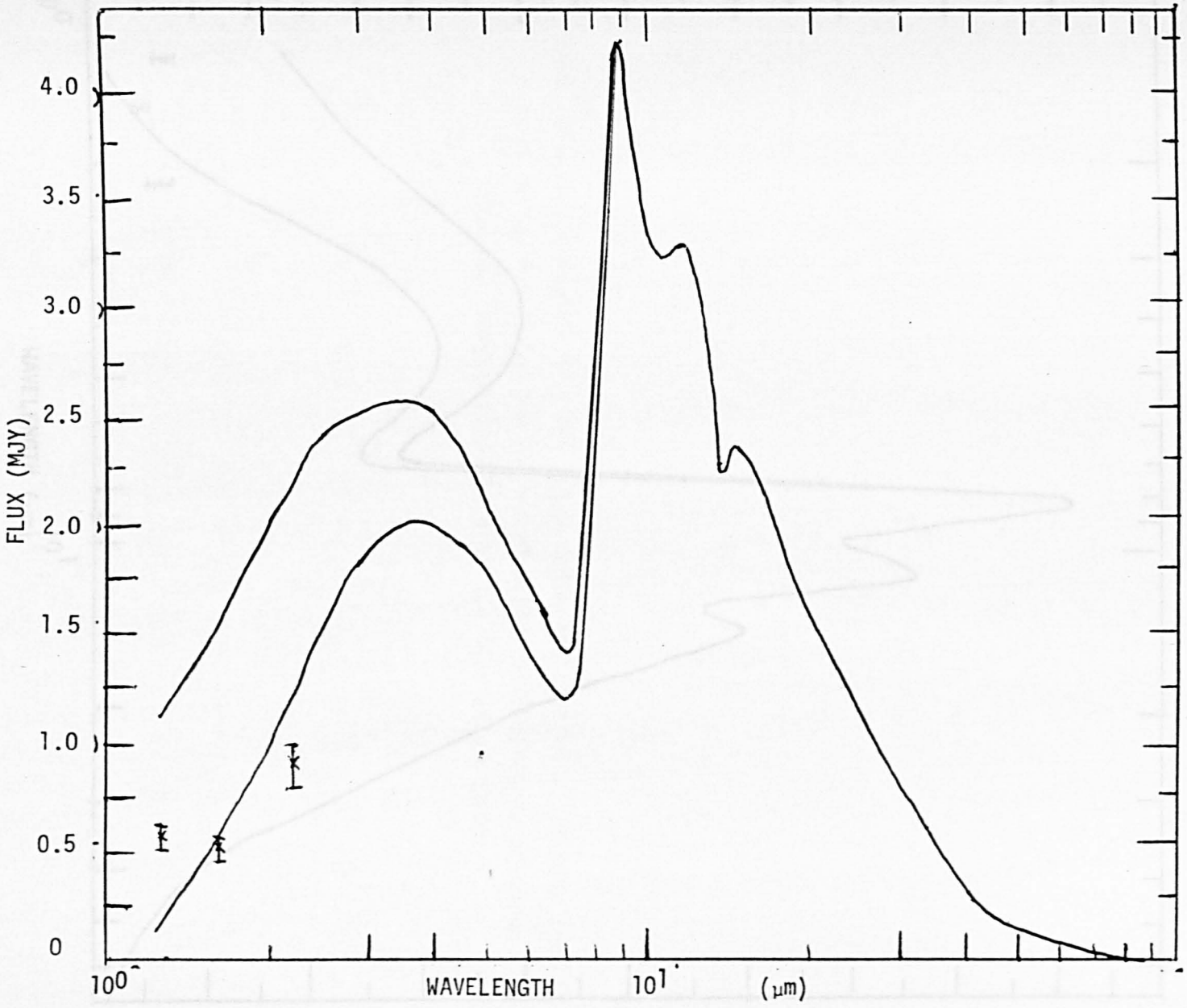
4.0
3.5
3.0
2.5
2.0
1.5
1.0
0.5
0
FLUX (MJY)
10^0
WAVELENGTH
10^1
(μm)

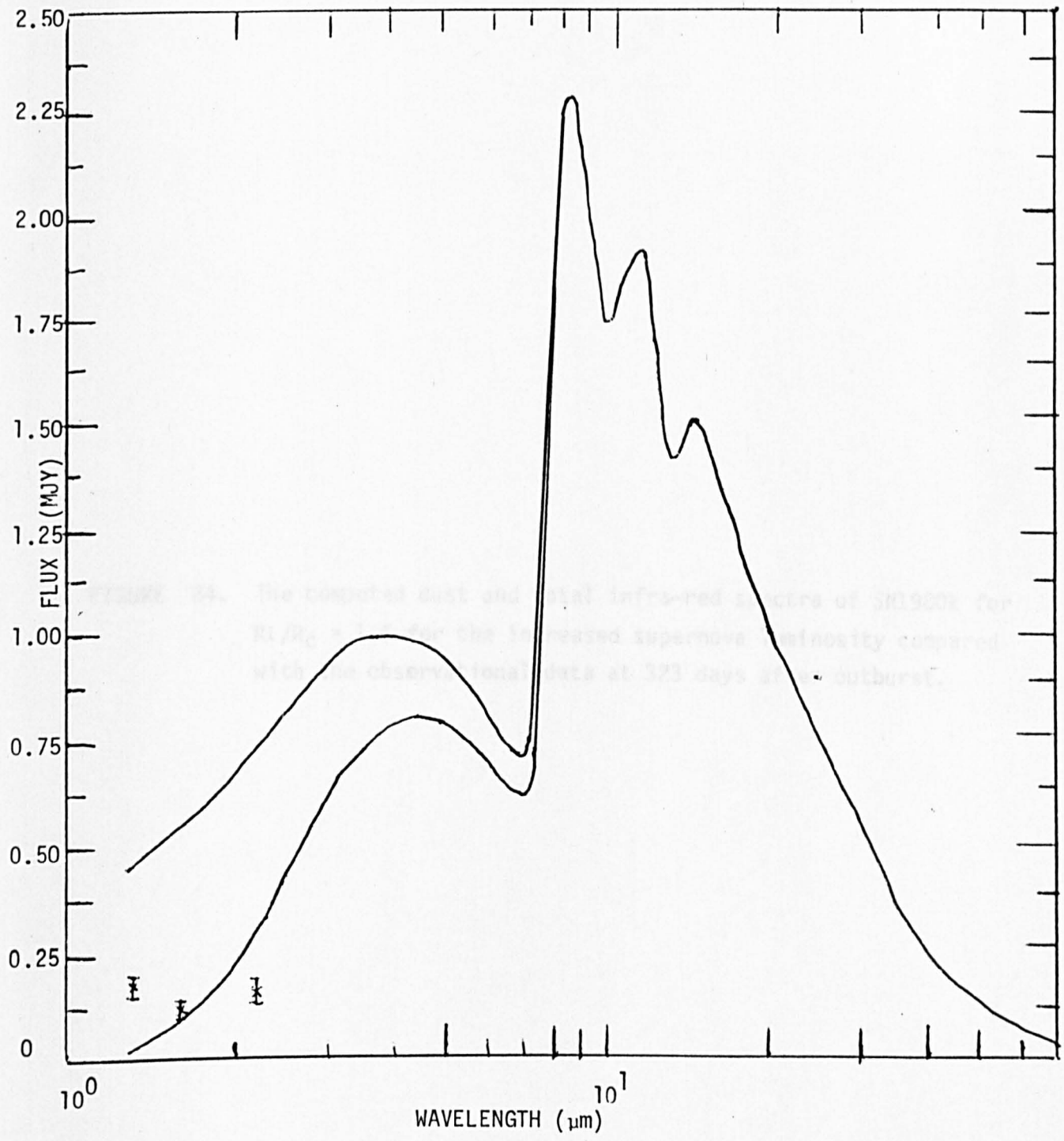
2.50
2.25
2.00
1.75
1.50
1.25
1.00
0.75
0.50
0.25
0
FLUX (MJY)
10^0
10^1
WAVELENGTH (μm)

FIGURE 84. The computed dust and total infra-red spectra of SN1980k for R_1/R_c = 1.6 for the increased supernova luminosity compared with the observational data at 323 days after outburst.

FIGURE 85. The computed dust and total infra-red spectra of SN1980k for R_1/R_c = 1.6 for the increased supernova luminosity compared with the observational data at 340 days after outburst.

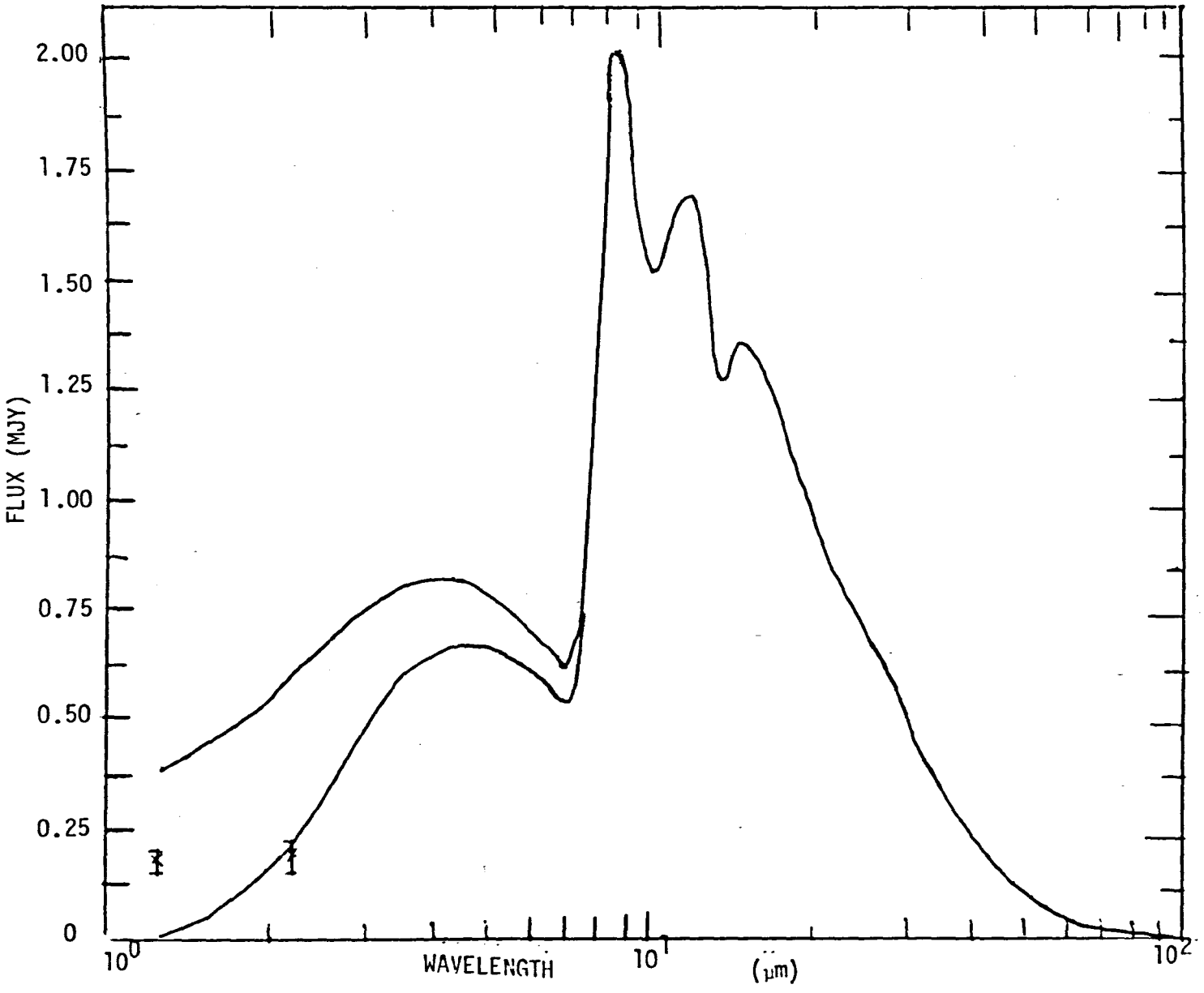
2.00
1.75
1.50
1.25
1.00
0.75
0.50
0.25
0
FLUX (MJY)
10^0
WAVELENGTH
10^1
(μm)
10^2

FIGURE 86. The computed dust and total infra-red spectra of SN1980k for R_1/R_c = 1.6 for the increased supernova luminosity compared with the observational dat at 357 days after outburst.

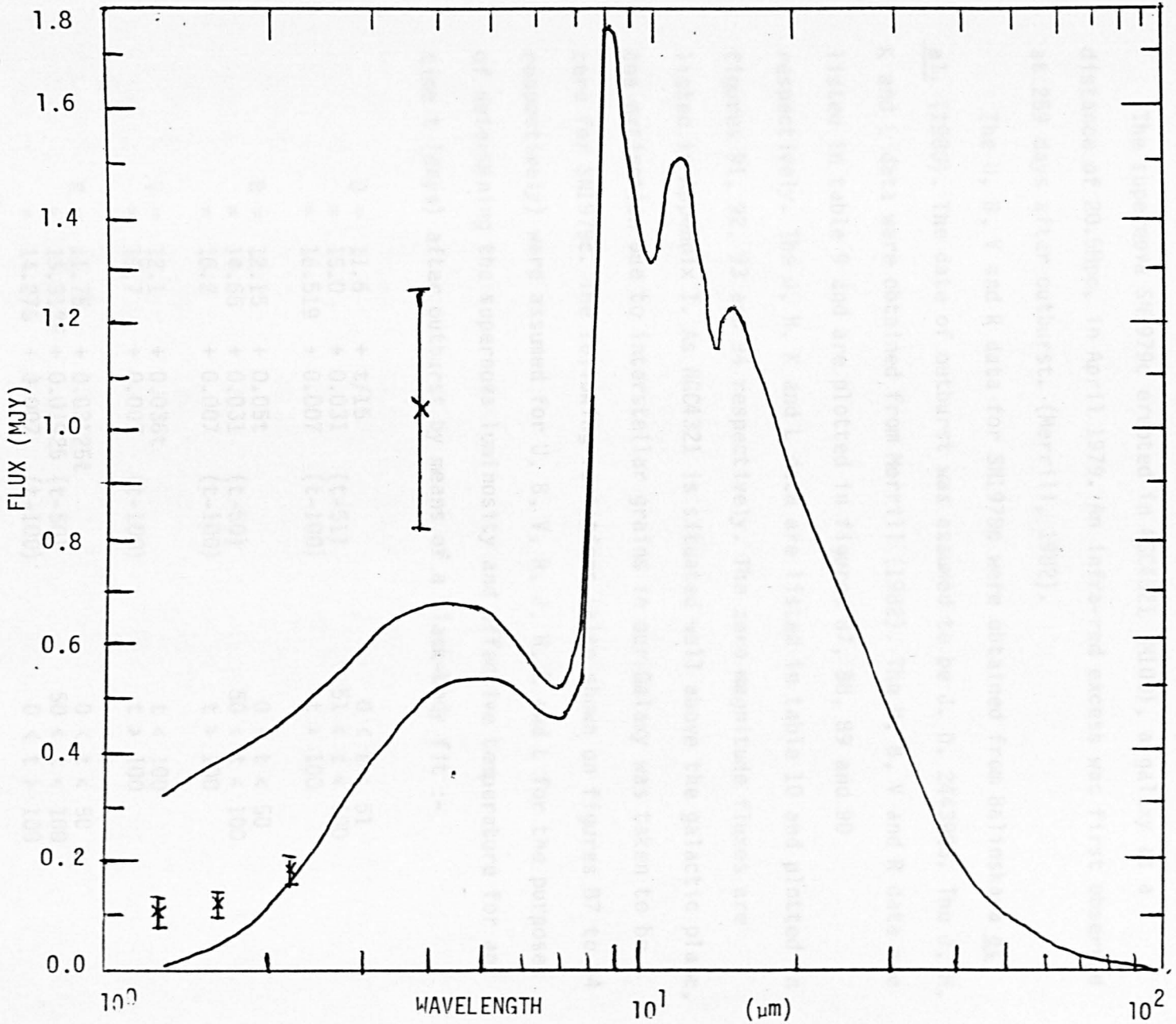
1.8
1.6
1.4
1.2
1.0
0.8
0.6
0.4
0.2
0.0
FLUX (MJY)
WAVELENGTH
(μm)

6.4 The application of the circumstellar dust model to SN1979c.

The supernova SN1979c erupted in NGC4321 (M100), a galaxy at a distance of 20.5Mpc, in April 1979. An infra-red excess was first observed at 259 days after outburst. (Merrill, 1982).

The U, B, V and R data for SN1979c were obtained from Balinskaya *et al.* (1980). The date of outburst was assumed to be J. D. 2443983. The J, H, K and L data were obtained from Merrill (1982). The U, B, V and R data are listed in table 9 and are plotted in figures 87, 88, 89 and 90 respectively. The J, H, K and L data are listed in table 10 and plotted in figures 91, 92, 93 and 94 respectively. The zero magnitude fluxes are listed in Appendix I. As NGC4321 is situated well above the galactic plane, the extinction due to interstellar grains in our Galaxy was taken to be zero for SN1979c. The following variations (also shown on figures 87 to 94 respectively) were assumed for U, B, V, R, J, H, K and L for the purposes of determining the supernova luminosity and effective temperature for any time t (days) after outburst by means of a black-body fit :-

U =	11.6	+ t/15		0 < t < 51
=	15.0	+ 0.031	(t-51)	51 < t < 100
=	16.519	+ 0.007	(t-100)	t > 100
B =	12.15	+ 0.05t		0 < t < 50
=	14.65	+ 0.031	(t-50)	50 < t < 100
=	16.2	+ 0.007	(t-100)	t > 100
V =	12.1	+ 0.036t		t < 100
=	15.7	+ 0.007	(t-100)	t > 100
R =	11.75	+ 0.03125t		0 < t < 50
=	13.3125	+ 0.01925	(t-50)	50 < t < 100
=	14.275	+ 0.007	(t-100)	0 < t > 100
J =	11.4	+ 0.0175t		t < 60
=	12.45	+ 0.01	(t-60)	60 < t < 100
=	12.85	+ 0.007	(t-100)	t > 100
H =	11.3	+ 0.015t		0 < t < 60
=	12.2	+ 0.01	(t-60)	60 < t < 100
=	12.6	+ 0.007	(t-100)	t > 100

TABLE 9

THE U, B, V, R DATA FOR SN1979c.

TIME AFTER SUPERNOVA OUTBURST (Days).	V	U	B	R
11.36	12.45	12.33	12.73	12.06
11.38	12.49	12.36	12.76	12.10
12.36	12.56	12.49	12.85	12.17
12.38	12.50	12.39	12.79	12.15
12.45	12.49	12.37	12.80	12.12
13.32	12.59	12.52	12.92	12.21
13.35	12.65	12.65	12.99	12.21
13.41	12.63	12.58	12.91	12.25
25.29	12.81	13.06	13.22	12.33
26.38	12.86	13.27	13.33	12.40
28.40	12.89	13.30	13.37	12.38
29.30	12.84	13.33	13.42	12.32
29.36	12.86	13.35	13.39	12.35
29.40	12.87	13.36	13.40	12.33
35.37	13.13	13.71	13.75	12.48
35.39	13.11	13.78	13.77	12.52
36.35	13.28	13.97	13.90	12.61
36.37	13.25	13.94	13.88	12.65
37.37	13.24	13.90	13.89	12.57
37.38	13.29	13.99	13.95	12.64

TABLE 9 (cont).

38.33	13.29	14.10	14.00	12.59
41.40	13.50	14.26	14.21	12.72
45.32	13.81	14.67	14.63	13.07
45.39	13.77	14.67	14.58	12.98
58.34	14.18	14.83	14.94	13.32
59.34	14.28		15.01	
63.33	14.36	14.83	15.06	13.46
67.32	14.55	14.99	15.23	13.62
71.33	14.63		15.24	13.67
92.28	15.26		15.64	14.11
98.30	15.44		15.79	14.27
246.61	18.26	18.30	18.67	17.13
302.59	18.62	18.40	18.93	17.46

TABLE 10

THE INFRA-RED DATA FOR SN1979c.

TIME AFTER OUTBURST (days)	J	H	K	L
5	11.55	11.30	11.10	10.45
17	11.70	11.33	11.10	10.48
24	11.83	11.84	11.22	
26	11.77	11.44	11.19	11.00
60	12.41	12.17	11.80	10.95
259	14.92	13.53	12.39	10.72
282	14.44	13.67	12.59	11.33
440	16.99	15.92	14.43	12.59

FLUXES(mJy) 25% errors assumed.

	J	H	K	L
259	1.83±0.45	4.15±1.04	6.98±1.75	15.92±3.98
282	2.84±0.71	3.65±0.91	5.81±1.45	9.08±2.27
440	0.27±0.07	0.46±0.11	1.07±0.27	2.84±0.71

FIGURE 87. SN1979c in NGC4321 : Magnitude U, for the first 200 days after outburst. The solid line is a fit to the observed data used in the black-body fit. The dotted line is predicted by the black-body fit. The crosses are the observed data points.

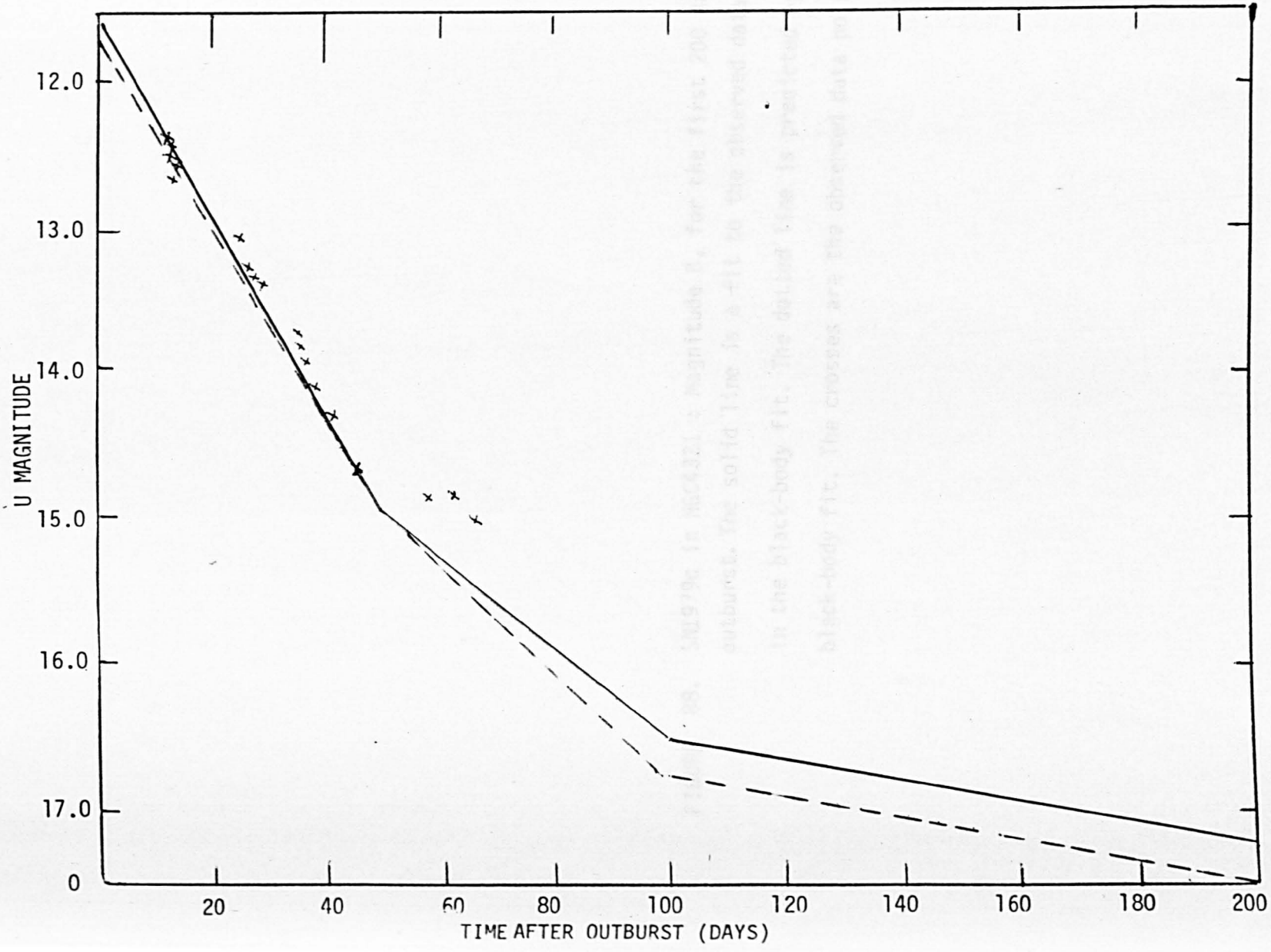
12.0
13.0
14.0
15.0
16.0
17.0
0
U MAGNITUDE
20
40
60
80
100
120
140
160
180
200
TIME AFTER OUTBURST (DAYS)

FIGURE 88. SN1979c in NGC4321 : Magnitude B, for the first 200 days after outburst. The solid line is a fit to the observed data used in the black-body fit. The dotted line is predicted by the black-body fit. The crosses are the observed data points.

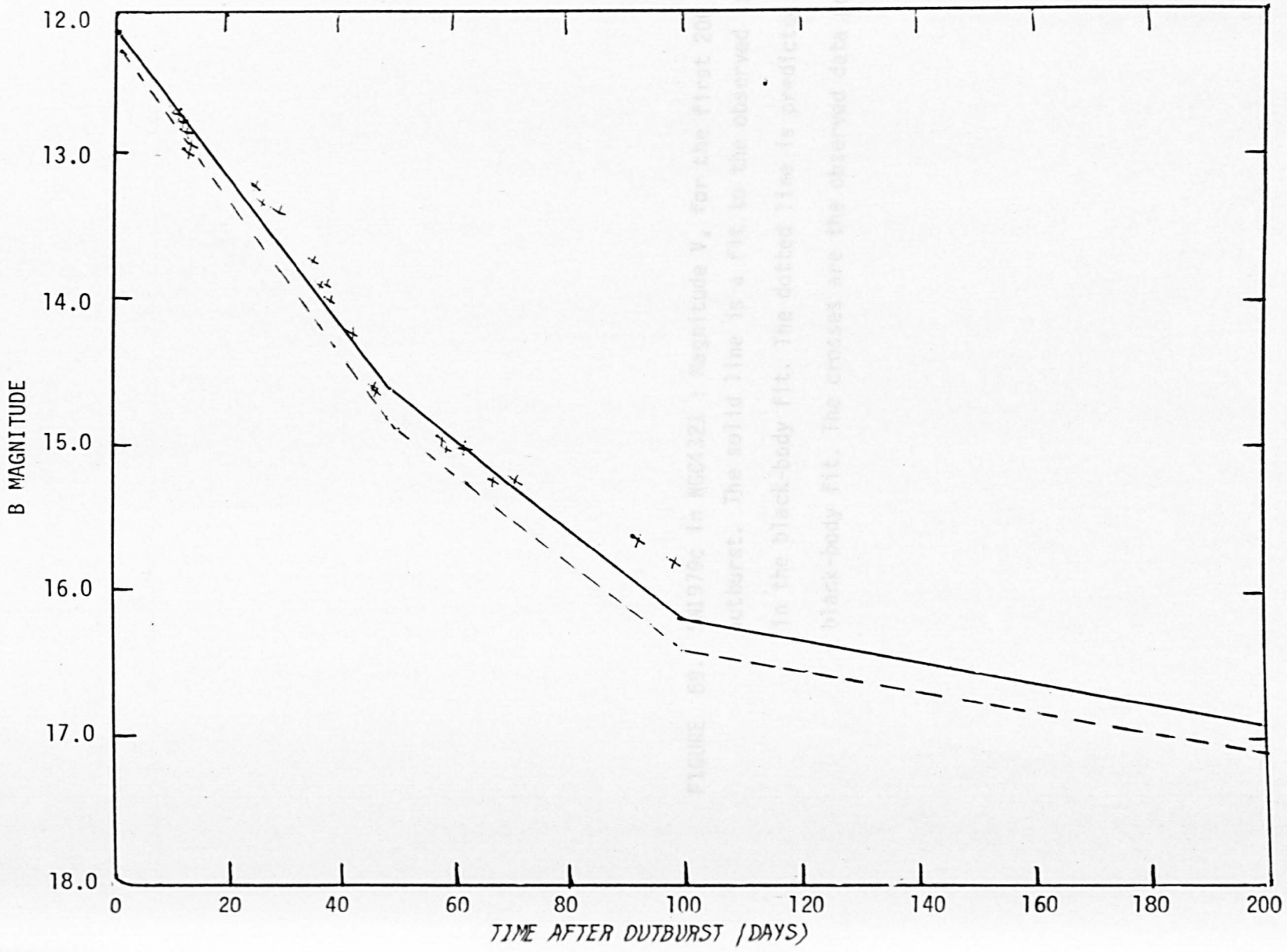
12.0
13.0
14.0
15.0
16.0
17.0
18.0
B MAGNITUDE
0
20
40
60
80
100
120
140
160
180
200
TIME AFTER OUTBURST (DAYS)

FIGURE 89. SN1979c in NGC4321 : Magnitude V, for the first 200 days after outburst. The solid line is a fit to the observed data used in the black-body fit. The dotted line is predicted by the black-body fit. The crosses are the observed data points.

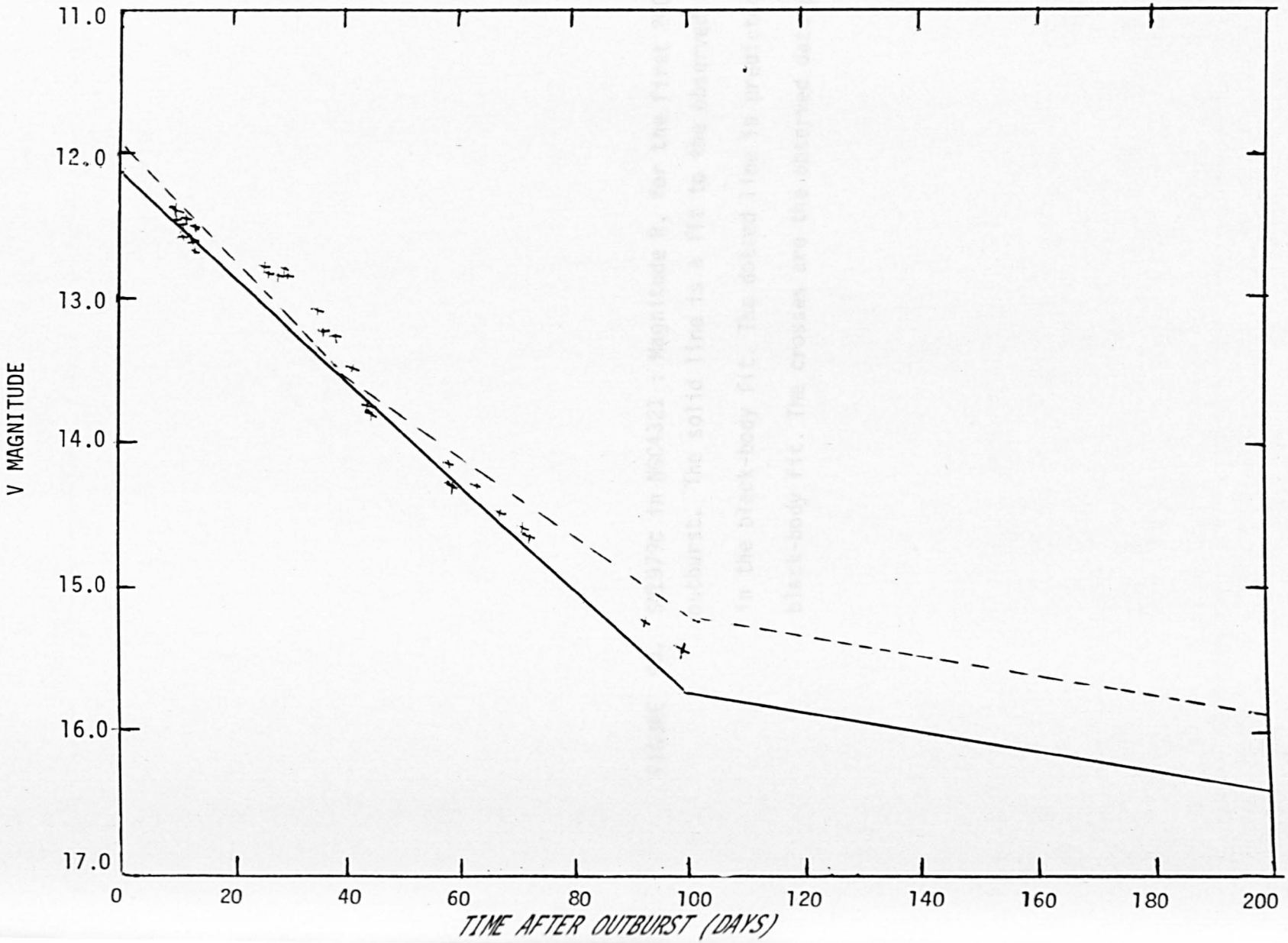
11.0
12.0
13.0
14.0
15.0
16.0
17.0
V MAGNITUDE
0
20
40
60
80
100
120
140
160
180
200
TIME AFTER OUTBURST (DAYS)

FIGURE 90. SN1979c in NGC4321 : Magnitude R, for the first 200 days after outburst. The solid line is a fit to the observed data used in the black-body fit. The dotted line is predicted by the black-body fit. The crosses are the observed data points.

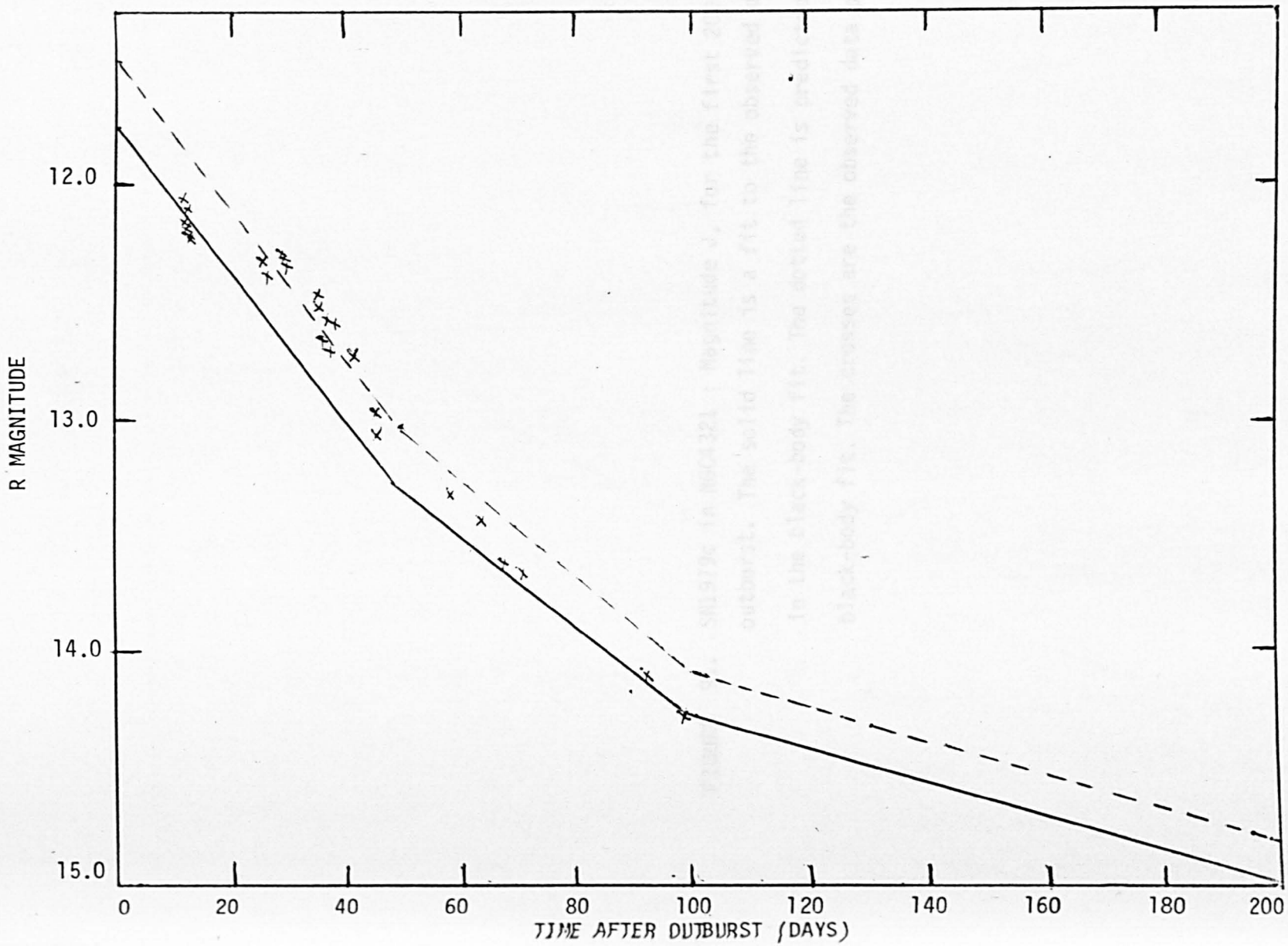
R MAGNITUDE
12.0
13.0
14.0
15.0
0
20
40
60
80
100
120
140
160
180
200
TIME AFTER OUTBURST (DAYS)

FIGURE 91. SN1979c in NGC4321 : Magnitude J, for the first 200 days after outburst. The solid line is a fit to the observed data used in the black-body fit. The dotted line is predicted by the black-body fit. The crosses are the observed data points.

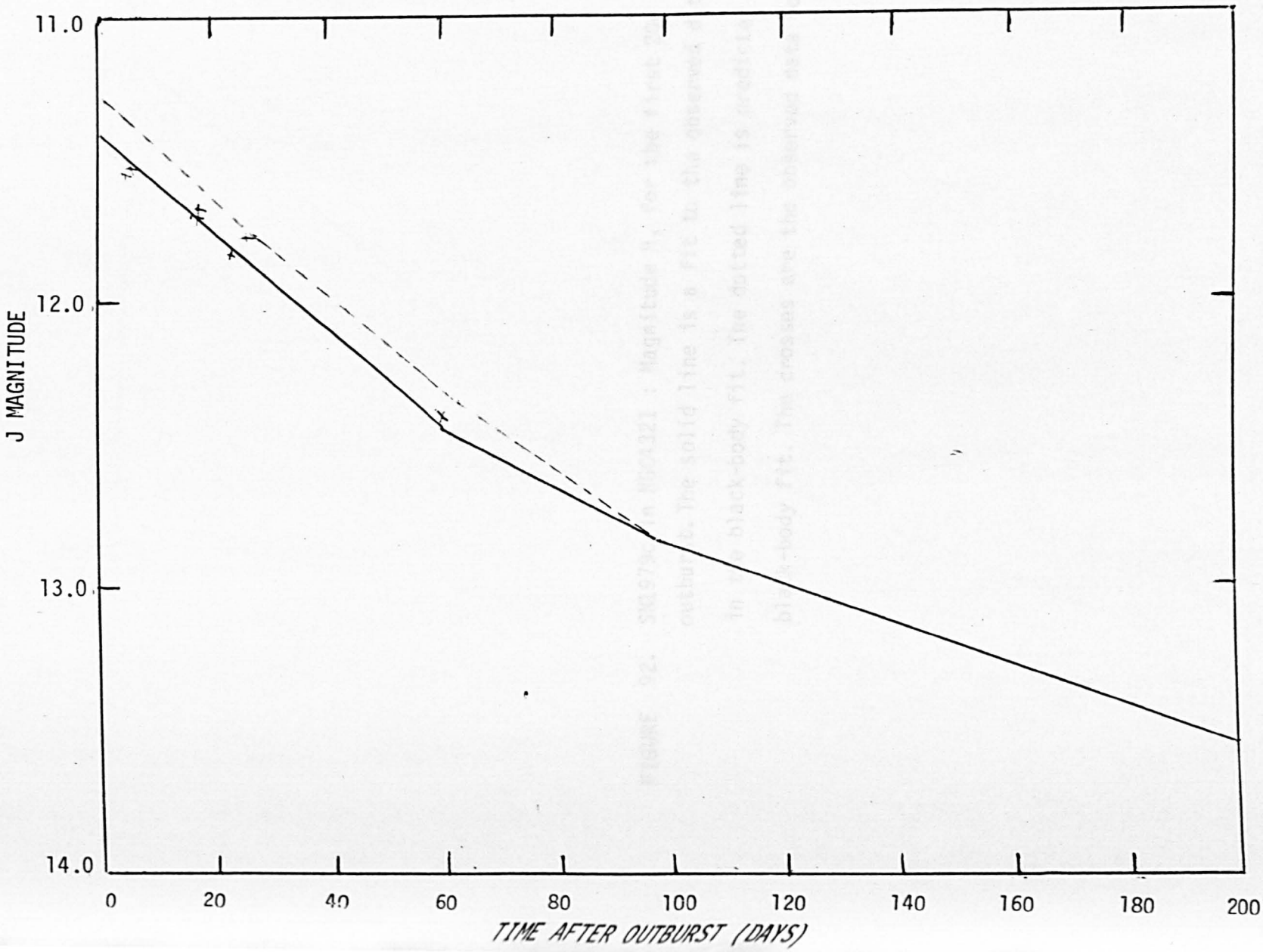
11.0
12.0
13.0
14.0
J MAGNITUDE
0
20
40
60
80
100
120
140
160
180
200
TIME AFTER OUTBURST (DAYS)

FIGURE 92. SN1979c in NGC4321 : Magnitude H, for the first 200 days after outburst. The solid line is a fit to the observed data used in the black-body fit. The dotted line is predicted by the black-body fit. The crosses are the observed data points.

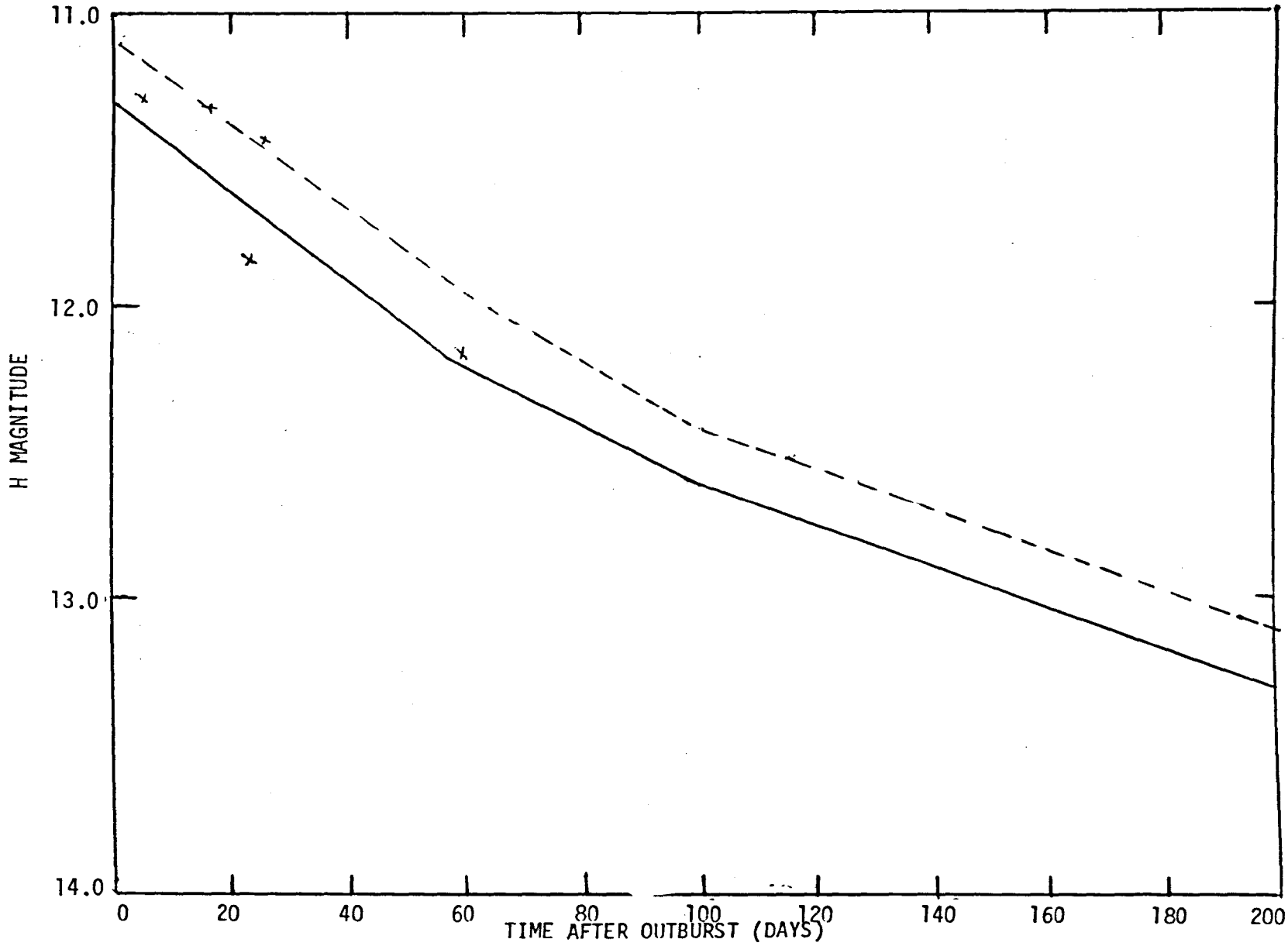
11.0
12.0
13.0
14.0
H MAGNITUDE
0
20
40
60
80
100
120
140
160
180
200
TIME AFTER OUTBURST (DAYS)

FIGURE 93. SN1979c in NGC4321 : Magnitude K, for the first 200 days after outburst. The solid line is a fit to the observed data used in the black-body fit. The dotted line is predicted by the black-body fit. The crosses are the observed data points.

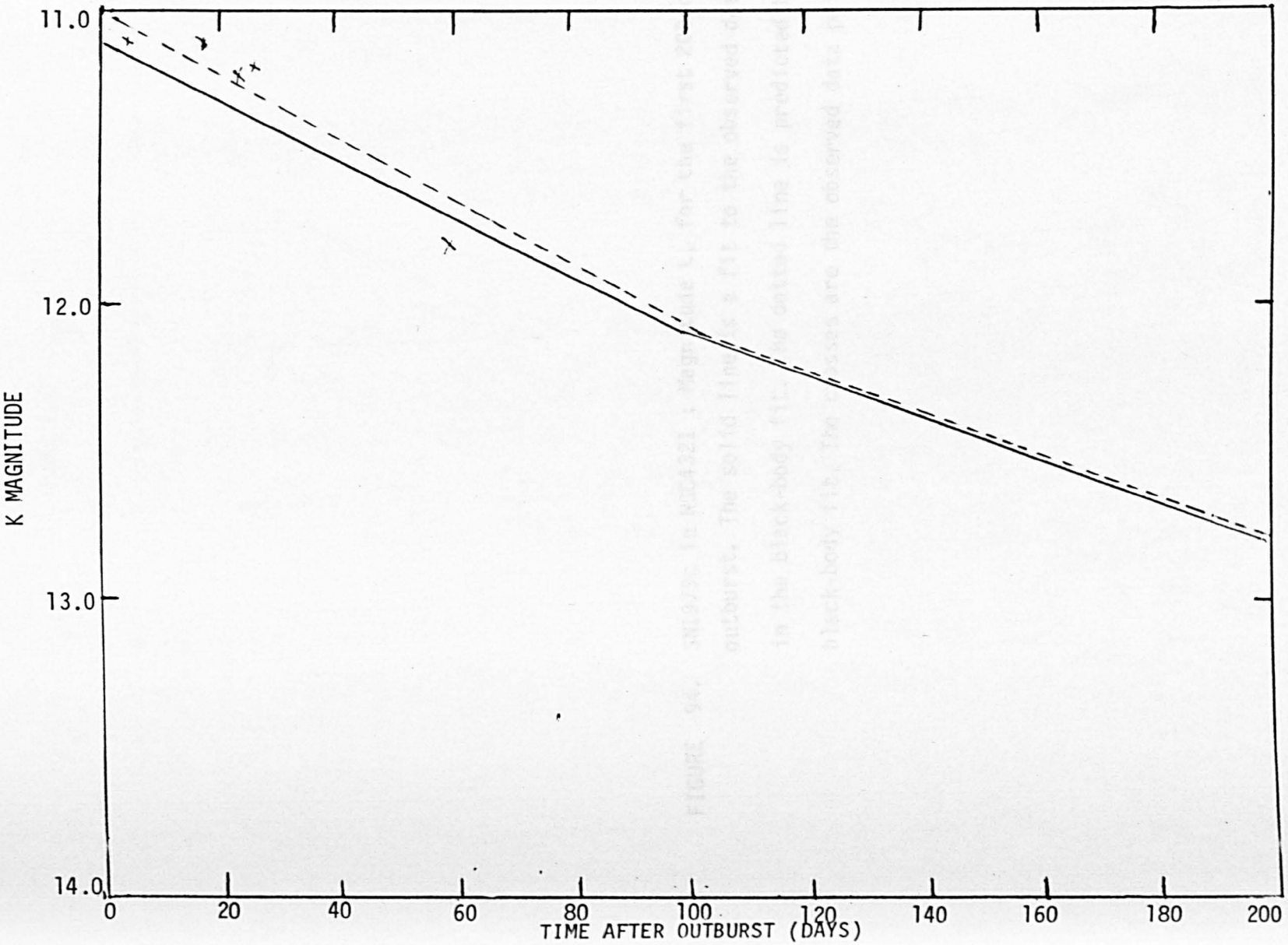
11.0
12.0
13.0
14.0
K MAGNITUDE
0
20
40
60
80
100
120
140
160
180
200
TIME AFTER OUTBURST (DAYS)

FIGURE 94. SN1979c in NGC4321 : Magnitude L, for the first 200 days after outburst. The solid line is a fit to the observed data used in the black-body fit. The dotted line is predicted by the black-body fit. The crosses are the observed data points.

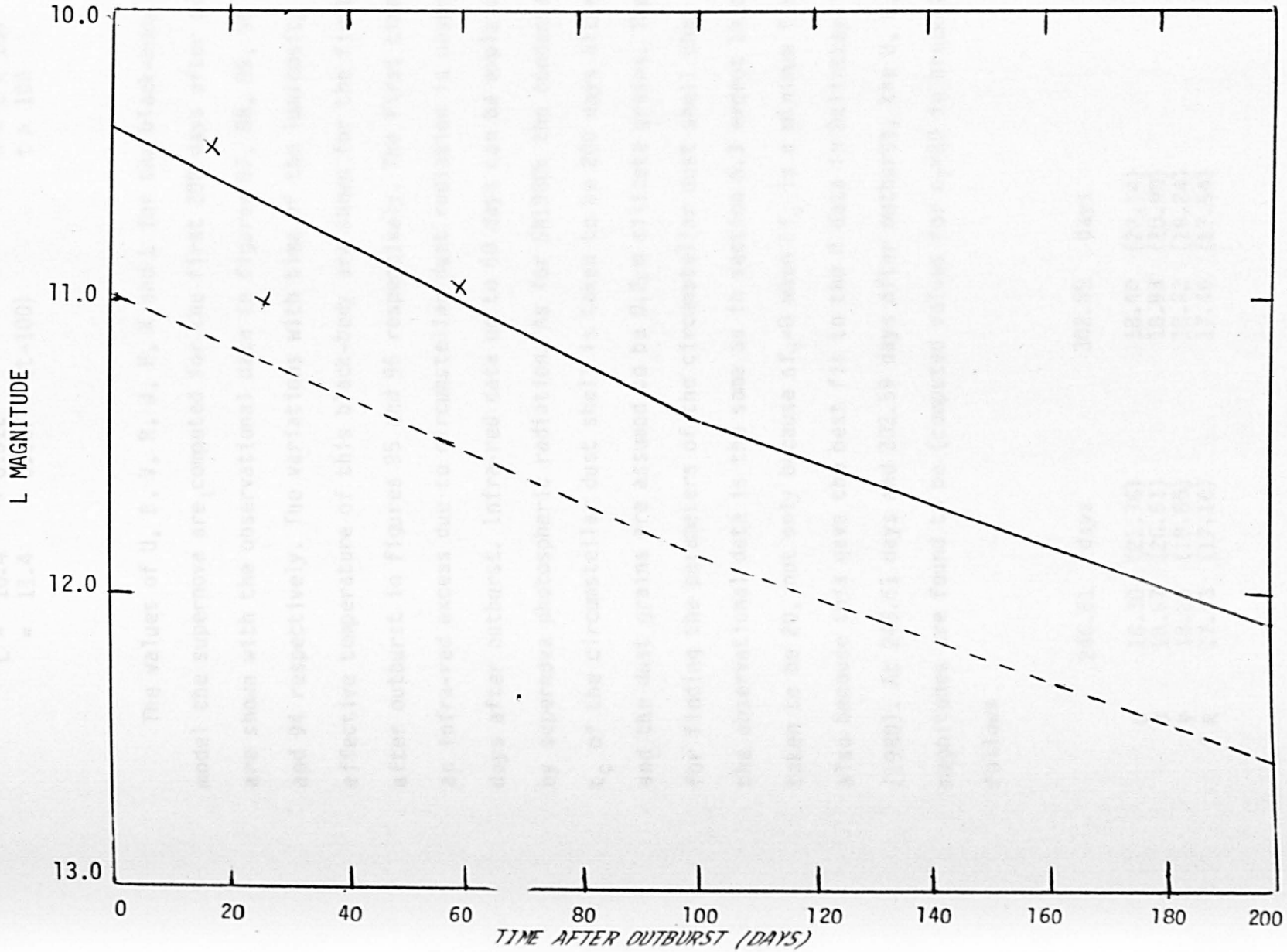
10.0
11.0
12.0
13.0
L MAGNITUDE
0
20
40
60
80
100
120
140
160
180
200
TIME AFTER OUTBURST (DAYS)

$$K = 11.1 + 0.01t \qquad 0 < t < 100$$
$$= 12.1 + 0.007\ (t-100) \qquad t > 100$$

$$L = 10.4 + 0.01t \qquad 0 < t < 100$$
$$= 11.4 + 0.007\ (t-100) \qquad t > 100$$

The values of U, B, V, R, J, H, K and L for the black-body used to model the supernova are computed for the first 200 days after outburst and are shown with the observational data in figures 87, 88, 89, 90 ,91, 92, 93 and 94 respectively. The variations with time of the luminosity and effective temperature of this black-body are shown for the first 200 days after outburst in figures 95 and 96 respectively. The first time at which an infra-red excess due to circumstellar dust radiation is observed is 259 days after outburst. Infra-red data up to 60 days can be explained entirely by supernova photospheric radiation. As for SN1980k the condensation time t_c of the circumstellar dust shell is taken to be 200 days after outburst and the dust grains are assumed to be 0.2μm silicate grains. The procedure for finding the parameters of the circumstellar dust shell that best fitted the observational data is the same as in section 6.3 except that c_T was taken to be 20, not only because $\Delta f_\nu \simeq 0$ when δf_ν is a minimum for $c_T=20$, but also because this gave the best fit to the R data in Balinskaya et al. (1980). At 246.61 days and 302.59 days after outburst, the U, B, V, R magnitudes are found to be (computed values for $c_T=20$ in brackets) as follows

	246.61 days		302.59 days	
U	18.30	(21.76)	18.40	(22.14)
B	18.67	(20.51)	18.93	(20.90)
V	18.26	(18.85)	18.62	(19.24)
R	17.13	(17.16)	17.46	(17.54)

The mean values of the computed magnitudes less the observed magnitudes for the two times increase by 0.20, 0.15, 0.13 and 0.10, for U,

FIGURE 95. SN1979c in NGC4321 : Luminosity for the first 200 days after outburst.

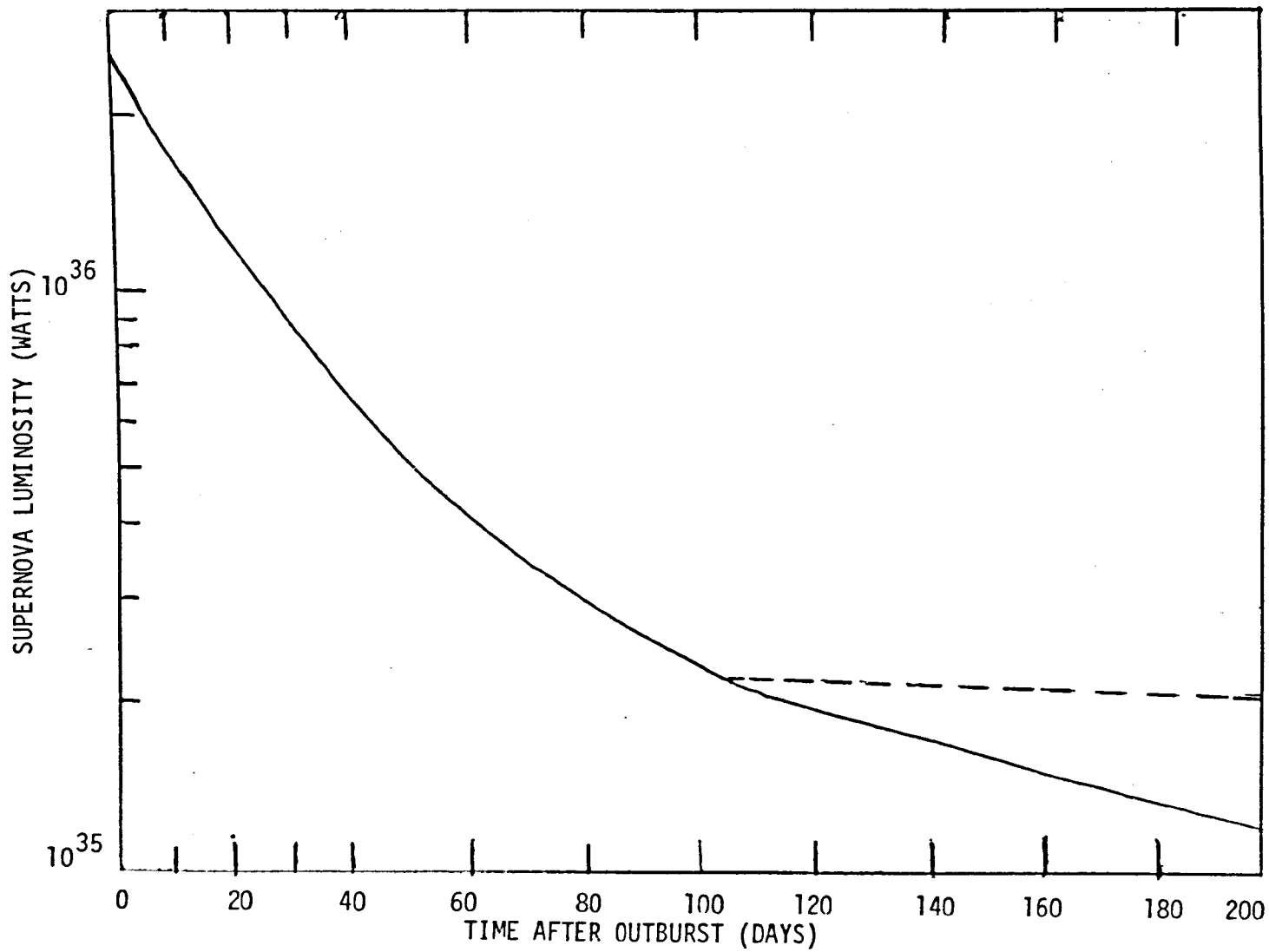
SUPERNOVA LUMINOSITY (WATTS)
10^{36}
10^{35}
0
20
40
60
80
100
120
140
160
180
200
TIME AFTER OUTBURST (DAYS)

FIGURE 96. SN1979c in NGC4321 : Effective temperature for the first 200 days after outburst.

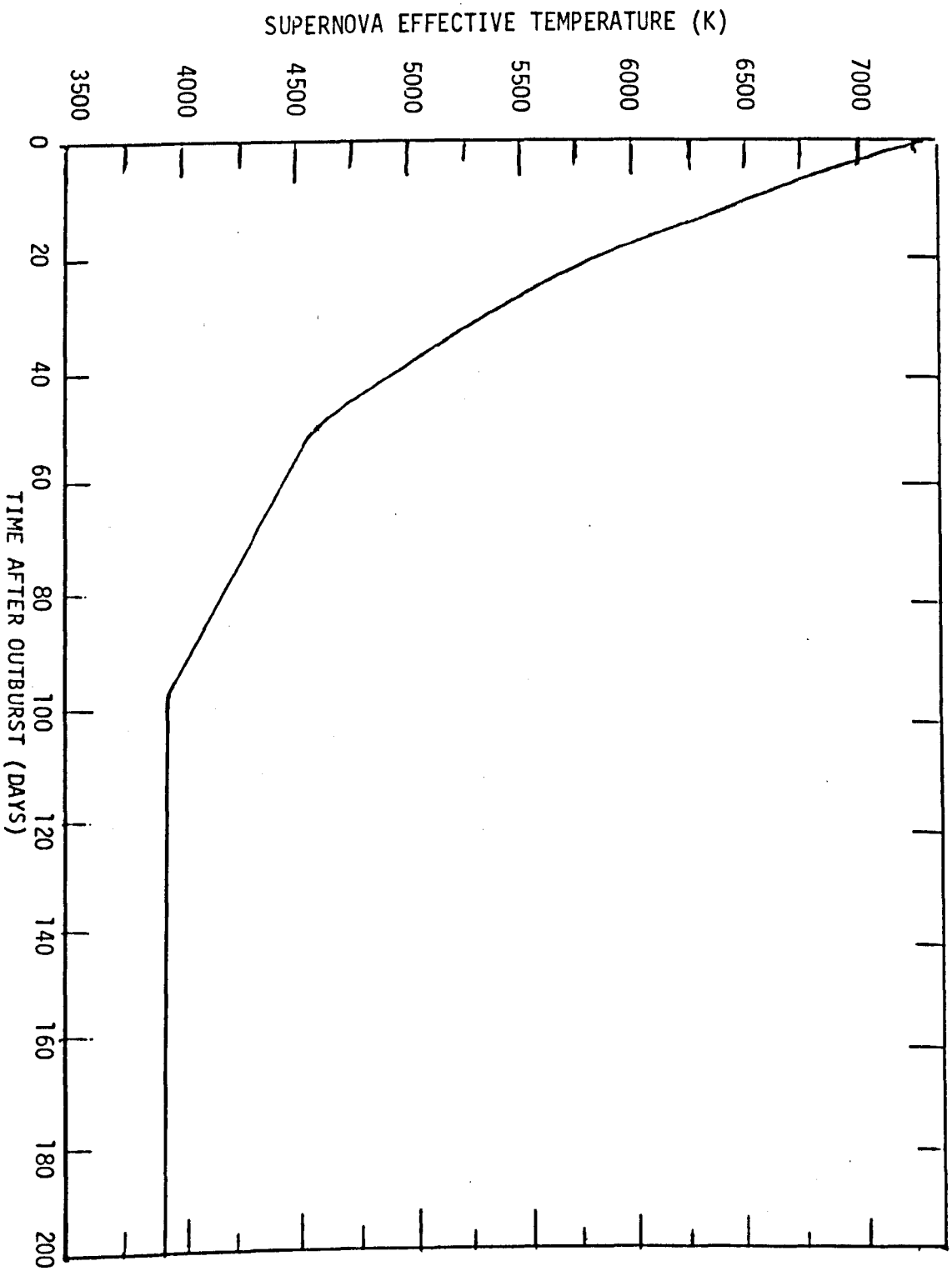
SUPERNOVA EFFECTIVE TEMPERATURE (K)
3500
4000
4500
5000
5500
6000
6500
7000
TIME AFTER OUTBURST (DAYS)
0
20
40
60
80
100
120
140
160
180
200

B, V and R respectively for each increase of one in the value of c_T. The discrepencies at U, B and V may be due to the fact that in practice a supernova is not strictly a black-body. The effect of emission lines for example could be significant. The effect of increasing the photospheric fluxes at late times is investigated later.

The number of observations at times of infra-red excess is only twelve in the case of SN1979c as opposed to fifteen in the case of SN1980k. While the number of infra-red observations at earlier times is nineteen as opposed to forty two for SN1980k. A better fit could be obtained for SN1979c especially at early times ($t < 200$ days) if more data were available. Comparison of the computed and observed fluxes for SN1979c at the earlier times (up to 60 days after outburst) yields $\Delta f_\nu = -0.015$ and $\delta f_\nu = 0.109$ so the time variations assumed for U, B, V, R, J, K and L at earlier times are reasonably appropriate. The rate of decline after 100 days after outburst was taken to be 0.007 magnitude per day in all wavebands, because slower and faster rates of decline led to values of Δf_ν for the later times which were respectively too negative and too positive (altering the rate of decline by 0.001 magnitudes per day changed Δf_ν by about 0.1).

The fits for the supernova photosphere derived above are now used to calculate the dust flux, for a dust shell of inner radius R_c and outer radius R_1. The best fit for $R_1/R_c > 1.6$ was found to occur for $R_c = 1.5 \times 10^{14}$m. The values of Δf_ν and δf_ν for the following values of R_c and R_1/R_c are tabulated :-

R_1/R_c	R_c 1.3×10^{14} (m)	1.4×10^{14} (m)	1.5×10^{14} (m)	1.6×10^{14} (m)	1.7×10^{14} (m)
1.3	-0.020(0.273)	-0.027(0.269)	-0.034(0.268)	-0.042(0.266)	-0.049(0.266)
1.6	-0.026(0.272)	-0.034(0.269)	-0.042(0.268)	-0.049(0.268)	-0.057(0.269)
1.8	-0.029(0.272)	-0.037(0.270)	-0.045(0.269)	-0.052(0.270)	-0.060(0.271)
2.0	-0.031(0.272)	-0.039(0.271)	-0.047(0.270)	-0.055(0.271)	-0.063(0.273)
2.2	-0.032(0.273)	-0.040(0.272)	-0.048(0.272)	-0.056(0.273)	-0.064(0.275)
2.5	-0.034(0.274)	-0.042(0.273)	-0.050(0.273)	-0.058(0.274)	-0.066(0.276)

It can be seen that the observations do not give any indication of the thickness of the dust shell. For every value of R_1/R_c investigated, the best fitting dust shell inner radius (R_c) is 1.5×10^{14} m. Spectra and light curves were then computed for three values of R_1/R_c; 1.6, 2.0 and 2.5. Three values were chosen as for SN1980k, to investigate the possiblity that observations further into the infra-red than L would give further information on the thickness of the circumstellar dust shell.

For R_1/R_c = 1.6, the dust shell mass is 4.025×10^{-3} solar masses, the optical depth is shown as a function of wavelength between 0.1μm and 50μm in figure 57. For R_1/R_c = 2.0 and 2.5, the dust shell mass is 5.032×10^{-3} solar masses and 6.290×10^{-3} solar masses respectively and the optical depths are the same as for R_1/R_c = 1.6 (i.e. the optical depth is held constant).

The dust and total flux spectra at 259 days after outburst are shown along with the observed fluxes taken from table 10 for R_1/R_c = 1.6, 2.0 and 2.5 in figures 97, 98 and 99 respectively. The silicate feature is again clearly visible, the dust and total flux spectra are also computed at 282 days and 440 days after outburst. The spectra at 282 days after outburst are shown with the observational data taken from table 10 for R_1/R_c = 1.6, 2.0 and 2.5 in figures 100, 101 and 102 respectively. Spectra at 440 days after outburst are shown with the observational data in table 10 for R_1/R_c = 1.6, 2.0 and 2.5 in figures 103, 104 and 105 respectively. It can be seen from figures 97, 98 and 99 that while the H and K fluxes predicted by the model are in agreement with the observed fluxes, the predicted J flux is between two and three standard deviations larger than the observed flux and the predicted L flux is a factor of three smaller than the observed flux. From figures 100, 101 and 102 the predicted J, H and K fluxes at 282 days after outburst are in agreement with the observed fluxes and the predicted L flux is a factor of two smaller than the observed flux. From figures 103, 104 and 105 the predicted K flux at 440 days after outburst is in agreement

FIGURE 97. The computed dust and total infra-red flux spectra of SN1979c in NGC4321 for R_1/R_C = 1.6 compared with the observational data at 259 days after outburst.

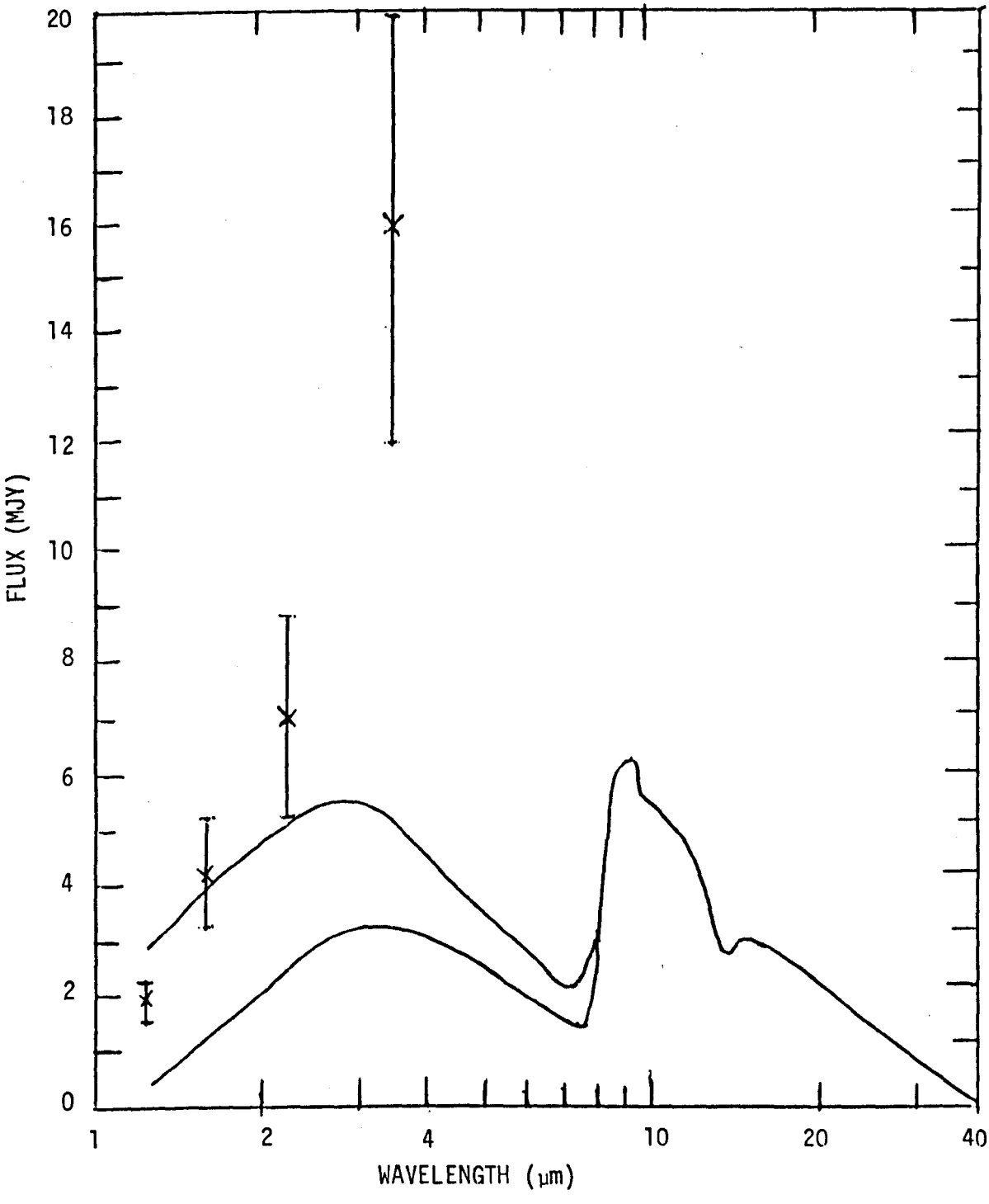
20
18
16
14
12
10
8
6
4
2
0
FLUX (MJY)
1
2
4
10
20
40
WAVELENGTH (μm)

FIGURE 98. The computed dust and total infra-red flux spectra of SN1979c in NGC4321 for R_1/R_C = 2.0 compared with the observational data at 259 days after outburst.

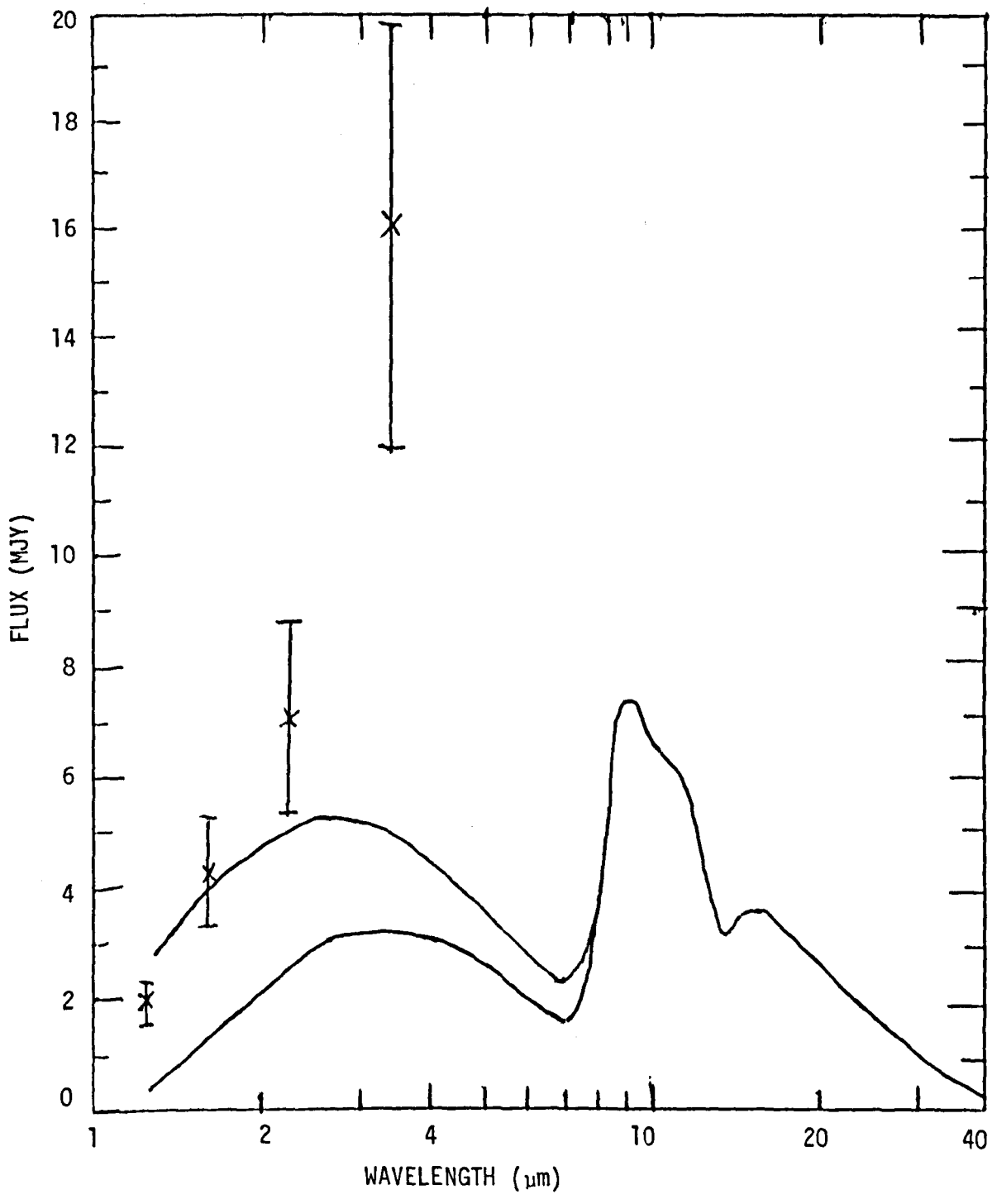
20
18
16
14
12
10
8
6
4
2
0
FLUX (MJY)
1
2
4
10
20
40
WAVELENGTH (μm)

FIGURE 99. The computed dust and total infra-red flux spectra of SN1979c in NGC4321 for R_1/R_C = 2.5 compared with the observational data at 259 days after outburst.

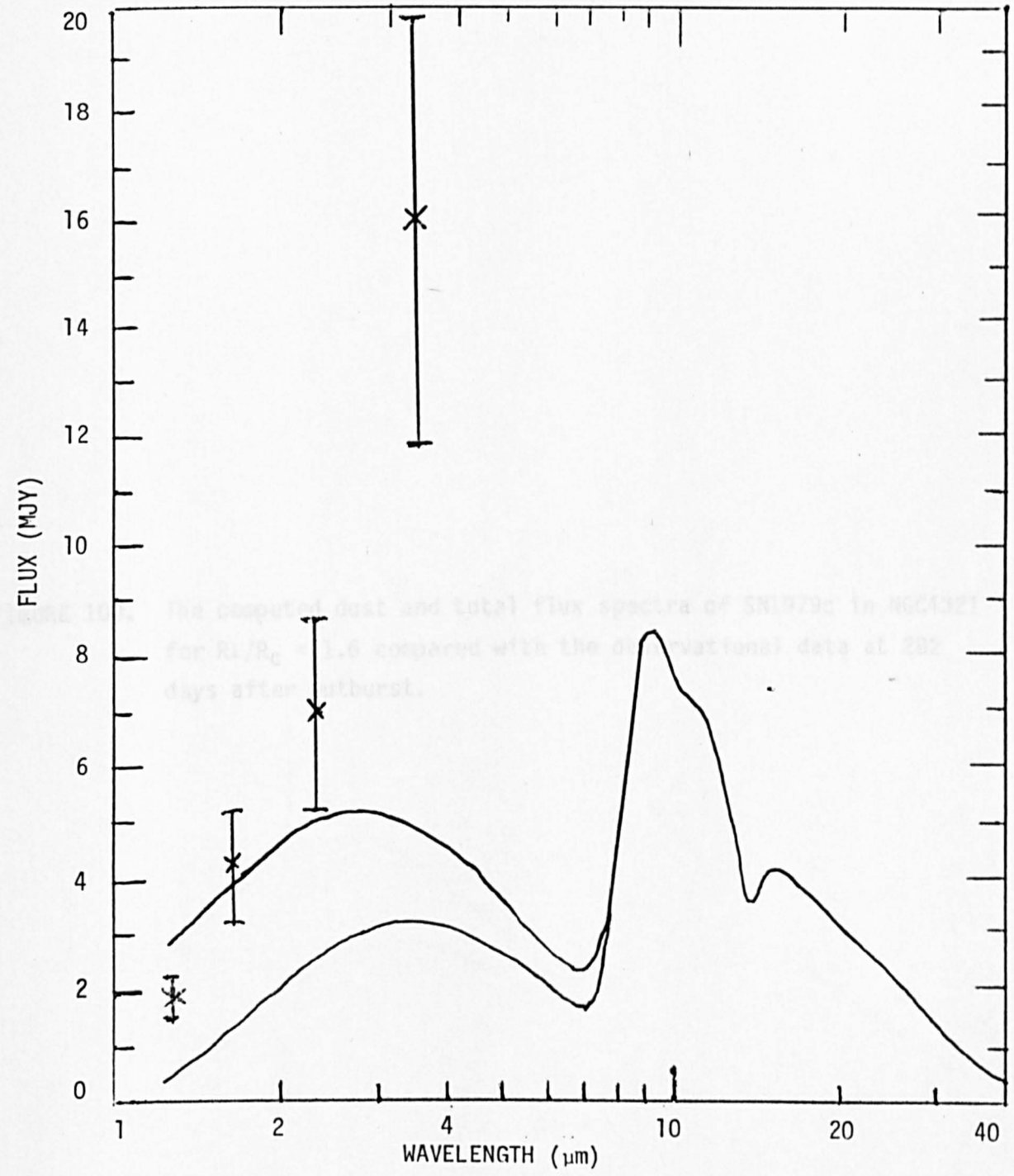
20
18
16
14
12
10
8
6
4
2
0
FLUX (MJY)
1
2
4
10
20
40
WAVELENGTH (μm)

FIGURE 100. The computed dust and total flux spectra of SN1979c in NGC4321 for R_1/R_c = 1.6 compared with the observational data at 282 days after outburst.

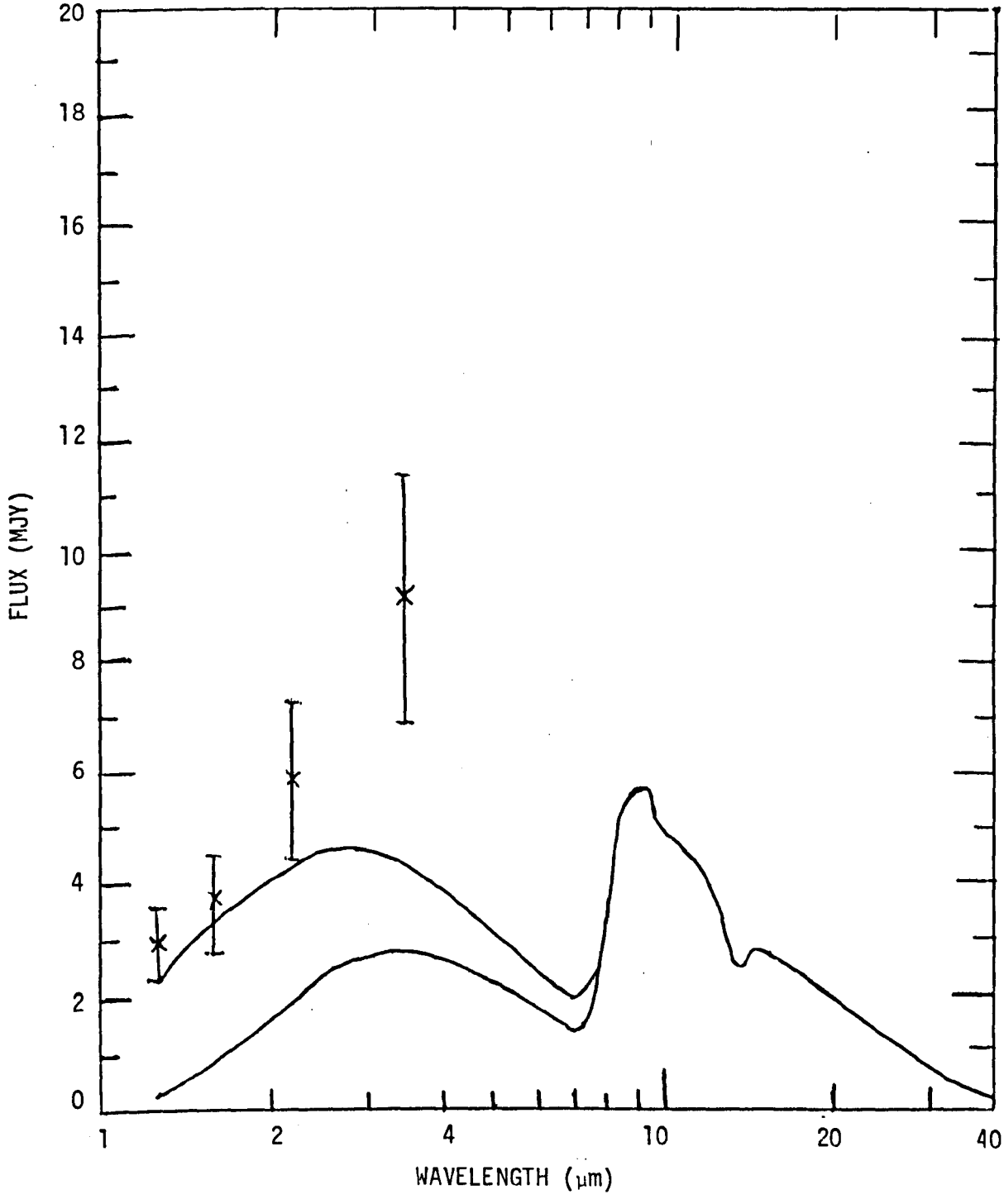
20
18
16
14
12
10
8
6
4
2
0
FLUX (MJY)
1
2
4
10
20
40
WAVELENGTH (μm)

FIGURE 101. The computed dust and total flux spectra of SN1979c in NGC4321 for $R1/R_C$ = 2.0 compared with the observational data at 282 days after outburst.

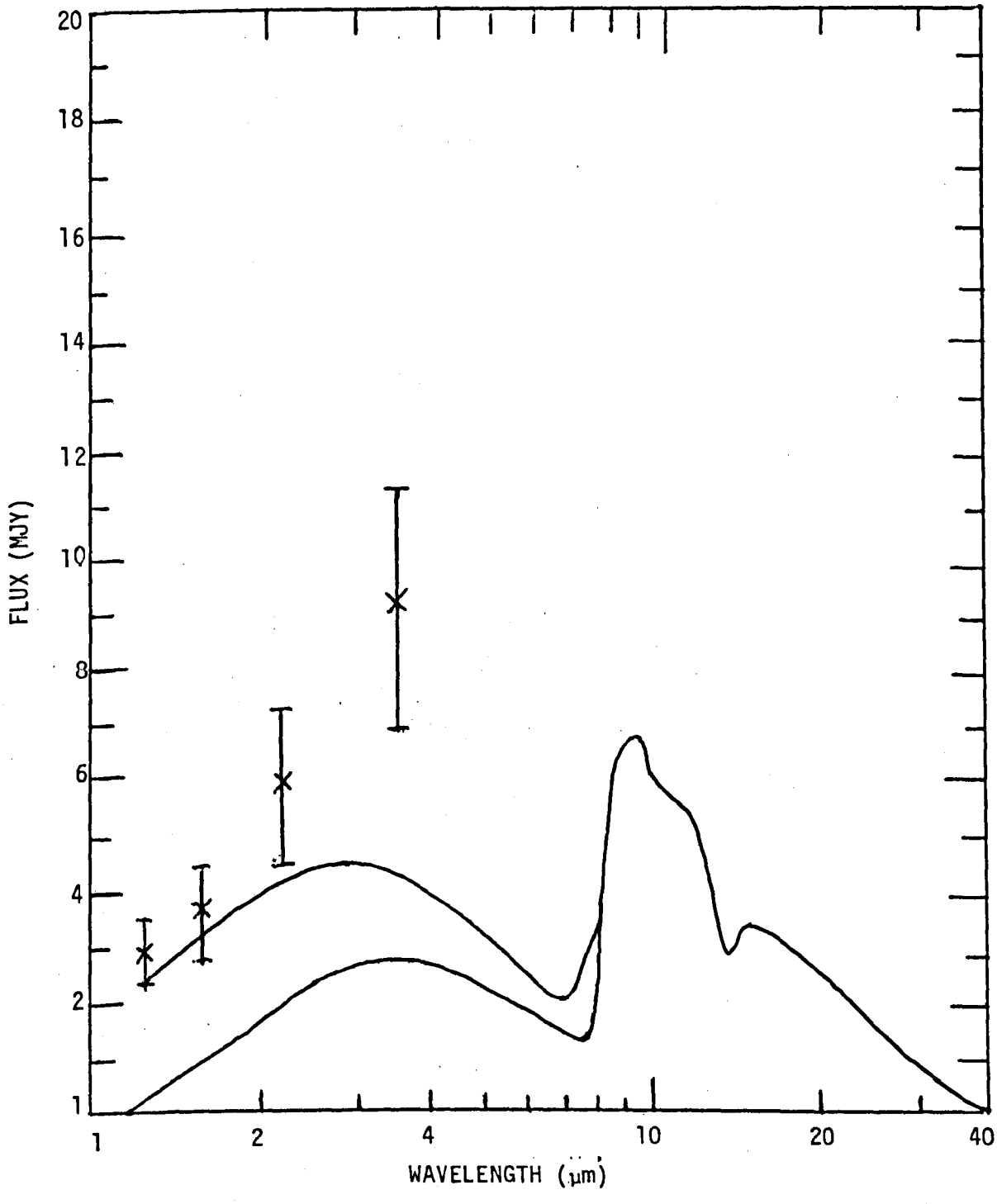
20
18
16
14
12
10
8
6
4
2
1
FLUX (MJY)
1
2
4
10
20
40
WAVELENGTH (μm)

FIGURE 102. The computed dust and total flux spectra of SN1979c in NGC4321 for R_1/R_C = 2.5 compared with the observational data at 282 days after outburst.

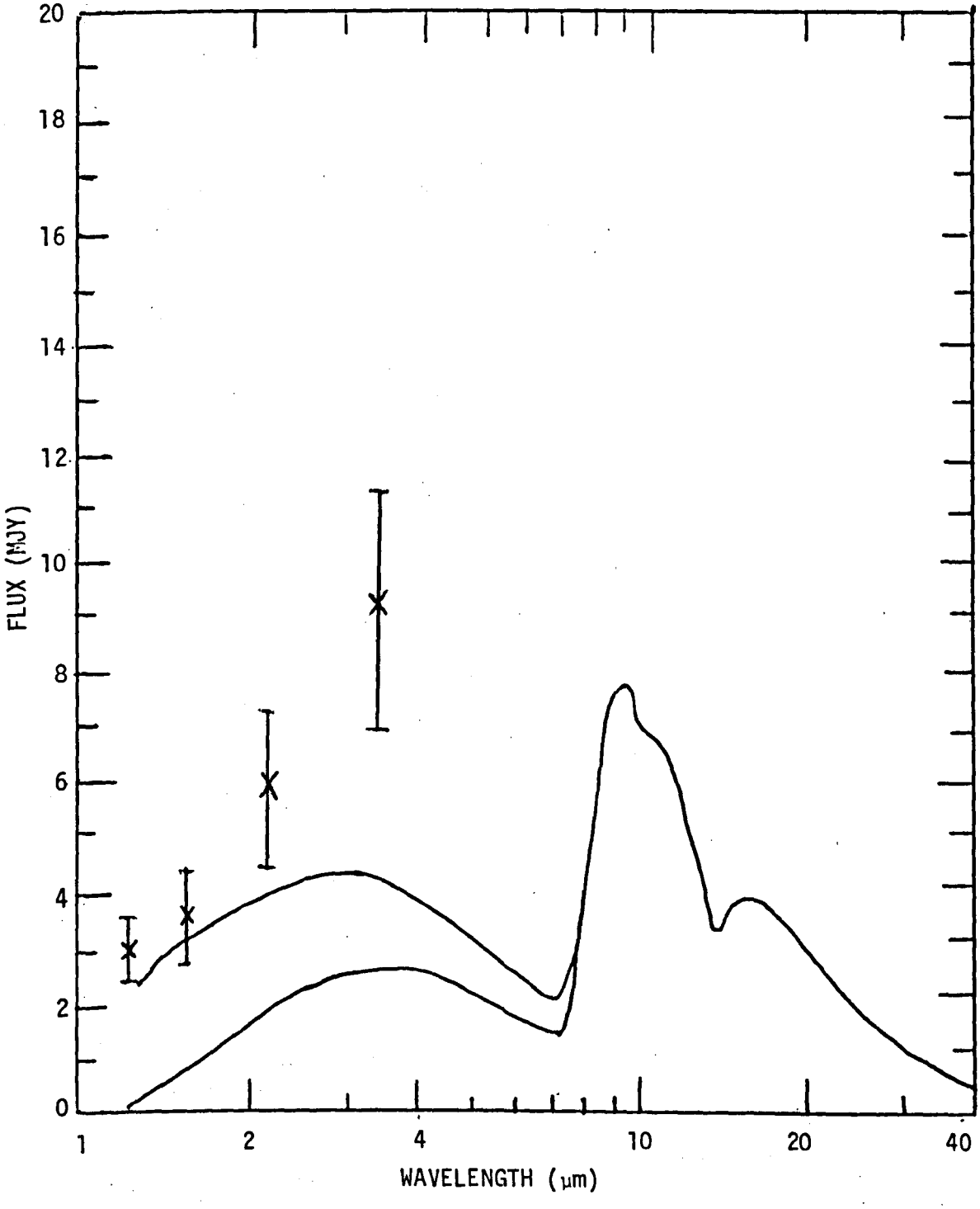
20
18
16
14
12
10
8
6
4
2
0
FLUX (MJY)
1
2
4
10
20
40
WAVELENGTH (μm)

FIGURE 103. The computed dust and total flux spectra of SN1979c in NGC4321 for R_1/R_c = 1.6 compared with the observational data at 440 days after outburst.

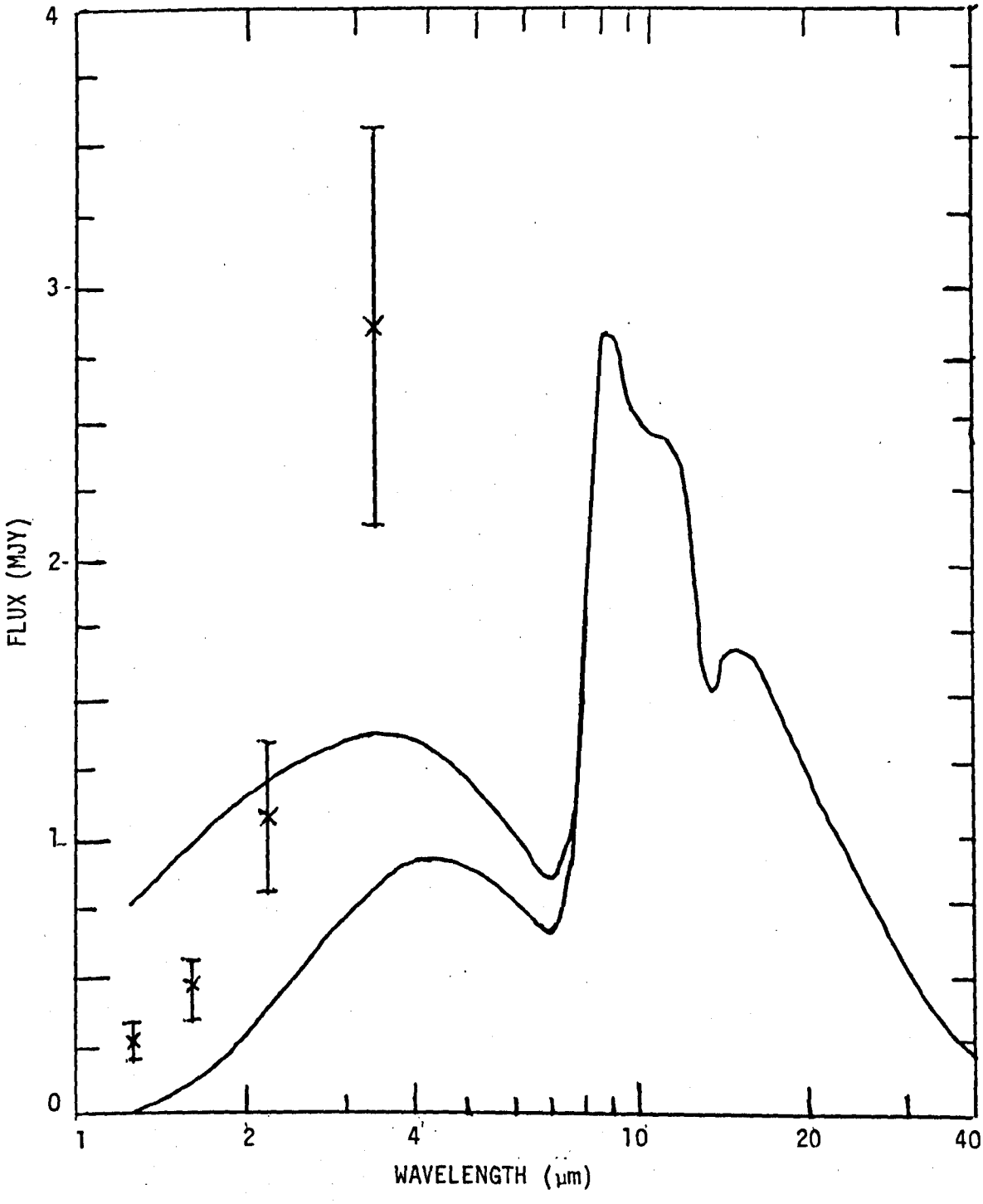
4
3
2
1
0
FLUX (MJY)
1
2
4
10
20
40
WAVELENGTH (μm)

FIGURE 104. The computed dust and total flux spectra of SN1979c in NGC4321 for R_I/R_C = 2.0 compared with the observational data at 440 days after outburst.

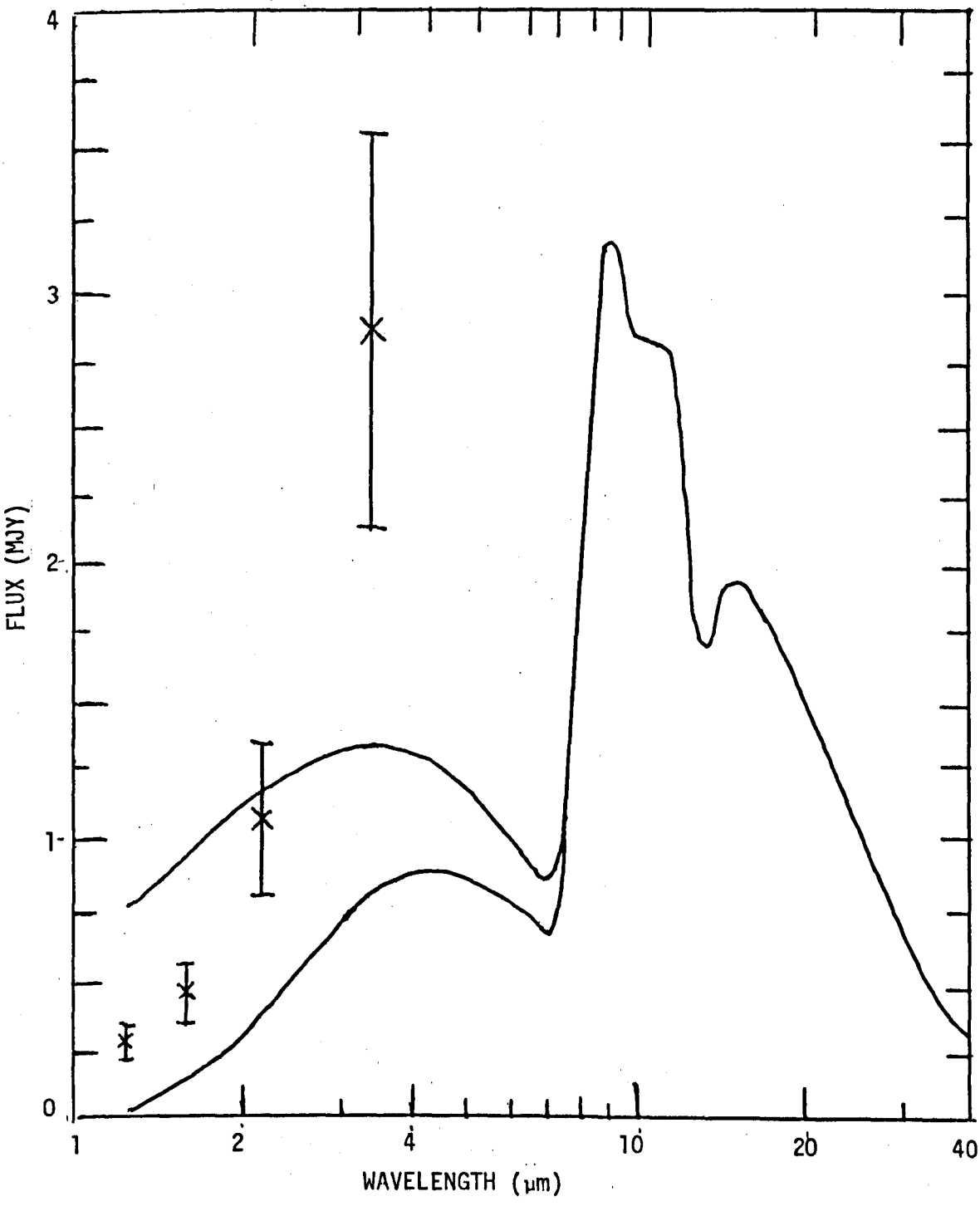
4
3
2
1
0
FLUX (MJY)
1
2
4
10
20
40
WAVELENGTH (μm)

FIGURE 105. The computed dust and total flux spectra of SN1979c in NGC4321 for $R1/R_c$ = 2.5 compared with the observational data at 440 days after outburst.

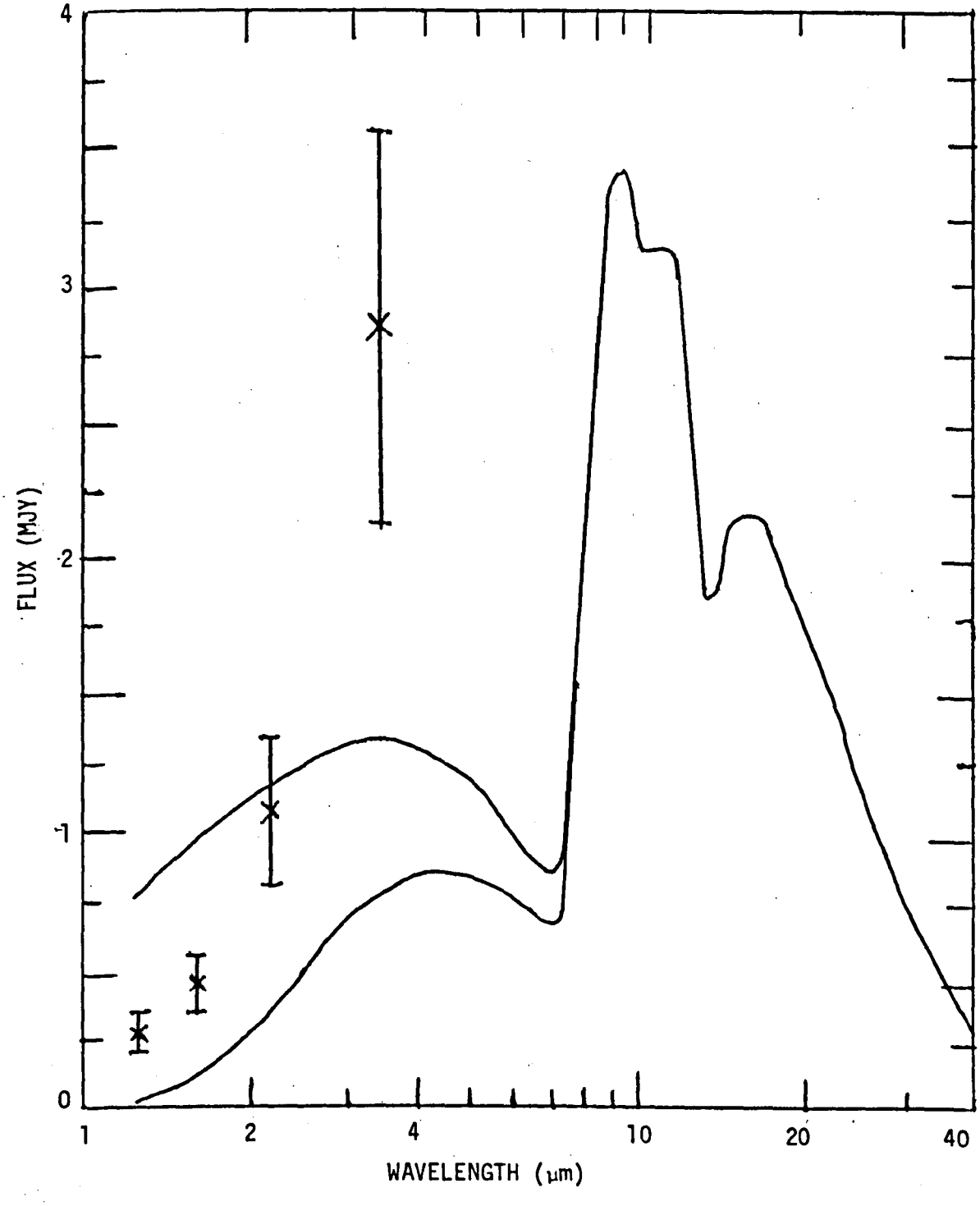
4
3
2
1
0
FLUX (MJY)
1
2
4
10
20
40
WAVELENGTH (μm)

with the observed flux while the predicted J and H fluxes are both a factor of three too big and the predicted L flux a factor of two too small. The observational errors on all points are taken to be 25% or 0.25 magnitudes (Merrill, 1982). The errors at J, H and K are expected to be much less; however, the observed increase of 0.48 magnitudes in J flux from 259 days to 282 days after outburst is probably entirley due to observational error since the flux decreases in the other three wavebands and the circumstellar dust shell must get cooler as the time after outburst is increased. The discrepancies at L may in part be due to the observational difficulties in observing accurately in this waveband. Similarly the discrepancies at J and K at 440 days after outburst may in part be due to the extreme difficulties encountered in observing SN1979c at this time (there was no visible object). On the other hand the fit may be improved by using a different theoretical approach and this is discussed later on in this chapter. Dwek (1982) attempts to fit the observational data at 259 days, 282 days and 440 days after outburst. There is no real attempt to fit J and H data in Dwek's paper because the supernova flux is not taken into account. The approach here is far more rigorous. The fits at K and L are reasonable but possible deficiencies to the method used to compute the flux in Dwek's paper have been detailed in section 6.3.

The supernova flux as a function of time for the first 800 days after outburst is shown at 3.4μm, 9μm and 20μm in figures 106, 107 and 108 respectively. The dust flux for the three cases R_1/R_c = 1.6, 2.0 and 2.5 is shown as a function of time for the first 800 days after outburst at 3.4μm, 9μm and 20μm in figures 109, 110 and 111 respectively. The light curves at 3.4μm represent the time variation of the flux in the near infra- red region of the spectrum, while light curves at 20μm represent the time variation of the flux in the far infra-red region of the spectrum. The time variation of the flux at 9μm describes the flux variation of the silicate peak. The abrupt drop in supernova flux and the increase from zero of the

FIGURE 106. SN1979c in NGC4321 : The computed supernova light curve at 3.4μm. (Excluding the dust contribution).

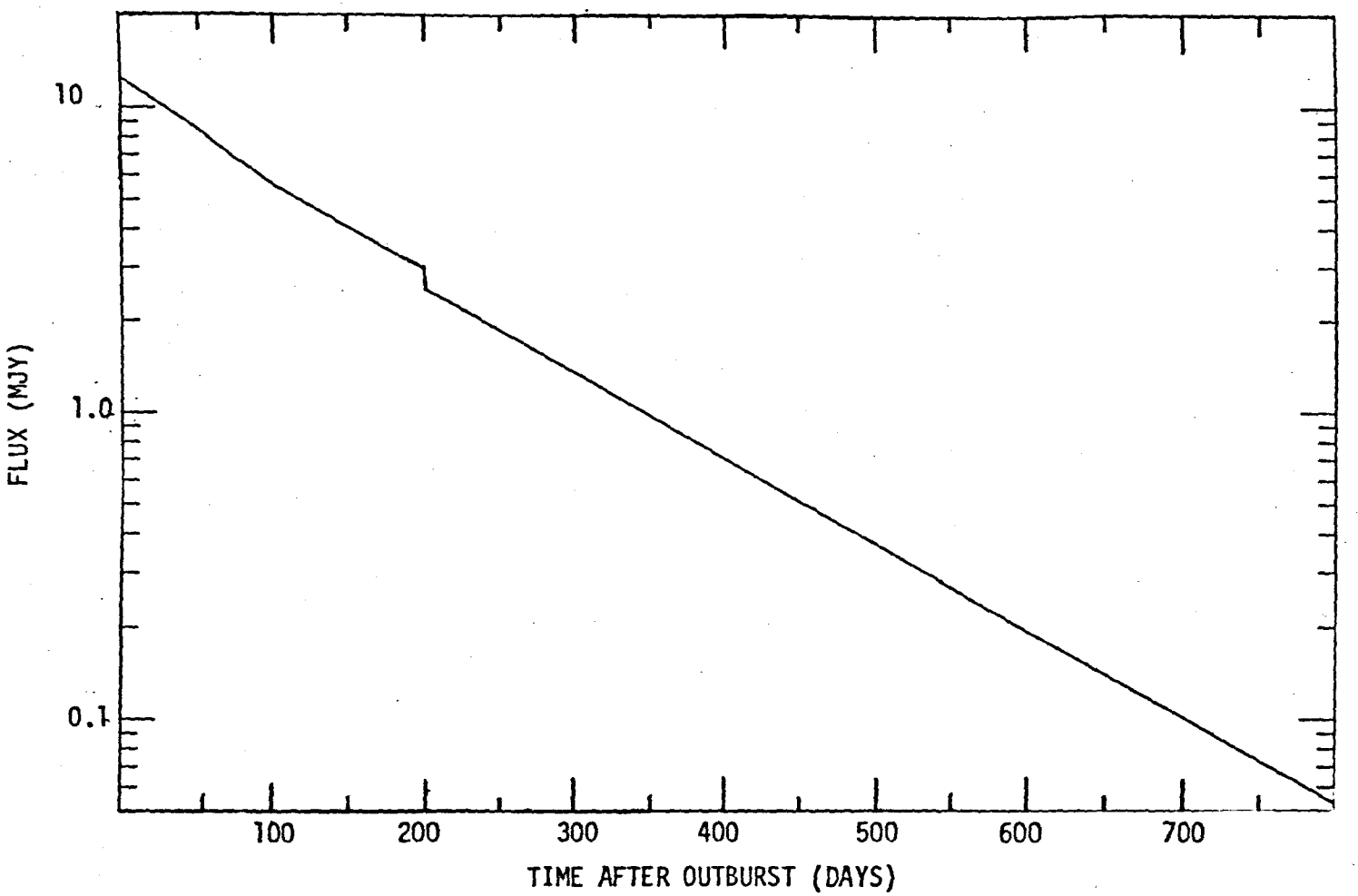
10
1.0
0.1
FLUX (MJY)
100
200
300
400
500
600
700
TIME AFTER OUTBURST (DAYS)

FIGURE 107. SN1979c in NGC4321 : The computed supernova light curve at 9μm. (Excluding the dust contribution).

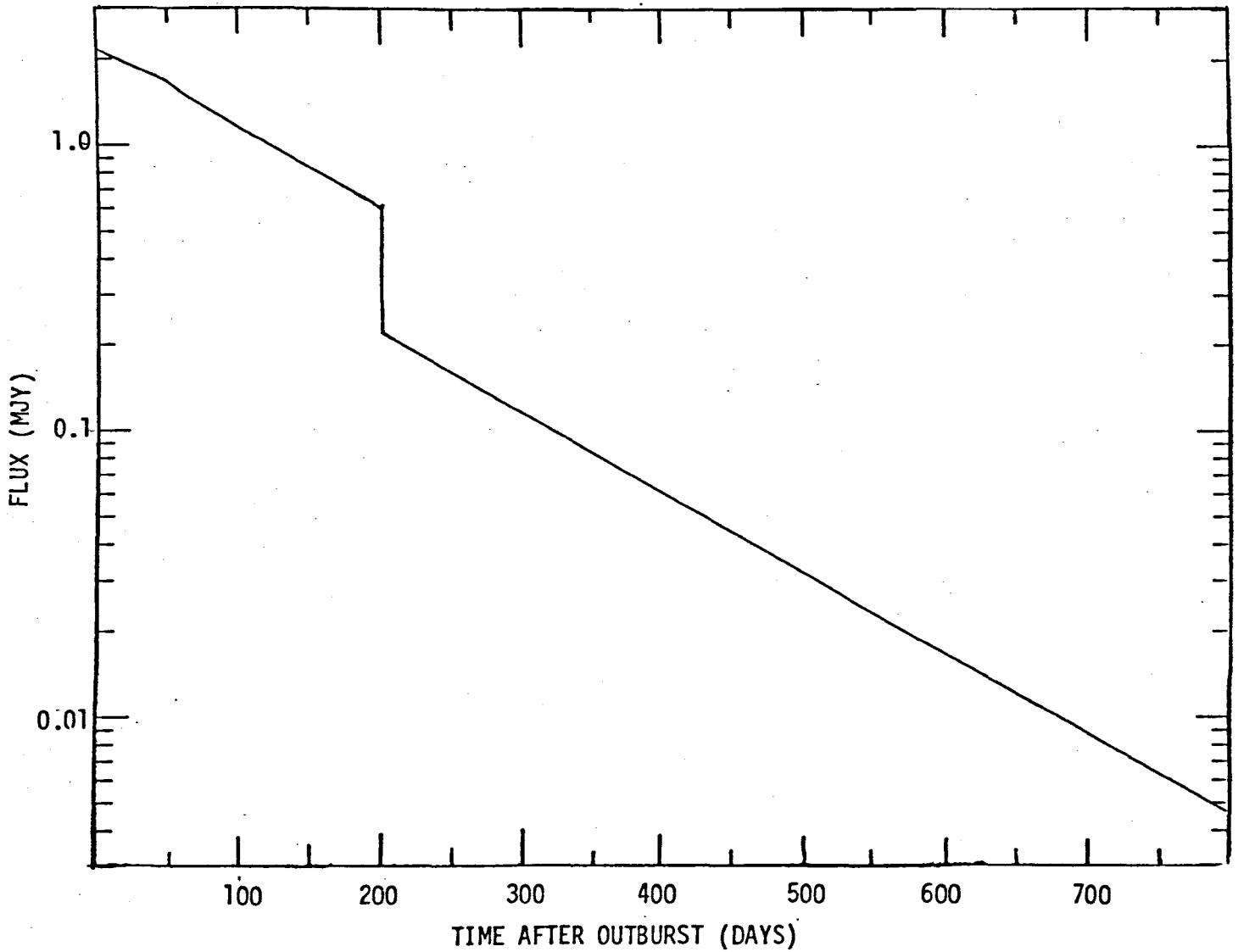
1.0
0.1
0.01
FLUX (MJY)
100
200
300
400
500
600
700
TIME AFTER OUTBURST (DAYS)

FIGURE 108. SN1979c in NGC4321 : The computed supernova light curve at 20μm. (Excluding the dust contribution).

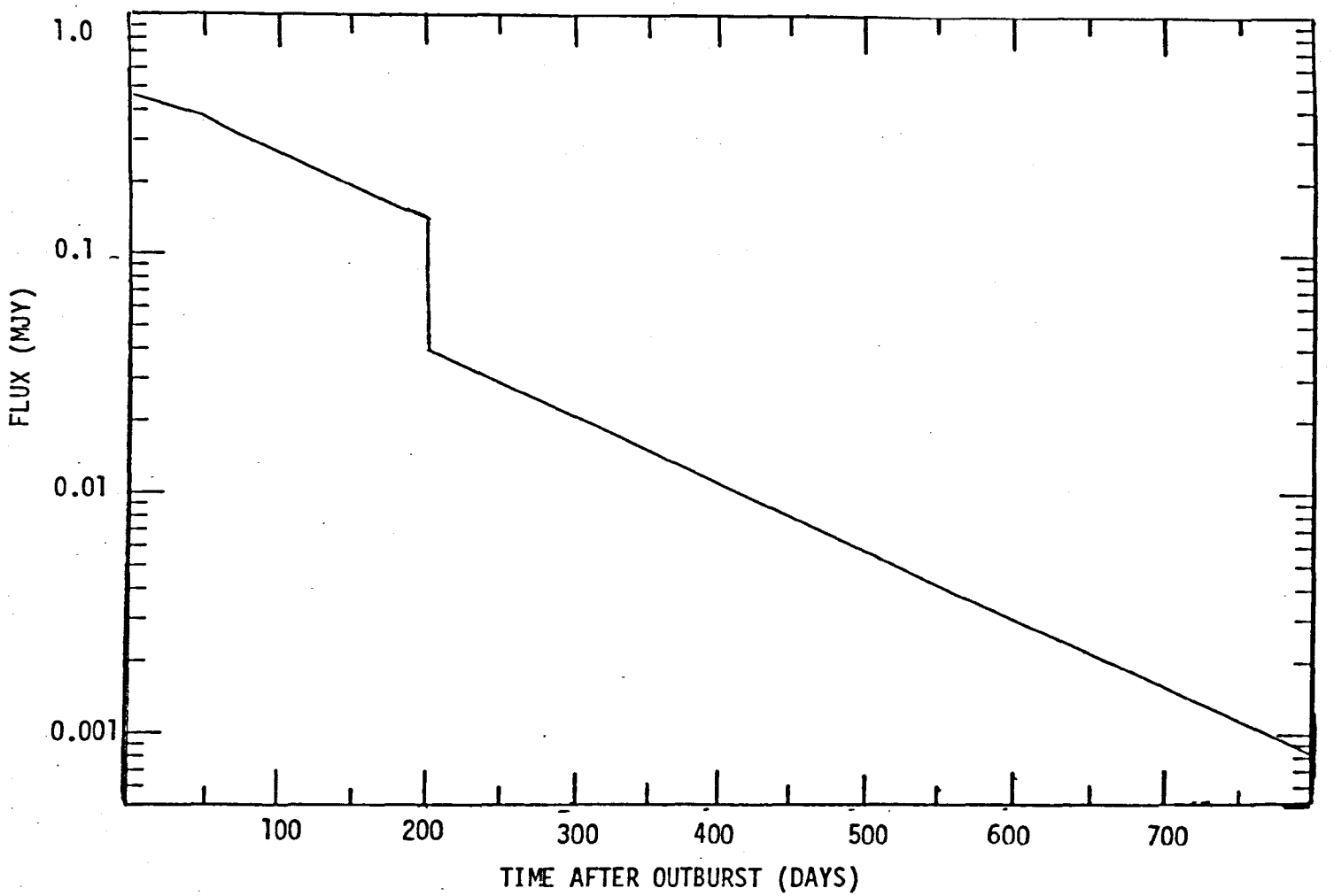
1.0
0.1
0.01
0.001
FLUX (MJY)
100
200
300
400
500
600
700
TIME AFTER OUTBURST (DAYS)

FIGURE 109. SN1979c in NGC4321 : The computed dust and total infra-red flux as a function of time for R_I/R_C = 1.6 at 3.4μm.

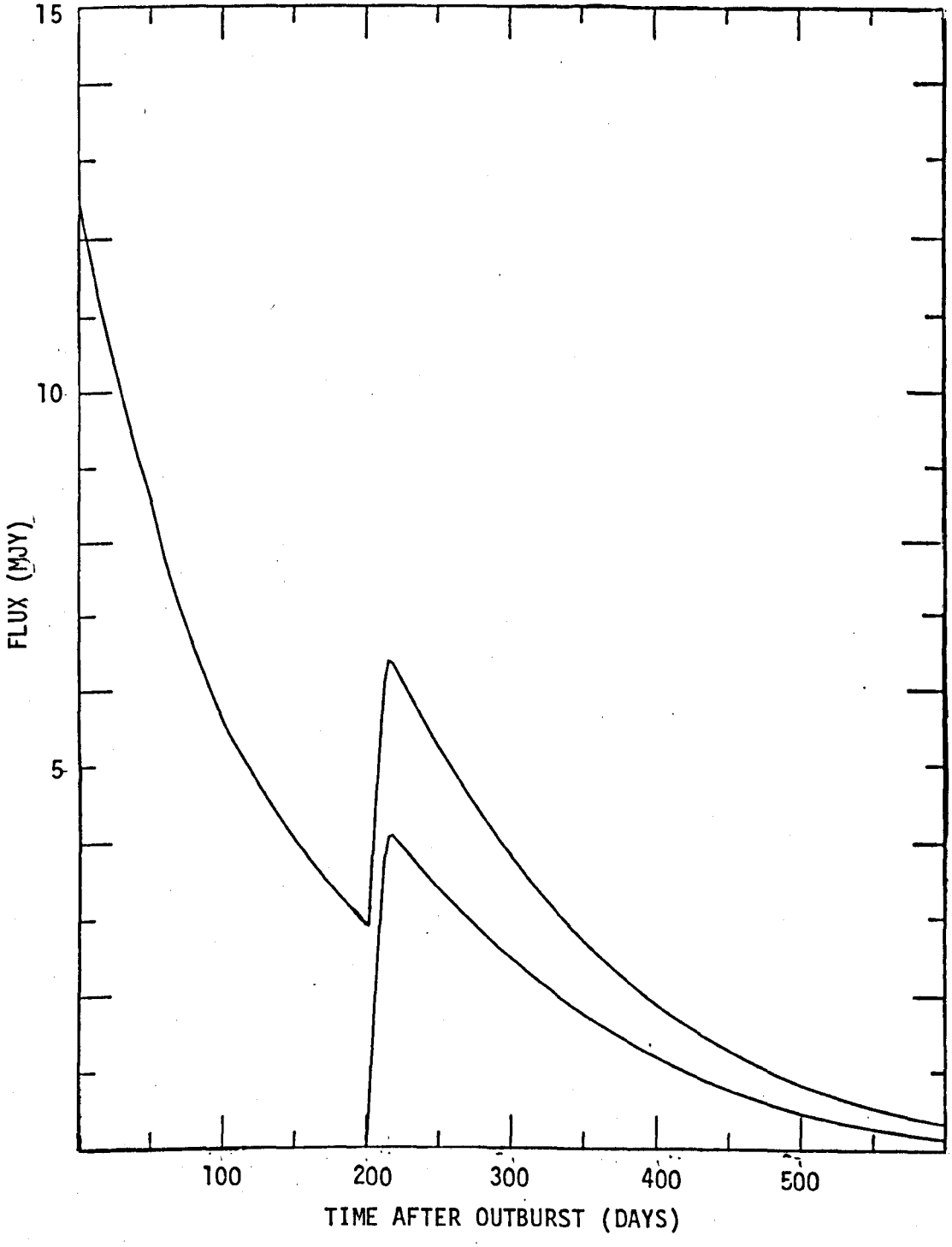
15
10
5
FLUX (MJY)
100
200
300
400
500
TIME AFTER OUTBURST (DAYS)

FIGURE 110. SN1979c in NGC4321 : The computed dust and total infra-red flux as a function of time for R_1/R_c = 1.6 at 9μm.

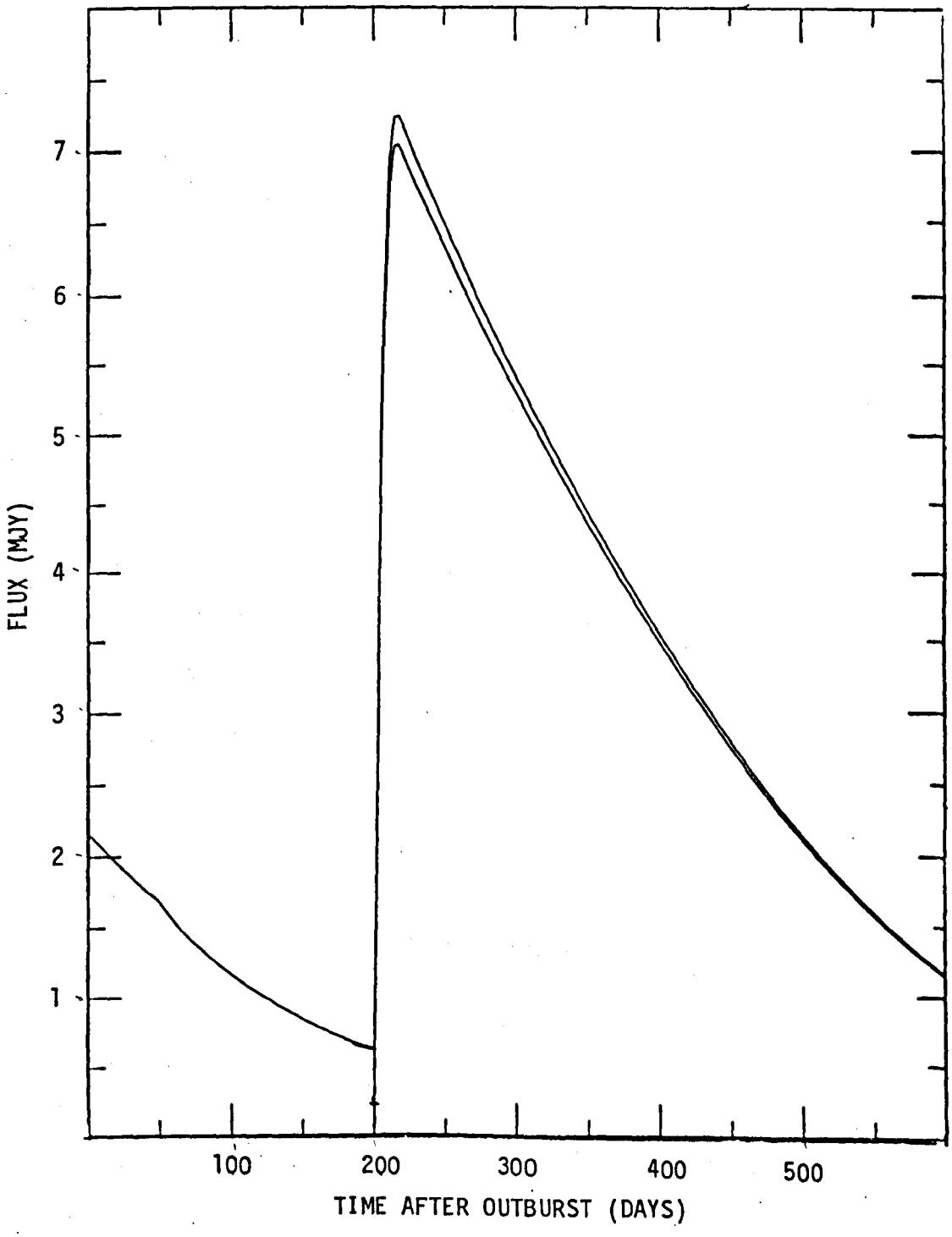
FLUX (MJY)
7
6
5
4
3
2
1
100
200
300
400
500
TIME AFTER OUTBURST (DAYS)

FIGURE 111. SN1979c in NGC4321 : The computed dust and total infra-red flux as a function of time for R_1/R_c = 1.6 at 20μm.

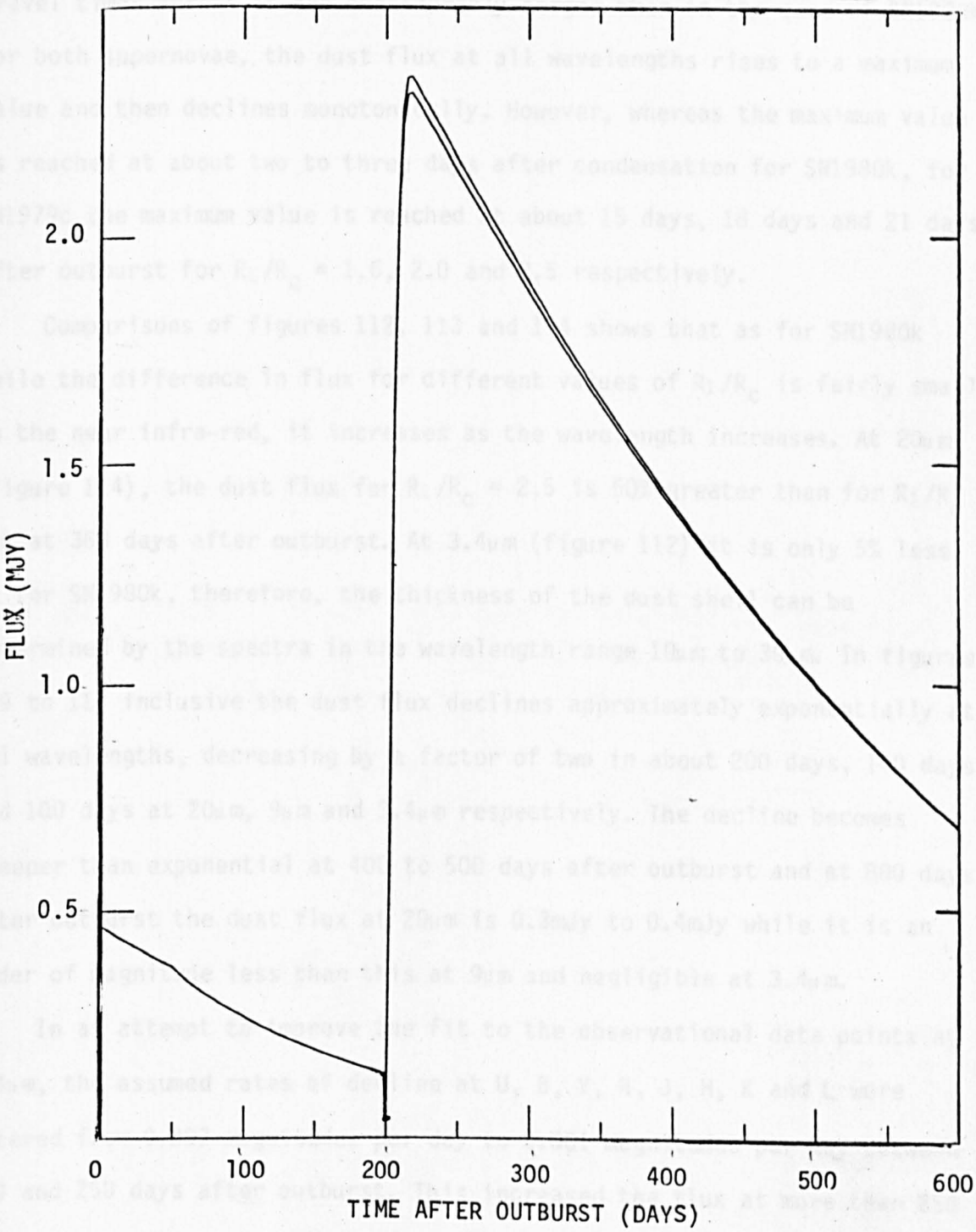
2.0
1.5
1.0
0.5
FLUX (MJY)
0
100
200
300
400
500
600
TIME AFTER OUTBURST (DAYS)

dust flux at 200 days after outburst is due to the condensation of the dust shell. The value of $2R_c/c$ is 11.6 days so R_1/c ranges from 18.6 days for R_1/R_c = 1.6 to 29.0 days for R_1/R_c = 2.5. The dust shell and so the light travel times across it are considerably larger than in the case of SN1980k. For both supernovae, the dust flux at all wavelengths rises to a maximum value and then declines monotonically. However, whereas the maximum value is reached at about two to three days after condensation for SN1980k, for SN1979c the maximum value is reached at about 15 days, 18 days and 21 days after outburst for R_1/R_c = 1.6, 2.0 and 2.5 respectively.

Comparisons of figures 112, 113 and 114 shows that as for SN1980k while the difference in flux for different values of R_1/R_c is fairly small in the near infra-red, it increases as the wavelength increases. At 20μm (figure 114), the dust flux for R_1/R_c = 2.5 is 50% greater than for R_1/R_c = 1.6 at 360 days after outburst. At 3.4μm (figure 112) it is only 5% less. As for SN1980k, therefore, the thickness of the dust shell can be determined by the spectra in the wavelength range 10μm to 30μm. In figures 109 to 114 inclusive the dust flux declines approximately exponentially at all wavelengths, decreasing by a factor of two in about 200 days, 140 days and 100 days at 20μm, 9μm and 3.4μm respectively. The decline becomes steeper than exponential at 400 to 500 days after outburst and at 800 days after outburst the dust flux at 20μm is 0.3mJy to 0.4mJy while it is an order of magnitude less than this at 9μm and negligible at 3.4μm.

In an attempt to improve the fit to the observational data points at 3.4μm, the assumed rates of decline at U, B, V, R, J, H, K and L were altered from 0.007 magnitudes per day to 0.001 magnitudes per day between 100 and 250 days after outburst. This increased the flux at more than 250 days after outburst by 0.9 magnitudes in all wavebands. The supernova effective temperature is of course unchanged but the increased supernova luminosity is shown as a broken line in figure 95. The optical depth of the circumstellar shell was left unchanged. As the light travel time across the

FIGURE 112. SN1979c in NGC4321 : The computed infra-red dust flux as a function of time for R_1/R_C = 1.6 (upper curve), 2.0 (middle curve) and 2.5 (lower curve) at 3.4μm.

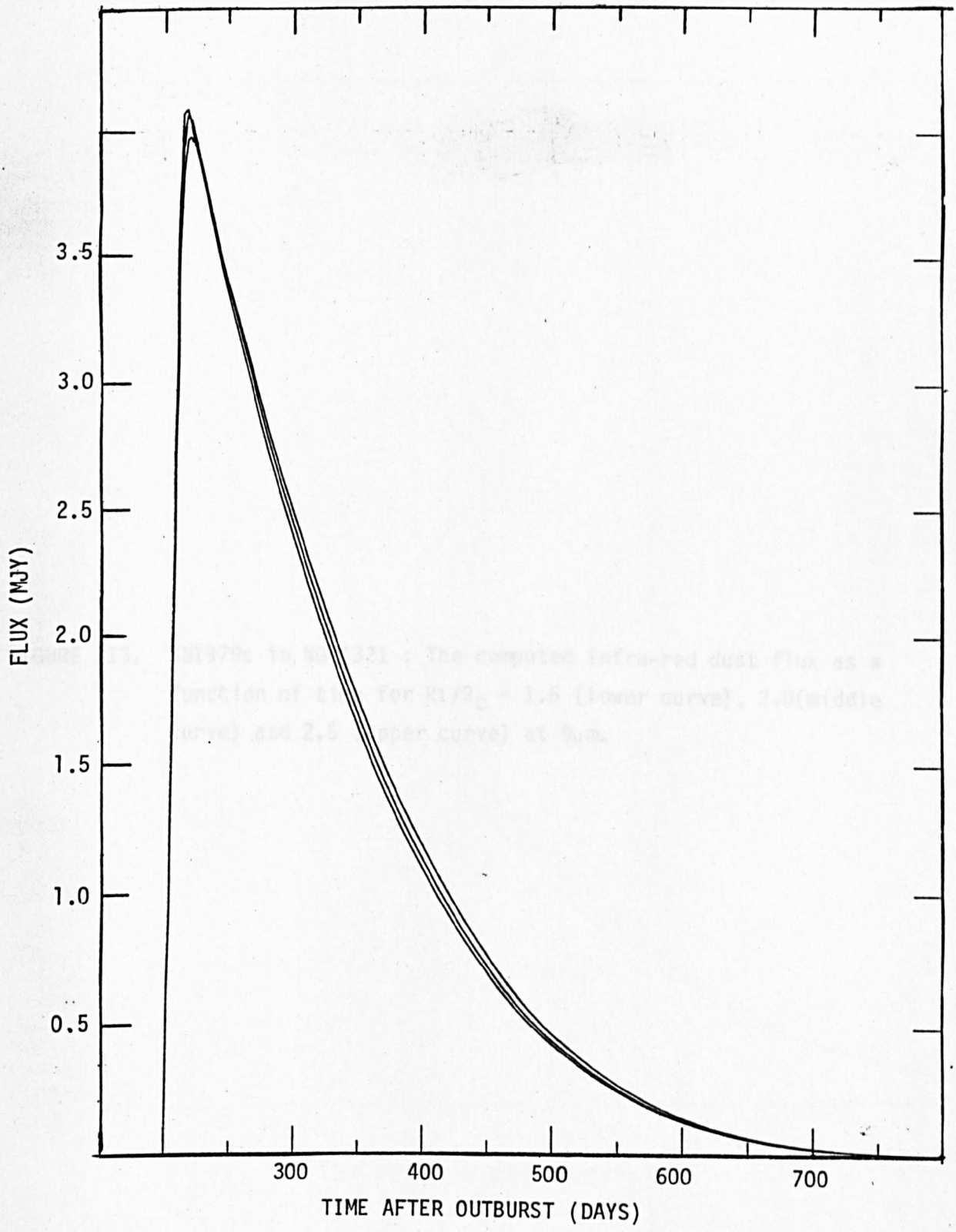
FLUX (MJY)
3.5
3.0
2.5
2.0
1.5
1.0
0.5
300
400
500
600
700
TIME AFTER OUTBURST (DAYS)

FIGURE 113. SN1979c in NGC4321 : The computed infra-red dust flux as a function of time for R_1/R_c = 1.6 (lower curve), 2.0(middle curve) and 2.5 (upper curve) at 9μm.

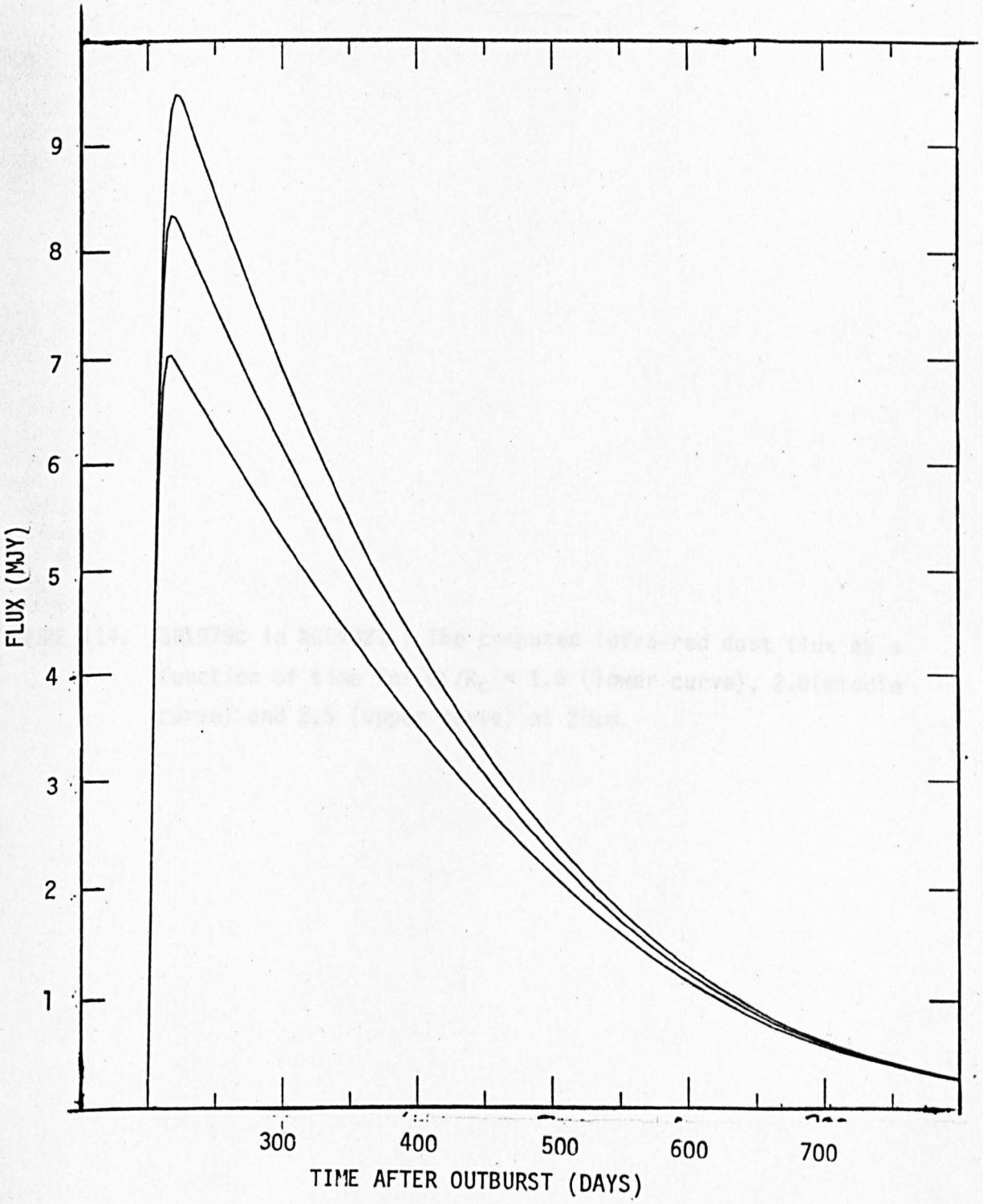
FLUX (MJY)
9
8
7
6
5
4
3
2
1
300
400
500
600
700
TIME AFTER OUTBURST (DAYS)

FIGURE 114. SN1979c in NGC4321 : The computed infra-red dust flux as a function of time for R_1/R_C = 1.6 (lower curve), 2.0(middle curve) and 2.5 (upper curve) at 20μm.

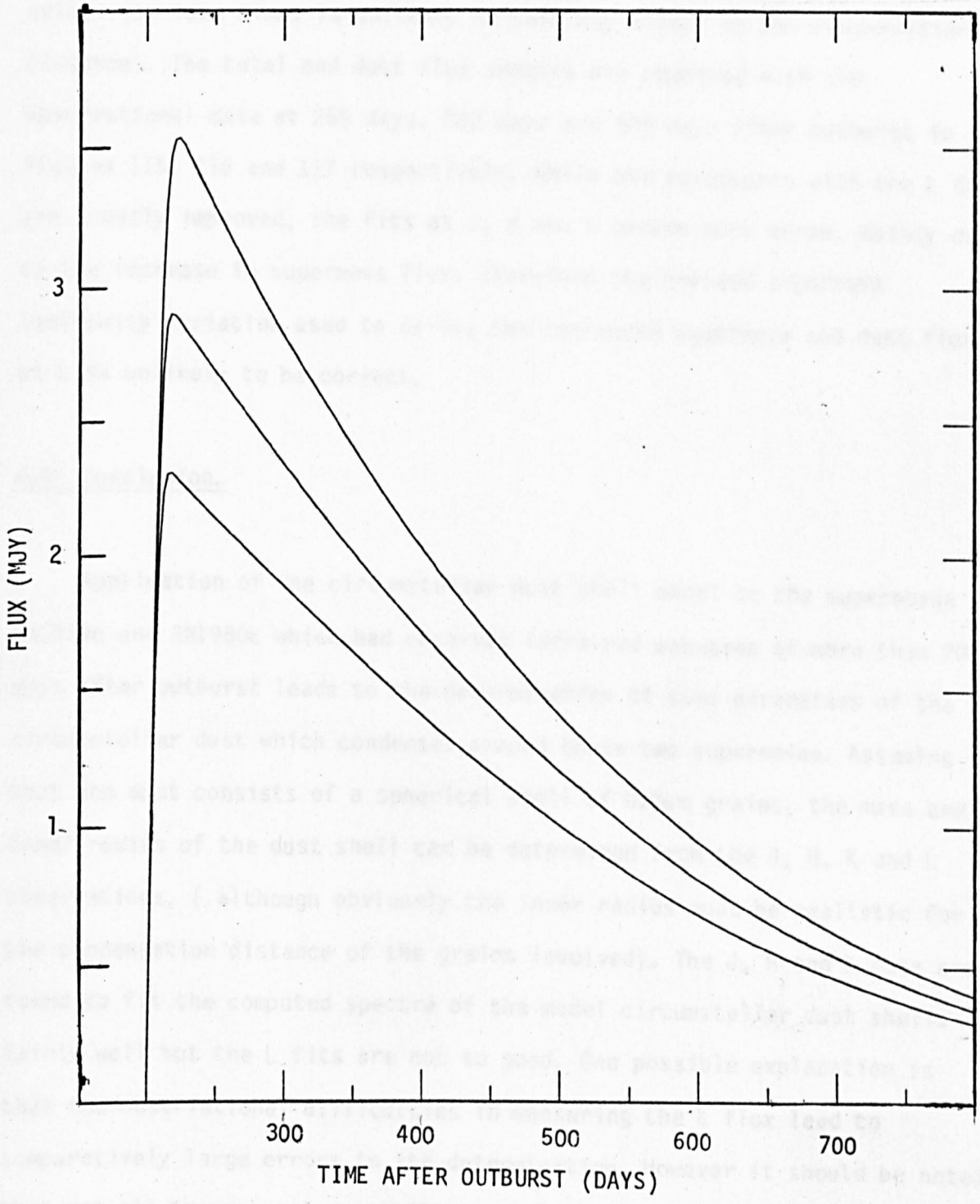
FLUX (MJY)
3
2
1
300
400
500
600
700
TIME AFTER OUTBURST (DAYS)

circumstellar dust shell is in this case around 10 to 20 days it was decided to leave R_c unchanged and let the increase in grain temperature give rise to more flux. (The effect of increasing the luminosity at relatively late times is unlikely to have any effect on the condensation distance). The total and dust flux spectra are compared with the observational data at 259 days, 282 days and 440 days after outburst in figures 115, 116 and 117 respectively. While the agreements with the L data are greatly improved, the fits at J, H and K become much worse, mainly due to the increase in supernova flux. Therefore the revised supernova luminosity variation used to derive the increased supernova and dust flux at L is unlikely to be correct.

6.5 Conclusion.

Application of the circumstellar dust shell model to the supernovae SN1979c and SN1980k which had observed infra-red excesses at more than 200 days after outburst leads to the determination of some parameters of the circumstellar dust which condenses around these two supernovae. Assuming that the dust consists of a spherical shell of 0.2μm grains, the mass and inner radius of the dust shell can be determined from the J, H, K and L observations, (although obviously the inner radius must be realistic for the condensation distance of the grains involved). The J, H and K data are found to fit the computed spectra of the model circumstellar dust shells fairly well but the L fits are not so good. One possible explanation is that the observational difficulties in measuring the L flux lead to comparatively large errors in its determination. However it should be noted that not all theoretical possibilities have been explored. Firstly, despite the fact that silicate grains are to be expected around type II supernovae, they may not be the grain type in reality. Should some other grain type be involved, for example, a conducting grain as discussed by Dwek (1982), this

FIGURE 115. The computed dust and total infra-red flux spectra of SN1979c in NGC4321 for R_1/R_c = 1.6 and the increased supernova luminosity compared with the observational data at 259 days after outburst.

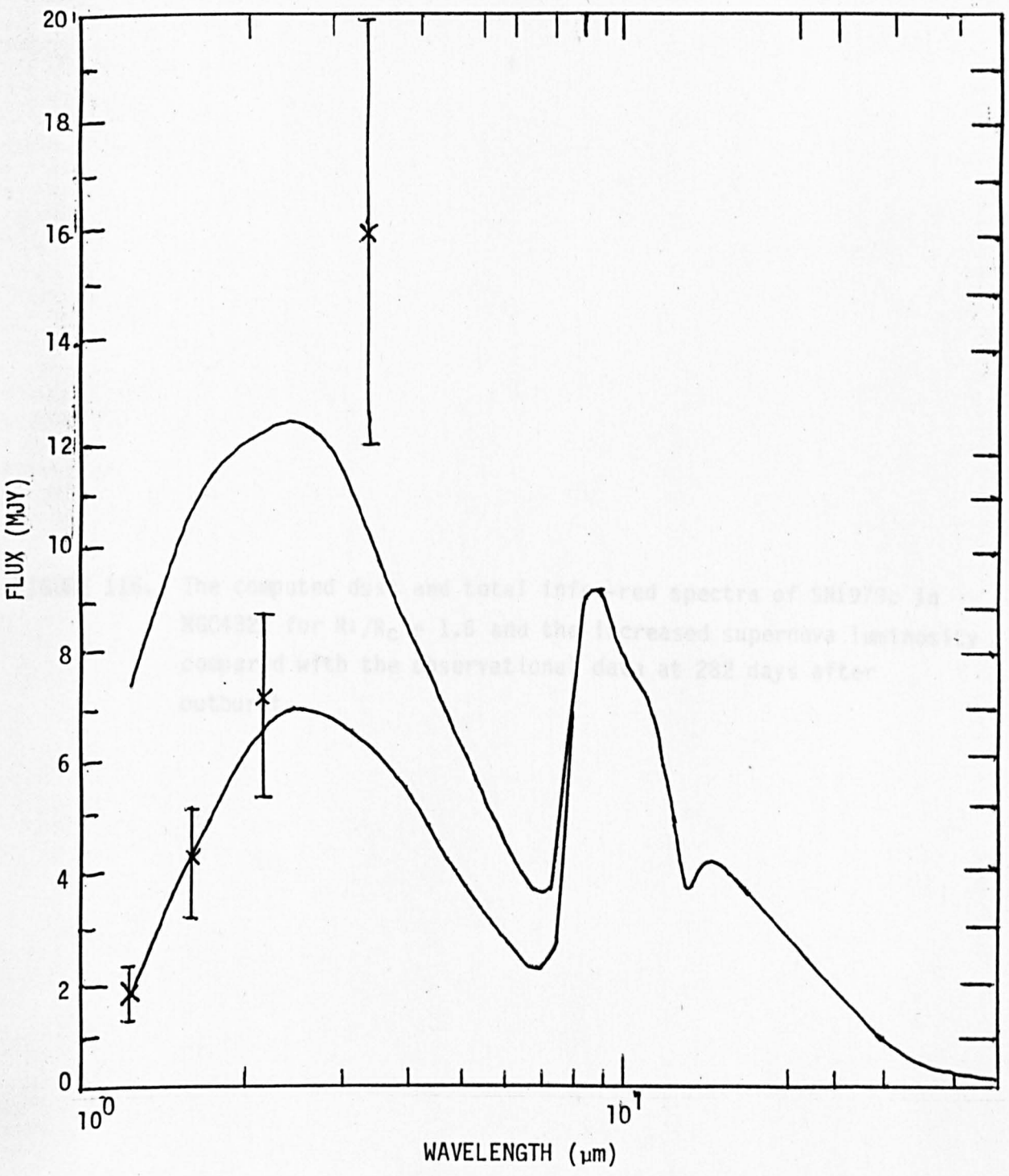
FLUX (MJY)
WAVELENGTH (μm)
0
2
4
6
8
10
12
14
16
18
20
10^0
10^1

FIGURE 116. The computed dust and total infra-red spectra of SN1979c in NGC4321 for R_1/R_C = 1.6 and the increased supernova luminosity compared with the observational data at 282 days after outburst.

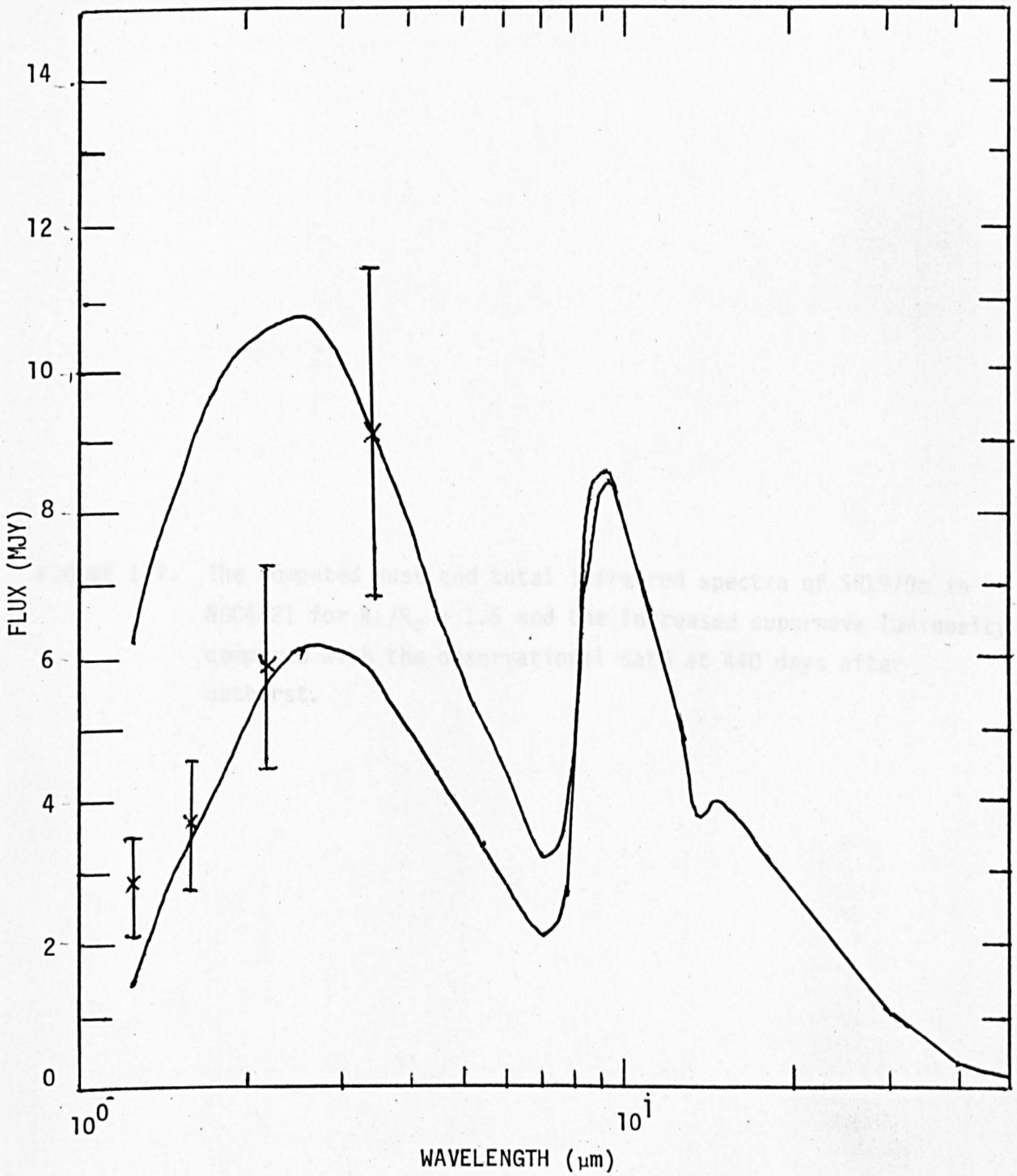
14
12
10
8
6
4
2
0
FLUX (MJY)
10^0
10^1
WAVELENGTH (μm)

FIGURE 117. The computed dust and total infra-red spectra of SN1979c in NGC4321 for R_1/R_c = 1.6 and the increased supernova luminosity compared with the observational data at 440 days after outburst.

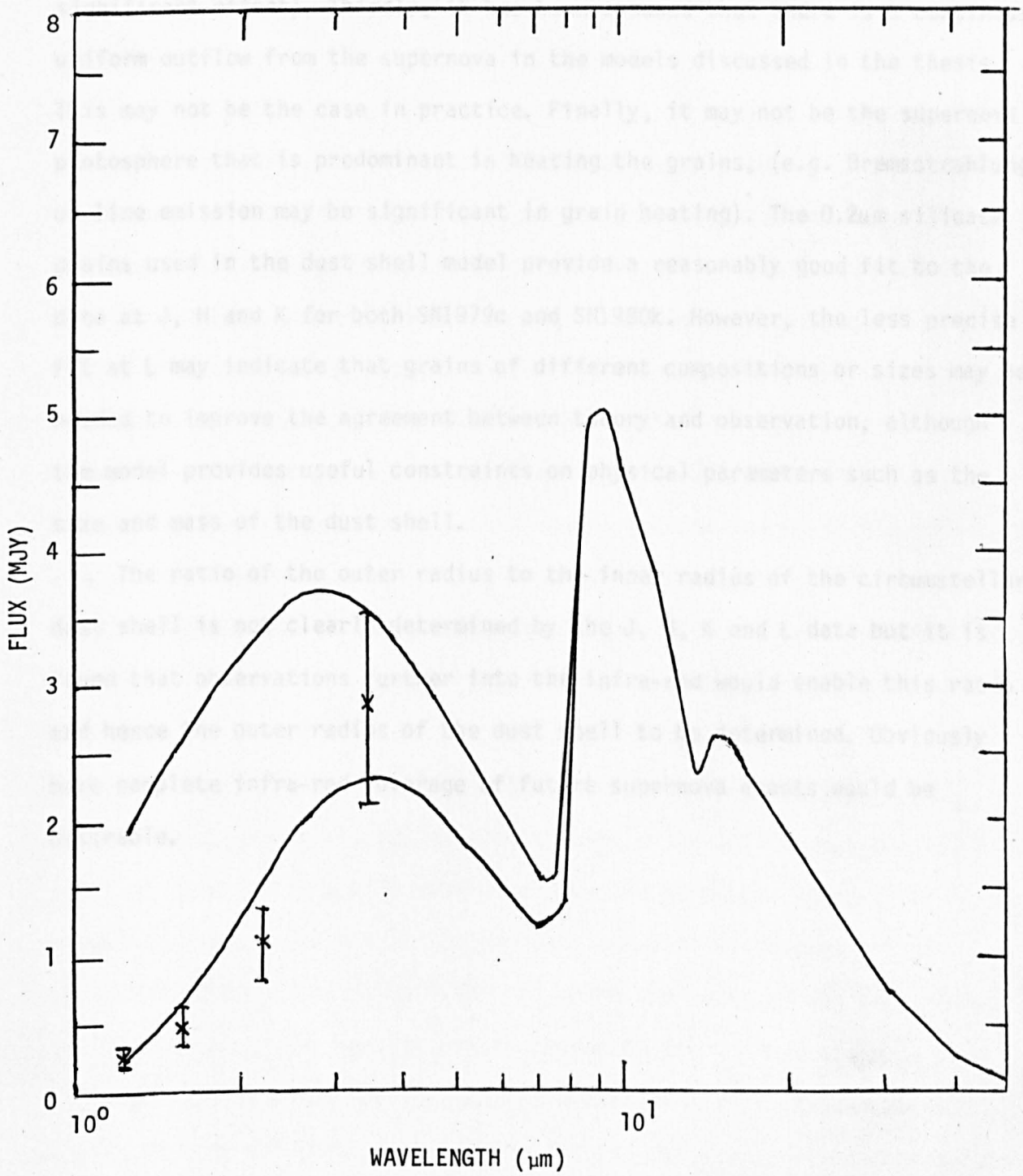
8
7
6
5
4
3
2
1
0
FLUX (MJY)
10^0
10^1
WAVELENGTH (μm)

could provide interesting constraints on the composition of the ejecta. Secondly, there is likely to be a distribution of grain sizes in the dust shell (even assuming a single grain size other that 0.2μm might have a significant effect). Thirdly, it has been assumed that there is a continous uniform outflow from the supernova in the models discussed in the thesis. This may not be the case in practice. Finally, it may not be the supernova photosphere that is predominant in heating the grains, (e.g. Bremsstrahlung or line emission may be significant in grain heating). The 0.2μm silicate grains used in the dust shell model provide a reasonably good fit to the data at J, H and K for both SN1979c and SN1980k. However, the less precise fit at L may indicate that grains of different compositions or sizes may be needed to improve the agreement between theory and observation, although the model provides useful constraints on physical parameters such as the size and mass of the dust shell.

The ratio of the outer radius to the inner radius of the circumstellar dust shell is not clearly determined by the J, H, K and L data but it is found that observations further into the infra-red would enable this ratio and hence the outer radius of the dust shell to be determined. Obviously more complete infra-red coverage of future supernova events would be desirable.

CHAPTER 7

THE INFRA-RED RADIATION FROM A DOUBLE CIRCUMSTELLAR DUST SHELL.

7.0 Introduction

It is evident that (for example Yamamoto et al. 1977) due to the different condensation temperatures of various grain forming materials ejected in the supernova explosion, these various materials will condense out at different distances from the supernova. It is envisaged therefore that a circumstellar dust shell could condense out around the supernova and that this dust shell could be composed of subshells of different grain types. As the supernova ejecta material flows outwards, first one grain material condenses and then a second material condenses to form mantles on the already condensed grains. Consequently a double dust shell condenses with an inner shell of homogeneous grains and and outer shell, (whose inner radius is the same as the inner shell's outer radius), of core-mantle grains.

An alternative hypothesis is that the presence of the layered circumstellar dust shell could arise through a pre-existing circumstellar shell of core-mantle grains present around the supernova progenitor. At outburst of the supernova all of the dust material evaporates out to a minimum distance from the supernova at which the cores of the core-mantle grains can exist. The mantles evaporate out to the minimum distance from the supernova at which the core-mantle grains can exist. These two distances form the inner shell of the double dust shell. Beyond the second distance, none of the dust evaporates and this region forms the outer shell of the double dust shell.

Clayton (1982) discussed the existence of a multi-layered grain type. The corundum core is surrounded by a layer of $MgAl_2O_4$ which is in turn

surrounded by a layer of $MgSiO_3$. The $MgSiO_3$ layer is covered by a mantle of more volatile material. It is explained by Clayton that such multi-layered grains created by successive condensations of grain materials account for the much greater depletion of aluminium than magnesium from interstellar gas. This strengthens the case for the formation of multi-layered grains in the supernova ejecta. In this chapter the formation of such core-mantle grains around supernovae is considered.

7.1 The Geometry Of The Double Dust Shell

It is assumed that the double circumstellar dust shell consists of an inner shell of inner radius R_c and outer radius R_0, and an outer shell of inner radius R_0 and outer radius R_1. All grains in the inner shell are assumed to be spherical, homogeneous, of the same radius a_1, the same composition, and so the same density s_1. All grains in the outer shell are assumed to have cores identical to grains in the inner shell, and to have spherical homogeneous mantles of the same radii a_2, the same composition, and so the same density s_2, but the mantles have a different composition to the cores. The number density of grains throughout both shells is given by

$$\begin{aligned} N_d(r) &= N_{od} r^{-\beta} && R_0 < r < R_1 \\ &= 0 && \text{otherwise} \end{aligned} \qquad (7.1.1)$$

where $\beta = 0, 1, \text{ or } 2.$

Assuming that the double dust shell has a total mass M_g,

$$M_g = \int_{R_c}^{R_1} N_d(r) \frac{4}{3}\pi a_1^3 s_1 4\pi r^2 dr + \int_{R_0}^{R_1} N_d(r) \frac{4}{3}\pi (a_2^3 - a_1^3) s_2 4\pi r^2 dr \qquad (7.1.2)$$

Substituting (7.1.1) in (7.1.2) we obtain

$$N_{od} = 3(3-\beta)M_g / 16\pi^2 (a_1^3 s_1 (R_1^{3-\beta} - R_c^{3-\beta}) + (a_2^3 - a_1^3) s_2 (R_1^{3-\beta} - R_0^{3-\beta})) \qquad (7.1.3)$$

As in the case of the circumstellar dust shell it is assumed that the grains are of unchanging radius and the net extinction of radiation along a light path through the dust shells is the extinction due to absorption by grains only.

It is useful to define:-

$$N_{i\nu} = N_{od}\pi a_i^2 Q_{abs}(j,a_i,\nu) \qquad (7.1.4)$$

where $j = h_0$ and $j = C_m$ refer respectively to the homogeneous and the core-mantle grains and i=1, 2 for homogeneous and core-mantle grains respectively.

The same coordinate system is used in the flux computation as is used in the circumstellar dust shell case. This coordinate system is illustrated in figure 118 which also defines the symbols. For the double dust shell equation (3.5.6) becomes

$$\tau_\nu'(r)=N_{od}\pi a_1^2 Q_{abs}(h_0,a_1,\nu)f_\beta(R_c,r) \qquad R_c < r < R_0$$

$$=N_{od}\pi (a_1^2 Qabs(h_0,a_1,\nu)f_\beta(R_c,R_0)$$

$$+ a_2^2 Q_{abs}(C_m,a_2,\nu)f_\beta(R_0,r)) \qquad R_0 < r < R_1 \qquad (7.1.5)$$

where the function f_β is defined in equation (3.5.7)

The flux seen by the observer per unit frequency interval at frequency ν at time t from a single grain at position $\underline{r}$ in a double dust shell is given by

FIGURE 118. The coordinate system for the double dust shell.

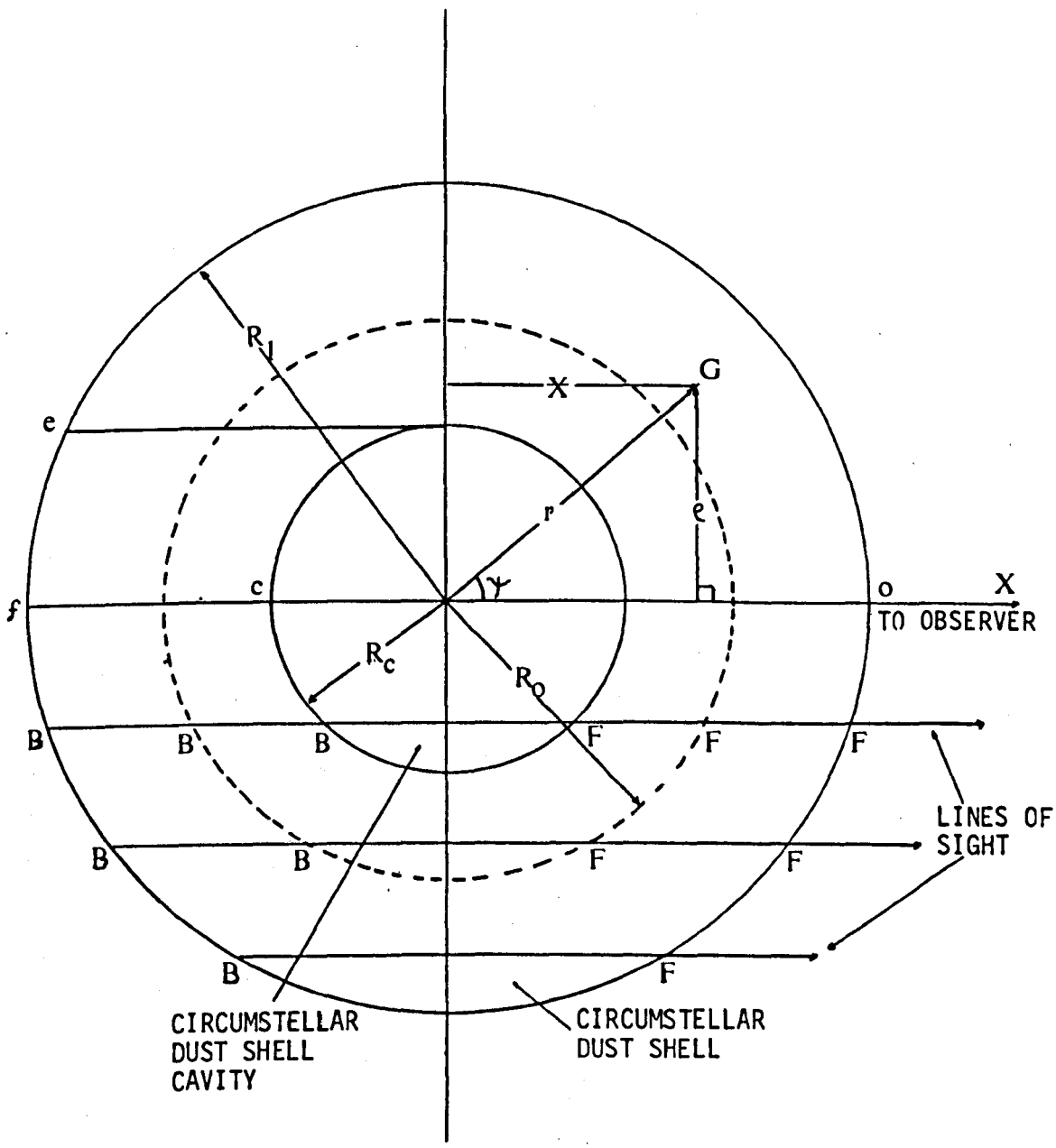
R_1
G
X
e
r
e
Ψ
c
o
X
f
TO OBSERVER
R_c
R_o
B
B
B
F
F
F
B
B
F
F
B
F
LINES OF SIGHT
CIRCUMSTELLAR DUST SHELL CAVITY
CIRCUMSTELLAR DUST SHELL

$$S_\nu(\psi,\rho,t)=\pi^{-1}D^{-2}\zeta'(\rho,\psi)B_\nu(r,\tau(\rho,\psi,t))$$
$$.\exp\Big(-\int_{\psi'=\psi}^{\psi'=\psi(F)} N_d(r')\zeta'(\rho,\psi')dx'\Big) \qquad (7.1.6)$$

where $\psi(F)$ represents the value of ψ at point F in figure 118. The grain absorption cross-section ζ' is given by:

$$\zeta'(\rho,\psi)=\pi a_1^2 Q_{abs}(h_0,a_1,\nu)$$
$$R_0 > \rho\,\mathrm{cosec}\psi > R_c$$
$$=\pi a_2^2 Q_{abs}(c_m,a_2,\nu)$$
$$R_1 > \rho\,\mathrm{cosec}\psi > R_0 \qquad (7.1.7)$$

Inside the cavity ($\rho\,\mathrm{cosec}\psi < R_c$), N_d is zero since there are no grains and $\zeta'(\rho,\psi)$ is therefore not defined inside the cavity.

To simplify the expression for the optical depth given in equation (7.1.8) below, the function $\phi_{1\beta}(\rho,\psi)$ and $\phi_{2\beta}(\rho,\psi)$ are defined. These functions represent the factors by which $N_{1\nu}$ and $N_{2\nu}$ must be multiplied to obtain the optical depth expressions across the double dust shell,

$$-\int_{\psi'=\psi}^{\psi'=\psi(F)} N_d(r')\zeta'(\rho,\psi')dx'$$
$$=(N_{1\nu}\phi_{1\beta}(\rho,\psi)+N_{2\nu}\phi_{2\beta}(\rho,\psi))\rho^{1-\beta} \qquad (7.1.8)$$

Equation (7.1.8) represents the optical depth of the grains across the double dust shell.

Substituting equations (6.1.21) (6.1.22) (7.1.1) (7.1.4) (7.1.7) into equation (7.1.8) yields the following equations, from which the optical depth from any point in the double dust shell can be derived:-

$$\phi_{1\beta}(\rho,\psi)=0 \quad \text{for } \rho > R_0 \text{ or } \rho < R_0 \text{ and } \psi<\psi(F'') \qquad (7.1.9a)$$

which is represented by lines of sight (ii) (iii) or (iv) in figure 118 and represents the region between F" and F on this figure.

$$\phi_{1\beta}(\rho,\psi)=\int_{\psi(B'')}^{\psi(F'')} \sin^{\beta-2}\psi'd\psi' \quad \text{for } R_c < \rho < R_0 \text{ and } \psi > \psi(B'') \qquad (7.1.9b)$$

The conditions for this are represented by lines of sight (ii) and (iii) in figure 118 and the region between B" and B.

$$\phi_{1\beta}(\rho,\psi)=\int_{\psi}^{\psi(F'')} \sin^{\beta-2}\psi'd\psi' \quad \text{for } R_c < \rho < R_0 \text{ and } \psi(B'') > \psi > \psi(F'') \text{ or } \rho < R_c \text{ and } \psi(F') > \psi > \psi(F'') \qquad (7.1.9c)$$

which is represented by lines of sight (ii) and (iii) and represents the region between B" and F" along these lines of sight.

$$\phi_{1\beta}(\rho,\psi)=\int_{\psi}^{\psi(B')} \sin^{\beta-2}\psi'd\psi' + \int_{\psi(F')}^{\psi(F'')} \sin^{\beta-2}\psi'd\psi' \quad \text{for } \rho < R_c \text{ and } \psi(B'') > \psi > \psi(B') \qquad (7.1.9d)$$

These conditions represent the line of sight (ii) in figure 118 and the region between B" and B'.

$$\phi_{1\beta}(\rho,\psi)=\int_{\psi(B'')}^{\psi(B')} \sin^{\beta-2}\psi'd\psi' + \int_{\psi(F')}^{\psi(F'')} \sin^{\beta-2}\psi'd\psi' \quad \text{for } \rho<R_c \text{ and } \psi(B) > \psi > \psi(B'') \qquad (7.1.9e)$$

which is represented also by the line of sight (ii) but indicates in this case the region between B and B" in figure 118. For $\phi_{2\beta}$ we have the

following conditions:-

$$\phi 2_\beta(\rho,\psi)=\int_{\psi}^{\psi(F)} \sin^{\beta-2}\psi' d\psi' \qquad \text{for } \rho > R_0 \text{ or } \rho < R_0 \text{ and } \psi < \psi(F'') \tag{7.1.10a}$$

These condtions are represented by the lines of sight (ii) (iii) or (iv) and the region between F and F" in figure 118.

$$\phi 2_\beta(\rho,\psi)=\int_{\psi}^{\psi(B'')} \sin^{\beta-2}\psi' d\psi' + \int_{\psi(F'')}^{\psi(F)} \sin^{\beta-2}\psi' d\psi' \qquad \text{for } \rho < R_0 \text{ and } \psi > \psi(B'') \tag{7.1.10b}$$

which represents the conditions along line of sight (iii) in figure 118 between regions B" and B.

$$\phi 2_\beta(\rho,\psi)=\int_{\psi(F'')}^{\psi(F)} \sin^{\beta-2}\psi' d\psi' \qquad \text{for } R_c < \rho < R_0 \text{ and } \psi(B'') > \psi > \psi(F'') \text{ or } \rho < R_c \text{ and } \psi(F') > \psi > \psi(F'') \tag{7.1.10c}$$

which represents lines of sight (ii) or (iii) in figure 118 and the region between B" and F".

$$\phi 2_\beta(\rho,\psi)=\int_{\psi(F'')}^{\psi(F)} \sin^{\beta-2}\psi' d\psi' \qquad \text{for } \rho < R_c \text{ and } \psi(B'') > \psi > \psi(B') \tag{7.1.10d}$$

which represents line of sight (ii) in figure 118 and the region between B' and B".

In the above equations $\psi(B)$, $\psi(B')$, $\psi(B")$, $\psi(F)$, $\psi(F')$ and $\psi(F")$ are the values of ψ (in terms of ρ) at the positions B, B', B", F, F' and F" respectively, which are illustrated in figure 118. The conditions $\psi(B)$, $\psi(B')$, $\psi(F)$ and $\psi(F')$ are defined in section 6.1 and $\psi(B")$ and $\psi(F")$ are defined by:-

$$\psi(F") = \tan^{-1}(\rho/(R_0^2-\rho^2)^{\frac{1}{2}}) \qquad (7.1.11)$$

$$\psi(B") = \pi - \tan^{-1}(\rho/(R_0^2-\rho^2)^{\frac{1}{2}}) \qquad (7.1.12)$$

Equations (7.1.9) and (7.1.10) are integrated in appendix (II).

The flux, S_ν, emitted after time t, by a single grain at position ρ, ψ in the double dust shell is given by equation (7.1.13) below. Equation (7.1.13) is obtained by substituting equations (3.5.2) and (7.1.8) into equation (7.1.6). Hence,

$$S_\nu(\psi,\rho,t) = \frac{2\pi h\nu^3}{c^2D^2}\,\zeta'(\rho,\psi)H_\nu(r,\tau(\rho,\psi,t))$$

$$.\exp(\rho^{1-\beta}(N_{1\nu}\phi_{1\beta}(\rho,\psi)+N_{2\nu}\phi_{2\beta}(\rho,\psi))) \qquad (7.1.13)$$

where H_ν is defined in chapter 3.

The surface brightness is given by:-

$$\sum_\nu(\rho,t) = D^2 \int_{\psi=\min(\psi(b):\psi(P))}^{\psi=\psi(F)} N_d(r)S_\nu(\psi,\rho,t)dx. \qquad (7.1.14)$$

as unit normal area of the double dust shell subtends solid angle D^{-2} to the observer. Substituting equations (6.1.1) (6.1.4) (7.1.2) (7.1.7) and

(7.1.13) into equation (7.1.14) yields:-

$$\sum_{\nu}(\rho,t)=2\pi h\nu^{3}c^{-2}(N_{1\nu}\sigma 1'_{\nu}(\rho,t)+N_{2\nu}\sigma 2'_{\nu}(\rho,t)) \qquad (7.1.15)$$

The expression $\sigma 1'_{\nu}(\rho,t)$ is derived from $\sigma'_{\nu}(\rho,\gamma,t)$ which is defined in equation (6.1.31) with the substitutions R_1 becomes R_0, and $Nc_{\nu}\rho^{1-\beta}\phi_{\beta}(\rho,\psi)-\tau^{ic}_{\nu}(\rho,\gamma)$ becomes $\rho^{1-\beta}(N_{1\nu}\phi 1_{\beta}(\rho,\psi) + N_{2\nu}\phi 2_{\beta}(\rho,\psi))$. The expression for $\sigma 2'_{\nu}$ is derived from $\sigma'_{\nu}(\rho,\gamma,t)$ with the substitution that R_c becomes R_0 and $N_{c\nu}\rho^{1-\beta}\phi_{\beta}(\rho,\psi)-\tau^{ic}_{\nu}(\rho,\gamma)$ becomes $\rho^{1-\beta}(N_{1\nu}\phi 1_{\beta}(\rho,\psi)+N_{2\nu}\phi 2_{\beta}(\rho,\psi))$.

Equation (7.1.15) is the integrated expression for the surface brightness for the double dust shell. The flux per unit frequency interval from the double circumstellar dust shell can be computed for any frequency, ν, and at any time, t, after outburst, from the following equation

$$f_{\nu}(t)=2\pi D^{-2}\int_{0}^{R_1}\sum_{\nu}(\rho,t)\rho d\rho \qquad (7.1.16)$$

7.2 The Computed Infra-Red Flux From A Composite Dust Shell

Two cases of double dust shells can be considered. In a carbon excess environment such as will be found around a type I supernova, silicon carbide grains can be thought of as nucleation centres for the formation of graphite grains. In an oxygen excess environment such as will be found around a type II supernova, corundum grains can be thought of as nucleation centres for the formation of silicate grains. As silicon is very much less abundant than carbon, and aluminium is very much less abundant than silicon, (assuming cosmic abundance), silicon carbide and corundum will only form if they condense before graphite and silicate respectively. Even if silicon carbide and corundum were to condense as mantles on graphite and silicate grains respectively, the mantles would be so thin that their

effect on the optical properties of the grains would be negligible. Furthermore, it is likely that the carbon necessary to form silicon carbide will already have condensed as graphite.

A double dust shell could conceivably be formed in one of two ways. One way is for a pre-existing dust shell of core-mantle grains to be partially evaporated by the supernova in such a way that for a range of distances from the supernova, the grain mantles are vapourized but not the cores. The other way is for the cores to condense from the supernova ejecta at a certain distance from the supernova. The mantles would condense on the cores at a greater distance from the supernova. Table 5 in chapter 4 gives the radii of the evaporated cavities of the four grain types while equation (4.1.3) gives the distance at anytime t after outburst at which grains of a particular type can condense. It can be seen from table 5 that neither type of double dust shell can be evaporated from a pre-existing dust shell of core-mantle grains as in both cases the cores, whatever the grain radius, are evaporated out to a much greater distance than the corresponding core-mantle grains. It is also found that silicon carbide grains cannot act as nucleation centres for the formation of graphite-mantle silicon carbide-core grains around type I supernovae because the minimum distance from the supernova at which a grain can condense is always much greater for the silicon carbide core than for either the corresponding core-mantle grains, or for homogeneous graphite grains of the same radius as the corresponding core-mantle grains. This is not, however, true in the case of silicate and corundum. At outburst, the minimum distance from the supernova at which the corundum cores can condense is much greater than for the corresponding core-mantle grains or for homogeneous silicate grains of the same radius as these core-mantle grains. At more than 20 days after outburst, however, this minimum distance is smaller for the corundum cores than for the corresponding core-mantle grains or homogeneous silicate grains of the same radius as these core-mantle grains. The explanation for

this must lie in the different variations with temperature of the Planck mean absorption efficiencies of the core-mantle grains, the homogeneous silicate grains, and the corundum cores, because the type II supernova effective temperature falls from 25,000K at outburst to 9300K at 20 days and to 6000K by 30 days after outburst, after which it remains constant. A similar explanation applies to the formation of silicon carbide cores and graphite mantles around type I supernovae. It can be seen from equation (4.1.3) that the condensation distance depends on the Planck mean absorption efficency of the grains at the supernova effective temperature. As it is the only one of the four scenarios considered likely, the condensation of a double dust shell of silicate-mantle corundum-core and homogeneous corundum grains around a type II supernova is considered.

As the radius of interstellar silicate grains was assumed in chapter 5 to be 0.15μm, this is taken to be the radius of the core-mantle grains. In chapter 3 it is shown that the probable ratio of the mantle radius to the core radius is about 2.2 for graphite-mantle silicon carbide-core grains and 3.77 for silicate-mantle corundum-core grains. The corundum cores therefore have a radius of about 0.04μm. The condensation time t_c of the double dust shell is taken to be 160 days after outburst, which is about the time at which infra-red excesses around type II supernovae begin to be observed. From equation (4.1.3) the cavity radius of the inner dust shell (of homogeneous corundum grains) is found to be 4.468×10^{13}m and the inner radius of the outer dust shell (of core-mantle grains) is found to be 1.945×10^{14}m. The outer radius of the outer dust shell is taken to be 3×10^{14}m (corresponding to an ejection velocity of 21700Km s^{-1}) and the mass of the composite dust shell is taken to be 5×10^{-4} solar masses, a figure between the solar masses of around 2×10^{-4} solar masses derived for the circumstellar dust shell around SN1980k and around 5×10^{-3} solar masses derived from the circumstellar dust shell around SN1979c. The expansion of the outer radius and the consequent increase in mass is discussed later in

the chapter. The grain number density throughout the double dust shell is given by the same $\beta = 2$ distribution described by equation (7.1.1), so no discontinuity in grain number density occurs at the interface between the two dust shells. From equations (7.1.3) and (7.1.5) the optical depth of the double dust shell is approximately given by $\tau_{\nu}^{cs} = 1.326\ Q_{abs}(h_0, a_1, \nu) + 1.974\ Q_{abs}(c_m, a_2, \nu)$.

The shape of the infra-red spectrum of dust heated by supernovae is determined to a large extent by the wavelength variation of the absorption efficiency, Q_{abs}, of the dust. The parameter Q_{abs} is shown as a function of wavelength for 0.15μm silicate grains and for 0.04μm corundum grains in figure 119. In figure 120, Qabs is shown for core-mantle grains of radii 0.03μm, 0.05μm, 0.1μm, 0.15μm and 0.25μm with a grain to core radius ratio of 3.77. In figure 121, Q_{abs} is shown for core-mantle grains of the same radii but with a grain to core radius ratio of 2.00. It can be seen from figure 119 that Q_{abs} for the corundum grains has prominent peaks at 12.7μm, 15.9μm, 20.8μm, and 26μm. It can be seen from figure 120 that Q_{abs} for the core- mantle grains peaks at 10μm, 14μm and 21.2μm. If the grain to core radius ratio is reduced from 3.77 to 2.00, it can be seen from figure 121 that Q_{abs} has peaks at the same wavelengths, but the 10μm peak becomes much less prominent, the 14μm and 21.2μm peaks become much more prominent and a 16μm peak, barely visible for a ratio of 3.77, becomes clearly visible for a ratio of 2.00. A barely visible peak at 26μm is also beginning to emerge. The core mantle peak at 10μm presumably arises from the optical properties of silicate and is similar to the silicate feature at about the same wavelength. The core-mantle peaks at 16μm, 21.2μm and 26μm presumably arises from the optical properties of corundum, as corundum grains have peaks at about the same wavelength. The 14μm peak, however, is peculiar to core-mantle grains. It does not appear for either silicate or corundum grains so its appearence in a circumstellar dust spectrum can be taken as a positive indication of the presence of silicate-mantle corundum-core

FIGURE 119. The variations with wavelength of the absorption efficiencies (Q_{abs}) of 0.15μm radius spherical homogeneous silicate grains (upper line at 1μm) and of 0.04μm radius spherical homogeneous corundum grains (lower line at 1μm).

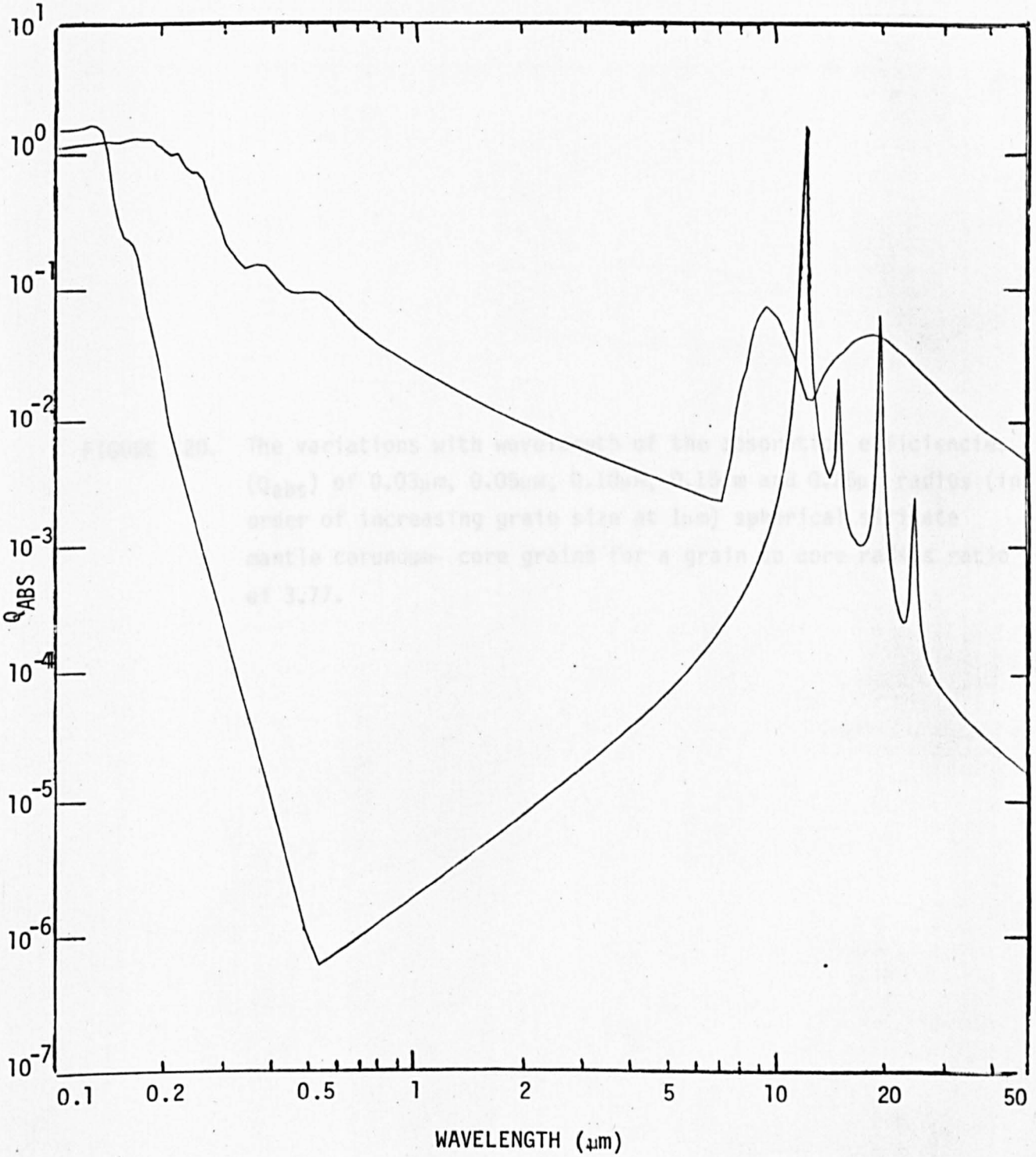
10^{1}
10^{0}
10^{-1}
10^{-2}
10^{-3}
10^{-4}
10^{-5}
10^{-6}
10^{-7}
Q_{ABS}
0.1
0.2
0.5
1
2
5
10
20
50
WAVELENGTH (μm)

FIGURE 120. The variations with wavelength of the absorption efficiencies (Q_{abs}) of 0.03μm, 0.05μm, 0.10μm, 0.15μm and 0.25μm radius (in order of increasing grain size at 1μm) spherical silicate mantle corundum- core grains for a grain to core radius ratio of 3.77.

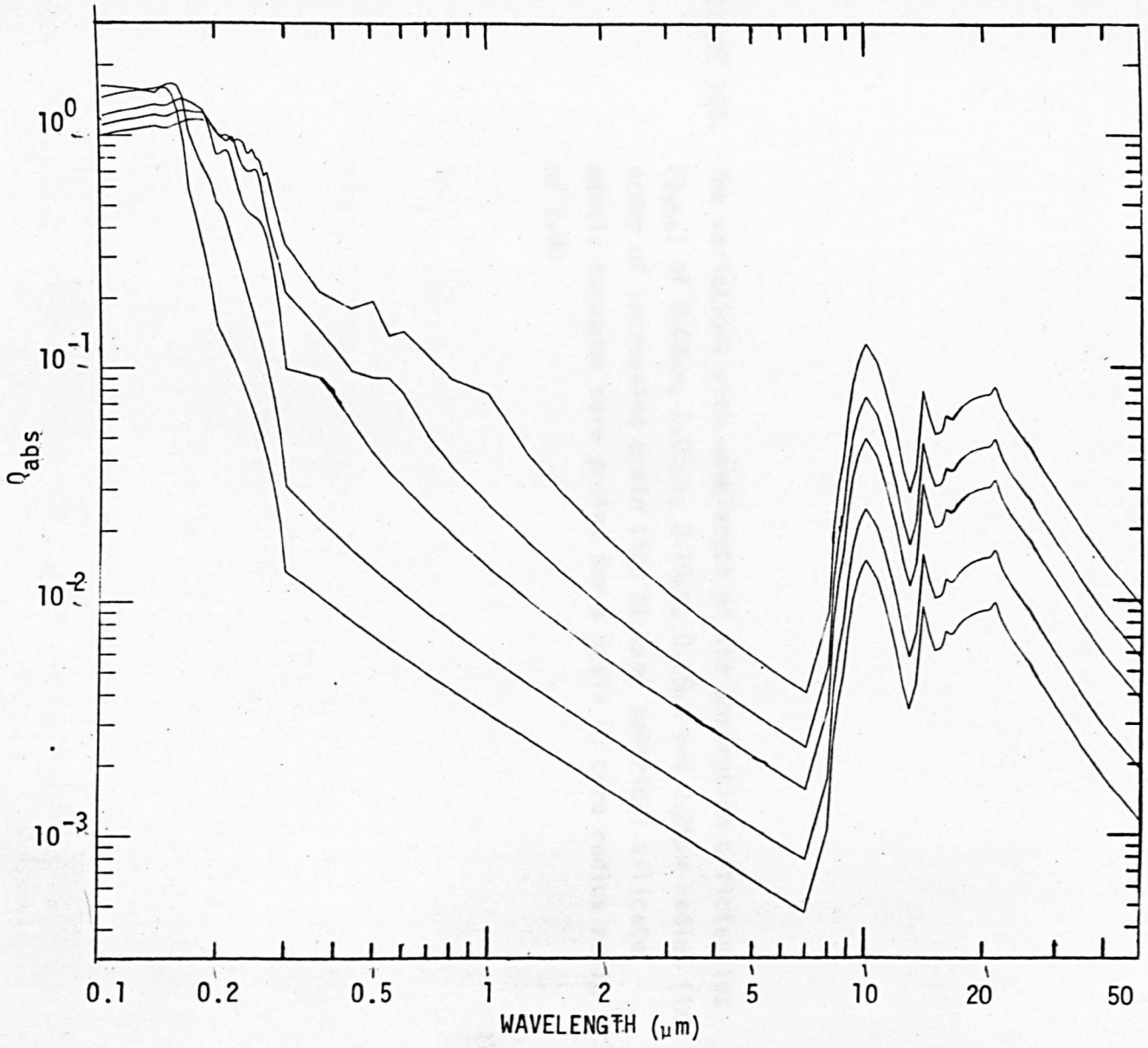
10^0
10^{-1}
10^{-2}
10^{-3}
Q_{abs}
0.1
0.2
0.5
1
2
5
10
20
50
WAVELENGTH (μm)

FIGURE 121. The variations with wavelength of the absorption efficiencies (Q_{abs}) of 0.03μm, 0.05μm, 0.10μm, 0.15μm and 0.25μm radius (in order of increasing grain size at 1μm) spherical silicate mantle corundum core grains for a grain to core radius ratio of 2.00

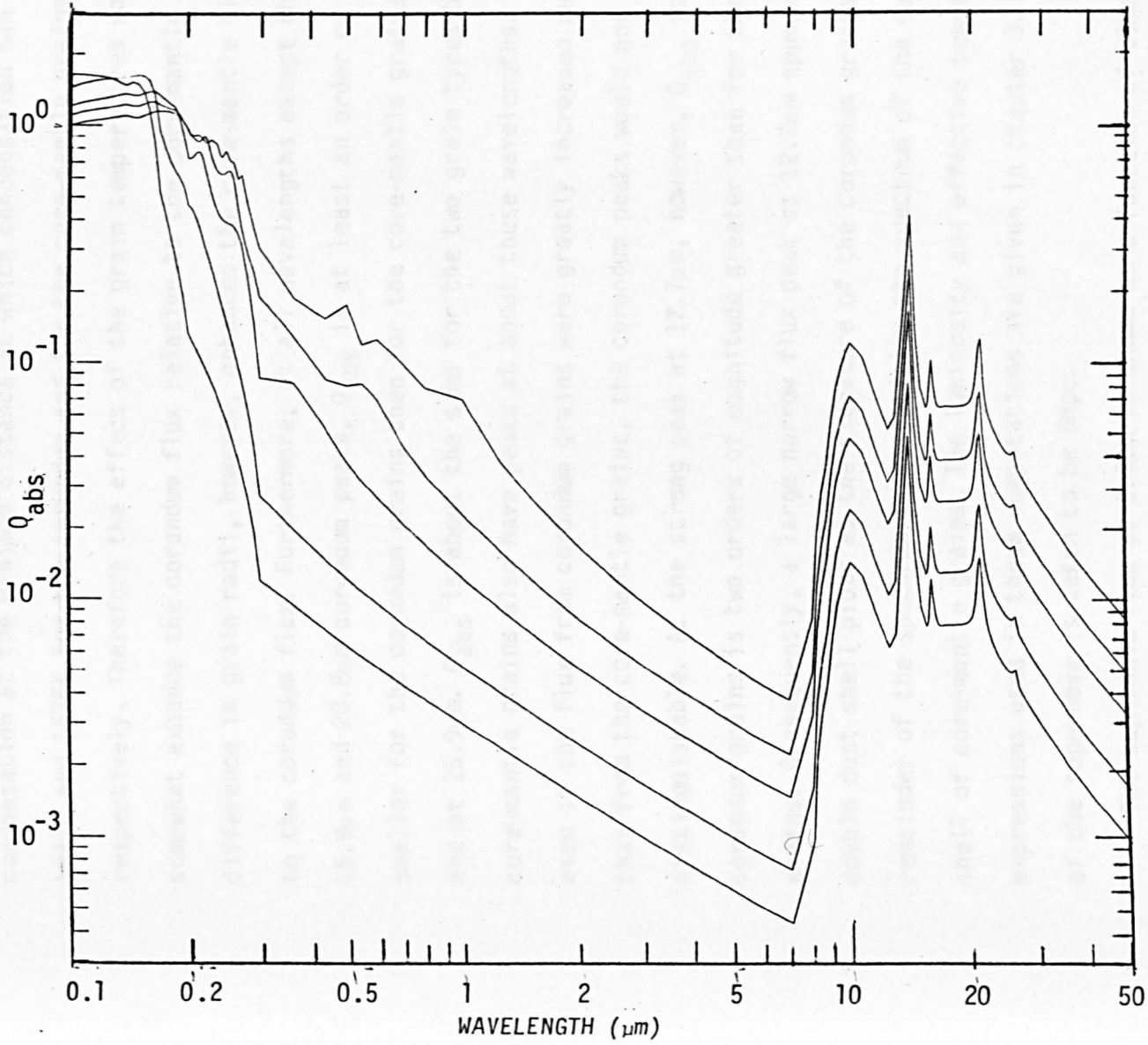
10^0
10^{-1}
10^{-2}
10^{-3}
Q_{abs}
0.1
0.2
0.5
1
2
5
10
20
50
WAVELENGTH (μm)

grains.

As the grain number density distribution in the composite dust shell is described by $\beta = 2$, the number of corundum grains is about 50% greater than the number of core-mantle grains. The grain temperatures at condensation at the minimum distance at which condensation can occur are 1941K and 1676K for the corundum and for the core-mantle grains respectively. Therefore the effect of the grain temperatures would be to somewhat exhance the corundum flux relative to the core-mantle flux. The difference in grain radii, however, enhances the core-mantle flux relative to the corundum flux. Furthermore, at all wavelengths except the 12.7μm, 15.9μm and 20.8μm corundum peaks, Q_{abs} is at least an order of magnitude smaller for the corundum grains than for the core-mantle grains. At 20.8μm and at 15.9μm. Q_{abs} is about the same for the two grain types but the core-mantle grains also have peaks at about these wavelengths. Therefore, even if the flux from corundum grains were greatly increased relative to that from the core-mantle grains, the corundum peaks would not be distinguishable. At the strong peak at 12.7μm, however, Q_{abs} for the corundum grains is two orders of magnitude greater than for the core-mantle grains. Consequently, a large narrow flux peak at 12.7μm appears in all the double dust shell plots as the signature of the corundum grains. The remainder of the spectrum is essentially the spectrum of the outer dust shell of core-mantle grains. The luminosity and effective temperature expressions used in these computations are given in chapter 3. The distance of the supernova is taken to be 5Mpc.

The supernova flux at 3.4μm is shown as a function of time for the first 750 days after outburst in figure 122. The flux rises to reach a maximum at about 30 days after outburst because of the decline in the supernova effective temperature from 25000K to 6000K. After this time the supernova effective temperature remains constant so the flux follows the variation of the supernova luminosity and declines exponentially with an

FIGURE 122. The supernova light curve at 3.4μm.

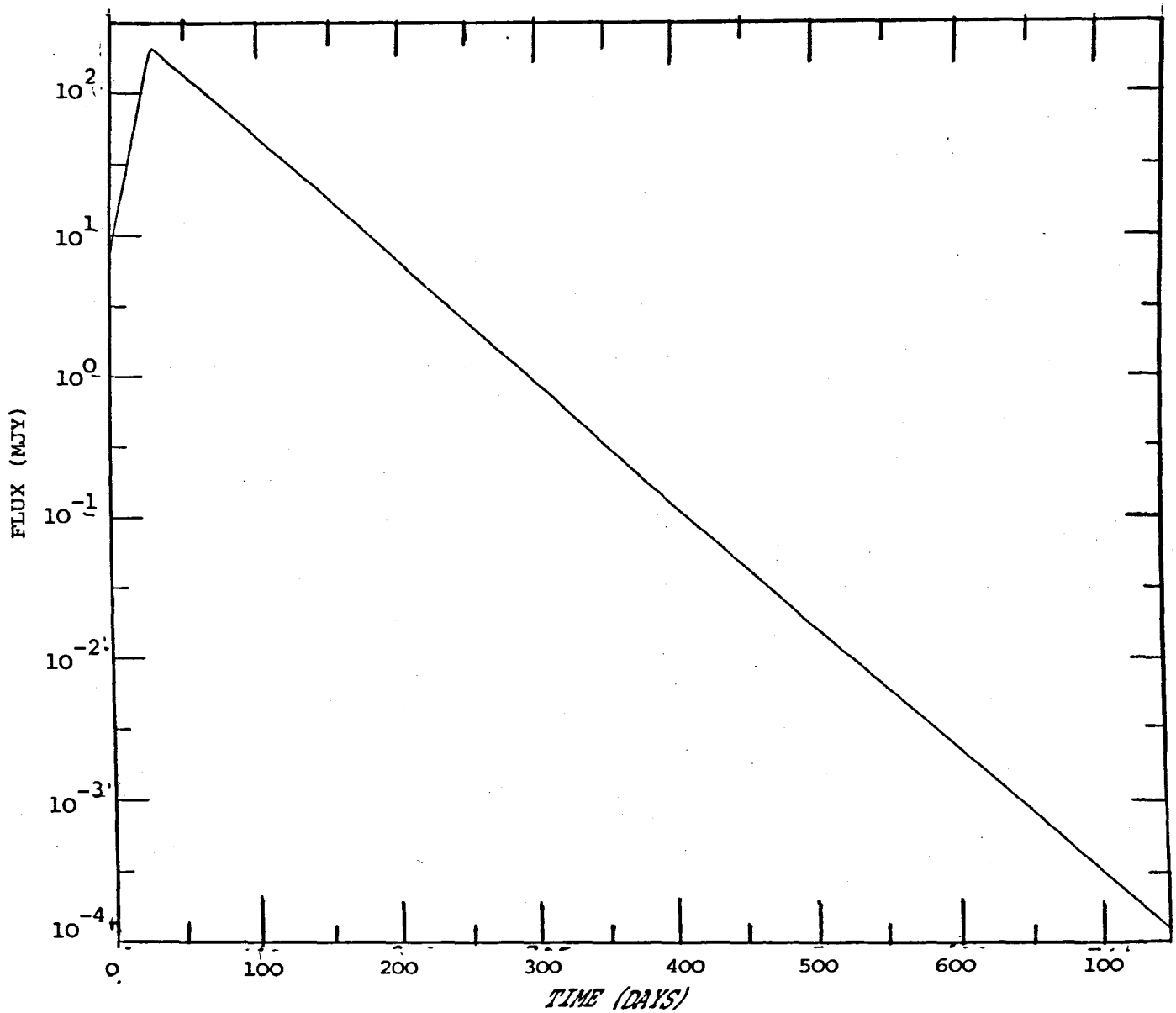
FLUX (MJY)
10^{2}
10^{1}
10^{0}
10^{-1}
10^{-2}
10^{-3}
10^{-4}
0
100
200
300
400
500
600
100
TIME (DAYS)

e-folding time of 50 days. The dust and total spectrum of the supernova and the double dust shell are shown at 200 days, 360 days, 500 days and 720 days after outburst in figures 123, 124, 125 and 126 respectively. In all four spectra the corundum peak is clearly visible, though the flux at all wavelengths at 720 days after outburst is too small to be observable. This peak, centred on 12.7μm is about 0.2μm wide at its base and has peak flux 76mJy, 11mJy, 0.6mJy and 0.6mJy at 200 days, 360 days, 500 days and 720 days respectively after outburst. The other features in the spectra are due to the core-mantle grains. The 10μm peak dominates the spectrum at 200 days and at 360 days after outburst with fluxes of 60mJy and 5.5mJy respectively. With a flux of 0.14mJy it is the smallest peak in the spectrum at 500 days after outburst and has completely vanished at 720 days after outburst. The 14μm peak has fluxes 26mJy, 3.8mJy, and 0.25mJy at 200 days, 360 days and 500 days respectively after outburst. It is smaller than the 10μm peak at the first two times but larger at 500 days. At 720 days after outburst, it too has disappeared. The 21μm core-mantle peak is barely distinguisable from the continuum at 200 and 360 days after outburst, but forms a very prominent peak at 500 days after outburst with a flux of 0.41mJy. This is compared with 14mJy and 2.8mJy, at 200 and 360 days, respectively after outburst. At 720 days after outburst, the peak flux is about 7μJy at about 30μm and this is due to the variation with wavelength of the Planck function at the temperature of the core-mantle grains rather than the wavelength dependence of Q_{abs}.

It has been assumed for the formation of this composite dust shell that the supernova ejecta from which the double dust shell condenses is ejected from the supernova over a period of order of hundreds of days, so that it stretches almost continually outwards from the centre of the supernova eruption at the time at which the double dust shell condenses. It is therefore considered possible that the outer radius R_1 and mass of the double dust shell may increase while the inner radii R_c and R_0 and the

FIGURE 123. The infra-red flux distribution from the composite dust shell at 200 days after outburst. Upper line shows total flux (dust flux + supernova flux); lower line shows dust flux only.

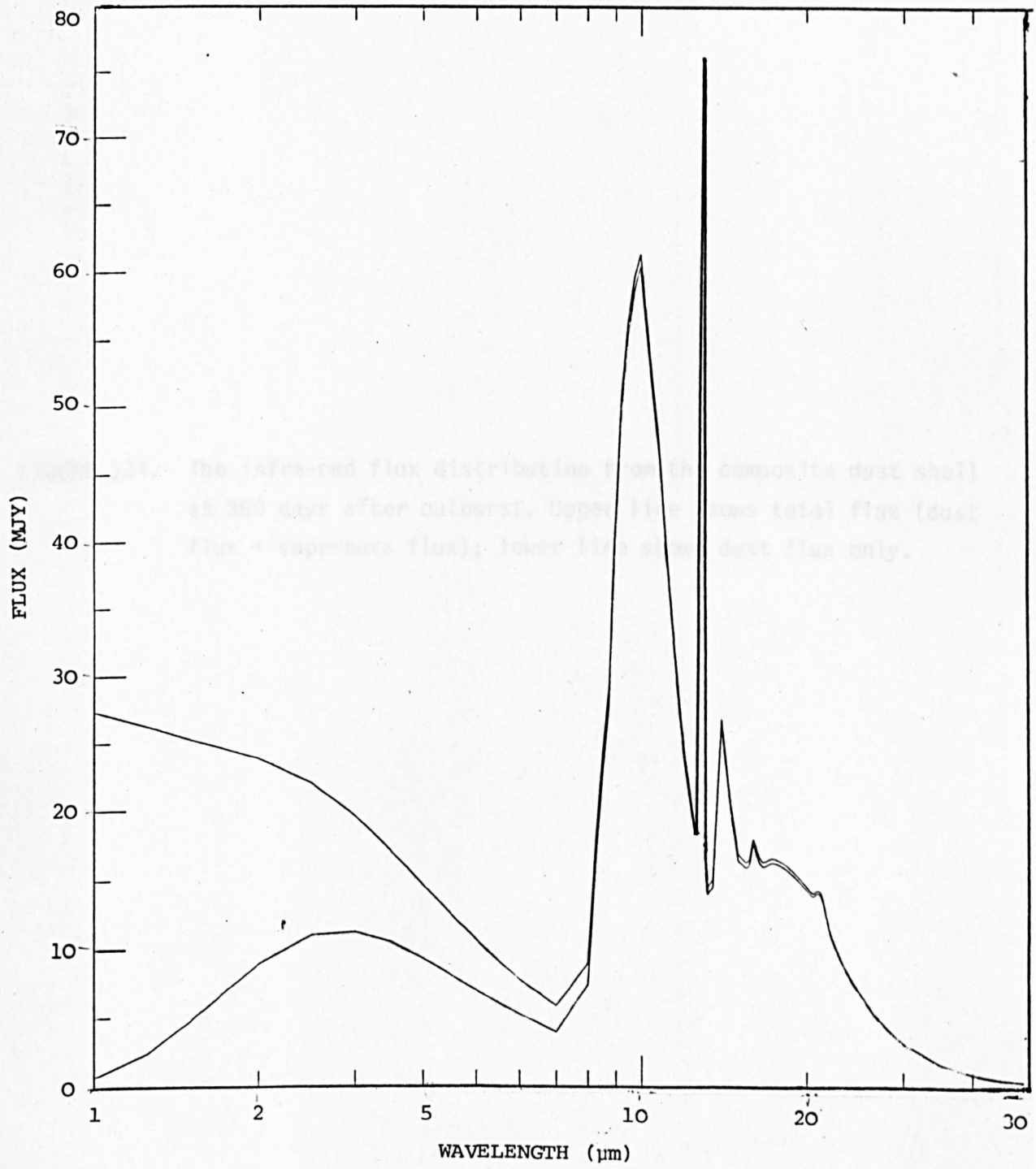
80
70
60
50
40
30
20
10
0
FLUX (MJY)
1
2
5
10
20
30
WAVELENGTH (μm)

FIGURE 124. The infra-red flux distribution from the composite dust shell at 360 days after outburst. Upper line shows total flux (dust flux + supernova flux); lower line shows dust flux only.

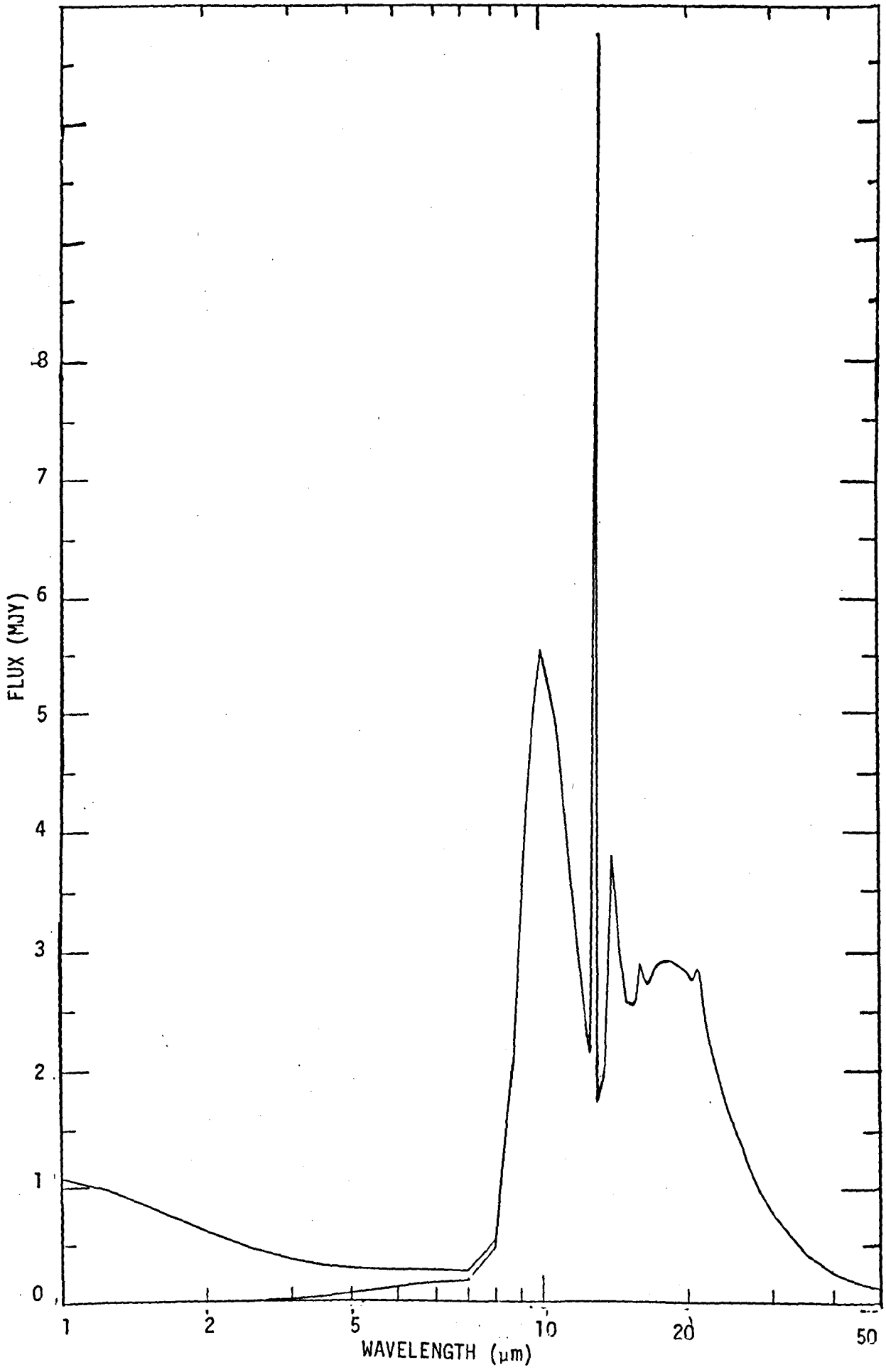
FLUX (MJY)
0
1
2
3
4
5
6
7
8
1
2
5
10
20
50
WAVELENGTH (μm)

FIGURE 125. The infra-red flux distribution from the composite dust shell at 500 days after outburst. Upper line shows total flux (dust flux + supernova flux); lower line shows dust flux only.

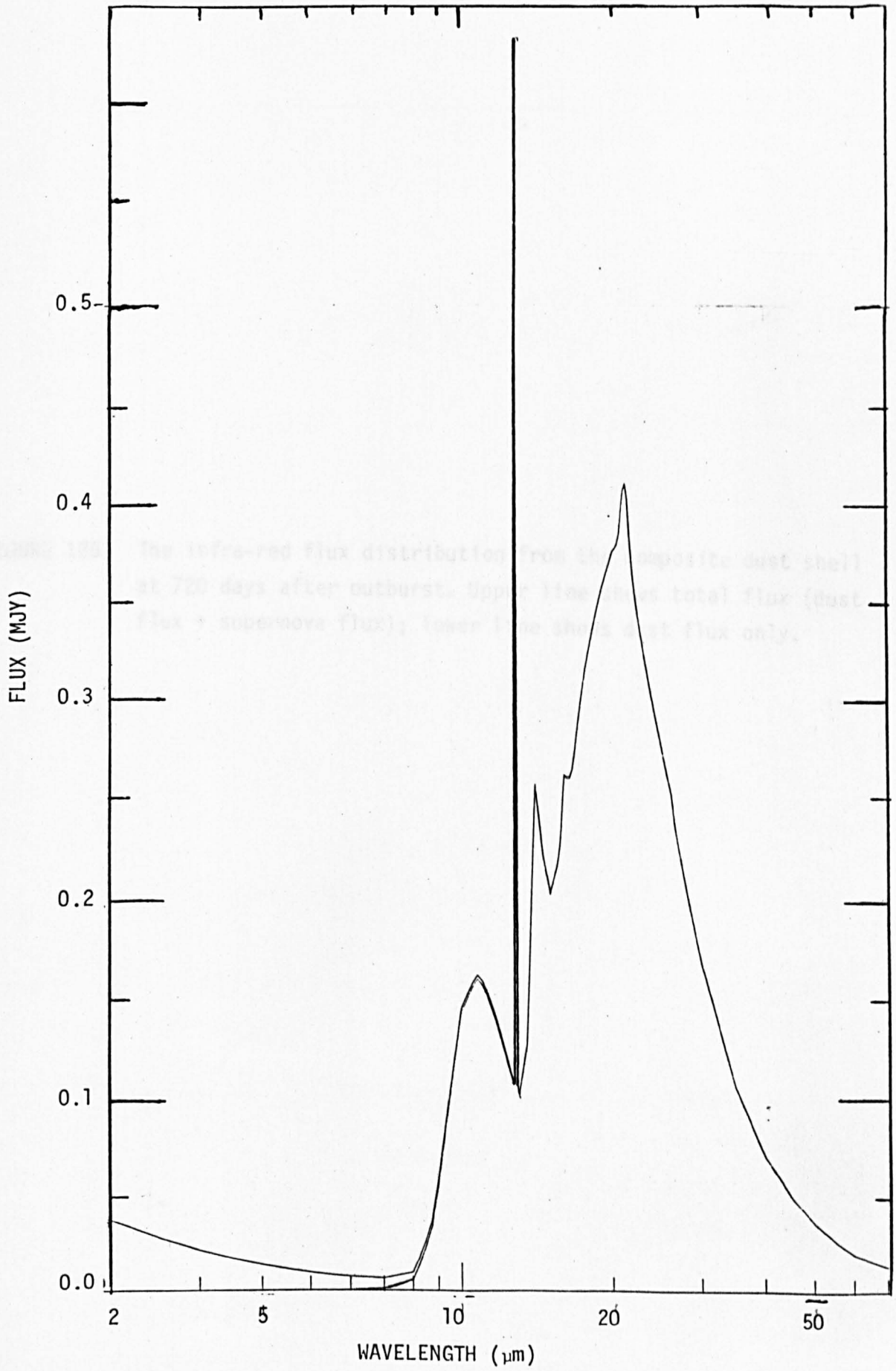
0.5
0.4
0.3
0.2
0.1
0.0
FLUX (MJY)
2
5
10
20
50
WAVELENGTH (μm)

FIGURE 126. The infra-red flux distribution from the composite dust shell at 720 days after outburst. Upper line shows total flux (dust flux + supernova flux); lower line shows dust flux only.

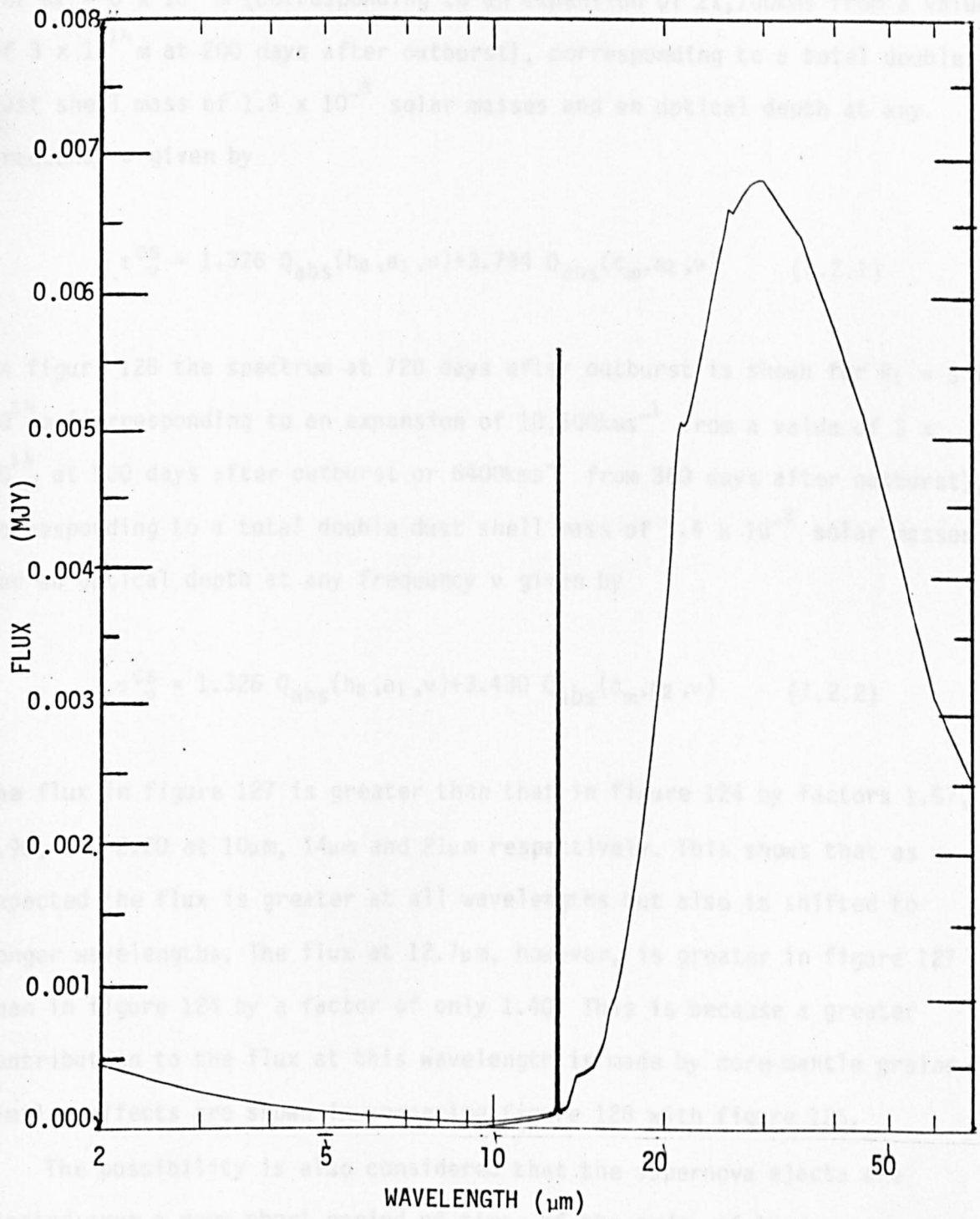
0.008
0.007
0.006
0.005
0.004
0.003
0.002
0.001
0.000
FLUX (MJY)
2
5
10
20
50
WAVELENGTH (μm)

grain number density at any particular distance from the supernova remain unchanged. In figure 127, the spectrum at 360 days after outburst is shown for $R_1 = 6 \times 10^{14}$m (corresponding to an expansion of 21,700kms from a value of 3×10^{14}m at 200 days after outburst), corresponding to a total double dust shell mass of 1.9×10^{-3} solar masses and an optical depth at any frequency ν given by

$$\tau_\nu^{cs} = 1.326\ Q_{abs}(h_0, a_1, \nu) + 3.794\ Q_{abs}(c_m, a_2, \nu) \qquad (7.2.1)$$

In figure 128 the spectrum at 720 days after outburst is shown for $R_1 = 5 \times 10^{14}$m (corresponding to an expansion of 10,500kms^{-1} from a value of 3×10^{14}m at 500 days after outburst or 6400kms^{-1} from 360 days after outburst), corresponding to a total double dust shell mass of 1.4×10^{-3} solar masses and an optical depth at any frequency ν given by

$$\tau_\nu^{cs} = 1.326\ Q_{abs}(h_0, a_1, \nu) + 3.430\ Q_{abs}(c_m, a_2, \nu) \qquad (7.2.2)$$

The flux in figure 127 is greater than that in figure 124 by factors 1.57, 1.90, and 2.20 at 10μm, 14μm and 21μm respectively. This shows that as expected the flux is greater at all wavelengths but also is shifted to longer wavelengths. The flux at 12.7μm, however, is greater in figure 127 than in figure 124 by a factor of only 1.40. This is because a greater contribution to the flux at this wavelength is made by core-mantle grains. Similar effects are shown in comparing figure 128 with figure 126.

The possibility is also considered that the supernova ejecta are ejected over a very short period of time, of the order of 10 days, so that a thin expanding dust shell is produced. Taking the expansion velocity to be 10^4kms^{-1} and the dust shell thickness to be the distance covered in 10 days of moving at this velocity (8.64×10^{12}m), this dust shell has inner and outer radii 1.296×10^{14}m and 1.3824×10^{14}m respectively at 160 days

FIGURE 127. The infra-red spectrum of the expanding composite dust shell at 360 days after outburst. (Dust flux only).

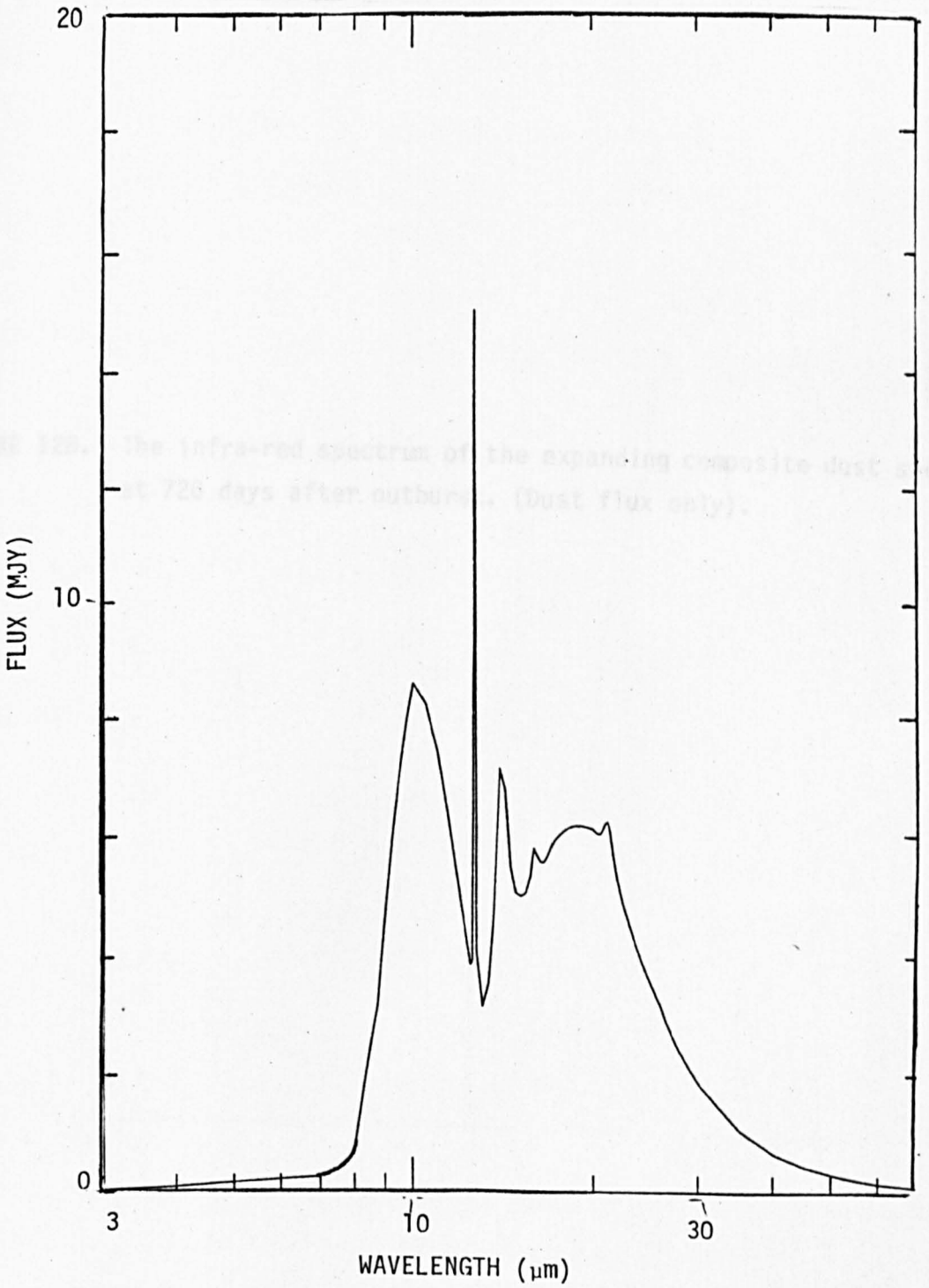
20
10
0
FLUX (MJY)
3
10
30
WAVELENGTH (μm)

FIGURE 128. The infra-red spectrum of the expanding composite dust shell at 720 days after outburst. (Dust flux only).

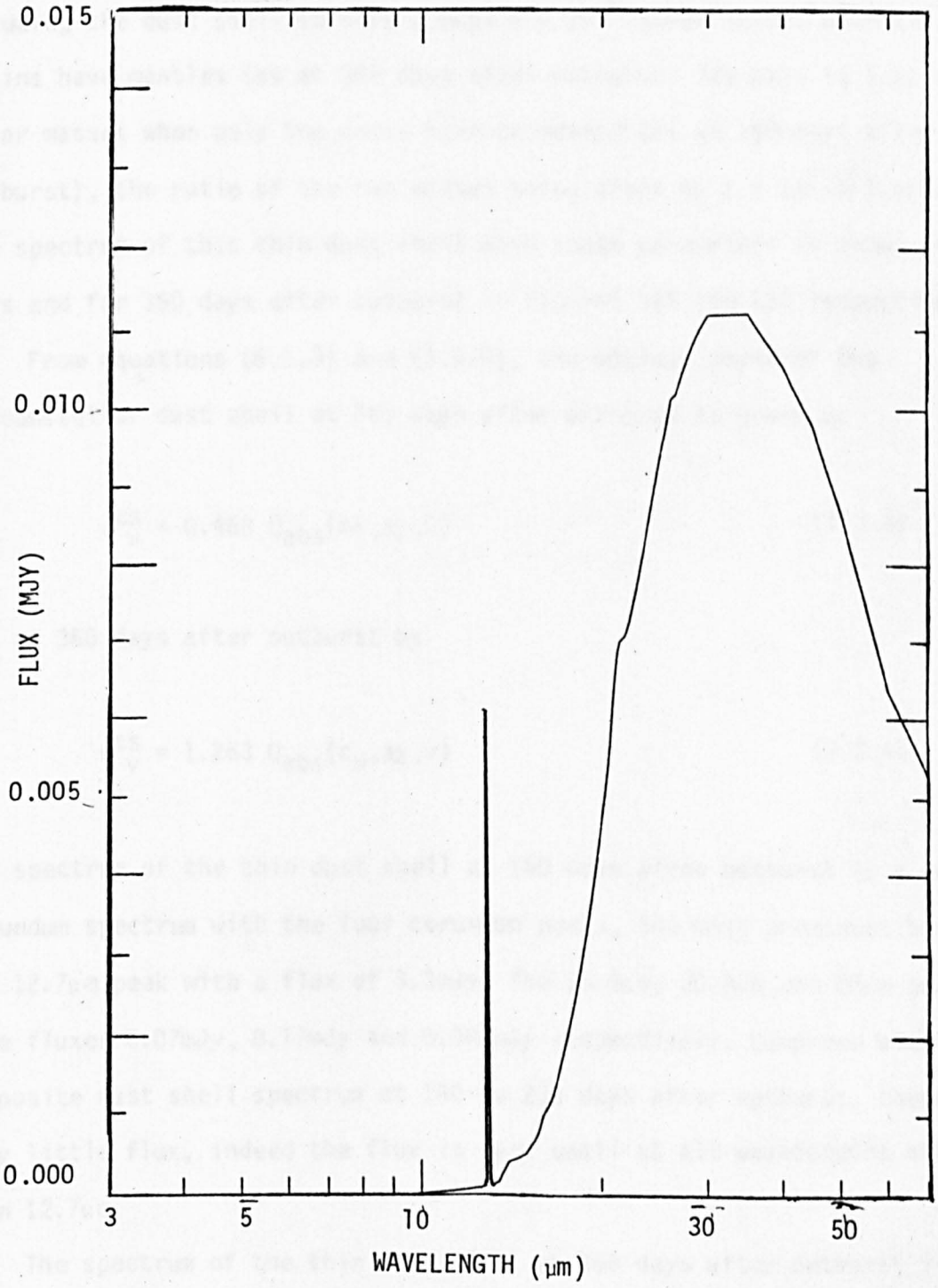
0.015
0.010
0.005
0.000
FLUX (MJY)
3
5
10
30
50
WAVELENGTH (μm)

after outburst and 3.024×10^{14}m and 3.1104×10^{14}m respectively at 360 days after outburst. At the earlier time, only the corundum cores will have condensed whereas at the later time, the mantles will also have condensed. Assuming the dust shell to have a mass 5×10^{-4} solar masses when all the grains have mantles (as at 360 days after outburst) its mass is 1.11×10^{-5} solar masses when only the cores have condensed (as at 160 days after outburst), the ratio of the two masses being given by $1 + (a_2^3 - a_1^3)\, s_2 / a_1^3 s_1$. The spectrum of this thin dust shell with these parameters is shown for 160 days and for 360 days after outburst in figures 129 and 130 respectively.

From equations (6.1.3) and (3.5.6), the optical depth of the circumstellar dust shell at 160 days after outburst is given by

$$\tau_\nu^{cs} = 0.468\, Q_{abs}(h_0, a_1, \nu) \qquad (7.2.3)$$

and at 360 days after outburst by

$$\tau_\nu^{cs} = 1.263\, Q_{abs}(c_m, a_2, \nu) \qquad (7.2.4)$$

The spectrum of the thin dust shell at 160 days after outburst is a pure corundum spectrum with the four corundum peaks, the most prominent being the 12.7μm peak with a flux of 3.3mJy. The 15.9μm, 20.8μm and 26μm peaks have fluxes 0.07mJy, 0.17mJy and 0.006mJy respectively. Compared with the composite dust shell spectrum at 180 to 200 days after outburst, there is very little flux, indeed the flux is very small at all wavelengths other than 12.7μm.

The spectrum of the thin dust shell at 360 days after outburst is similar to the double dust shell spectra except that there is no 12.7μm corundum peak. The flux is also greater than in the double dust spectrum at 360 days after outburst by a factor of about nine between 10μm and 20μm. The probable explanation for this is that although the thin dust shell is

FIGURE 129. The infra-red spectrum of the thin composite dust shell at 160 days after outburst. (Dust flux only).

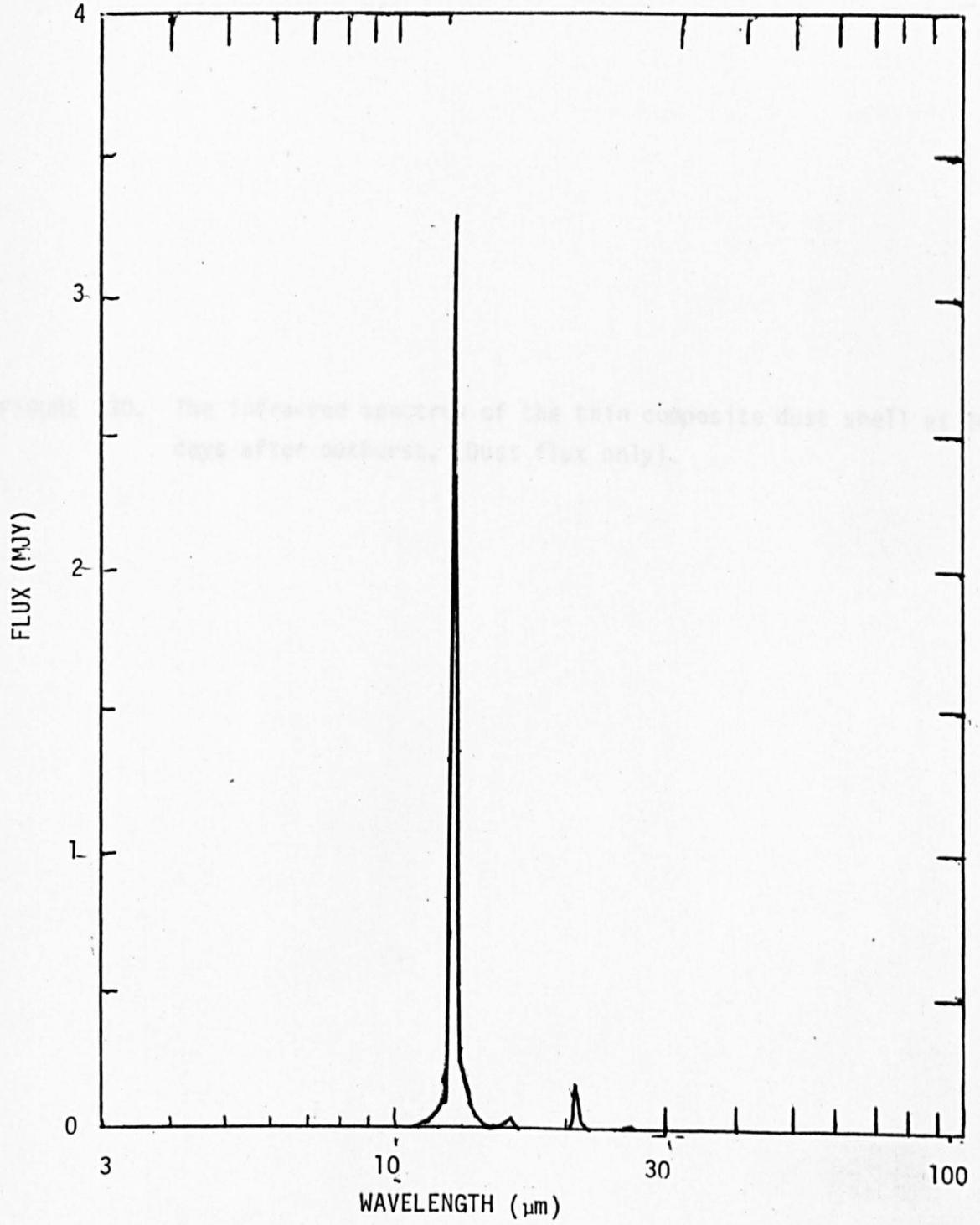
4
3
2
1
0
FLUX (MJY)
3
10
30
100
WAVELENGTH (μm)

FIGURE 130. The infra-red spectrum of the thin composite dust shell at 360 days after outburst. (Dust flux only).

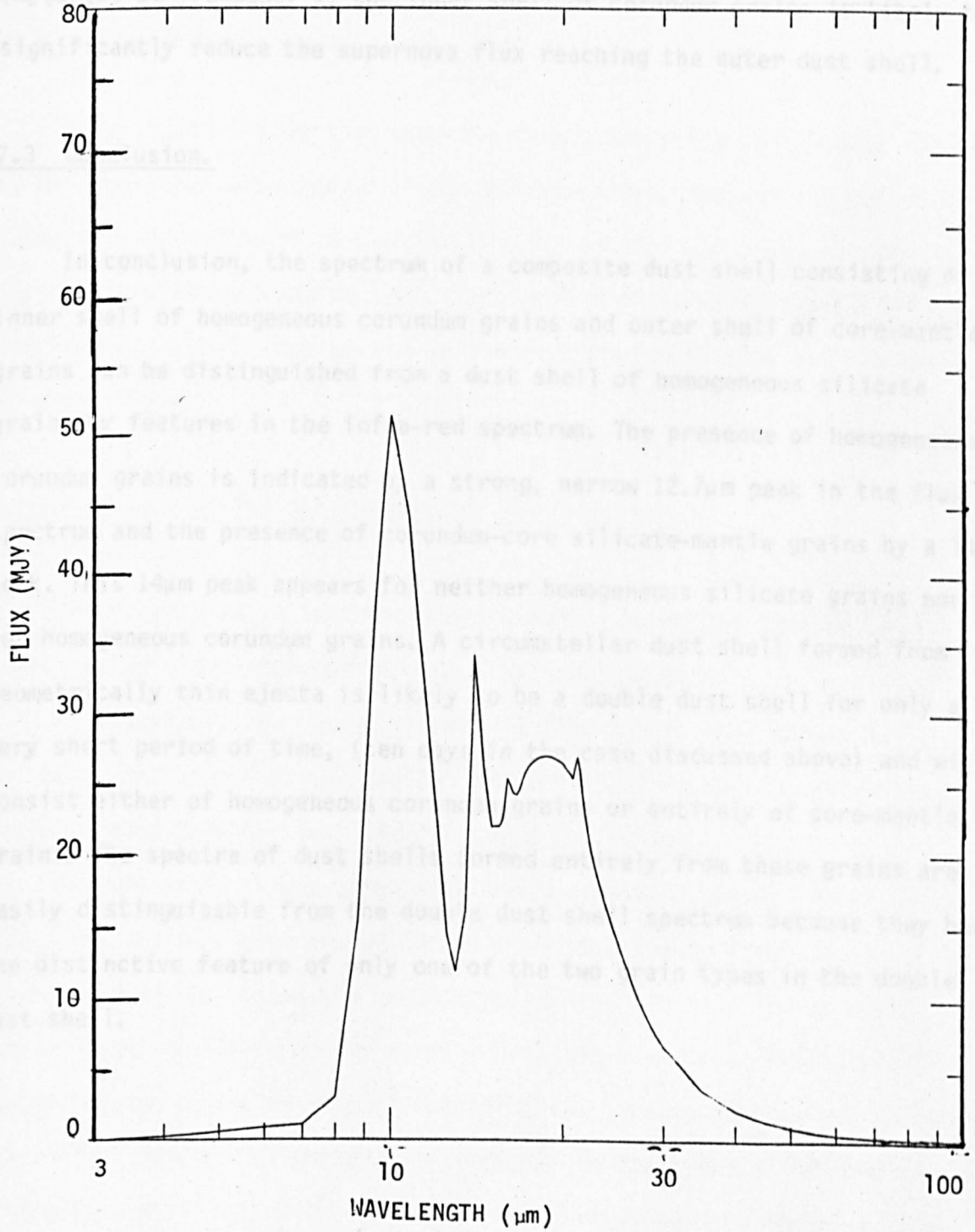
80
70
60
50
40
30
20
10
0
FLUX (MJY)
3
10
30
100
WAVELENGTH (μm)

further from the supernova, there are no corundum grains between the thin dust shell and the supernova. However, there are in the case of the outer shell of the double dust shell and with an optical depth of 1.326 Q_{abs} (h_0, a_1, ν) at frequency ν, the inner shell of corundum grains is likely to significantly reduce the supernova flux reaching the outer dust shell.

7.3 Conclusion.

In conclusion, the spectrum of a composite dust shell consisting of an inner shell of homogeneous corundum grains and outer shell of core-mantle grains can be distinguished from a dust shell of homogeneous silicate grains by features in the infra-red spectrum. The presence of homogeneous corundum grains is indicated by a strong, narrow 12.7μm peak in the flux spectrum and the presence of corundum-core silicate-mantle grains by a 14μm peak. This 14μm peak appears for neither homogeneous silicate grains nor for homogeneous corundum grains. A circumstellar dust shell formed from geometrically thin ejecta is likely to be a double dust shell for only a very short period of time, (ten days in the case discussed above) and will consist either of homogeneous corundum grains or entirely of core-mantle grains. The spectra of dust shells formed entirely from these grains are easily distinguisable from the double dust shell spectrum because they have the distinctive feature of only one of the two grain types in the double dust shell.

CHAPTER 8

SUGGESTIONS FOR FURTHER WORK

8.0 Introduction

This chapter summarizes what the thesis has achieved and describes how it has contributed to our knowledge of supernovae. Section 8.1 below summarizes the achievements of the thesis. Section 8.2 below suggests further work which could be done. Section 8.3 provides an overall conclusion for this chapter and condenses the general aims and achievements of this thesis.

8.1 A Summary Of The Achievements Of The Thesis

This thesis has attempted detailed modelling of the heating of interstellar and circumstellar grains by supernovae.

In chapter 2, the recent literature relevant to this thesis is reviewed. In chapter 3, the optical properties of various grain materials are described together with the supernova properties.

In chapter 4, it was shown that condensation of grains in the ejecta of supernovae is instantaneous in all realistic cases, which is useful in providing constraints on the parameters such as the velocity at which material can be realistically ejected from the supernova. The effect of depletion and expansion on grain condensation is also considered. Further, the evaporation of the cavity is considered in the light of the forces acting on the grains, (e.g. the force of gravitation, radiation pressure, and viscous drag are considered).

In chapter 5, the case of infra-red emission from interstellar grains composed of graphite and a composite silicate is considered. The ratio of

silicate:graphite grains in a galaxy is varied and the resulting infra-red fluxes are computed. Other parameters such as the inclination of the galaxy to the observer's line of sight, the grain number density and the depth of the supernova into the galaxian plane are also varied. Furthermore, the effect of the heating by background starlight is considered. The geometry of the problem is described in detail. The modelling shows that the infra-red flux emitted by such grains due to supernova heating can be detected at far infra-red wavelengths (~100μm) for several years (~10years) after the supernova outburst.

Chapter 6, contains a model of a circumstellar dust shell around a supernova. Modelling has been attempted for the supernovae SN1979c in NGC4321 and SN1980k in NGC6946. This modelling provides a good fit to the observational data available. A black body fit is undertaken for the U, B, V data available for SN1979c and SN1980k repectively. A dust shell composed of corundum and a composite silicate is used in the models. Such models are useful in providing constraints on parameters such as the mass of the dust shell being observed, the composition of the supernova ejecta, and the grain temperature. The geometry of the problem is also detailed in this chapter.

In chapter 7, the case of a double circumstellar dust shell is modelled. The effect of material condensing out at different temperatures and thereby forming a composite dust shell is considered. The cases of a geometrically thick and a thin dust shell are each considered in turn. Such modelling provides useful constraints on the time over which material is ejected from the supernova. The case of an expanding outer shell is also considered. There are quite striking differences between the composite dust shell case and the single circumstellar dust shell case, and the potential uses of this and the modelling undertaken are discussed below in section 8.2.

8.2 Suggested Further Work

In chapter 5 the case of infra-red emission from interstellar grains heated by a supernova was considered. The grain materials were graphite and a composite silicate. It would be interesting to compute the fluxes for silicates of different compositions (so-called dirty silicates) and for graphites with differing impurity contents. It would also be interesting to model infra-red fluxes assuming non-spherical grains, as this is likely to be the case in practice. It has also been assumed that the galaxy being modelled was a uniform infinite plane parallel slab. The effect of a more realistic grain density distribution, and grain radius distribution would also provide interesting further work.

With the advent of the Shuttle Infra-Red Telescope Facility (S.I.R.T.F), it should be possible to obtain data on supernovae at far infra-red wavelengths (~100μm). The present Infra-Red Astronomical Satellite (I.R.A.S) does not have the resolution or sensitivity to obtain such infra-red data. Provided that observations are conducted away from the Galactic plane, the effects of contamination from interstellar dust in our Galaxy should be negligible. Since many supernovae have occurred during the past two to three years, and the model discussed in chapter 5 indicates that far infra-red emission from interstellar dust heated by extragalactic supernovae should be detectable for about 10 years after outburst, there are several such objects which could be observed with S.I.R.T.F. The model discussed in chapter 5 can also be used to determine the depth of a supernova in its parent galaxy. It would be useful therefore to obtain such data to study the positions of supernovae in galaxies. This could reveal information regarding extinction in the parent galaxy.

Chapter 6 deals with modelling a single circumstellar dust shell for the supernovae SN1979c in NGC4321 and SN1980k in NGC6946, using silicate and corundum. It would be interesting to repeat the data fitting procedure

using grains having a different composition and optical properties, and using different grain distributions across the dust shell. It is concluded in chapter 6 that further observations at near infra-red (~1μm to 10μm) wavelengths are needed. More observations are needed in particular of type I supernovae, in order to determine if type I supernovae like type II supernovae have circumstellar dust shells. Such work may also reveal further information about the events leading up to the explosion mechanism of these different supernovae.

It would be useful to have more observational data on such supernovae. Both infra-red data and U, B, V data are desirable, in order that better fits could be obtained. Almost continual observational coverage of supernovae events is required.

In chapter 7, the case of a composite dust shell with fixed inner radii (R_c and R_o) and an expanding outer radius R_1, was considered together with the case of a pre-existing composite dust shell.

It would be useful to attempt to determine observationally if the material in such circumstellar dust shells around supernovae is pre-existing or condensed or whether this varies from supernova to supernova. If a circumstellar shell condensed, a sudden rise in the near infra-red flux would occur at the condensation time, since it has been shown in chapter 4 that condensation is essentially instantaneous for all realistic cases. If the circumstellar shell were pre-existing around the progenitor a gradual rise in the infra-red excess would result from the time of outburst. At present the instrumentation available is not sensitive enough to detect this gradual rise in its early stages. The two different mechanisms cannot therefore presently be distinguished.

In considering the case of the condensing double dust shell it is not known if R_o and R_c will change with time. In chapter 7 for this case it was assumed that the rate at which material condensed at the inner edge of the cavity of radius R_c was equal to the rate at which the material condensed

at the inner edge of the shell of radius R_o. Whilst the cavity radius may contract with time due to the decreasing luminosity of the supernova, the cavity radius could equally well still be expanding if material is still being ejected from the supernova. The behaviour of the cavity radius at relatively late times (t~100 days) is therefore likely to be quite complex. It would however be useful to undertake a detailed study of this phenomenon, thereby obtaining expressions for the behaviour of the inner radii R_o and R_c. Infra-red fluxes could then be recomputed using these expressions to determine what effect the behaviour of R_o and R_c as a function of time has on the computed fluxes.

It would also be useful to obtain observational results regarding the period of time over which material may be ejected from the supernova. Very little seems to be known about this at present. The period of time over which material is ejected from the supernova may not only influence the cavity radius R_c (and perhaps the inner dust shell radius R_0), but it will also determine the geometrical extent of the dust shell.

Observations of condensed double dust shells around supernovae when compared to computed spectra would provide information about the rate at which material is ejected from the supernova. A short ejection time would provide a homogeneous shell. However a long ejection time would tend to provide a multi-layered dust shell. It would also be interesting to model a multi-layered dust shell for several different materials.

The double dust shell model discussed in chapter 7 indicated that different infra-red spectral features would be observable compared to those for a single dust shell for the materials discussed. Such modelling is useful when compared with observations in indicating whether the dust shell around a supernova is a single layered dust shell or a multi-layered dust shell. Although the instrumentation available to-date does not have the sensitivity to indicate this, it is thought that future instrumentation would enable this to be done. Such observations would need to be undertaken

using instrumentation situated above the atmosphere, because of absorption of radiation around the 16μm wavelength feature by the Earth's atmosphere. In fact, in general this type of work requires instrumentation with improved resolution. It would help to have such instruments available in the near future.

The planned fully automated Berkeley University supernova search (Kare et al 1982) would be of particular use in continually scanning galaxies each night and discovering supernovae almost at outburst. The present hap-hazard system of discovering supernovae has certain drawbacks. Firstly, very often the fainter supernovae are discovered in retrospect by accident, whilst plates are being scanned for other purposes. Secondly, even if a supernova is discovered and reported, the means of reporting such events often means that it is days before the discovery is generally known. This means that data immediately at the supernova outburst cannot be collected. Therefore, little or no data are available at or just after a supernova outburst. The Berkeley group supernova search should also mean that more supernovae are discovered with its continual scanning of galaxies. The discovery rate varies at the moment from 1 to 8 supernovae per year. The expected rate with the automated Berkeley search will be 1 to 2 supernovae per week (Kare et al. 1982).

Further work needs to be done to specifically determine the progenitors of type I supernovae. The nature of the progenitor could provide information regarding whether type I supernovae also have circumstellar dust.

8.3 Conclusion

This thesis set out to attempt to model the infra-red flux emitted from interstellar and circumstellar grains heated by supernovae. Previous to this study, very little work had been done on the infra-red astronomy of

supernovae and thus very little data were available. However, the data which were available have been fitted into the circumstellar dust shell model which provided a good fit to these data.

It is concluded that a great deal of information can be obtained about supernovae and their progenitors from a study of the infra-red emission arising from the heating of grains by supernovae.

APPENDIX I

MAGNITUDE WAVEBANDS

TABLE A1

$A\lambda/Av$	MAGNITUDE	WAVELENGTH λ (μm)	$\Delta\lambda$ (μm)	$\log_{10} f_\nu(m=0)$
1.58	U	0.365	0.068	-22.73
1.32	B	0.440	0.098	-22.37
1.00	V	0.550	0.089	-22.42
0.69	R	0.700	0.220	-22.55
0.46	I	0.900	0.240	-22.65
0.29	J	1.250	0.380	-22.77
0.19	H	1.600		-22.97
0.10	K	2.200	0.480	-23.20
0.05	L	3.400	0.700	-23.51
0.00	M	5.000		-23.74

In the above table, λ is the central wavelength and $\Delta\lambda$ the bandwidth of the magnitude waveband, and $f_\nu(m=0)$ is the zero magnitude flux in $Wm^{-2}\ Hz^{-1}$. The information on H was derived from Wamsteker (1981) and the remainder from Allen (1973).

The parameter A_λ is the interstellar extinction at wavelength λ, and A_ν is the interstellar extinction in the visual waveband. The interstellar extinction at M is taken to be zero because it is very small.

APPENDIX II

This appendix gives a detailed solution to equations (7.1.9) and (7.1.10) in chapter 7.

Substituting equations (6.2.9) (6.2.10) (6.2.11) (6.2.12) (7.1.11) (7.1.12) into equation (7.1.9) and (7.1.10) yields the sets of equations (II.1) and (II.2) respectively.

$$\phi_{1\beta}(\rho,\psi) = 0 \quad \text{for } \rho \geq R_o \text{ or } \rho < R_o \text{ and } \psi \leq \tan^{-1}(\rho/(R_o^2-\rho^2)^{\frac{1}{2}})$$

$$= -2(R_o^2-\rho^2)^{\frac{1}{2}}/\rho \qquad \text{for } \beta=0$$

$$= 2\ln(\tan\tfrac{1}{2}(\tan^{-1}(\rho/(R_o^2-\rho^2)^{\frac{1}{2}}))) \qquad \text{for } \beta=1$$

$$= 2\tan^{-1}(\rho/(R_o^2-\rho^2)^{\frac{1}{2}}) - \pi \qquad \text{for } \beta=2$$

$$\text{for } R_c \leq \rho \leq R_o \text{ and } \psi \geq \pi - \tan^{-1}(\rho/(R_o^2-\rho^2)^{\frac{1}{2}})$$

$$\phi_{1\beta}(\rho,\psi) = \cot\psi - (R_o^2-\rho^2)^{\frac{1}{2}}/\rho \qquad \text{for } \beta=0$$

$$= \ln(\tan\tfrac{1}{2}(\tan^{-1}(\rho/R_o^2-\rho^2)^{\frac{1}{2}}))\cot\tfrac{1}{2}\psi) \qquad \text{for } \beta=1$$

$$= \tan^{-1}(\rho/(R_o^2-\rho^2)^{\frac{1}{2}}) - \psi \qquad \text{for } \beta=2$$

$$\text{for } R_c \leq \rho < R_o \text{ and } \pi - \tan^{-1}(\rho/(R_\rho^2-\rho^2)^{\frac{1}{2}}) \geq \psi > \tan^{-1}(\rho(R_o^2-\rho^2)^{\frac{1}{2}}) \quad \rho < R_c$$

$$\text{where } \tan^{-1}(\rho/(R_c^2-\rho^2)^{\frac{1}{2}}) \geq \psi > \tan^{-1}(\rho/(R_o^2-\rho^2)^{\frac{1}{2}})$$

$$\phi_{1\beta}(\rho,\psi) = \cot\psi - (R_o^2-\rho^2)^{\frac{1}{2}}/\rho + 2(R_c^2-\rho^2)^{\frac{1}{2}}/\rho \qquad \text{for } \beta=0$$

$$= \ln(\tan\tfrac{1}{2}(\tan^{-1}(\rho/(R_o^2-\rho^2)^{\frac{1}{2}}))\cot\tfrac{1}{2}\psi\cot^2\tfrac{1}{2}(\tan^{-1}(\rho/(R_c^2-\rho^2)^{\frac{1}{2}}))) \qquad \text{for } \beta=1$$

$$= \tan^{-1}(\rho/(R_o^2-\rho^2)^{\frac{1}{2}}) - \psi + \pi - 2\tan^{-1}(\rho/(R_c^2-\rho^2)^{\frac{1}{2}}) \qquad \text{for } \beta=2$$

$$\text{for } \rho < R_c \quad \pi - \tan^{-1}(\rho/(R_o^2-\rho^2)^{\frac{1}{2}}) \geq \psi \geq \pi - \tan^{-1}(\rho/(R_c^2-\rho^2)^{\frac{1}{2}})$$

$$\phi_{1\beta}(\rho,\psi) = 2((R_c^2-\rho^2)^{\frac{1}{2}}/\rho-(R_o^2-\rho^2)^{\frac{1}{2}}/\rho) \qquad \text{for } \beta=0$$

$$= 2\ln(\tan\tfrac{1}{2}(\tan^{-1}(\rho/(R_o^2-\rho^2)^{\frac{1}{2}}))\cot\tfrac{1}{2}(\tan^{-1}(\rho/(R_c^2-\rho^2)^{\frac{1}{2}}))) \qquad \text{for } \beta=1$$

$$= 2(\tan^{-1}((R_o^2-\rho^2)^{\frac{1}{2}}/\rho)-\tan^{-1}((R_c^2-\rho^2)^{\frac{1}{2}}/\rho)) \qquad \text{for } \beta=2$$

for $\rho<R_c$ $\quad \pi-\tan^{-1}(\rho/(R_1^2-\rho^2)^{\frac{1}{2}}) \geq \psi > \pi-\tan^{-1}(\rho/(R_o^2-\rho^2)^{\frac{1}{2}})$

(II.1)

$$\phi_{2\beta}(\rho,\psi) = \cot\psi-(R_1^2-\rho^2)^{\frac{1}{2}}/\rho \qquad \text{for } \beta=0$$

$$=\ln(\tan\tfrac{1}{2}(\tan^{-1}(\rho/(R_1^2-\rho^2)^{\frac{1}{2}})\ \cot\tfrac{1}{2}\psi) \qquad \text{for } \beta=1$$

$$= \tan^{-1}(\rho/(R_1^2-\rho^2)^{\frac{1}{2}})-\psi \qquad \text{for } \beta=2$$

for $\rho \geq R_o$ or $\rho<R_o$ $\quad \psi \leq \tan^{-1}(\rho/(R_o^2-\rho^2)^{\frac{1}{2}})$

$$\phi_{2\beta}(\rho,\psi) = \cot\psi-(R_1^2-\rho^2)^{\frac{1}{2}}/\rho+2(R_o^2-\rho^2)^{\frac{1}{2}}/\rho \qquad \text{for } \beta=0$$

$$= \ln(\tan\tfrac{1}{2}(\tan^{-1}(\rho/(R_1^2-\rho^2)^{\frac{1}{2}}))\cot\tfrac{1}{2}\psi\cot^2\tfrac{1}{2}(\tan^{-1}(\rho/(R_o^2-\rho^2)^{\frac{1}{2}}))) \qquad \text{for } \beta=1$$

$$= \tan^{-1}(\rho/R_1^2-\rho^2)^{\frac{1}{2}})-\psi+\pi-2\tan^{-1}(\rho/(R_o^2-\rho^2)^{\frac{1}{2}}) \qquad \text{for } \beta=2$$

for $\quad \rho<R_o \quad \psi>\pi-\tan^{-1}(\rho/(R_o^2-\rho^2)^{\frac{1}{2}})$

$$\phi_{2\beta}(\rho,\psi) = (R_o^2-\rho^2)^{\frac{1}{2}}/\rho-(R_1^2-\rho^2)^{\frac{1}{2}}/\rho \qquad \text{for } \beta=0$$

$$= \ln(\tan\tfrac{1}{2}(\rho/(R_1^2-\rho^2)^{\frac{1}{2}})\cot\tfrac{1}{2}(\rho/R_o^2-\rho^2)^{\frac{1}{2}})) \qquad \text{for } \beta=1$$

$$= \tan^{-1}(\rho/(R_1^2-\rho^2)^{\frac{1}{2}})-\tan^{-1}(\rho/(R_o^2-\rho^2)^{\frac{1}{2}}) \qquad \text{for } \beta=2$$

for $\rho<R_c$ $\quad \tan^{-1}(\rho/(R_c^2-\rho^2)^{\frac{1}{2}}) \geq \psi > \tan^{-1}(\rho/(R_o^2-\rho^2)^{\frac{1}{2}})$

$\pi-\tan^{-1}(\rho/(R_o^2-\rho^2)^{\frac{1}{2}}) \geq \psi \geq \pi-\tan^{-1}(\rho/(R_c^2-\rho^2)^{\frac{1}{2}})$

$$R_c \leq \rho < R_o \quad \pi - \tan^{-1}(\rho/(R_o^2-\rho^2)^{\frac{1}{2}}) > \psi > \tan^{-1}(\rho/(R_o^2-\rho^2)^{\frac{1}{2}}) \qquad (II.2)$$

APPENDIX III

Reduction of the U.K.I.R.T. Data

In this appendix the method used to reduce the U.K.I.R.T. data obtained for supernovae in September 1982, December 1982 and January 1983 is described. These data are not actually used in any modelling in the thesis due to the absence of corresponding U, B, V data for these supernovae.

The Method of Reduction

Suppose we wish to determine the K magnitude of the supernova in NGC7713, on night 1 (that is 13th/14th September 1982) of the September observing run. This object was measured at 10.45 U.T. The method of reduction is as follows:-

Calibration stars are chosen around the time at which the supernova measurements were taken, in order to determine (a) the extinction in the atmosphere and (b) the calibration of the supernova flux. Suitable calibration stars are FR8729, HD1160, FR9601, and HD1160, listed in tables A3 to A6 respectively. The data for each object are based on different numbers of integrations because observations are accumulated until the errors are of an acceptable level. The standard K magnitudes for these stars are given in table A7.

Airmass is given by the formula Airmass = $(AM)_0$. Sec Z, where Z is the zenith angle and the quantity $(AM)_0$ changes with time. For the calibration stars, errors in instrumental magnitude are neglible. The 5.43 correction on FR9601 is due to the high load resistor being used in this case, to avoid signal saturation.

The "SETMAG" of the system for each measurement can now be

calculated by subtracting the calibration magnitude from the instrumental magnitude. The resulting SETMAG gives a measure of the gain of the system. Thus, if we assume the telescope and detectors and electronics have constant gain, then any variation in the SETMAG must be due to atmospheric extinction. We now have instrumental magnitudes minus the calibrated magnitudes given in table A8. Thus we have an extinction of ~0.9 magnitudes per unit airmass, (see figure A1). This is actually a very high result, demonstrating that it was a poor night. A good night on U.K.I.R.T. should give only ~0.1 to 0.2 magnitudes per unit airmass at K, (see table A9).

Having established the above calibration we are now in a position to estimate the magnitude of the supernova in NGC7713. In table A2, the K magnitude of this supernova is given as

Instrumental magnitude	=	-6.19
Error	=	0.05
Airmass	=	1.89

Since this measurement was done with the high load resistor, the standard FR9601 was also measured on the high load. First we estimate the extinction correction for NGC7713. Going from 1.89 to 1.15 (the airmass of the FR9601 calibration) clearly reduces the airmass by 0.74 and so should brighten the magnitude by

$$0.74 \times 0.9 = 0.67 \text{ magnitudes}$$

If the airmass changes appreciably during a long integration then the average of the airmasses should be taken at the beginning and end of the measurement.

Thus the K magnitude of the supernova in NGC7713 is equal to

$$7.34 + (13.34 - 6.19) - 0.67$$

↑	↑	↑	↑
Calibration value of the standard star	Measurement of the calibration star	Measurement of SN7713	Extinction correction

$$= + 13.91$$

Errors in the magnitude measurement at J, H, K, and L are typically of the order of ±0.05. Thus the magnitude at K of the supernova in NGC7713 (on this particular night at the specified time) was +13.91 ± 0.05. A similar process is repeated to obtain the magnitude of this and other supernovae at J, H and L.

FIGURE A1. The variation of Setmag with Airmass for the calibration stars at magnitude K.

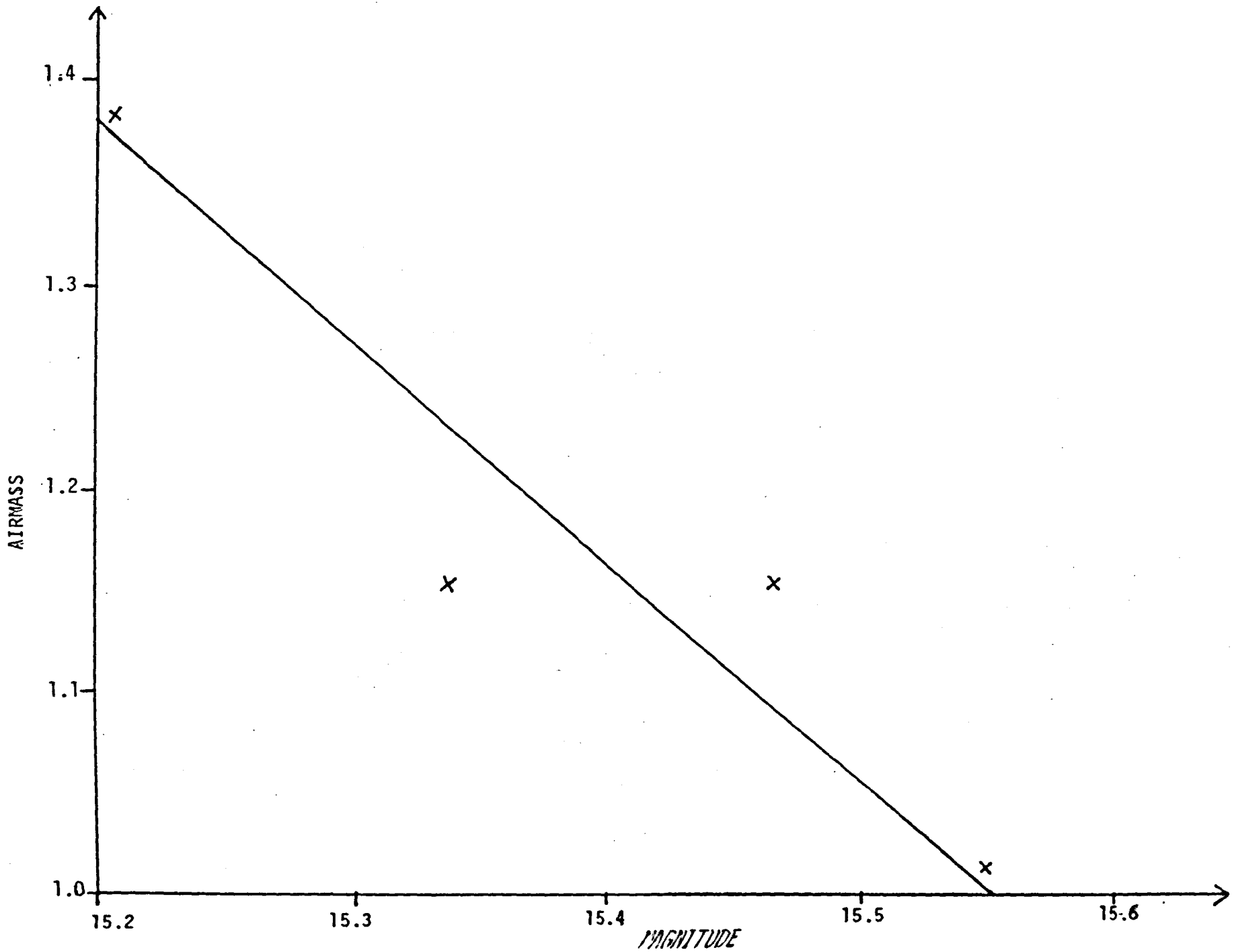
1.4
1.3
1.2
1.1
1.0
AIRMASS
15.2
15.3
15.4
15.5
15.6
MAGNITUDE

TABLE A2

THE RAW DATA FOR SN7713

AT MAGNITUDE K

```
FF K

Filter Found : Shift= -1
OK
>NOMODE 0
Nodding is under manual control
OK
>SECS 15000
OK
>SECS
Integration Time Unchanged from (msecs) : 15000
Analogue PSD Mode
OK
>LEFT

 Run :   9      31.62     mV   times  1   15000 msecs     Filter :K
App RA: 23 35 27.13   LST: 23 33 21.80   Hour angle:  0.03 hr E
   Dec:-38  1 59.00    UT: 10 22 56.97       Airmass: 1.8798
No logfile open

Time        I  R-L         (R+L)/2    Ins. Mag.   Error
OK
 =>R
10:24:01    1  282.05       14716.      -6.126          0.0000 =>L
10:26:09    3  417.49       14728.      -6.418          0.1183 =>L
10:27:01    4  359.60       14710.      -6.411          0.0644 =>R
10:27:58    5  266.27       14719.      -6.350          0.0903 =>L
10:29:03    6  227.67       14730.      -6.206          0.0730 =>R
10:30:19    7  286.54       14732.      -6.267          0.0870 =>L
>STOPC
OK
>LEFT
OK
10:32:12    8  260.23       14740.      -6.241          0.0809 =>R
10:33:23    9  344.84       14710.      -6.253          0.0714 =>L DELETE 6
10:33:51    9  14859.       7429.3      -6.290          0.0681OK

10:35:26   10  205.09       14756.      -6.244          0.0763 =>R
10:36:25   11  331.10       14745.      -6.250          0.0680 =>L
10:37:31   12  319.71       14733.      -6.251          0.0615 =>R
10:38:35   13  314.55       14757.      -6.250          0.0562 =>L
10:39:28   14  388.11       14799.      -6.269          0.0536 =>R
10:40:22   15  179.07       14712.      -6.234          0.0608 =>L
10:41:13   16  317.24       14751.      -6.235          0.0566 =>R
10:42:05   17  345.15       14698.      -6.243          0.0530 =>L
10:43:35   18  254.54       14738.      -6.230          0.0516 =>R
10:44:42   19  199.15       14740.      -6.209          0.0536 =>L
10:45:39   20  221.78       14717.      -6.193          0.0534>MAG

  19 integrations of   30.000     seconds

App RA: 23 35 27.40   LST: 23 56 18.60   Hour angle:  0.35 hr W
   Dec:-38  1 60.00    UT: 10 45 50.04       Airmass: 1.8906

**********************

Filter :K

Mean       =  300.032
St. Dev.   =  69.8934

Ins Mag.   =  -6.193
 -Airmass  =  -6.193
 +Offset   =   9.287
 Error     =   0.053
**********************
```

TABLE A3

THE RAW DATA FOR FR8729

AT MAGNITUDE K

```
OK
FF K

Filter Found : Shift= -1
OK
>LEFT

 Run :  3        100.0      mV   times  1    5000 msecs     Filter :K
App RA: 22 56 37.60    LST: 22 20 19.60   Hour angle:  0.60 hr E
   Dec: 20 40 30.00     UT:  9 10  6.76      Airmass: 1.0113
No logfile open

Time        I  R-L          (R+L)/2     Ins. Mag.   Error
OK
 =>R
09:10:26    1  42159.        46723.       -11.56          0.0000 =>L
09:10:49    2  41655.        46935.       -11.56          0.0060 =>R >MAG


   2 integrations of   10.000      seconds

App RA: 22 56 37.67    LST: 22 21 13.20   Hour angle:  0.59 hr E
   Dec: 20 39 19.00     UT:  9 11  0.21      Airmass: 1.0107

**********************

Filter :K

Mean       =  41906.6
St. Dev.   =  356.413

Ins Mag.   = -11.556
 +Airmass  = -11.556
 +Offset   = -11.556
 Error     =   0.006
**********************
```

TABLE A4

THE RAW DATA FOR HD1160

AT MAGNITUDE K

```
OK
FF K

Filter Found : Shift= -1
OK
:LEFT

 Run :   7       10.00      mV   times  1     5000 msecs     Filter :K
App RA: 24 15  4.00    LST: 22 30 44.80  Hour angle:  1.74 hr E
   Dec:  4  9 12.00     UT:  9 20 30.26      Airmass: 1.1530
No logfile open

Time        I  R-L          (R+L)/2     Ins. Mag.    Error
OK
 =>R
09:20:51    1  2348.7        4679.9       -8.427          0.0000 =>L
09:21:15    2  2361.6        4670.2       -8.430          0.0027 =>R
09:21:35    3  2358.1        4670.9       -8.431          0.0016>MAG


   3 integrations of    10.000      seconds

App RA: 24 15  4.26    LST: 22 31 54.80   Hour angle:  1.72 hr E
   Dec:  4  8  4.00     UT:  9 21 40.04      Airmass: 1.1504

**********************

Filter :K

Mean        =  2356.14
St. Dev.    =  6.69836

Ins Mag.    =  -8.431
 +Airmass   =  -8.431
 +Offset    =   7.049
 Error      =   0.002
**********************
```

TABLE A5

THE RAW DATA FOR FR9601

AT MAGNITUDE K

```
FF K

Filter Found : Shift= -1
OK
>RIGHT

 Run :  12        31.62      mV   times 10,    5000 msecs     Filter :K
App RA:  0  5 50.80    LST:  0 47  6.70   Hour angle:  0.69 hr W
   Dec: -7 38 12.00     UT: 11 36 29.82       Airmass: 1.1465
No logfile open

Time        I  R-L          (R+L)/2     Ins. Mag.   Error
OK
 =>L
11:36:55    1 0.21665E+06 0.14699E+06 -13.34          0.0000 =>R
11:37:35    2 0.21669E+06 0.14753E+06 -13.34          0.0004>MAG

   2 integrations of    10.000      seconds

App RA:  0  5 50.73    LST:  0 48 15.50   Hour angle:  0.71 hr W
   Dec: -7 38 13.00     UT: 11 37 38.40       Airmass: 1.1476

**********************

Filter :K

Mean       =  216671.
St. Dev.   =  116.370

Ins Mag.   = -13.340
 +Airmass  = -13.340
 +Offset   =   2.140
 Error     =   0.000
**********************
```

TABLE A6

THE RAW DATA FOR HD1160

AT MAGNITUDE K

```
OK
FF K

Filter Found : Shift= -1
OK
>RIGHT

 Run :  19       10.00      mV   times  1     5000 msecs     Filter :K
App RA:   0 15   2.80    LST:   2 59 39.70   Hour angle:   2.74 hr W
   Dec:   4  8 36.00     UT: 13 48 41.03       Airmass: 1.3680
No logfile open

Time        I  R-L         (R+L)/2     Ins. Mag.    Error
OK
 =>L
13:49:07    1  1868.3       4676.2       -8.179          0.0000 =>R
13:49:36    2  1813.9       4654.1       -8.163          0.0148 =>L
13:50:13    3  1861.0       4671.8       -8.167          0.0092 =>R
13:50:39    4  1886.0       4685.7       -8.172          0.0083>MAG

   4 integrations of   10.000      seconds

App RA:   0 15   3.07    LST:   3  1 44.00   Hour angle:   2.78 hr W
   Dec:   4  8 37.00     UT: 13 50 45.04       Airmass: 1.3786

**********************

Filter :K

Mean       =   1857.30
St. Dev.   =   30.8100

Ins Mag.   =   -8.172
 +Airmass =   -8.172
 +Offset   =   12.598
 Error     =    0.008
**********************
```

Table A7

Object	Calibrated K Magnitude from Tables	Airmass	Instrumental Magnitude (Ins. Mag.)
FR8729	3.99	1.01	-11.56
HD1106	7.04	1.15	- 8.43
FR9601	7.43	1.15	-13.34 + 5.34 + -7.91
HD1160	7.04	1.38	- 8.17

The formulae used to reduce the data listed in table V(i) were

For J SETMAG = -22.422 + 0.289 AM

errors 0.085 0.0675

For H SETMAG = -21.614 + 0.257 AM

errors 0.061 0.051

For K SETMAG = -21.207 + 0.244 AM

errors 0.055 0.046

where AM is airmass

The errors quoted above are the errors in the numerical coefficients and were obtained using a least squares fit to the data in table V(i).

Table A8

Object	SETMAG = Ins. Mag.- Calibration Mag.	Airmass
FR8729	-15.55	1.01
HD1160	-15.47	1.15
FR9601	-15.34	1.15
HD1160	-15.21	1.38

Table A9

Typical atmospheric extinction at UKIRT

Magnitude	Extinction
J	0.12
H	0.08
K	0.10
L	0.15

Table A10 below lists the standard stars used in the data reduction and table A11 below lists the reduced supernova data. The U.K.I.R.T. data given in tables A10 and A11 below were obtained using U.K.I.R.T. on 27th/28th December 1982 (G. Pearce and P.M. Williams).

Table A10

The standard stars used in the data reduction for 27th/28th December, 1982

Time (UT) h m s	Target	Aperture (mm)	Filter	Airmass	Reduced Instrumental Magnitude
5 17 25.39	HD1160	5	H	1.0820	-14.281
5 21 41.00	"	5	K	1.0880	-13.905
5 35 45.95	GL5827	5	K	1.2334	-13.455
5 38 42.51	"	5	J	1.2408	-13.757
5 40 50.38	"	5	H	1.2464	-13.561
10 50 58.40	HD40335	5	H	1.0857	-14.870
10 58 51.19	"	5	K	1.0960	-14.492
11 00 28.12	"	5	K	1.0983	-14.503
11 02 8.62	"	5	H	1.1007	-14.879
11 09 58.85	GL299	5	H	1.0486	-13.458
11 11 20.22	"	5	K	1.0472	-13.351
11 13 55.51	"	5	J	1.0445	-13.767
11 49 49.33	HD40335	5	H	1.2034	-14.840
11 51 24.31	"	5	K	1.2080	-14.487
12 01 47.11	GL299	5	K	1.0188	-13.309
12 03 23.81	"	5	J	1.0187	-13.770
12 06 50.27	"	5	H	1.0187	-13.441
13 37 08.42	"	5	L	1.0998	- 7.085
13 48 41.98	"	5	K	1.1205	-13.235
13 51 04.41	"	5	J	1.1290	-13.658
13 52 43.42	"	5	H	1.1328	-13.334
15 47 42.00	"	5	J	1.7282	-13.550
15 50 01.99	"	5	H	1.7521	-13.249
15 52 37.68	"	5	K	1.7792	-13.137

Table A11

U.K. I.R.T. supernova data obtained on night 2 (27th to 28th December 1982)

Time (UT)			Target	Filter	Magnitude
h	m	s			
06	13	20	SN4237	K	15.65
06	28	17	SN4237	J	16.02
06	46	59	SN4237	H	15.74
08	04	47	SN1187	K	15.37
08	16	39	SN1187	J	15.89
08	35	39	SN1187	H	15.98
14	51	28	SN5485	K	15.85
15	09	55	SN5485	K	15.62
15	28	13	SN5485	J	16.99

APPENDIX IV

LIST OF SYMBOLS USED IN THE THESIS

a	Grain radius.
A_ν	The optical depth at frequency ν due to interstellar extinction.
A_ν^*	The absorption, scattering or extinction in magnitudes at frequency ν due to interstellar dust.
a_1	Nucleation centre radius (core radius of grain).
a_2	Mantle radius of grain.
a_∞	Final grain radius.
a_c	Circumstellar grain radius.
a_i	Grain radius of type i (i=g for graphite, i=s for silicate).
B^i	Parameter in the black-body fit.
$B_\nu(r,t)$	Flux per unit frequency interval at frequency ν, from unit area of a black-body, distance r from the centre of the supernova heated by supernova radiation seen at time t.

$B(\nu,T)$	Planck function for frequency ν and temperature T.
c	Speed of light.
c'	A constant associated with grain condensation theory.
c_1, c_2, c_3	Parameters in the refractive index of corundum.
c_T	The coefficient of Q_{abs} in the expression for the optical depth of the circumstellar dust shell to supernova radiation.
D	Distance of supernova to observer.
d_{is}	Total mass density of interstellar grain material.
D_r	Grain acceleration due to ambient gas viscosity.
E(B-V)	Colour excess at B-V due to interstellar dust.
f_i	Fraction by number of interstellar grains of type i. (i=s for silicate, i=g for graphite).
F_i	Fraction by mass of interstellar grains of type i (i=g for graphite, i=s for silicate).
f_ν	Flux per unit frequency interval at frequency ν.

f_ν^{cal} The computed flux per unit frequency interval at frequency ν, corresponding to f_ν^{obs}.

f_ν^{obs} The observed flux per unit frequency interval at frequency ν.

f_β A function that determines grain number density.

F_ν Ambient starlight flux.

G Gravitational constant.

G_r Grain acceleration due to gravitational attraction by a supernova.

h Planck's constant.

H_* Rate at which grains absorb ambient starlight.

$H_\nu(r,t)$ Part of $B_\nu(r,t)$.

I Inclination of Galaxy to observer.

$I_\beta(t)$ A function of time after the beginning of grain condensation.

$I_{\nu i}$ Contribution from any grains infront of the cavity (at times for which $ct<R_1$) but behind the paraboloid of revolution.

$J(x_T)$	A function used in grain condensation theory.
K	Boltzmann Constant.
K_1', K_2'	Constants concerned with supernova light curves.
L_1, L_2, L_3, L_4	Parameters in the type I supernova effective temperature and luminosity variations.
L	Parameter in the black-body fit.
L_o	Peak luminosity of supernova.
L_ν	Luminous flux per unit frequency interval.
$L_\odot$	Solar luminosity.
$L_*(t)$	Supernova luminosity at time t after outburst.
L_{IR}	Infra-red luminosity of a nova or supernova.
M	Supernova absolute magnitude at time t.
m	Mass of monomer.
M_i	Mass density of interstellar grains of type i (i=s for silicate, i=g for graphite).

m_1 Real part of refractive index.

m_2 Imaginary part of refractive index.

M_{-6} Mass loss rate in units of $10^{-6} M_\odot yr^{-1}$.

mg Mass of a grain (rest mass).

m_g' Non-rest mass of grain.

M_g Circumstellar dust shell mass.

M_o Supernova absolute magnitude at outburst.

M_* Supernova Mass.

$M_\odot$ Solar Mass.

n Number density of gas particles.

n(t) Number density of grain monomers at time t after the beginning of condensation.

N_o Total number density of interstellar grains.

N_{oc} Coefficient in the circumstellar dust grain number density distribution.

N_{od} Coefficient in power law function in circumstellar grain distribution.

N_{oi} Number density of interstellar grains of type i (i=g for graphite, i=s for silicate).

$N_{1\nu}$ $N_{od}\pi a_1^2 Q_{abs}(a_1,\nu)$

$N_{2\nu}$ $N_{od}\pi a_2^2 Q_{abs}(a_2,\nu)$

n_c Number density of ambient carbon.

$N_c(r)$ Circumstellar grain number density at distance r from the supernova.

N_{co} Number density of grains at beginning of condensation.

$N_{c\nu}$ $N_{oc}\pi a_c^2 Q_{abs}(a_c,\nu)$.

$N_d(r)$ Circumstellar grain number density of distance r from the supernova in the double dust shell case.

$N_{gs\nu}$ The interstellar extinction per unit length divided by π.

n_H Number density of hydrogen atoms.

N_L Number of layers evaporating from a grain.

n_m Number of monomers in a grain at time t after beginning of condensation.

$n_v(t)$ The number density of monomers in the gas.

p A parameter used in the black-body fit.

P_r Grain acceleration due to radiation pressure.

$Q_{abs}(\nu)$ Grain absorption efficiency.

$Q_{ext}(\nu)$ Grain extinction efficiency.

$Q_{sca}(\nu)$ Grain scattering efficiency. The radiation scattering efficiency of a grain.

$\overline{Q_{abs}}$ The Planck mean of Q_{abs}.

$\overline{Q_{ext}}$ The Planck mean of Q_{ext}.

$\overline{Q_{sca}}$ The Planck mean of Q_{sca}.

Q'_{gc} Quantity corresponding to T'_{gc}.

Q_{ggi} Q_{gi} for temperature T_{ggi}.

Q_{gi} $Q_{abs}T_{gi}^4$.

Q'_{gi} Quantity defined by equation (5.2.10).

Q_{goi} Quantity used in the grain temperature interpolation.

$Q_{pr}(\nu)$ Grain radiation pressure efficiency (Planck mean Q_{pr}).

$\overline{Q_{pr}}$ Planck mean of Q_{pr}.

R Depth of the supernova into galaxy.

$\underline{R}$ Perpendicular vector from supernova to front-edge of galactic dust plane.

r Distance of a grain from the supernova.

$\underline{r}$ Radius vector from the supernova.

r_o Distance from the supernova at which condensation begins.

R_o Outer radius of inner shell and inner radius of outer shell for the double dust shell.

R_1 Interstellar cavity radius or outer radius of circumstellar dust shell.

R_c Circumstellar cavity radius.

$R_c'(t)$ Minimum distance from the supernova at which a grain can exist at time t after outburst.

R_{cm} The value of the cavity radius R_c of the model circumstellar dust shell for which $\nabla f_\nu = 0$.

R_{cs} The value of the cavity radius R_c of the model circumstellar dust shell for which $\delta f\nu$ is a minimum.

$R_p(t)$ The radius of the circle formed by the interstellar dust illuminated by the supernova at time t after outburst.

r_p, r_{p+1} r values at which Q_{gi} is computed for interpolation.

r_v Distance from the supernova at which grains vapourizes.

R_* Supernova black-body radius at time t.

s Bulk density of Grain material.

s_1 Core density.

s_2 Mantle density.

s_c Density of circumstellar. grain material.

s_i	Density of grain material (i=g for graphite, i=s for silicate).
S_ν	Flux per unit frequency interval at frequency ν at time t from a grain at position r.
$S_{\nu i}$	Infra-red flux from a grain of type i.
t	Time after the supernova outburst.
t(a) ... t(f)	The times after outburst at which the paraboloid of revolution crosses points (a) to (f) of the circumstellar dust shell (see figure 39).
T	Temperature of the radiation field.
t_o	e-folding time of the supernova light curve.
t_o'	Time at which the supernova has magnitude M_o.
T_o	A constant associated with grain sublimation.
t_1, t_2	Parameters of the type II supernova effective temperature variation.
t_1' t_2'	Time constants in the variation of the supernova magnitude.

$t_3 \ldots t_7$	Paramters in the type I supernova effective temperature and luminosity variations.
t_c	Condensation time of circumstellar dust shell.
t_c'	Time taken for 99% of the grain to condense.
$T_e(t)$	Supernova effective temperature at time t.
$T_{evap}(t)$	Grain evaporation temperature.
t_f	Life-time of a supernova flash.
T_{gc}	The temperature of a circumstellar dust grain heated by ambient starlight only.
T_{gi}	Grain temperature.
T_{gi}'	The temperature of an interstellar dust grain of type i heated by ambient starlight only.
T_{ggi}	The set of temperatures used in the determination of the grain temperature.
T_{gsb}	Sublimation temperature of a grain.
T_i	The black-body temperatures of ambient starlight (i=1,2,3).

t_q, t_{q+1} Set of t values at which Q_{gi} is computed for interpolation.

T_v Temperatures at which a grain vapourizes instantaneously.

U_o Binding energy per molecule of material.

U_4 Velocity of a shock wave in units of 10^4 kms^{-1} moving into the circumstellar medium.

V Grain velocity.

$\dot{V}$ Acceleration of a grain.

V_1 The wind velocity in units of 10kms^{-1} caused by the moving shock wave.

V_{ej} Supernova ejecta velocity.

V_s The sound speed in the ejecta.

V_{sc} Rate of increase of the supernova black-body radius.

W Dilution factor $(R^*/r)^2$.

W_i Dilution factors for ambient starlight, (i=1,2,3).

x — Distance along the line of sight towards the observer from the plane through the supernova, normal to the line of sight.

$x(M)$ — The value of x at which a line of sight crosses the front edge of the interstellar dust plane.

$x(P)$ — The value of x at which a line of sight (defined by ρ and γ or by ρ, y, and z) crosses the paraboloid of revolution.

$x(U)$ — The value of x at which a line of sight crosses the back edge of the interstellar dust plane.

x_T — Ratio of grain radius to final grain radius.

$x_\zeta(\rho)$ — The path length through the interstellar dust cavity along a line of sight.

y — Coordinate in the plane perpendicular to the line of sight.

z — Coordinate in the plane at right angles to y.

α — Sticking probability.

α' — Temperature exponent in expression for Q_{gi}.

β Exponent of r in grain number density distribution.

γ Angular coordinate in the cylindrical system of polar coordinates used.

Γ Parameter in silicon carbide refractive index.

$\Gamma_1\ \Gamma_2\ \Gamma_3\ \Gamma_4\delta$ Parameters in silicon carbide refractive index.

$\delta(a)$ ... $\delta(e)$ The functions (equal to 1 or 0) which determine whether or not a particular integral contributes to the circumstellar dust brightness.

Δf_ν The mean deviation of the logarithm to the base 10 of the f_ν^{cal} from the logarithm to base 10 of the corresponding value of f_ν^{obs}.

δf_ν The standard deviation of the logarithm to the base 10 of the f_ν^{cal} from the logarithm to the base 10 of the corresponding value of f_ν^{obs}

Δ_i Parameter in the refractive index of silicon carbide.

Δ_τ Optical thickness of the shell.

$\varepsilon_0, \varepsilon_1, \varepsilon_2, \varepsilon_3, \varepsilon', \varepsilon''$ Quantities concerned with the computation of refractive index.

$\zeta'(\rho,\psi)$ A function equal to zero in the cavity of the double dust shell or outside the double dust shell but $a_1^2\ Q_{abs}\ (a_1,\nu)$ in the inner shell and $a_2^2\ Q_{abs}\ (a_2,\nu)$ in the outer shell.

$\zeta^{cs}(\rho,\psi')$ A function equal to zero inside the circumstellar dust cavity and unity otherwise.

$\zeta^{is}(\rho,x)$ A function equal to zero inside the interstellar dust cavity and unity otherwise.

η Viscosity of ambient gas.

Θ Thickness of the galactic dust plane.

κ Opacity of the circumstellar shell.

κ_ν Linear absorption coefficient.

λ Wavelength of radiation.

$\lambda_0,\lambda_1,\lambda_2$ Wavelengths used for computing refractive indices of grain materials.

μ A constant associated with collisional heating of grains.

ν Frequency of radiation.

ν_L Molecular vibration frequency of the lattice.

ν_o A frequency used in computing the refractive indices of various grain materials.

Σ_o Surface brightness of the supernova photosphere at time t_o'.

$\Sigma_\nu(\rho,\gamma)$ The surface brightness of the dust at frequency ν along the line of sight defined by (ρ,γ).

ρ The perpendicular distance to a grain from the line of sight passing through the supernova.

ρ_o An integration limit. The distance corresponding to the angular distance $\tan^{-1}(\rho_o/D)$.

$\rho_c(\gamma)$ The value of ρ for which the front of the interstellar dust plane intersects the paraboloid of revolution.

ρ_{cty} The value of ρ for which the paraboloid of revolution crosses the interstellar dust cavity.

ρ_g Ambient gas density.

σ Stefan's constant.

$\sigma_{1\nu}', \sigma_{2\nu}'$ The integrals in the expression for the interstellar dust surface brightness.

σ_{ν}' The integral in the expression for Σ_{ν} in the case of the circumstellar dust shell.

$\sigma_{\nu i}$ The integrals in the expression for the interstellar dust surface brightness.

$\tau(\rho, x, t)$ The time at which the observer sees the supernova radiation with which a grain at (ρ, x) is in thermodynamic equilibrium when the grain's radiation is seen at time t.

$\tau_{cav}(\rho)$ The reduction in the interstellar optical depth due to the light path through the interstellar dust cavity.

τ_{sput} Life-time of a grain against desruction by sputtering.

$\tau_{\beta\nu}$ The optical depth at frequency ν to interstellar grain radiation due to circumstellar dust.

$\tau_{\nu}'(r)$ Optical depth to supernova radiation of frequency ν distance r from the supernova.

τ_{ν}^{cs} The optical depth at frequency ν to supernova radiation due to circumstellar dust (at the observer).

$\tau_\nu^{ic}(\rho,\gamma)$ The extinction of circumstellar dust radiation by interstellar dust grains in the parent galaxy.

$\tau_\nu^{is}(\rho,\gamma)$ The optical depth at frequency ν to supernova radiation due to interstellar grains (at the observer).

$\tau*(r)$ $\tau_\nu'(r)$ with $Q_{abs}(\nu)$ replaced by Q_{abs} (T_e).

$\phi_{1\beta},\phi_{2\beta}$ Functions in the expression for the optical depth of circumstellar dust grains to circumstellar dust radiation in the double dust shell case.

ϕ_β A function in the expression for the optical depth of circumstellar dust grains to circumstellar dust radiation.

ψ A coordinate in the circumstellar dust shell case.

$\psi(B'),\psi(F')$etc. The value of ψ for which the line of sight crosses B',F' etc, (see figure 39).

χ Ratio of mass abundance of grain forming materials.

χ' Exponent of r used in interpolating Q_{gi}.

χ_{Al} The steady-state fraction of Aluminium.

APPENDIX V

THE AUTHOR'S PUBLISHED PAPERS